Titre: Title:	The effects of thermal transients on flange sealing
Auteur: Author:	Warren Brown
Date:	2001
Type:	Mémoire ou thèse / Dissertation or Thesis
Référence: Citation:	Brown, W. (2001). The effects of thermal transients on flange sealing [Thèse de doctorat, École Polytechnique de Montréal]. PolyPublie. https://publications.polymtl.ca/7051/

INFORMATION TO USERS

This manuscript has been reproduced from the microfilm master. UMI films the text directly from the original or copy submitted. Thus, some thesis and dissertation copies are in typewriter face, while others may be from any type of computer printer.

The quality of this reproduction is dependent upon the quality of the copy submitted. Broken or indistinct print, colored or poor quality illustrations and photographs, print bleedthrough, substandard margins, and improper alignment can adversely affect reproduction.

In the unlikely event that the author did not send UMI a complete manuscript and there are missing pages, these will be noted. Also, if unauthorized copyright material had to be removed, a note will indicate the deletion.

Oversize materials (e.g., maps, drawings, charts) are reproduced by sectioning the original, beginning at the upper left-hand corner and continuing from left to right in equal sections with small overlaps.

ProQuest Information and Learning
300 North Zeeb Road, Ann Arbor, MI 48106-1346 USA
800-521-0600

UNIVERSITÉ DE MONTREAL

THE EFFECTS OF THERMAL TRANSIENTS ON FLANGE SEALING

WARREN BROWN
DÉPARTEMENT DE GÉNIE MÉCANIQUE
ÉCOLE POLYTECHNIQUE DE MONTRÉAL

THÈSE PRÉSENTÉE EN VUE DE L'OBTENTION
DU DIPLÔME DE PHILOSOPHIAE DOCTOR
(GÉNIE MÉCANIQUE)
NOVEMBRE 2001

UNIVERSITÉ DE MONTREAL

ÉCOLE POLTECHNIQUE DE MONTREAL

Cette thèse intiulée:

THE EFFECTS OF THERMAL TRANSIENTS ON FLANGE SEALING

présentée par: BROWN, Warren

en vue de l'obtention du diplôme de: Philosophiae Doctor

a été dûment acceptée par le jury d'examen constitué de:

M. OSTIGUY Germain, Ph.D., président

M. DERENNE Michel, MScA., directeur de recherche

M. BOUZID Abdel-Hakim, Ph.D., codirecteur de recherche

M. BLACH Adolph, Ph.D., membre

M. MARCHAND Luc, Ph.D., membre

DEDICATION

To the many people who have given me encouragement to succeed.

ACKNOWLEDGEMENTS

I would like to express my sincere gratitude to my supervisors, Mr Michel Derenne and Dr Hakim Bouzid, for their guidance, valued discussion and good humour throughout this project.

I would also like to thank Mr David Reeves, of Chevron Ltd, for his support in obtaining the funding to build the principal experimental test rig and his valued assistance in obtaining the site measured data.

I wish to acknowledge the assistance I have received from the staff and my fellow students in the Section of Applied Mechanics at Ecole Polytechnique. In particular Dr Luc Marchand, Serge Plamandon and Nour Aimene for their assistance in bringing the principal experimental test rig to life.

Finally I would like to thank my wife, Sara, for her love and support throughout my studies, and for agreeing to live so far away from the beach for these past three years.

RÉSUMÉ

Ce travail a pour objet de déterminer le gradient thermique qui se développe dans les composants d'un assemblage à brides boulonnées et d'analyser les effets mécaniques qui en résultent lors d'une fluctuation de température du fluide contenu. Le résultat de ce travail sera utilisé pour développer une nouvelle méthode de conception des assemblages boulonnés utilisés en température. Cette recherche a permis de déterminer la température et la réponse dynamique de chaque composant de la bride pendant la fluctuation thermique. Cette réponse thermique a été utilisée pour déterminer les effets mécaniques (contrainte et déformation) sur chaque composant de la bride.

Les équations théoriques ont été développées afin de déterminer les gradients de température existant dans la bride un fois celle-ci en équilibre thermique. Les équations sont aussi utilisées, avec certaines modifications, pour déterminer le profil de température à différents stades durant la réponse dynamique de la bride. Ces profils sont alors utilisés pour déterminer la réponse mécanique (contrainte et déformation) de l'assemblage. La méthode analytique finale permet d'analyser tous les effets de température sur le comportement mécanique d'un assemblage à brides boulonnées. Elle pourra être simplifiée pour développer une méthode de calcul concernant ces effets qui sera utilisable dans la conception des assemblages à brides boulonnées à haute température.

La méthode des éléments finis a été utilisée pour confirmer les équations théoriques de la distribution de température et de l'interaction mécanique qui en résulte. Des expérimentations effectuées sur un assemblage de 3 pouces ont été réalisées pour vérifier les résultats analytiques. Également, des données thermiques prises sur des échangeurs de chaleur d'une raffinerie de pétrole ont été comparées aux résultats analytiques. Des essais ont aussi été réalisés en laboratoire sur un banc d'essais spécifiquement construit

pour vérifier la réponse mécanique (contrainte, déformation) des brides aux effets de température. Ce banc d'essais représente un assemblage de 24 pouces de diamètre nominal, avec 24 boulons.

ABSTRACT

The analysis developed in this project is used to determine the thermal and mechanical effects of temperature on the operation of bolted flanged joints. The goal of the study was to provide a theoretical basis for the development of a method of analysis of these effects, to be used in the design process of pressure vessel and piping equipment. The research established the temperature profile of the joint components during steady state operation and also during dynamic thermal transients. These temperature profiles were then used to determine the mechanical effects (deformation and load) on each of the joint components.

Analytical equations were developed to determine the steady state temperature profile of the joint components. These equations were then modified, and extended, to allow the determination of the temperature profile in the joint at critical stages during thermal transient operation. These temperature profiles were then used to determine the mechanical deformation and also the mechanical interaction of the joint components. The complete analytical method allows the analysis of the full effects of temperature on bolted flanged joints.

Finite Element Analysis is used to verify the developed theoretical equations, for both the temperature distribution and the subsequent mechanical interaction. The analytical results for steady state temperature distribution where also verified by comparison to experimentation on a NPS 3 inch ASME flange and by comparison with temperature measurements taken on operational heat exchangers in a refinery. The developed theoretical method for the analysis of the transient effects of temperature was verified by comparison to Finite Element Analysis. Additionally, laboratory experimentation was performed on a specially constructed 24 inch test rig to confirm the overall validity of both the Finite Element Analysis and the developed analytical approach.

CONDENSÉ EN FRANÇAIS

Introduction

Les assemblages à brides boulonnées sont utilisés dans la fabrication des réservoirs sous pression pour permettre l'assemblage de la tuyauterie connexe ou pour donner accès à l'intérieur de ces équipements. Cependant, ces assemblages sont le point faible des installations pressurisées et ils sont bien souvent la cause des fuites du fluide pressurisé qu'ils contiennent. Ces fuites peuvent être mineures et ne demander qu'un resserrage des boulons pour étancher l'assemblage. Par contre, elles peuvent aussi se transformer rapidement en accident grave pouvant entraîner la destruction des équipements par explosion suivie d'un incendie et éventuellement la mort de personnes qui se trouvent à proximité.

Les hautes températures d'opération et les chocs thermiques transitoires sont reconnus comme étant les facteurs principaux qui peuvent donner naissance à des fuites dans les équipements pressurisés (Payne, J.R., 1985). Cependant, les méthodes actuelles de conception ne prennent pas en compte les effets de température sur l'intégrité des assemblages boulonnés; seules les variations des propriétés avec la température des matériaux utilisés sont considérées. Actuellement, les températures des fluides contenus dans ces équipements sont de plus en plus élevées et donc le risque d'accidents, associés avec des fuites potentielles, est plus grand. Les possibilités d'incendie et de fermetures des installations sont donc aussi plus importantes. Ainsi, les coûts résultant d'une conception inadéquate qui ne fait pas intervenir l'effet de la température peuvent devenir très élevés.

Objectif de l'étude

L'objectif du présent travail est de développer une méthodologie d'analyse théorique pour déterminer les effets de la température sur l'intégrité mécanique des assemblages à brides boulonnées. Cette méthodologie pourrait alors être simplifiée pour établir une série de lignes directrices pouvant être utilisées dans les procédures de conception des codes de calcul des réservoirs sous pression. À partir d'équations analytiques, la méthodologie proposée concerne le calcul des contraintes et déformations du joint d'étanchéité, des boulons et des brides durant le régime transitoire du démarrage d'une installation et/ou durant les cycles thermique subséquents. Cette approche permet d'incorporer facilement cette méthodologie d'analyse dans les méthodes de calcul communément utilisées dans la conception des assemblages. Afin de simplifier la méthode, les équations développées se limitent à l'analyse en régime permanent et sont basées sur des conditions de service existants au moment le plus critique des transitoires de température. Cette approche a été vérifiée par comparaison avec une analyse par éléments finis (FEA), avec des mesures prises sur des installations existantes et avec une expérimentation en laboratoire faite sur un assemblage réel.

La philosophie d'analyse adoptée

Le développement de cette approche a été divisé en quatre étapes représentant chacune un processus analytique particulier. Pour chaque étape, ce processus est distinct des autres afin de permettre une vérification point par point de l'approche dans son ensemble. Les quatre étapes sont les suivantes:

1- Détermination de la distribution de température en régime permanent dans l'assemblage et des déformations qui en résultent pour chacun de ses composants (dilatations thermiques) dues à la température du fluide contenu.
2- Détermination de l'interaction mécanique existant entre les composants de l'assemblage une fois le régime permanent de température établi.

3- Détermination de la distribution de température en régime transitoire dans l'assemblage due à un changement brusque de la température du fluide contenu.
4- Détermination de l'interaction mécanique existant entre les composants de l'assemblage causée par le régime transitoire de température.

Chacune de ces étapes comprend quatre niveaux dans le processus d'analyse qui sont les suivants :

1- Faire l'analyse théorique du phénomène et écrire les équations correspondantes.
2- Vérifier ces équations en les comparant à plusieurs applications d'une analyse par éléments finis.
3- Vérifier une nouvelle fois théorie et équations par comparaison des résultats avec une expérience de laboratoire.
4- Confirmer l'application de la théorie par comparaison avec des mesures obtenues sur des installations existantes d'échangeurs de chaleur.

Les composants des assemblages à brides boulonnées sont représentés à la figure 0.3. Dans de tels assemblages, des hypothèses sur la géométrie sont généralement posées pour simplifier leur analyse. Ainsi, ils sont considérés comme étant symétriques par rapport à l'axe central de la tuyauterie et par rapport aux brides qui les composent, ces brides étant supposées identiques.

D'une façon générale, l'analyse mécanique des effets du boulonnage et de la mise en pression de ces assemblages montre qu'il y a une rotation des brides due à l'excentricité qui existe entre l'application de la force de boulonnage et le point d'application de la résultante de la réaction du joint d'étanchéité (voir Walters et al., 1927 et 1937). Cette rotation a tendance à faire se rapprocher les brides de façon plus importante du côté extérieur que du côté intérieur. Cet effet s'appelle encore la « mise en parapluie des brides ». L'application de la pression interne du fluide, quant à elle, produit deux effets.

Premièrement, il y a apparition d'une force axiale qu'on appelle « l'effet de fond » qui réduit la charge de compression appliquée sur le joint par le boulonnage initial et qui augmente la rotation des brides. Deuxièmement, il y a une expansion radiale de la tuyauterie (ou du réservoir) qui est restreinte par l'anneau des brides et qui cause un effet qu'on appelle « l'effet tonneau » qui s'accompagne d'un transfert de moment à l'anneau des brides et donc d'une rotation additionnelle de celles-ci (voir figure 0.4).

La mise en température de l'assemblage est traitée de la même manière que la mise en pression. Ici, les brides agissent exactement comme des ailettes de refroidissement installées sur la tuyauterie, ce qui donne naissance à des gradients de température dans les directions axiales et radiales (voir figure 0.5) et donc à des différentiels d'expansion thermique dans les composants de l'assemblage. D'une façon générale, puisque les boulons restent à une température plus basse que les brides, il en résulte un accroissement de la charge dans les boulons et donc de la charge sur le joint d'étanchéité. Cependant, puisque la tuyauterie (ou le réservoir) reste plus chaude que l'anneau des brides, le différentiel d'expansion radiale entre ces deux composants créera un transfert de moment à l'anneau des brides résultant en une diminution de la rotation des brides et donc une diminution de la charge dans les boulons et de la charge transmise au joint d'étanchéité.

À la suite d'un transitoire de température du fluide contenu, la tuyauterie (ou le réservoir) chauffe plus vite que l'anneau des brides et que les boulons. Cet effet dynamique a tendance à augmenter les deux effets précédemment mentionnés et peut, selon la géométrie de l'assemblage, donner une réduction ou un accroissement de la charge sur le joint d'étanchéité.

Les étapes de la méthodologie

Ce sont tous les effets mécaniques qui seront déterminés dans les quatre étapes de la méthode d'analyse présentée précédemment.

Étape 1

La première étape consiste à déterminer la distribution de température en régime permanent dans l'assemblage pour la température de service du fluide contenu. L'assemblage est divisé en quatre parties de géométrie simple à savoir : la paroi du réservoir ou de la tuyauterie, les brides, les boulons et le joint d'étanchéité (voir figure 0.3). Chacune de ces parties est analysée séparément en utilisant des solutions analytiques existantes. La paroi du réservoir ou de la tuyauterie est traitée comme un anneau creux à paroi épaisse et de longueur infinie tandis que la bride est analysée comme un anneau à paroi épaisse mais d'épaisseur finie si on néglige son moyeu de géométrie plus complexe. Cette approximation est valable puisque, une fois les températures de ces anneaux respectifs calculées, on peut, par interpolation entre ces deux valeurs, obtenir si nécessaire la température du moyeu.

Les boulons sont analysés comme des masses recevant de la chaleur des brides au niveau du cercle de boulonnage et perdant de la chaleur vers l'environnement extérieur. Le joint d'étanchéité est considéré comme étant à la même température que les parties de l'anneau des brides avec lesquelles il est en contact. Il est supposé que la perte de chaleur de tous ces éléments se fait par radiation et convection à partir de leur surface extérieure et qu'elle peut s'exprimer par une relation linéaire à partir de la différence de température entre cette surface extérieure et l'environnement ambiant; cette relation est communément appelée la « loi de Newton du refroidissement » (Carslaw and Jaeger or Moon and Spencer, 1961).

Finalement, les équations développées pour déterminer la distribution de température en régime permanent de chaque composant sont les équations 2.1 à 2.8 pour les parois, 2.16 à 2.24 pour les brides, 2.45 à 2.50 pour les boulons. Ces équations et la philosophie de l'analyse qui les sous-tend sont vérifiées par comparaison avec des résultats obtenus d'une analyse par éléments finis. Avec cette analyse, plusieurs passes correspondant à une sélection d'assemblages de dimensions différentes, ont été faites et une

représentation graphique de chacune a été obtenue. Les graphes produits donnent le pourcentage de température par rapport à celle du régime permanent en fonction du temps. Ils permettent à un utilisateur d'obtenir premièrement, le moment pour lequel le régime permanent de température est atteint et deuxièmement, la température de l'anneau de bride et celle des boulons à ce moment. En plus, des essais de laboratoires ont été effectués et des mesures sur site pour des géométries particulières d'assemblages ont été faites. Cela a permis de déterminer deux valeurs importantes qui sont la valeur du coefficient de transfert de chaleur du film extérieur, h_o (h_o = 23 W/(m^2.°C), et celle du coefficient de transfert de chaleur de contact, h_{cb} (h_{cb} = 3000 W/(m^2.°C).

Étape 2

Une fois le régime permanent des températures déterminé, leurs effets sur la déformation (dilatation thermique) de chaque composant doivent être calculés. Ceci constitue la deuxième étape de la méthodologie d'analyse. Ces effets peuvent être évalués en considérant trois composantes essentielles de déformation qui sont explicitées à la figure 3.2 et qui sont les suivantes :

- Effet #1 : Expansion axiale différentielle des composants due à un gradient radial de température.
- Effet #2 : Expansion radiale différentielle de la paroi du réservoir ou de la tuyauterie et du moyeu par rapport à l'anneau de la brides induite par un gradient de température axial et qui crée la rotation de l'anneau de la bride.
- Effet #3 : Expansion radiale différentielle du moyeu par rapport à l'anneau de la bride causée par un gradient radial de température dans cet anneau. Ce gradient décroissant restreint l'expansion radiale de la partie intérieure de cet anneau par rapport au moyeu et crée une force de cisaillement et un moment à l'interface bride-moyeu. Il en résulte une rotation de la bride qui a tendance à réduire la charge dans les boulons.

Les équations 2.9 (paroi réservoir ou tuyauterie) et 2.28 (anneau de bride) permettent d'évaluer l'expansion radiale de la bride. L'évaluation de cette expansion est un aspect important de la méthodologie d'analyse, surtout dans le cas de deux brides opérant à des températures différentes. Dans un tel cas, cette expansion peut détruire physiquement le joint d'étanchéité si la construction de ce dernier ne permet pas de supporter la force de cisaillement qui va s'y développer. L'équation 2.26 permet de déterminer l'expansion axiale de l'anneau de bride à sa partie interne et au niveau du cercle de boulonnage. L'équation 2.51 permet d'obtenir l'expansion des boulons. En utilisant l'équation 2.30, la pression équivalente, due à la plus grande expansion différentielle du réservoir ou de la tuyauterie, est déterminée. Ensuite, à partir des équations 3.1 à 3.13 et 3.18, l'analyse de l'interaction mécanique des composants peut être faite. Toutes ces équations et la méthodologie sous-jacente sont vérifiées par comparaison avec des résultats de analyse par éléments finis et des mesures faites sur site pour des géométries particulières d'assemblages.

Étape 3

La troisième étape de la méthodologie consiste à déterminer le régime transitoire de température. Pour tous les assemblages, la masse et par conséquent l'inertie thermique de l'anneau de bride est beaucoup plus grande que celle de la coque du réservoir ou de la tuyauterie. Il y a donc un écart subséquent entre l'accroissement de température de la coque ou tuyauterie et celui de l'anneau de bride et des boulons. Ceci à deux effets : au départ, la coque ou tuyauterie est à une température plus élevée et donc les effets #2 et #3 mentionnés précédemment sont prépondérants, ce qui veut dire qu'il y a une réduction subséquente de la charge dans les boulons au fur et à mesure que la température de la bride augmente. Cependant, la partie intérieure de l'anneau de bride devenant plus chaude pendant que les boulons restent plus froids, l'expansion axiale (effet #1) domine et la charge dans les boulons et celle sur le joint d'étanchéité vont augmenter. L'ensemble de ces effets sont visualisés à la figure 4.1 dans le cas d'une analyse par éléments finis faite sur le chauffage d'une bride d'un échangeur de chaleur de 37 pouces de diamètre nominal.

Le cycle de refroidissement dans un transitoire de température peut être négligé dans cette analyse, car il est moins important que le cycle de chauffage. Ceci est dû au fait que les effets différentiels entre coque ou tuyauterie et anneau de bride sont inversés et conduisent à l'augmentation de la force de boulonnage. De plus, les boulons refroidissant plus vite que les brides, il y a une tendance supplémentaire à accroître encore cette force. Il semble donc que, dans un assemblage à brides boulonnés, la tendance à la fuite se produira au chauffage plutôt qu'au refroidissement. Ceci est clairement montré à la figure 4.2 dans le cas de résultats d'une analyse par éléments finis faite sur le refroidissement d'une bride du même échangeur de chaleur de 37 pouces de diamètre nominal étudié précédemment à la figure 4.1. Dans cet exemple, il apparaît que le cycle de refroidissement a, d'une façon générale, un effet moindre que le cycle de chauffage.

La méthodologie d'analyse se concentre donc sur le cycle de chauffage d'un transitoire de température. Elle consiste à déterminer les transitoires de température de la coque ou tuyauterie et de l'anneau de bride. Un programme d'ordinateur a été écrit en langage C++ en utilisant la méthode des différences finies pour calculer l'évolution des températures de la coque (ou tuyauterie) et de l'anneau de bride en fonction du temps et en utilisant des variables non dimensionnelles bien sélectionnées. Cette façon de faire est détaillée à l'annexe B.

Étape 4

La quatrième étape consiste à déterminer les effets mécaniques d'un régime transitoire. La procédure utilisée est présentée dans les tableaux 5.2 et 5.3, dans les équations 4.3 et 5.1 ainsi qu'aux figures 4.3a à 4.5. Cette procédure permet le calcul de la réduction maximale de la charge de boulonnage (ou de contrainte dans les boulons). Elle permet aussi, par l'évaluation de la rotation de la bride, de déterminer la déflexion maximale de la bride due à cette rotation. La connaissance de cette déflexion est importante car une rotation excessive de la bride peut entraîner la détérioration du joint d'étanchéité et

conduire à l'apparition d'une fuite pouvant être grave. Pour certains types d'assemblages, il peut aussi être nécessaire d'apporter une attention particulière au maximum d'augmentation de la charge de boulonnage, au cas où le joint serait susceptible de s'endommager à cause d'une surcharge trop grande.

Validation expérimentale en laboratoire

Pour s'assurer de la justesse de la méthodologie d'analyse développée dans ce travail, un banc d'essais a été construit. Ce banc est constitué d'un réservoir à brides boulonnées de 24 pouces de diamètre nominal représenté à la figure 6.1. Les brides de ce réservoir ont été conçues selon le Code de l'ASME, Section VIII (1998b) avec une configuration similaire aux brides d'échangeurs de chaleur. Ce vaisseau est chauffé intérieurement par des éléments chauffants contrôlés électroniquement de telle façon que le taux de chauffage puisse être modifié et que la température du régime permanent puisse être maintenue constante. Ce réservoir est complètement instrumenté, y compris tous les 24 boulons, pour permettre la mesure des températures de tous les composants, de la charge dans tous les boulons et des déflexions des brides en deux points placés radialement.

Les tests ont consisté à appliquer des cycles de température à cet assemblage et à enregistrer les températures des brides, leur déflexion et la charge dans les boulons durant les cycles. Les mesures obtenues ont été comparées aux méthodes de calcul développées pour vérifier leur validité. Cette vérification a permis de confirmer la validité de la méthodologie d'analyse proposée pour étudier les effets de température sur l'intégrité des assemblages à brides boulonnées sous pression. Un total de dix tests ont été effectués et sont identifiés au tableau 6.1 avec leurs paramètres d'essais. Les résultats obtenus sont présentés graphiquement et les figures 6.14 à 6.17 montrent les températures des composants de l'assemblage en fonction de la charge moyenne dans les boulons. En général, en plus de montrer une excellente répétitivité, ces résultats expérimentaux indiquent une bonne concordance avec les prédictions de l'analyse théorique. La charge de boulonnage chute dramatiquement durant les premiers moments

du chauffage et doucement se met à augmenter au fur et à mesure que l'ensemble se stabilise en température. Au cours du refroidissement, l'inverse se produit, mais l'effet est moins important qu'au cours du chauffage. Ceci confirme que les effets du refroidissement peuvent être négligés comme il a été dit précédemment.

Une fois la température de l'assemblage stabilisée (300°C par exemple) après le chauffage à partir de la température ambiante, la contrainte dans les boulons a diminué en moyenne de 15 MPa (voir figures 6.13 à 6.17). Ce résultat se compare bien aux prédictions faites par la méthode analytique (13 MPa) ainsi qu'aux résultats de la méthode d'analyse par éléments finis (18 MPa). La différence entre les deux méthodes est due au fait que la méthode numérique donne une température des boulons plus haute que la méthode analytique, conduisant ainsi à une réduction plus grande de la contrainte dans les boulons.

Quelques résultats concernant les changements de température au cours du chauffage et de la variation de la contrainte dans les boulons sont présentés graphiquement aux figures 6.18 à 6.20. Dans la figure 6.19, des résultats d'analyse par éléments finis sont ajoutés aux mesures faites pendant le test 2b. La concordance est très bonne entre les résultats expérimentaux et les méthodes analytique et numérique, aussi bien dans la valeur de la réduction de la contrainte dans les boulons que dans la forme de cette variation au cours du temps. Les petites différences en température qui existent durant le régime transitoire ne semblent pas avoir d'effets significatifs sur la différence de contrainte dans les boulons.

La figure 6.20 présente toutes les variations de la contrainte dans les boulons en fonction des valeurs correspondantes obtenues par l'analyse par éléments finis. Comme on peut le voir, la concordance est excellente et les résultats expérimentaux apparaissent très répétitifs. Les seules différences notables se produisent quand on change les paramètres de test comme le taux de chauffage (test 3c), l'addition d'une plaque à tubes (test 4a) ou durant la première passe avec le joint d'étanchéité de type « a » (tests 1a et 4a). La

relaxation qui se produit au cours du premier cycle thermique apparaît à l'évidence comme étant le résultat d'un décalage dans la charge des boulons. Cependant, même si la perte de charge est plus grande, il apparaît quand même que la forme générale des courbes est la même.

La figure 6.21 compare les tests 2b et 2c réalisés respectivement à un taux de chauffage de 48°C/min et de 16°C/min. Comme prévu, la pente due à la variation de charge transitoire du boulonnage est plus petite pour le test 2c. Plus important cependant, est le peu de différence qu'il y a entre les deux tests, dans la grandeur de la variation de charge du boulonnage. En effet, les pertes maximales de la charge de boulonnage sont à toute fin pratique, identiques compte tenu de la précision des mesures, bien que les taux de chauffage soient dans un rapport de trois. Ce résultat est en accord avec l'analyse par éléments finis faite avec un coefficient de transfert de chaleur interne de 47 W/(m².°C)(voir la figure 6.22). La très petite différence dans la variation de la charge de boulonnage pour des taux de chauffage différents résulte probablement de la faible valeur du coefficient de transfert de chaleur interne. Cependant, par comparaison des résultats de l'analyse par éléments finis obtenus pour un coefficient de transfert de chaleur interne plus grand (400 W/(m^2.°C)) et pour des taux de chauffage différents (voir figure 6.23), on s'aperçoit qu'il y a peu de différence dans la variation de la charge de boulonnage résultante. Ceci indique que le taux de chauffage peut être négligé comme paramètre d'étude. De plus, en supposant un taux de chauffage infini (chauffage instantané), on obtient des valeurs conservatives pour la variation de la charge de boulonnage et on évite ainsi les problèmes associés à la connaissance des variations réelles de la température du fluide transporté ainsi qu'à la connaissance du coefficient de transfert de chaleur interne.

Conclusion

La méthode analytique développée permet à un utilisateur d'évaluer tous les aspects essentiels des effets de température sur le comportement mécanique d'un assemblage à brides boulonnées pressurisés. Cette méthode est cependant limitée aux assemblages symétriques qui sont uniformément chauffés et il y a donc un grand nombre d'assemblages qui n'entrent pas dans cette catégorie. Quand même, cette méthode fournit une base solide qui permettra d'étendre cette analyse à l'étude de ces autre types d'assemblages et de prendre en compte des effets comme :

- l'utilisation de brides non symétriques,
- le chauffage circonférentiel non uniforme,
- le fluage éventuel des composants de l'assemblage,
- la construction non normalisée d'assemblages à brides boulonnées.

Pour être introduite dans les procédures de conception courantes des assemblages à brides boulonnées, cette méthode d'analyse demande à être simplifiée. Des lignes directrices doivent être développées lorsque la conception de ces assemblages demande l'analyse des effets de température. Ceci permettra au concepteur de savoir quand une telle analyse supplémentaire est requise.

Malgré tout, la méthodologie développée permet au concepteur de tels assemblages (ou réservoirs) de prendre en compte les effets de température, s'il le souhaite. Il a été démontré que la méthode d'analyse peut être utilisée avec suffisamment de précision pour déterminer analytiquement les déformations et contraintes des différents composants de l'assemblage, aussi bien durant le régime permanent d'opération en température qu'au cours des régimes transitoires de chauffage ou refroidissement. On pense aussi qu'elle peut être étendue facilement à toutes les configurations d'assemblages (ou de réservoirs) existants.

En plus, la formulation analytique de cette méthodologie la rend plus puissante et plus universelle qu'une méthode numérique comme celle des éléments finis et aussi plus rapide, si correctement automatisée. Les facteurs d'opération comme les coefficients de transfert de chaleur réels qui ont été déterminés dans cette étude sont requis pour faire une analyse par éléments finis qui soit utile. Ces facteurs n'étaient pas disponibles dans la littérature technique avant que ce travail ne soit fait. L'étude expérimentale a aussi fourni une base réaliste avec laquelle une solide évaluation de cette méthodologie a été faite.

Enfin, il a été démontré que pour certaines configurations d'assemblages, les effets de température pouvaient être plus importants que les effets de mise en pression. La fréquence des fuites qui surviennent dans les échangeurs de chaleur confirme ce résultat. Il apparaît donc nécessaire de prendre en compte les effets de température dans les procédures de conception des assemblages à brides boulonnées.

La présente étude permet donc de faire un premier pas dans la mise en place de la prévention des effets néfastes qui affectent l'intégrité des assemblages sous pression et qui ont des répercussions sur les coûts d'opération des installations, sur la sécurité du personnel qui y travaille et sur l'environnement qui est bien souvent négligé.

TABLE OF CONTENTS

NOMENCLATURE

α = material thermal diffusivity (m^2/s)

α_p = pressure flange compliance factor, per Eqn. 4.3. [Wesstrom, 1951]

α_f, α_b, α_g = coefficients of thermal expansion for flange, bolt, gasket (m/m/°C)

δ_1, δ_2 = flange deflection at C - load state 1, 2 (m) [Wesstrom, 1951]

ξ = Variable relating temperature profile and radial location in cylinder [Figure 4.5]

ν_f, ν_s = Poisson's ratio of flange, shell material

μ = viscosity of internal fluid at calorific temperature (g/(m.s))

μ_w = viscosity of internal fluid at pipe wall temperature (g/(m.s))

θ'_f, θ'_h = rotation of the flange ring and hub due to differential thermal loading (radians).

θ_f = flange rotation (radians)

θ = non-dimensional temperature (T/T_i)

ϕ_b = bolt nominal diameter (m).

ϕ_n = equivalent nut diameter = across flats dimension of nut (m).

φ_n = the positive roots of Equation 3.13

ρ = material density (kg/m^3)

τ = Fourier Number (non-dimensional time, per Eqn. B.7)

A = flange external diameter (m) [ASME, 1998b]

A_f = internal fluid flow area of flange (m^2)

B = flange internal diameter (m) [ASME, 1998b]

C = bolt pitch circle diameter (m) [ASME, 1998b]

c = material specific heat (J/(kg.°C))

D = factor, defined by Eqn 4.10.

d = gap between the two flanges in the axial direction (m).

E_f = Young's modulus of flange material (MPa)

$f(z)$ = function of the temperature gradient on the inner radius in the z direction

G = gasket load reaction diameter (m) [ASME, 1998b]

g_1 = thickness of the hub (m) [ASME, 1998b]

H_{G2} = operational gasket load (N) [ASME, 1998b]

H_i, H_e = internal surface, external surface Biot Number

h_0 = hub length (m) [ASME, 1998b]

h_{cb} = heat contact transfer coefficient for the bolt/flange interface (W/(m².°C)).

h_D, h_G, h_T = flange load moment arms (m) [ASME, 1998b]

h_{fb} = approximated heat transfer coefficient from the flange to the bolt in the bolt hole region (W/(m².°C)).

h_i, h_{os} = heat film transfer coefficient for inside and outside surfaces (W/(m².°C)).

$h_o = h_{os}/k_f$ = modified film transfer coefficient for flange outside surface as defined in Carslaw et al(1959).

$h_e = h_{os}$ for shell region and modified h_{os} [Equation 5.1] for flange region.

$I_o()$, $I_1()$ = Modified Bessel Functions of the 1st kind, order 0 and 1 respectively

K = A/B (ASME, 1998b)

$K_o()$, $K_1()$ = modified Bessel Functions of the 2nd kind, order 0 and 1 respectively

k = thermal conductivity of the internal fluid (W/(m.°C))

k_f= thermal conductivity of the flange material (W/(m.°C))

k_s, k_i = thermal conductivities for the vessel shell and insulation (if applicable) (W/(m.°C)).

L_s = effective thermal length of the shell. (m)

l_0, l_1, l_2 = effective bolt length - unloaded, load state 1, 2 (m) [Wesstrom, 1951]

l_e = length of exposed bolt above nut (m).

l_n = thickness of nut (m).

M = edge moment per unit of circumference at flange/shell intersection (N.m/m)

M_1, M_2 = flange moment - load state 1, 2 (N.m) [Wesstrom, 1951]

n = number of roots used for Bessel equation calculations

P = internal pressure (MPa)

P_r = Prandtl number for the internal fluid flow.

Q = overall joint compliance (m/N) [Wesstrom, 1951]

Q_1^{in} = heat flow across the nut/flange contact surface (W)

Q_1^{out} = heat flow from the exposed section of the bolt (W)

Q_2^{in} = heat flow from the flange to bolt in the bolt hole area (W)

Q_2^{out} = heat flow from the nut surface (W)

Q_n = heat flow across R_n (W)

q = heat flow per unit length (W/m)

q_f = flange compliance (incl. ring and hub) (m/N) [Wesstrom, 1951]

q_g, q_b = gasket, bolt compliances (m/N) [Wesstrom, 1951]

q_r = flange compliance for pressure effects (m/N) [Wesstrom, 1951]

R = non-dimensional radius (r/r_i)

R_1 = internal wall film resistance of the shell wall. (°C/W)

R_2 = internal wall film resistance of the flange thickness. (°C/W)

R_3 =sum of internal (through thickness) and external film resistance of the shell.(°C/W)

R_4 = sum of internal (through thickness) and external film resistance of the flange.(°C/W)

R_5 = internal resistance between the shell and the flange. (m.°C/W)

R_{af} = resistance of the fluid/flange wall interface at the internal diameter (m.°C/W)

R_{as} = resistance of the fluid/shell wall interface at the internal diameter (m.°C/W)

R_{bf} = internal resistance of the flange inner section across the thickness (m.°C/W)

R_{bs} = internal resistance of the shell wall across the thickness (m.°C/W)

R_{cf} = resistance of the flange/air interface over the outer section (m.°C/W)

R_{cs} = resistance of the shell insulation (m.°C/W)

R_{ds} = resistance of the shell/air interface at the external diameter (m.°C/W)

R_e = Reynolds number for internal fluid flow.

R_{sf} = resistance of the shell to flange heat flow (m.°C/W)

r_e = outer radius of the hub at the intersection with the flange (m).

r_{ext} = ($r_i + t_s$) for shell, r_e for flange ring inner section and r_f for flange outer section (m)

r_f = outer radius of the flange (m).

r_h = radius of the middle of the equivalent hub [$(B + t_h)/2$] (m)

r_i = inner radius of vessel/pipe (m)

r_{int} = r_i for the flange ring inner section and r_e for the outer section (m)

r_{sm} = radius of the middle of the vessel/pipe wall (m)

S = radial shear force per unit of circumference at flange/shell intersection (N/m)

T_b = bolt temperature (°C)

T_{cn} = thermocouple number n.

T_e = flange temperature at hub outer radius (°C).

$T_f(r)$, $T_s(r)$ = flange, shell temperature at radius r (°C)

T_{fi} = flange wall inside surface temperature (°C).

T_i, T_o = inside fluid and outside (ambient) fluid temperatures (°C).

T_{si}, T_{so} = shell wall inside and outside surface temperatures (°C).

$t_e = (2t_f - d)$; $t_f < t_e < 2t_f$ = the equivalent thickness of the flange (m)

t_f = thickness of the flange (m)

t_g = gasket thickness (m)

t_h = equivalent hub thickness (m), per Eqn. 4.6.

t_s, t_i = thickness of the vessel shell and insulation (if applicable) (m).

t_{ts} = thickness of the tubesheet (if applicable) (m).

u'_f, u'_h = radial deflection of the flange ring, hub due to differential thermal loading (m).

$u_s(r)$, $u_f(r)$, $u_h(r)$ = radial expansion of the shell, flange, hub at radius (r) (m).

v_0, v_1, v_2 = gasket thick. in unloaded, load state 1 and load state 2 (m) [Wesstrom, 1951]

v_b = axial expansion of the bolt (m).

v_f = average axial expansion of the flange and half the gasket thickness (m).

v_f^h = flange axial deflection due thermal differential loading (m).

v_g = axial expansion of the gasket (m).

$v_s(r)$, $v_f(r)$ = axial expansion of the shell, flange at radius (r) (m).

W_1, W_2 = bolt load – load state 1, 2 (N) [Wesstrom, 1951]

w = fluid mass flowrate (g/s)

Z = non dimensional axial distance (z/r_i)

z = axial distance along cylinder (m)

LIST OF ABBREVIATIONS

ASME = American Society of Mechanical Engineers

ASTM = American Society for Testing and Materials

FEA = Finite Element Analysis

HOBT = Hot Blow Out Test

NPS = Nominal Pipe Size

PVRC = Pressure Vessel Research Council

RFWN = Raised Face, Welding Neck Flange

TTRL = Tightness Testing and Research Laboratory

LIST OF FIGURES

LIST OF TABLES

LIST OF APPENDICES

INTRODUCTION

0.1 Introduction to the problem

Bolted flange joints are used in the manufacture of pressure vessels and piping to provide ease of assembly or internal equipment access. However, these joints are quite often the weak link in the pressure system and the failure of a pressure containing component is most likely to occur at the bolted flange joint location. This type of failure can have a variety of consequences, ranging from a minor inconvenience, requiring tightening of the joint, to major loss of equipment and life in a subsequent fire or explosion.

High temperature operation and transient thermal shock are well recognised causes of such pressure vessel joint leakage (Payne, J.R. (1985)). However, the present flange design methods do not address the effects of temperature on the integrity of the bolted joint, other than the flange material properties. Due to the high temperature of the fluid contained by the joint there is an increased hazard to personnel associate with any leakage from this type of joint. Additionally, the likelihood of fire and/or subsequent plant or unit shutdown means that the relative cost due to inadequate design in this area can be extremely high.

In petroleum refineries around the world there are a variety of techniques currently employed in dealing with joint failures. Most of them are, however, only instigated after the advent of leakage and are expensive to employ. Listed following are some examples of the estimated cost to refineries caused by such joint failures. In addition, Figures 0.1

and 0.2 illustrate the type of costly solution that is often employed in cases of flange leakage where it is not possible to seal the joint by re-tightening.

The below figures are approximate and were obtained from a survey of petroleum refinery operations and maintenance personnel:

- For one refinery, an average of more than 8 instances of severe leakage per year occurred in the 8 year period, 1992-2000.
- The cost of lost production due to severe leakage, resulting in crude plant shutdown, is in excess of US$250,000 per day of plant shutdown
- The annual cost per refinery for on-line temporary leak sealing or steam-lancing, is often in excess of US$350,000 / year
- The largest single incident cost directly attributable to a leaking joint in one refinery was US$7,000,000. This included equipment replacement costs and lost production costs due to a resulting plant fire.

Figure 0.1 – Steam Leak on Reboiler

Figure 0.2 – Temporary Clamp (Costing in excess of US$50,000)

A sound design and analysis method would enable the operating companies to eliminate these costs, better protect the environment, and eliminate the possibility of loss of life due to joint leakage. It would appear therefore that there is adequate reason for the inclusion of an additional design step in the pressure vessel design codes to fully address the effects of temperature on the flange joint integrity.

The objective of this project was to develop a theoretical analysis methodology to determine the effects of temperature on flange joints. This methodology may then be simplified, in order to create a series of guidelines and formulae for analysing the effects of temperature to be used in conjunction with code flange design procedures. Using analytical equations, the developed methodology addresses the gasket, bolt and flange deflections and stresses during transient thermal start-up and/or subsequent thermal cycling of the joint. This approach enables the methodology to be easily incorporated into the existing, commonly used, analytical methods of flange design. For simplification of the method, the developed equations were limited to steady state (non-transient) analysis and were based on the service conditions at the critical (worst-case) time during thermal transients. The final design philosophy was verified by comparison to Finite Element Analysis (FEA), site data and experimental laboratory testing.

0.2 Causes of joint failure

Failure of pressure vessel joints due to temperature transients may be defined solely as failure due to joint leakage. In general, for the majority of flange joints, it is impractical to consider actual bolt or flange mechanical failure. This is due to two reasons:

1. Deformation (rotation) of the sealing faces of the flange, which occurs with deformation of the flange or bolt components during yielding, will cause the joint to leak (and therefore release the driving pressure force) prior to the actual mechanical failure point of those components.

2. Secondly, thermal loading is a secondary loading. That is to say, the driving force for material yielding is diminished as yielding occurs. It is therefore not possible for temperature alone to drive flange or bolt mechanical failure.

Hence, it is acceptable, when analysing the effects of temperature on a flange designed in accordance with design codes in a ductile material, to focus on gasket sealing failure as the sole mode of joint failure. There are two principle causes of gasket sealing failure, which can be further separated into subcategories of failure:

1. Loss of gasket load
   1.1. Loss of load due to relaxation/creep of the gasket at temperature
   1.2. Loss of load due to flange deflection caused by joint component thermal interaction
   1.3. Loss of load due to poor load distribution caused by increased flange rotation
2. Physical destruction of the gasket
   2.1. Gasket degradation with time (e.g: oxidation of graphite)
   2.2. Radial shearing of gasket due to radial movement of flanges caused by differences in mating flange temperatures
   2.3. Crushing of gasket due to increased load caused by joint component thermal interaction

From the above list, items 1.1 and 2.1 are primarily properties of the gasket used in the joint. This study focused on the mechanical interaction of the flange and as such did not specifically examine these two causes of failure. However, some aspects of the study, such as determining the actual temperature distribution in the joint, are necessary for assessing the likelihood of these two modes of failure occurring.

In order to assess the likelihood of joint failure due to temperature, one must examine the joint during two operational phases:

1. Steady State Operation, where a gradient exists between the temperature of the contained fluid and the external surrounds.
2. Dynamic Operation, during plant start-up, shut-down or operational fluctuations, where the contained fluid temperature varies sharply, causing dynamic thermal gradients in the flange components.

In addition, the following variables must be considered in the thermal analysis of the joint behaviour:

- Gasket stiffness and thickness
- Material properties (gasket, flange and bolts)
- Flange stiffness
- Bolt stiffness
- Internal fluid temperature and heat transfer properties
- External temperature (including insulation or cooling)
- Internal pressure
- Initial bolt stresses
- Flange dimensions & configuration

From the consideration of these variables the parameters which determine the response of the joint (and therefore the likelihood of joint leakage) to temperature can be determined. These parameters may be summarised as below:

- Joint component temperatures
- Gasket stresses during all operational phases
- Flange deflections during all operational phases

The developed analysis methodology enables the determination of the joint failure parameters. These parameters are listed following, with the failure criterion for each parameter listed following it in brackets:

- Change in bolt stress (max/min)

{calculated value exceeds material allowable at modified design temperature}

- Change in gasket stress and distribution (max/min)
  {calculated value exceeds maximum allowable stress for gasket or is less than the required sealing stress}
- Change in bolt temperature (max)
  {temperature exceeds maximum for bolt material vs. creep}
- Change in gasket temperature (max)
  {value exceeds guidelines for gasket type}
- Differential expansion of flanges in radial direction (max)
  {calculated value exceeds a percentage of the gasket width for the gasket type}
- Flange rotation and stresses (max)
  {calculated value exceeds allowable stresses at the design temperature}

The analysis of the effects of temperature on flanged joints is complicated by certain non-linearities in the analysis. These include:

- Thermal transients
- Gasket behaviour
- Component material properties vs. temperature
- Component material creep and relaxation

However, by careful consideration and simplification of the non-linearities a conservative methodology was developed, which is essentially a steady-state analysis conducted at certain critical points in the thermal cycle of the flanged joint.

0.3 Objectives and analysis description

Due to the non-linearities involved and the interaction between the joint components, a comprehensive method of analysis to determine the effects of temperature on the sealing of flange joints would be extremely complex. In order that the analysis be as simple as possible, each non-linearity and interaction was analysed to determine if it could be

neglected or must be incorporated into the analytical approach. The simplification process, however, required that the initial analytical approach was comprehensive and included all variables. It was then proven, by comparison with the comprehensive analysis, that any simplifications made were acceptable.

To ensure that the comprehensive analysis was approached in an orderly manner, it was separated into four consecutive stages of development. Each stage encompassed a single stand-alone analytical process. This enabled a step by step verification of each stage of the analysis upon its completion.

The four stages were as follows:

1. Determination of the steady state temperature distribution and subsequent joint component deflections (thermal expansions).
2. Determination of the joint component mechanical interaction due to the steady state effects.
3. Determination of the dynamic (transient) temperature distribution due to an instantaneous internal fluid heat load.
4. Determination of the joint component mechanical interaction due to the dynamic effects.

Each of these stages incorporated four steps in the analysis process, as listed below:

a) Determine the comprehensive analytical equations and associated analytical theory.
b) Verify these equations by comparison with several analysis cases using Finite Element Analysis.
c) Further verify the theory and equations by comparison with laboratory experimentation.
d) Confirm the overall applicability of theory by comparison with on-site measurement of heat exchanger flanges.

The components of a basic flange joint are drawn in Figure 0.3. In the analysis of flange joints several simplifying assumptions are commonly made. For simplicity of analysis the joint is assumed to be symmetric about the central axis (axisymmetric) and it is also generally assumed that the mating flanges are identical and therefore symmetry may also be assumed in the flange pair direction.

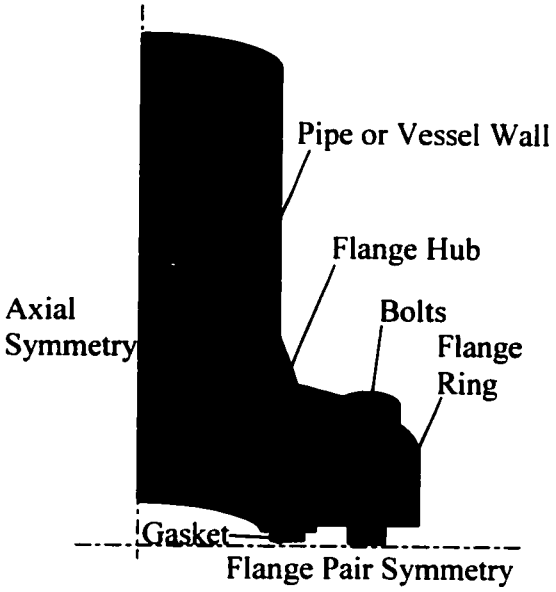

Figure 0.3 – Components of a flange joint

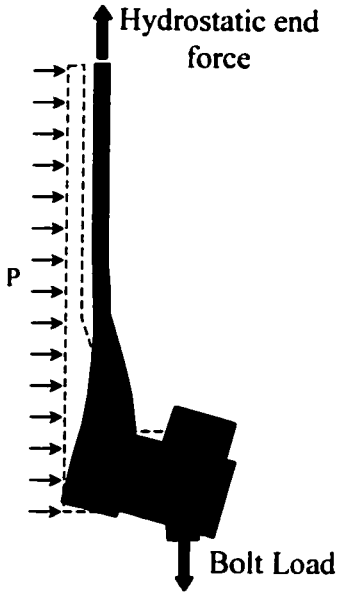

Figure 0.4 – Deformation due to initial bolting load and internal pressure load

The commonly used methods for the mechanical analysis of the effect of bolting and pressure forces (refer to Waters, et. al., 1927 and Waters, et. al., 1937) demonstrate that there is an associated flange rotation (inward cupping of the flanges towards each other) due to the eccentricity of the bolt loading by comparison to the gasket reaction point. There are a series of elastic interaction equations that may be used to determine, given the elasticity of the components, the deformations and subsequent component stresses. This is based on the above assumptions of symmetry and the assumption that the flange is a ring coupled to an infinite shell.

These equations indicate that upon application of the bolt load, the flange is rotated as the bolt load is transferred to the gasket. However, with the application of a pressure load there are two effects that occur. A hydrostatic end force acts along the vessel wall, which decreases the gasket load and induces further flange rotation. Additionally there is a "hoop effect", where the internal pressure causes radial expansion of the vessel wall. This radial expansion is restrained by the flange ring, causing a transfer of moment onto the flange ring, which induces further flange rotation (refer to Figure 0.4). Thus, depending on the relative elasticities of the three components, the bolt load may either increase or decrease with application of internal pressure.

The effects of temperature loading on the joint can be treated similarly to pressure loading. The flange acts essentially as a cooling fin to the vessel shell, which leads to a temperature gradient in the radial and axial directions (refer to Figure 0.5). This causes differential axial thermal expansion of the flange components. Since the bolt will be at a lower temperature than the flange, the differential expansion will result in an increase in bolt and gasket load. However, offsetting this is an effect similar to the pressure hoop effect. Since the shell will be operating at a higher temperature than the flange ring there will be differential expansion in the radial direction between these two components, causing a transfer of moment to the flange ring, flange rotation and subsequent reduction in bolt and gasket load (refer to Figure 0.6).

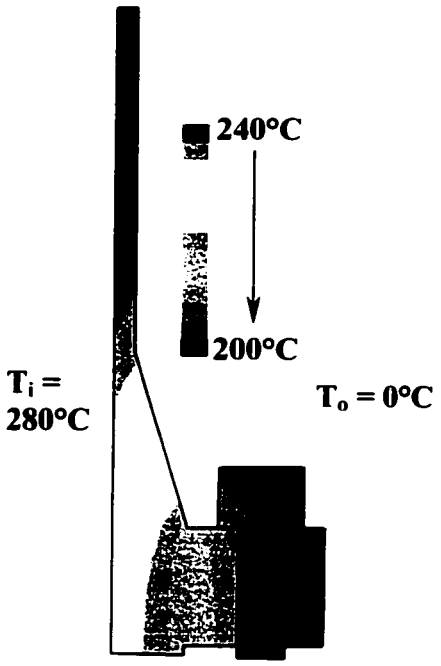

Figure 0.5 – Joint temperature distribution

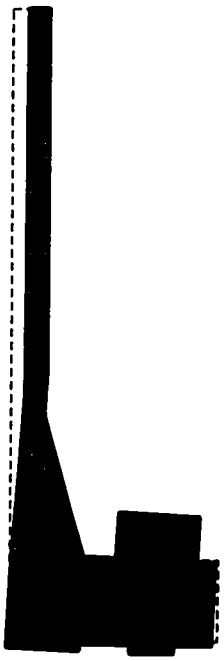

Figure 0.6 – Deformation due to temperature loading

During a thermal transient in the contained fluid there will be a dynamic effect, where the vessel shell heats quicker than the flange ring and bolts. This will lead to an increase in both the previously mentioned effects and, depending on the joint geometry, could lead to either a reduction or increase in gasket load. It is these mechanical effects of temperature that will be determined in the subsequently developed analysis method.

In order to aid the simplification of the analysis, it will be further restricted to encompass only the following sizes of flange joint:

0.25m < Flange internal diameter < 2m

0.025 < Ratio of flange thickness/internal diameter < 0.5

1.05 < Ratio of flange outside diameter/internal diameter < 3.0

0.05 < Ratio of flange thickness/outside diameter

The flange diameter limitation is made from experience, which suggests that flanges of internal diameter less than 0.25m will not have a leakage problem associated with temperature. Additionally, the limitations on the other parameters, such as the flange thickness, are established from an analysis of existing standard flange and heat exchanger flange dimensions. These dimensional limitations should encompass all heat exchanger flanges and most larger piping flanges.

CHAPTER 1

LITERATURE RESEARCH SUMMARY

1.1 Introduction

The problem of leakage of bolted flanged joints due to thermal transients is well documented. Payne (1985) performed the most comprehensive survey of the causes of flanged joint failure. The paper includes the identification of the most common causes of leakage and the variation in effect of these causes by comparison to joint size, rating and service. The survey clearly indicates thermal transients on the bolted joint as one of the major sources of failure. In addition Hsu, et. al.(1990), Hsu, et.al. (1994), Winter, et. al. (1996) and Hsu, et. al. (1992) present the American Pressure Vessel Research Council (PVRC) research programs during the past 10 years and include a brief explanation for the necessity behind this research work. The PVRC has been actively addressing the problem of thermal effects on pressure vessel flange joints in various studies during this time.

However, to date, there has not been a general theoretical analysis of this problem performed. There have been several papers on the effects of thermal transients on the sealing of specific joints, under specific operational constraints, but no general design philosophies presented. Although there have been some simplified attempts to address the effects of thermal gradients on the joint interaction there has been no real effort put into the determination of the actual thermal gradients which exist in the joint during operation. Hence it is not possible, without reverting to the use of finite element analysis,

for the present day flanged joint designer to address the possible detrimental effects of thermal transients on the joint.

The following literature summary outlines the articles pertinent to this study written in the period 1935-2001. They are subdivided into the subject areas of flange thermal interaction, flanged joint mechanical interaction, heat transfer and thermal stress analysis, general gasket behaviour and finite element analysis of flanged joints. A brief summary of the relevance of each paper to this research is included.

1.2 Flange thermal interaction

The papers, which address the subject of this study most closely, are Sawa, et. al. (1995a) and Sawa, et. al. (1996a). These papers utilise finite cylinder heat transfer theory to examine the distribution of temperature in an insulated, 3inch class 150 ASME B16.5 flange due to various thermal gradients. However, the theory is not fully detailed and it is therefore difficult to confirm the accuracy of the equations presented or utilise the detailed methodology. In addition, the relevance of the presented theory has not been verified for large diameter flanges or flanges without insulation. A third paper by Sawa, et. al. (1998) continues with approach of previous papers, but includes an examination of the effects of using a spiral wound gasket in the 3" experimental rig.

Perhaps the most generalised treatment of the problem is given by Dudley (1961), who outlines an analytic approach to solving the stresses and deflections of flanges due to a temperature difference between the flange ring and vessel shell. However, it is simplistically assumed that the thermal distribution in the shell and flange ring are uniform and the actual thermal distribution or the effects this would have on the analysis assumptions are not examined.

Kerkhof (1951) presents an approach to the treatment of static thermal loading in flange design, based on bolt load reduction due solely to flange material property changes

(creep). Some experimental results are given to confirm the theory, however once again the actual thermal gradients are not examined.

The paper by Singh, et. al. (1979b) presents an analytic methodology to assess the radial growth of the flanges and tubesheet in a heat exchanger joint. It simplistically treats the flanges as infinite cylinders with no heat loss from the outer surface and no assessment of the axial expansion or analysis of the joint component interaction is presented.

The remaining papers in this section tend to focus on the solution of specific thermal gradient problems, most commonly employing finite element analysis to establish the joint temperature distribution. Sawa, et. al. (1993) utilises Finite Element Analysis (FEA) and experimental analysis to examine the distribution of temperature and the effects of temperature on a 65mm nominal bore diameter aluminium flange due to various thermal gradients. Sawa, et. al. (1996b) continues with the approach of the previous paper, utilising a flat cover to replace one of the matching flange pairs.

The paper by Nau, et. al. (1985a) utilises FEA to examine temperature gradients, specifically the lag of the bolt temperature behind the flange temperature, in several standard B16.5 flanges during a transient thermal gradient. They appear, however, to neglect heat transfer to the atmosphere from the exterior of the flange (modelling a perfectly insulated flange).

Martens, et. al. (1994) outline an analysis, using finite element analysis, of a problematic heat exchanger joint configuration with failure directly attributable to thermal gradients. The calculated thermal gradients, subsequent stresses and a final solution of the use of a fully welded bellows type gasket are all presented. Raju (1980) also presents a simplistic axisymmetric FEA approach to the general solution of thermal and mechanical loading on flange joints.

Interesting research on heat transfer between flanges has been performed by the Russian researchers Kosykh, et. al. (1989) and Krylov, et. al. (1987). These papers present thermal transients on pipeline valve bonnet flanges and include analysis of the effect of contact heat transfer between the two flanges. Krylov, et. al. (1986) also outlines the effects of contact stresses and stress uniformity on the flow of heat in sectional connections of power plant pipeline valves.

Perhaps one of the most comprehensive studies of a problematic joint was performed by Bickford, et. al. (1989a). This paper summarises the findings of an ASME investigation into a problematic reboiler flange joint. It includes sections on the background of the joint, joint failure history, presentation of a detailed FEA model and results, comparison with an analytic solution and a detailed discussion of the results. Three other papers from this study are Winter (1988), Bickford, et. al. (1989b) and Chao (1998), which are earlier papers presenting in more detail the bolting procedures used and the FEA study completed.

Another excellent paper, which is also somewhat more general, is that of Winter, et. al. (1996). It looks at the effects of thermal transients on a series of standard joint configurations, specifically: gasket temperature, effect of thermal transfer coefficients and weldneck vs. lap joint flange configurations. The paper is written from a practical perspective and presents FEA and field data for the various joint configurations.

Similar work, from a slightly more theoretical perspective, has been performed by Scliffet (1993) who examines the effects of thermal transients on an 80mm cl.1500 and a 150mm cl.600 standard ANSI B16.5 flange joint. Experimental results for the flange temperature distribution and flange loading are presented and confirmed using FEA. A second paper by Scliffet (1994) presents the results of thermal testing on an 80mm NB flanges and specifically examines the bolt temperature lag effects and confirms the experimental results with FEA results.

The nuclear power industry has produced some excellent work on a specific problematic configuration of flanged joint that occurs commonly on the head of large diameter high temperature vessels used in the reactors. Spaas, et. al. (1977) used FEA and experimental analysis to examine a 702mm internal diameter, high pressure, non-standard flange (nuclear PWR vessel head). The paper contains a comprehensive collection of data on the transient thermal gradients and subsequent effects on the bolt loading, flange rotation and stresses. Bakker, et. al. (1977) outline the philosophy and equations used in this previous paper, including the FEA code, thermal gradients, flange rotation and bolt stresses.

Andresso (1984) examines the effects of thermal and pressure gradients on a 450NB manway flange using FEA. The relative component loadings and deflections with respect to time (gradient position) are presented. Andreosso, et. al. (1985) utilises FEA and photo-elastic analysis to estimate the effect of a thermal gradient on the flange and cover of a 450mm NB manway cover. Finally Qu, et. al. (1989) present experimental results of transient thermal gradients on a 1000mm I.D. high pressure non-standard flange (nuclear PWR vessel head), including thermal gradients, bolt loading and flange distortion.

There were also several studies into the effects of thermal gradients completed prior to the widespread use of finite element analysis. These studies generally utilised direct measurement of temperature gradients and resulting bolt and flange stresses. One such paper is Carlson, et. al. (1951), which outlines thermal testing of three different configurations of 225mm I.D. flanges. Thermal gradients during thermal transients (increasing and decreasing) are presented. Similar work was performed by the British Flange Committee, which examined the effects of thermal gradients on stresses and joint creep. Johnson, et. al. (1954), Tapsell (1939) and Gough (1936) detail this high temperature testing of flanges in the creep range. Flange thermal gradients and loading are presented for insulated flange joints of several sizes. The papers also examine the effects of temperature on gaskets and the variation of loading due to different bolt

configurations. Further analysis of this work is presented in Bailey (1937) and Bernard (1963), who summarise the findings of the previous papers and present further analytic treatment of the results.

Two theoretical papers on the creep effects of temperature are Marine (1938) and Waters (1938). These papers give an analytic overview of the effects of high temperature on flange joints in terms of component creep. However, no analysis of actual thermal gradients is presented. A paper by Price (1996) presents a simplified overview of thermal effects on flanges, although no experimental or theoretical analysis is presented.

1.3 Flange mechanical interaction

There has been much work performed over the years on the subject of the mechanical interaction of the flange joint. A brief summary of the work performed is listed below, however, a comparison of the various studies and methodologies will not be presented. The reader should refer to existing sources of this information such as Blach (1981), which presents an excellent review of the history of the current design equations and of available literature on all aspects of flange design. Additionally BS (1969), provides a critical review of the ASME VIII and Taylor Forge design methods and also outlines deficiencies in flange design standards (most of theses deficiencies are still current today). Rose (1970) includes a section on the various methodologies currently used for flange design and also an extension of the work by Murray, et. al.(1961) on flange design is also presented.

Flange design is not an exact art, there are a multitude of variables which must be considered in order to ensure a sound design. Schneider, et. al. (1982), Waters, et. al. (1934) and Labrow (1947) all provide a general discussions on some pertinent points regarding flange design which should be considered when trying to establish design philosophies.

The initial work on the mechanical behaviour of the flanged joint and the development of this theory into the present ASME VIII design methodology is covered in various papers such as Waters, et. al. (1927), who performed the initial work on design of flanges using flat plate theory, including extensive experimental testing on the deflection and stresses of flanges. Holmberg, et. al. (1932) developed the theory further by eliminating some of the governing loading assumptions made by Waters, et. al (1927). Jasper, et. al. (1936) present an outline on the design of flanged joints based on the analysis of Holmberg, et. al (1932). Waters, et. al. (1937) expand on the original analysis of flanged joints using flat plate theory. It is this work that was later modified to form the basis of the ASME Code. Rossheim, et. al. (1938) present experimental testing of heat exchanger flanges for bolt load and flange rotation due to internal pressure, with comparison to the Waters et. al. (1937) theory.

Additional work on the refinement of the early philosophies was completed in the 1950's and 1960's. Roberts (1950) examines the effects of bolt spacing and gasket creep on gasket load and joint sealing. Wesstrom, et. al. (1951) extends the author's original work on flange design, using flat plate theory to include joint component interaction due to internal pressure. Horvay, et. al. (1954) outlines a treatment of flange analysis where the shell is not perpendicular to the flange, using flat plate theory. Lake, et. al. (1957) modifies the previous approach to flange design by reasoning that it is acceptable to allow minor plastic deformations of the flange hub. Donald, et. al. (1959) conducted extensive experimental testing on flange interaction in comparison with the Waters, et. al (1951) theory and Donald, et. al. (1959) experimentally examines the interaction of joint components and flange sealing characteristics. Murray, et. al. (1961) used computer analysis to eliminate many of the approximations previously made in flange design and confirmed their approach experimentally for the design of large diameter flanges. In their analysis the flange ring is treated as a ring, rather than a flat plate. Van Campen, et. al. (1960) treats the flange hub as a ring using detailed equations and presents a comparison between this approach and that of Murray, et. al. (1961).

Since the 1960's work has been performed sporadically on further understanding the complexities of joint interaction. Boissenot, et. al. (1977) examined the suitability of flange design using an elastoplastic design philosophy. Experimental and FEA results for a 400NB flange are presented. Bouzid (1994) summarises the various approaches to joint design and, by using a combination of the various exact methods, including joint interaction, develops a more accurate solution to flange design. Jaep (1951), Singh, et. al.(1983), Thomson (1989), Brown (1993) and Bouzid, et. al. (1994) all extend the approach of Waters, et. al (1951) to include such factors as bolt bending, joint interaction, gasket properties, joint relaxation and flange rotation on the ability of the joint to seal. Experimental work and FEA to confirm the analysis is also presented in these papers.

Cascales, et. al.(1987) presents a simplification of the analysis outlined by Murray, et. al (1961). Nagy (1994) further develops the work done by Murray et. al. (1961), presenting a more precise method for the calculation of the modification of bolt loads due to internal pressure. Fessler, et. al. (1972) outlines a series of deflection and stress tests on 100NB flanges of various materials.

Some new design philosophies were established by Sawa, et. al. (1993) who approached the analysis of flanges as a hollow cylinder, using axisymmetric elastic analysis. The author also includes the localised deflection of the flange and nut in modifying the bolt loads. Sawa, et. al. (1991), Sawa, et. al. (1991), Morohoshi, et. al. (1989), Sawa, et. al. (1986), Sawa, et. al.(1985a), Sawa, et. al. (1985b), Sawa, et. al. (1979), Varga, et. al. (1995) and Sawa, et. al. (1985c) all follow a similar approach to the previous paper, except that a flange hub, blind flange, bending moment or joint component interaction is included in the analysis. Experimental verification of the analysis is presented. Sawa, et. al. (1983) examines the analysis of flanges by equating the flange to a beam on an elastic foundation, with experimental results.

The inclusion of a tubesheet in the joint is a common complication in the design of high temperature joints. There are several papers written solely on the design aspects of this complexity. Osweiller (1996) details the differences between the current methods of heat exchanger tubesheet design. Kenny, et. al. (1963) examines the deflection of flanges, specifically when used on a tubesheet joint. Several general papers on tubesheet design are Miller (1953), Duncan (1956), Yu (1956), Gardner (1952), Horvay (1952), Downey, et. al. (1964), Duncan, et. al. (1963) and Singh (1979a). All present general equations and methodologies for the design of heat exchanger tubesheets.

The localised deformation of the bolt is generally not included in the modern design of flanged joints. It is, however, a variable which may have a large effect on the overall joint interaction. Thompson, et. al. (1976), Sawa, et. al. (1979), Motosh (1976), Lehnhoffet. al. (1996), Inoue, et. al. (1986) and Grosse, et. al. (1990) all examine the effects of localised deformation under the bolt head during the loading of a bolted joint, but not necessarily for a flanged joint containing a gasket.

A final factor, which will have an effect on joint performance, is that of an external bending moment acting across the joint. Blick (1950), Blach, et. al. (1992), Sawa, T., et. al. (1995), Laviolette, et. al. (1996), Blach, et. al. (1992), Tschiersch, et. al. (1996), Koves (1996) and Bouzid, et. al. (1998) all examine the effects of bending moments on the sealing and stresses in bolted joints.

1.4 Heat transfer and thermal stress analysis

Establishing the exact nature of the thermal gradients in a joint is considered of critical importance to creating a sound design philosophy on this subject. Carslaw, et. al. (1959) examines the theoretical solution of thermal gradients for a variety of heat transfer cases. Additionally the treatment of other aspects, such as the overall heat flow and effects of flange separation on the thermal profiles are covered in Kern, et. al. (1972), which presents a discussion and analysis of extended surfaces (fins) and their effect on heat transfer in a body.

Upon establishment of the thermal gradients, these must then be related to flange deformations and stresses. Boley, et. al.(1960) and Parkus (1976) examine the stresses, produced by a given thermal gradient, in bodies of various configurations, including cylinders, disks and non-axisymmetric thermal gradients. Additionally, Goldberg (1953) outlines an analytic solution to the stresses in a circular plate due to thermal gradients.

The analysis of thermal gradients under transient conditions is a somewhat more difficult subject, requiring simplification of the flange to a cylindrical representation. There has been much work done, for a variety of applications, on thermal transients in cylinders and flat plates. Some of the more recognised of these works are listed following. Dahl (1924) presents generalised solutions for heat conductance in hollow cylinders with transient thermal gradients. Kent (1932) and Heisler (1953) outline general solutions for transient thermal stresses in slabs and cylindrical pressure vessels, including analytical treatment and calculated charts.

Kent (1931) follows a similar approach to the previous two papers, specifically for thin cylinders including the effects of end restraints. Newman (1936) and Heisler (1947) examine the theory and present charts for the solution of transient heat conduction in slabs and solid cylinders. Olson (1942) presents a numerical chart approach to the solution of thermal gradients in solid cylinders and slabs during thermal transients.

Goodier (1957) presents an analysis for the stresses in a hollow cylinder due to thermal gradients, including non-axisymmetric thermal gradients. MacNeil (1971) presents a chart approach to the solution of thermal transient stresses in pipes. Bochkov, et. al. (1990) outlines a method of analysis for thermal distribution and stresses in a solid cylinder. Ladopoulos, et. al. (1994) presents a numerical method of the analysis for three dimensional thermoelastic stresses.

Whilst there has been little work performed on thermal gradients in bolted joints of the type used on pressure vessel equipment, there has been considerable work performed on bolted joints, with or without gaskets, when used in such areas as electrical components or satellite attachments. Some of this technology is transferable to pressure vessel joints. Lee, et. al. (1993), Lee, et. al. (1996), Mittlebach, et. al. (1992), Mantelli, et. al. (1998), Fletcher, et. al. (1989), Mittelbach, et. al. (1994), Bradley, et. al. (1971) and Itoh, et. al. (1992) all examine the flow of heat through single bolt plate joints. The analysis presented relates the contact pressure to the rate of heat flow. Experimental confirmation of the theory used is presented for small diameter bolts. Kumano, et. al. (1993), Kumano, et. al. (1995) and Kumano, et. al. (1994) all experimentally and theoretically examine the thermal heat flow and its effect on bolt stresses in a single bolt bolted joint. Mantelli, (1998) examines the thermal contact resistance of satellite bolted flanged joints. Analytic solutions and experimental results are presented.

Additionally the examination of the effects of thermal transients on simple configurations, such as infinite cylinders, has been widely researched. Some aspects of this research may be applicable to the simplified model of a bolted joint during thermal transients. Hence a selection of papers on such topics are presented following. Chen (1989) presents a numerical analysis for the thermal stresses and deflections in a non-uniform cylindrical cross section. Jahanian, et. al. (1990) examines the effect of temperature dependant properties on the solution of cylindrical thermal stresses. Galishin, et. al. (1991) analyse the effects of shell discontinuities and non-uniform

thermal profiles on cylindrical stresses. Jahanian (1996) outlines the effect of material non-linearity (strain-hardening) on the thermal stresses in a cylinder.

Renji, et. al. (1985), Shevchenko, et. al. (1991) and Galishin, et. al. (1991) present analyses of the effects of a stiffening ring on the transient stresses in a cylinder. Chen, et. al. (1991) presents a numerical analysis of the effects of a stiffening ring on the transient stresses in a cylinder. Houtman (1978) addresses transient thermal stresses in a cylinder with a rigid end discontinuity. Mukoed, et. al. (1989) look at the effects of geometrical and physical non-linearities on the thermal stresses in a cylindrical shell. Tooth, et. al. (1998), Russo, et. al. (1994) and Tooth, et. al. (1989) examine the effects of circumferentially varying thermal gradients on the thermal stresses in a cylindrical pressure vessel. Zibdeh (1990) and Smith (1984) discuss the failure probability for thermally stressed cylindrical vessels.

1.5 General gasket behaviour

The selection of a gasket and characterisation of the gasket behaviour in the design process is a subject of great complexity which was not fully understood until fairly recently. The are many aspects to be considered in the utilisation of gaskets. An excellent reference for this information is Winter (1990). This is a general paper on gasket selection, which explains many of the necessary aspects of gasket behaviour.

The present ASME pressure vessel design code (ASME 1998b) philosophy incorporates an approximation of the gasket behaviour by specifying a required gasket seating stress and operating stress for different gasket materials and configurations. The writers of the code established these "gasket factors" at the time of the introduction of flange design to the code. ASME (1942) provides the original modifications to the ASME pressure vessel codes, which saw the inclusion of the "m" and "y" gasket factors. Rossheim, et. al. (1943) is the first revision to the "m" and "y" factors and includes a discussion on the applicability of these factors.

Since this initial work, many studies have been conducted on specific gasket types, under specific operational conditions. One important aspect of gasket behaviour to this project is the gasket elasticity properties, as these affect the joint mechanical interaction. There are many papers on the subject of gasket testing. Listed following are some of them, which include sections on gasket elasticity properties. Swick (1977) provides a simplified theory for establishing the gasket stress at leakage, including a model for the gasket modulus of elasticity. Cascales, et. al. (1987) presents an analytic model for gasket load recovery under operational loading. Soler (1980) outlines a model for the non-linear behaviour of a gasket and presents a comparison with linear approximations. Bazergui, et. al. (1989), Derenne, et. al. (1996), Birembaut, et. al. (1994), Derenne, et. al. (1996) and Derenne, et. al. (1997a) present test results for graphite gaskets, both flexible and metal insert, and outline the high temperature behaviour, relaxation and elasticity properties for this type of gasket.

Bazergui (1977) and Bartonicek, et. al. (1995) both present elasticity testing on spiral wound gaskets. Derenne, et. al. (1997b) presents testing of PTFE gaskets, including elasticity and relaxation. Derenne, et. al. (1994a), Derenne, et. al. (1994b) and Marchand, et. al. (1986) outline the general philosophy for the testing of gaskets, including elevated temperature testing and temperature effect on the gasket modulus. Birembaut, et. al. (1987) presents and discusses the effects of temperature on the mechanical properties of sheet gasket materials. Nishida et. al. (1996) outlines the effect of operational temperature on the mechanical properties of spiral wound gaskets. Bazergui, et. al. (1986) and Bazergui, et. al. (1988) present general testing philosophies for gaskets, including gasket elasticity properties. Birembaut, et. al. (1997) compares different gasket testing procedures and outlines the variation of gasket elastic properties for different gasket types. Birembaut, et. al. (1992) examines gasket elasticity and relaxation, including the variation between different manufacturers. Bazergui, et. al. (1988) presents a general overview of the elevated temperature behaviour for gaskets.

An additional important aspect of gasket interaction in flange design, especially for high temperature joints, is that of gasket relaxation during joint operation. Many authors have explored this phenomenon, however, due to the multitude of gasket types and materials, this effect is far from being completely defined. Thorn (1949) is an early paper on the relaxation properties of asbestos sheet gasket materials. Bazergui (1984) presents the short-term (initial) relaxation of various gaskets. Farnam (1951), Smoley, et. al. (1963) and Marchand, et. al. (1996) examine the relaxation characteristics of sheet gasket materials, including the effects of elevated temperature. Kraus, et. al. (1982), Marchand, et. al. (1993), Bouzid, et. al.. (1994), Bouzid, et. al. (1996), Bouzid, et. al. (1997), Nagy (1996) and Nagy (1997) address the relationship of gasket relaxation with respect to joint interaction.

Nau (1996) wrote a general paper on the operational characteristics of gaskets, in which the various mechanisms of gasket load relaxation versus time are described and a design theory presented. Kockelmann, et. al.(1990) presents relaxation data for flexible graphite and metal insert graphite gaskets, the effects of temperature on relaxation are also examined. Latte, et. al. (1996) presents the relaxation and leakage properties in modified PTFE gasket materials. Vignaud, et. al. (1986) addresses the relaxation characteristics of spiral wound gaskets, including a comparison between two gaskets made by different manufacturers.

Two papers of general interest to this study, as they address specific gasket failure modes in high temperature joints, are Winter, et. al. (1985), which outlines a failure mode of spiral wound gaskets due to inward buckling of the windings at high temperature and Berbee (1998), which details the use of metal reinforced graphite gaskets to replace other gasket types in problematic services such as high temperature heat exchanger joints.

1.6 Finite element analysis of flanged joints

The use of Finite Element Analysis (FEA) to study the operational interaction of the flanged joint is becoming increasingly popular as general purpose finite element programs become more accessible and easier to use. The following papers all use FEA to study flanged joints. They are interesting to this study as they present a comparison of the different methods of analysis that may be used. In particular, the modelling of the gasket and the bolts are aspects which cause the most difficulty when using general FEA programs to analyse flange joints. Cartraud, et. al. (1994) outlines a FEA model for gasket behaviour which includes non-linear, transverse isotropic, plastic, isotropic hardening and surface failure criterion to accurately model the actual gasket material behaviour. Some comparison with experimental results is also presented. Maddren, et. al.(1995) and Lin, et. al. (1997) examine the use of FEA code to study the flow of heat in single bolt bolted joints, particularly with respect to contact stress levels and subsequent heat flow. Nishioka, et. al. (1979) presents a 2D FEA analysis of standard flanges, specifically with respect to stress levels, effect of hub radius and taper, comparison with code calculations and effective gasket loading.

Zerres, et. al. (1998) outlines a 3D FEA model of a standard flange, with comparison to present analytical design procedures. Fessler, et. al. (1974) examines the flange material stress levels and creep rates for a 250NB integral flange. Experimental and photoelastic results confirming the flange model are presented. Nerli, et. al. (1974) presents a numerical methodology for evaluation of integral flange rotation. Fukuoka, et. al. (1998) utilises 3D FEA to examine the effects of flange facing on stress levels and the variation of stresses in the flange in the circumferential direction caused by the non-axisymmetric presence of bolt holes.

Smith, et. al. (1996) proposes a method of modelling spiral wound gasket behaviour in FEM and includes the 2D analysis of several standard flanges to confirm the model. Hwang, et. al. (1994) examines the difference between 2D and 3D FEA modelling of a

standard flange joint under various operational loads. Stallings, et. al. (1992) gives a simple methodology for the modelling of bolt preload in flange joints. Hollinger, et. al. (1996) presents a methodology for making a comparison between FEA results and present analytical design equations. Nau (1985) details a simple FEA approach to analysis of the joint, using shell and isoparametric plate elements. Kim, et. al. (1998) presents a FEA of a bolted joint (manway cover) which includes contact analysis of the bolt and nut, including threads. Bushnell (1984) examines the physical relationships and equations used in the numerical analysis of shells. Ghoneim, et. al. (1990) uses FEA to examine the load capacity of standard API flanges.

CHAPTER 2

STEADY STATE TEMPERATURE ANALYSIS

2.1 Analytic method outline

2.1.1 General description

In order to determine the steady state temperature distribution in the joint components due to heating of the joint by an internal fluid, the joint is broken into four separate components (refer to Figure 2.1) and each of these components is analysed separately. In this way the geometry becomes easier to model using existing analytical solutions.

The vessel wall or pipe is treated as a thick, infinite length hollow cylinder. This is perhaps an excessive approach, as in most cases the thickness to diameter ratio is such that thin cylinder equations may be used. However, it will result in a more accurate, if slightly more complex, analysis. The flange hub is not analysed, as once the shell and flange temperatures are calculated one can interpolate between the two values to obtain the hub temperature, if required.

In all cases it is assumed that heat is lost from the outer surface of each component by radiation and convection, which may be expressed in a linear form relating to the temperature difference between the surface and ambient. This relationship is commonly termed "Newton's Law of Cooling" (Carslaw and Jaeger, 1959; Moon and Spencer, 1961) and will hold true as long as either the radiation or the convection regimes do not dominate; that is, as long as the surface is not at a high temperature (too high and

radiation dominates) and the external fluid has a low velocity (otherwise convection will dominate). The general case of pressure vessel joint operation meets the above restrictions as they rarely operate at temperatures above 400°C and also are rarely cooled by external flow of fluid.

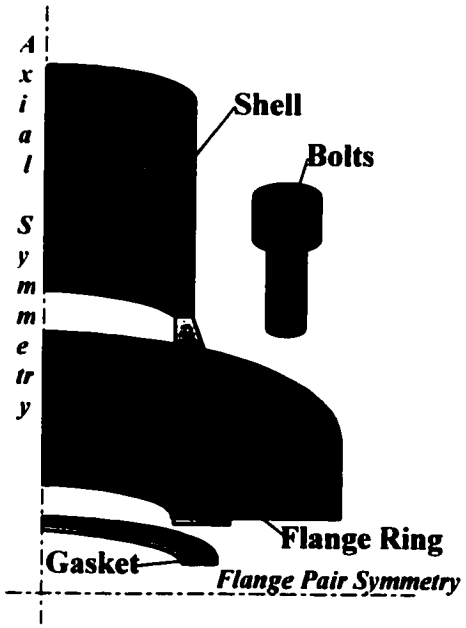

Figure 2.1 – Joint components for steady state temperature analysis

2.1.2 Vessel wall temperature distribution

To analytically establish the steady state thermal distribution in a flange as a whole, it is necessary to commence by treating the shell and flange ring as separate components and, if required, to then include the effects of heat transfer between these two components. The heat transfer between the two components must be combined as the flange acts, effectively, as a cooling fin to the shell. This is due to the fact that the thermal resistance for the flange ring section is lower than that of the shell region. There is, therefore, a net transfer of heat from the shell section to the flange ring section. This leads to a slight overall increase in the flange temperature and a decrease in the shell temperature. This effect is particularly pronounced in small diameter flanges.

This heat transfer between the shell and flange will be further examined in Section 2.1.6. To analyse the shell alone, it is assumed to be an infinite length, thick walled, hollow cylinder, for which the standard thermal resistances per unit length for each section of the shell and insulation are defined in Equations 2.1 to 2.4 following, which are taken from Ozisik (1985).

$$R_{as} = \frac{1}{2\pi \cdot r_i \cdot h_i} \tag{2.1}$$

$$R_{bs} = \frac{1}{2\pi \cdot k_s} \cdot \ln\left(\frac{r_i + t_s}{r_i}\right) \tag{2.2}$$

$$R_{cs} = \frac{1}{2\pi \cdot k_i} \cdot \ln\left(\frac{r_i + t_s + t_i}{r_i + t_s}\right) \tag{2.3}$$

$$R_{ds} = \frac{1}{2\pi \cdot (r_i + t_s + t_i) \cdot h_{os}} \tag{2.4}$$

The total heat flow per unit length of shell can, therefore, be defined as per Equation 2.5.

$$q_s = \frac{(T_i - T_o)}{R_{as} + R_{bs} + R_{cs} + R_{ds}} \tag{2.5}$$

The inside and outside shell wall temperatures and the radial temperature gradient in the shell are calculated using Equations 2.6 to 2.8.

$$T_{si} = T_{so} + q_s \cdot R_{bs} \tag{2.6}$$

$$T_{so} = T_o + q_s \cdot (R_{ds} + R_{cs}) \tag{2.7}$$

$$T_s(r) = T_{so} + (T_{si} - T_{so}) \left[\ln\left(\frac{r_i + t_s}{r}\right) \Big/ \ln\left(\frac{r_i + t_s}{r_i}\right) \right] \tag{2.8}$$

2.1.3 Vessel wall thermal expansion

The previously calculated temperature profile may be integrated in order to determine the radial expansion of the shell, per Equation 2.9 for an infinite cylinder from Boley et.al. (1960), with the integral evaluated per Equation 2.10.

$$u_s(r) = \frac{\alpha_s}{r \cdot (1-\nu)} \cdot \left[(1+\nu) \cdot \int_{r_i}^{r} T_s(r) \cdot r \cdot dr + \frac{(1-3\nu) \cdot r^2 + (1+\nu) \cdot r_i^2}{2r_i \cdot t_s + t_s^2} \cdot \int_{r_i}^{r_i+t_s} T_s(r) \cdot r \cdot dr \right] \quad 2.9$$

$$\int T_s(r) \cdot r \cdot dr = \tfrac{1}{2} \cdot r^2 \cdot \left[T_{so} + (T_{si} - T_{so}) \cdot \ln\left(\frac{r_i + t_s}{r_i} \right)^{-1} \cdot \left(\ln\left(\frac{r_i + t_s}{r} \right) + \tfrac{1}{2} \right) \right] \quad 2.10$$

2.1.4 Flange ring temperature distribution

The flange ring is modelled as two components (refer to Figure 2.2). The inner section is approximated by a thick cylinder of thickness equal to g_1, where g_1 is the flange hub thickness at the intersection with the flange ring. There is no thermal dissipation from this inner section of the ring. The second region is that of the exposed flange ring. This section is modelled as a finite length cylinder with heat loss from the upper and lower flat surfaces and the outer radius. The thickness of this ring (t_e) is taken as proportional to the flange thickness (t_f) and the gap (d) between the flange pairs (t_e=2.t_f - d)), with t_e restricted to $t_f < t_e < 2.t_f$. This modification is made in order to account for the affect on the thermal dissipation of the proximity of the two flanges. The equation models almost zero heat loss from the bottom surface of the flange for the case of a very close flange pair. Conversely, for a widely spaced flange pair, the factor of influence becomes zero and the heat loss from both upper and lower surfaces are considered equal.

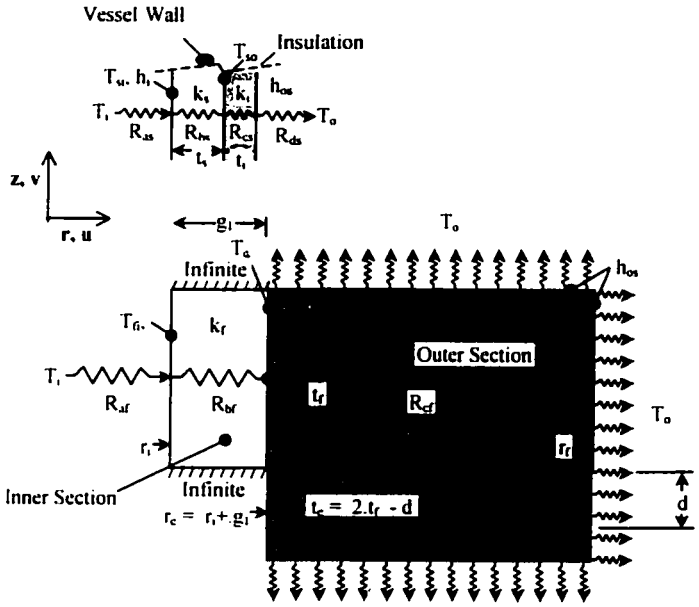

Figure 2.2 – Flange temperature analysis model

For the inner section, the thermal resistances (R_{af} and R_{bf}) are calculated as for the shell (except that g_i is used in place of t_s). Equations 2.11 through to 2.13 define the thermal profile in a finite cylinder and are taken from Carslaw et. al. (1959).

$$T_f(r,z) = 2\cdot\sum_{n=1}^{\infty}\frac{(\varphi_n\cos(\varphi_n z)+h_o\sin(\varphi_n z))\cdot\phi(r;n)}{\left[(\varphi_n{}^2+h_o{}^2)\cdot t_e+2h_o\right]\cdot\phi(r_e;n)}\cdot\int_0^{t_c}\left[f(z)\cdot(\varphi_n\cos(\varphi_n z)+h_o\sin(\varphi_n z))\right]\cdot dz \qquad 2.11$$

$$\phi(r;n) = I_o(r\varphi_n)\cdot[\varphi_n\cdot K_1(r_o\varphi_n)-h_o\cdot K_o(r_o\varphi_n)]+K_o(r\varphi_n)\cdot[\varphi_n\cdot I_1(r_o\varphi_n)+h_o\cdot I_o(r_o\varphi_n)] \qquad 2.12$$

Where φ_n are the non-zero, positive roots of the equation:

$$\tan(\varphi_n \cdot t_e) = \frac{2\varphi_n \cdot h_o}{\varphi_n^{\,2} - h_o^{\,2}}$$

2.13

These equations may be simplified by assuming a constant internal temperature with respect to z and therefore ignoring the temperature gradient in the axial (z) direction, which will be shown later, by comparison to FEA results, to be negligible. Therefore, a single radial thermal profile for the flange ring may be developed at z equal to t_e, and is given below in Equation 2.14.

$$T_f(r) = T_o - 2\cdot(T_e - T_o)\cdot\sum_{n=1}^{\infty}\frac{(h_o\cdot\cos(\varphi_n t_e) - h_o - \varphi_n\cdot\sin(\varphi_n t_e))\cdot\phi(r;n)}{\left[(\varphi_n^{\,2} + h_o^{\,2})\cdot t_e + 2h_o\right]\cdot\phi(r_e;n)}$$

2.14

The temperature at the inner edge of the flange ring (T_e) is calculated using the balance of the heat flow for an extended surface with uniform heat flow across the base area (as we have assumed), from Kern, et. al. (1972) as defined by Equation 2.15.

$$q = -2\cdot\pi\cdot r_e\cdot k_f\cdot\left.\frac{\partial T_f(r)}{\partial r}\right|_{r=r_e}$$

2.15

The heat dissipated from the outer flange ring can therefore be calculated for $r = r_e$ using Equations 2.16 and 2.17.

$$\frac{\partial\phi(r_e;n)}{\partial r} = \phi'(r_e;n) = \varphi_n\cdot\left[I_1(r_e\varphi_n)\cdot[\varphi_n\cdot K_1(r_o\varphi_n) - h_o\cdot K_0(r_o\varphi_n)] - K_1(r_e\varphi_n)\cdot[\varphi_n\cdot I_1(r_o\varphi_n) + h_o\cdot I_0(r_o\varphi_n)]\right]$$

2.16

$$q = 4\cdot\pi\cdot r_e\cdot k_s\cdot(T_e - T_o)\cdot\sum_{n=1}^{\infty}\frac{(h_o\cdot\cos(\varphi_n t_e) - h_o - \varphi_n\cdot\sin(\varphi_n t_e))\cdot\phi'(r_e;n)}{\left[(\varphi_n^{\,2} + h_o^{\,2})\cdot t_e + 2h_o\right]\cdot\phi(r_e;n)}$$

2.17

Since there is no heat dissipation from the inner section of the flange ring, the heat flow per unit length is constant through the inner and outer sections. Using a similar approach to that used for the shell, the section resistances may be calculated (Equations 2.18 to 2.21). The value of q_f for the flange ring section may therefore be expressed as in

Equation 2.22 and the temperatures at r_e and r_f may be calculated using Equations 2.23 and 2.24.

$$R_{af} = \frac{1}{2\pi \cdot r_i \cdot h_i} \tag{2.18}$$

$$R_{bf} = \frac{\ln\left(\frac{r_e}{r_i}\right)}{2\pi \cdot k_f} \tag{2.19}$$

$$R_{cf} = \frac{1}{2\pi \cdot r_e \cdot \beta} \tag{2.20}$$

where

$$\beta = 2 \cdot k_f \cdot \sum_{n=1}^{\infty} \frac{\left(h_o \cdot \cos(\varphi_n t_e) - h_o - \varphi_n \cdot \sin(\varphi_n t_e)\right) \cdot \phi'(r_e; n)}{\left[\left(\varphi_n^2 + h_o^2\right) \cdot t_e + 2h_o\right] \cdot \phi(r_e; n)} \tag{2.21}$$

$$q_f = \frac{(T_i - T_o)}{R_{af} + R_{bf} + R_{cf}} \tag{2.22}$$

$$T_{fi} = T_e + q_f \cdot R_{bf} \tag{2.23}$$

$$T_e = T_o + q_f \cdot R_{cf} \tag{2.24}$$

2.1.5 Flange ring thermal expansion

The previously determined gradients are used to calculate the axial flange deflection according to the theory of a circular disc with radial temperature variation (Boley et. al., 1960). The total axial expansion of the flange is approximated as the expansion occurring directly above the gasket, between the gasket and the mid-plane of the flange (including the gasket), and the expansion occurring at the bolt circle, between the point of application of the bolt force and the mid-plane of the flange ring.

Thus the inner section of the flange axial displacement, including half the gasket, is calculated using Equation 2.25.

$$v_f = \frac{\alpha_f \cdot t_f + \alpha_g \cdot t_g}{r_e^{\,2} - r_i^{\,2}} \cdot \int_{r_i}^{r_e} T_f(r) \cdot r \cdot dr$$

2.25

The integral is evaluated using Equation 2.10 and this gives us the expansion that occurs in the line of the gasket load reaction. The axial displacement at the bolt circle can be calculated using Equation 2.25, but omitting the gasket terms, and using the integral of the thermal gradient for the outer ring (Equation 2.26). The integral of $\phi(r;n)$ is calculated using Equation 2.27. These two axial expansions are then added together, to give the equivalent flange and gasket axial expansion (v_f).

$$\int_{r_e}^{r} T_f(r) \cdot r \cdot dr = \frac{1}{2} \cdot T_o \cdot r^2 - 2 \cdot (T_e - T_o) \cdot \sum_{n=1}^{\infty} \frac{(h_o \cdot \cos(\varphi_n t_e) - h_o - \varphi_n \cdot \sin(\varphi_n t_e)) \cdot \int_{r_e}^{r} \phi(r;n) \cdot r \cdot dr}{\left[(\varphi_n^{\,2} + h_o^{\,2}) \cdot t_e + 2h_o\right] \cdot \phi(r_e;n)}$$

2.26

$$\int \phi(r;n) \cdot r \cdot dr = r/\varphi_n \cdot (I_1(r\varphi_n) \cdot [\varphi_n \cdot K_1(r_o\varphi_n) - h_o \cdot K_0(r_o\varphi_n)] - K_1(r\varphi_n) \cdot [\varphi_n \cdot I_1(r_o\varphi_n) + h_o \cdot I_0(r_o\varphi_n)])$$

2.27

Due to the possibility of different radial expansion across the gasket face between mating flanges causing gasket failure, it is necessary to calculate the value of the flange radial expansion at the gasket outer diameter. The radial expansion of both inner and outer sections can be calculated using the equation for a short cylinder or disk from Boley et.al. (1960), as outlined in Equation 2.28. The integrals are evaluated using Equation 2.10 for the inner section and Equation 2.29 for the outer section.

$$u_f(r) = \frac{\alpha_f}{r} \cdot \left[(1+\nu) \cdot \int_{r_{int}}^{r} T_f(r) \cdot r \cdot dr + \frac{(1-\nu) \cdot r^{\,2} + (1+\nu) \cdot r_{int}^{\,2}}{r_{ext}^{\,2} - r_{int}^{\,2}} \cdot \int_{r_{int}}^{r_{ext}} T_f(r) \cdot r \cdot dr \right]$$

2.28

$$\int \phi(r;n) \cdot r \cdot dr = r/\varphi_n \cdot (I_1(r\varphi_n) \cdot [\varphi_n \cdot K_1(r_o\varphi_n) - h_o \cdot K_0(r_o\varphi_n)] - K_1(r\varphi_n) \cdot [\varphi_n \cdot I_1(r_o\varphi_n) + h_o \cdot I_0(r_o\varphi_n)])$$

2.29

Finally, in addition to the axial and radial expansion of the flange, there is a moment applied by the vessel shell onto the flange ring due to the shell being at a higher temperature than the flange and thus expanding in the radial direction more than the flange ring. As the ring restrains the shell in the radial direction there is a resultant moment transmitted to the flange (in much the same way as the hoop effects of internal pressure increase the flange rotation). For clarity and conformity with existing philosophy, the effects of this differential expansion are treated identically to these pressure hoop effects.

The radial expansion of the shell and the flange are calculated at the middle radius of the shell (r_{sm}) using Equation 2.9 for the shell and Equation 2.28 for the flange ring. The difference between the two can then be calculated and related to an equivalent pressure that would be required to obtain the same radial difference in an open thin cylinder. This effect can be evaluated using Equation 2.30. However, this value may not be compared directly to a design pressure as, with normal pressure loading, the flange rotates due to both the longitudinal and the hoop components of pressure. Hence the value calculated by this equation should be reduced, depending on the relative rigidities of the joint components, for direct comparison with a design pressure. Nonetheless, it gives an indication as to the magnitude of this effect, and is used as a design load in later sections.

$$P_{eq} = \frac{E_s \cdot t_s}{r_{sm}^{\ 2}} \cdot \left(u_s(r_{sm}) - u_f(r_{sm})\right)$$

2.30

2.1.6 Flange/shell temperature interaction

With certain flange types it is necessary to account for the flow of heat from the shell to the flange. This effect decreases with increasing internal diameter to shell wall thickness ratio (r_i/t_s), due to the fact that for a larger diameter the external shell resistance decreases (R_{ds}) and the internal resistance (R_5) increases. It may therefore be conservatively stated that if $R_5 > 10.R_{ds}$ then the effects of thermal transfer between the

flange and shell will be negligible and this section may be disregarded. By using the expressions for R_5 and R_{ds} (Equations 2.4 and 2.36) and simplifying the previously stated limit it can therefore be stated that the interaction may be disregarded if :

$$(h_o.(r_i + t_s)/((r_i + t_s)^2-r_i^2)) < 10. \qquad 2.31$$

To analytically model this effect in a simple manner several simplifying assumptions regarding the heat flow must be made. These assumptions may be outlined using the electrical circuit analogy detailed below (refer to Figure 2.3). In this analogy it is assumed that the internal resistance to heat flow is small in relation to the external film resistance so that the gradient within the shell wall is very small. It can therefore be assumed that the heat flow occurs at the inside of the shell wall. Whereas, in reality the flow will occur across the full thickness of the hub. The individual resistances are therefore evaluated using Equations 2.32 through to 2.34.

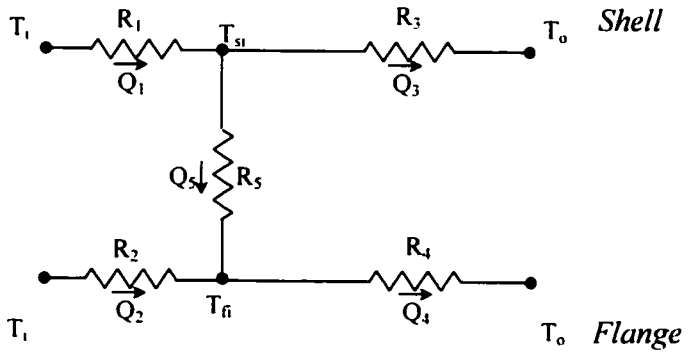

Figure 2.3 – Flange/shell heat flow analogy

$$R_1 = R_{as}/L_s \qquad 2.32$$

$$R_2 = R_{af}/t_f \qquad 2.33$$

$$R_3 = (R_{bs} + R_{cs} + R_{ds})/L_s$$

2.34

$$R_4 = (R_{bf} + R_{cf})/t_f$$

2.35

$$R_5 = L_s/(2\pi \cdot k_s \cdot (r_o^2 - r_i^2))$$

2.36

Since there is no additional heat loss, other than the external surfaces, the heat flow in must equal the heat flow out. Therefore the heat flow may be defined (Equation 2.37) and the inner flange wall and the shell wall temperatures may be calculated using (Equations 2.38 and 2.39). As the heat flow is related to the effective resistance and the temperatures, the final system temperatures and heat flows can be calculated using Equations 2.40 and 2.41. These values then replace the previous equations for the flange (q_f from Equation 2.22) and the shell (q_s from Equation 2.5) and the analysis is completed as previously outlined.

$$Q_1 + Q_2 = Q_3 + Q_4$$

2.37

$$T_{fi} = 1/D \cdot \left[(C-1) \cdot \left(\frac{T_i}{R_1} + \frac{T_o}{R_4} \right) + C \cdot \left(\frac{T_i}{R_2} + \frac{T_o}{R_5} \right) \right]$$

2.38

$$T_{si} = 1/A \cdot \left(\frac{T_i}{R_1} + \frac{T_o}{R_4} + \frac{T_{fi}}{R_3} \right)$$

2.39

$$q_f = Q_4/t_f = (T_{fi} - T_o)/(R_4 \cdot t_f)$$

2.40

$$q_s = Q_3/L_s = (T_{si} - T_o)/(R_3 \cdot L_s)$$

2.41

where

$$A = \left(\frac{1}{R_1} + \frac{1}{R_4} + \frac{1}{R_3} \right) \qquad 2.42$$

$$C = 1 + \left(\frac{R_1 \cdot R_4}{R_4 \cdot R_3 + R_1 \cdot R_3} \right) \qquad 2.43$$

$$D = \left(\frac{C}{R_2} + \frac{C}{R_5} + \frac{1}{R_3} \right) \qquad 2.44$$

2.1.7 Bolt temperature

The bolt receives heat flow from two sources, a) contact between the bolt head and the flange and b) radiation/convection from the flange bolt hole to the bolt. There are many variables affecting the degree of heat transfer by the latter source, such as bolt hole clearance and the length of the bolt in the flange (Gough, 1936). It is not feasible to include all of these variables when calculating the bolt temperature. To do so would result in an extremely complex relationship, which would not be workable in a flange design situation. The bolt temperature is therefore calculated using the following simplifying assumptions:

1) Heat flow to the bolt, via the nut, from the flange is assumed to follow existing contact heat transfer theory. The contact surface is assumed to be the entire underside of the nut.

2) The clearance between the flange and the bolt in the bolt hole is assumed to be a loose fit (based on standard flange dimensions) and thus the heat transfer between the bolt and flange through the flange thickness is primarily by radiation and convection, rather than contact. This will not be the case if the bolt is threaded into the flange or the bolt hole clearance is tight. In these cases the contact heat

conduction will result in much higher heat transfer rates, and the bolt/flange interface resistances, R_{ab} and R_{bb}, should be taken as equal to 1.0 and 0 respectively.

3) The heat loss from the nuts and from any exposed portion of the bolt between the two flanges is calculated as heat transfer to atmosphere from a cylinder having an outer diameter equal to the bolt nominal diameter or nut external diameter (across flats dimension) as applicable.

The bolt heat transfer model can therefore be drawn as per Figure 2.4.

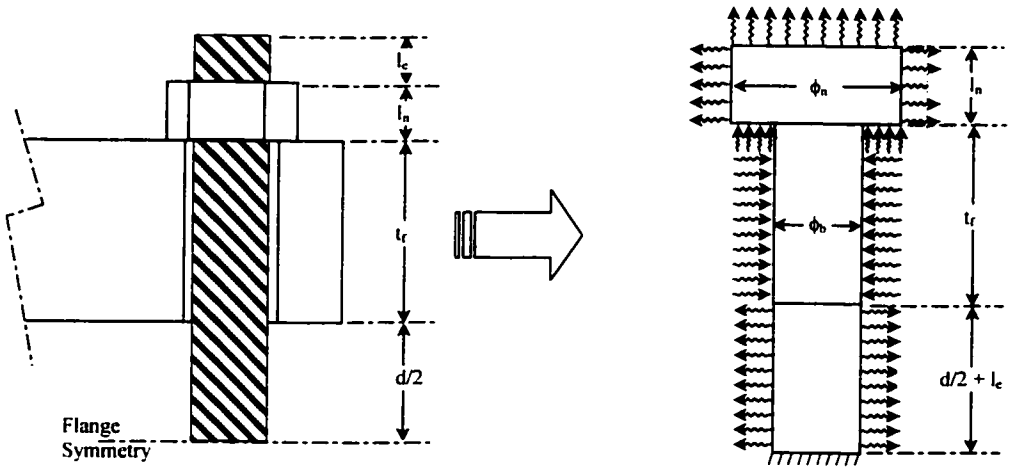

Figure 2.4 – Bolt Heat Flow Model

The flange temperature $T_f(r_b)$ at the bolt circle (r_b) from Equation 2.14 is used to calculate the temperature of the bolt. The exposed length of the bolt (d) will, in general, be less than the thickness of the flange and therefore it is reasonable to assume that the bolt temperature is uniform in both the radial and longitudinal directions. Thus the bolt temperature can be found by following the lumped mass heat balance (refer to Figure 2.5).

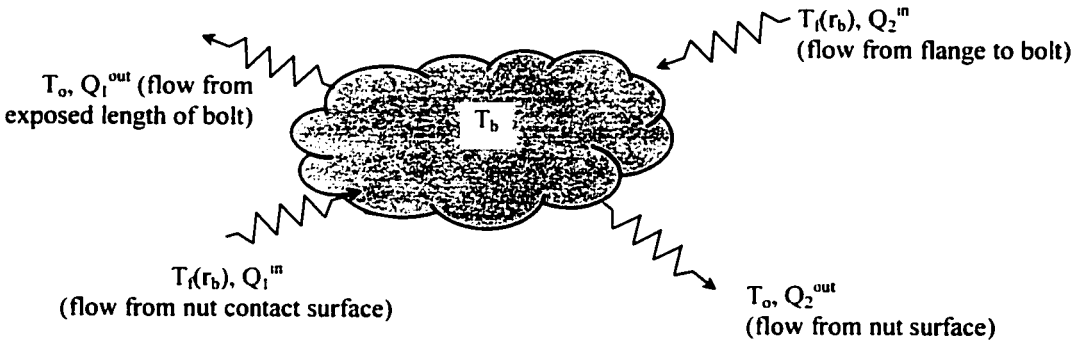

Figure 2.5 – Bolt heat transfer analogy

The governing equations for each heat flow case are defined by Equations 2.45 to 2.48 (Ozisik, 1985).

$$Q_1^{in} = h_{cb} \cdot \frac{\pi}{4}\left(\phi_n^{\,2} - \phi_b^{\,2}\right) \cdot \left(T_f(r_b) - T_b\right) = \frac{1}{R_{ab}} \cdot \left(T_f(r_b) - T_b\right) \qquad 2.45$$

$$Q_2^{in} = h_{fb} \cdot \pi \cdot \phi_b \cdot t_f \cdot \left(T_f(r_b) - T_b\right) = \frac{1}{R_{bb}} \cdot \left(T_f(r_b) - T_b\right) \qquad 2.46$$

$$Q_1^{out} = h_{os} \cdot \pi \cdot \phi_b \cdot \left(d/2 + l_e\right) \cdot \left(T_b - T_o\right) = \frac{1}{R_{cb}} \cdot \left(T_b - T_o\right) \qquad 2.47$$

$$Q_2^{out} = h_{os} \cdot \pi \cdot \left(\phi_n \cdot l_n + \tfrac{1}{4} \cdot \phi_n^{\,2}\right) \cdot \left(T_b - T_o\right) = \frac{1}{R_{db}} \cdot \left(T_b - T_o\right) \qquad 2.48$$

The heat transfer coefficient from the flange to bolt in the bolt hole, h_{fb}, can be determined by considering the resistance to include the external film transfer coefficient (h_{os}) on both the hole internal diameter and the bolt external diameter and a value for conductance across the air gap between the flange and the bolt. If, for simplification, the nominal diameter of the bolt is used for both cases of the film transfer resistance, this gives an equivalent film coefficient of $h_{os}/2$. The air gap can be represented by

conductance across an assumed gap of 3mm, on diameter, with the value of the thermal conductivity of air taken as 0.05 W/(m.°C) (Touloukian et. al., 1970). The approximated heat transfer coefficient is therefore defined by Equation 2.49.

$$h_{fb} = \frac{1}{2/h_{os} + 0.06}$$

2.49

The bolt temperature is therefore calculated as per Equation 2.50.

$$T_b = \frac{\left(\frac{1}{R_{ab}} + \frac{1}{R_{bb}}\right) \cdot T_f(r_b) + \left(\frac{1}{R_{cb}} + \frac{1}{R_{db}}\right) \cdot T_o}{\frac{1}{R_{ab}} + \frac{1}{R_{bb}} + \frac{1}{R_{cb}} + \frac{1}{R_{db}}}$$

2.50

The subsequent axial expansion of the bolt, for half of the length, can then be calculated as per Equation 2.51.

$$v_b = \alpha_b \cdot T_b \cdot (t_f + d/2)$$

2.51

2.1.8 Gasket temperature

The temperature of the gasket will vary, depending on the gasket face configuration and the gasket material. However, for the majority of gasket configurations, where the gasket is relatively thin and is compressed between the two flange faces, it is thought to be acceptable to assume that the gasket operating temperature gradient is the same as that of the flange face across the gasket width. This is due to the fact that the contact heat transfer area between the flange and the gasket is large by comparison to the gasket thickness and the gasket external heat transfer area. This simplification means that no further calculation is required to determine the gasket operating temperature.

2.2 Verification of analysis method

2.2.1 Comparison with finite element results

The calculation of the steady state temperature distribution in a fairly simple form such as a flange may be easily and accurately performed using finite element analysis. In cases of relatively simple heat transfer, such as this, the accuracy of the FEA results should be very high. Hence, in order to confirm that the developed theoretical equations are able to accurately model the temperature profile, and the subsequent material expansion, a comparison was performed between the results of the theoretical equations and FEA.

Since the theory of thermal gradients in an infinite cylinder is a fairly simple calculation and a well established process, it was not considered necessary to check the analytic theory detailed previously for the shell by comparison with FEA. Likewise, the theory detailed for the heat transfer from the flange to the bolt was similarly simple and well established. Thus the temperature distribution and subsequent deformation of the flange ring was considered the only aspect of the analysis requiring confirmation by FEA.

2.2.1.1 Analysis description

In order to verify the analytic method three FEA models having similar dimensions to the flange ring of flanges used later in the experimentation phase were constructed. Each model was analysed with steady state loading of a 250°C temperature difference between the outer surfaces and the inner surface. The program was run with three different inner surface film heat transfer coefficients (h_i) and two external film heat transfer coefficients (h_{os}) for each model, giving a total of three models and nine different load cases as outlined in Table 2.1. In all cases the material properties used were those of ASTM A-105 flange material; k_f = 0.047 W/(m.°C), α_f = 1.25e-5 m/m/°C, E_f = 190,000 MPa (ASME, 1998a).

Table 2.1 – Details of the FEA models used for comparison.

Model	r_i (mm)	r_f (mm)	t_f (mm)	r_e (mm)	h_i (W/m²/°C)	h_o (W/m²/°C)
FR1-A	39	95	22.5	57	150	30
FR1-B	39	95	22.5	57	1500	30
FR1-C	39	95	22.5	57	1500	90
FR2-A	127	222	46.2	160	150	30
FR2-B	127	222	46.2	160	1500	30
FR2-C	127	222	46.2	160	1500	90
FR3-A	535	606	58.7	554	150	30
FR3-B	535	606	58.7	554	1500	30
FR3-C	535	606	58.7	554	1500	90

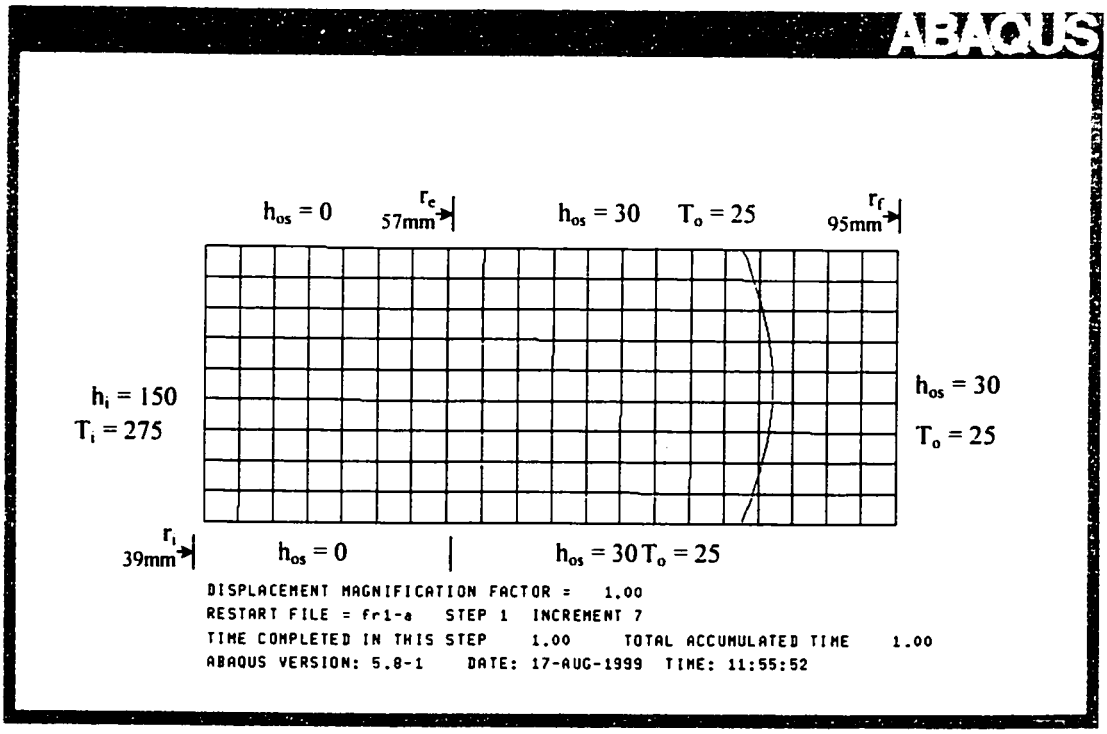

Figure 2.6 – Example of axisymmetric ring FEA model (FR1-A)

The FEA was performed using the ABAQUS general finite element program (ABAQUS, 1999). Due to the symmetry of the ring an axisymmetric analysis using four node elements (CAX4) was performed. A plot of an example model (FR1-A) is shown in Figure 2.6. The other models are all similar in construction. The temperature and deformation results of the FEA were then compared with those predicted by the theory previously outlined in Sections 2.1.5 and 2.1.6.

2.2.1.2 FEA results comparison

From the graphs (Figures 2.7 to 2.17) it can be seen that the accuracy of the theoretical equations by comparison to the FEA results are quite good. The theoretical equations appear to indicate a higher temperature for cases when the internal film coefficient is of the same order as the external film coefficient. However the difference between the FEA results and the theory is never more than 5% of the temperature difference between external and internal temperatures. This is considered sufficiently accurate for the determination of flange operational temperatures, especially taking into account that the external film coefficient will be an order of magnitude smaller than the inner film coefficient.

Comparison of the FEA results for temperatures at the mid-point and the surface of the model demonstrate that the temperature difference never exceeds more than a few degrees. As these models are fairly indicative of the sizes of flanges to be encountered this is considered sufficient support of the previously made assumption that the thermal gradient in the axial direction may be neglected. Additionally, from Figures 2.8 to 2.16 it may be seen that there is good agreement between the theoretical equations and the FEA results for the radial expansion of the flange ring. The results of the theoretical equations are in almost exact agreement with the FEA results. The axial expansion values for the theory versus the FEA are compared in Figure 2.17. The values are in good agreement, with the maximum error being less than 5%, which is considered sufficiently accurate for the determination of the joint mechanical behaviour.

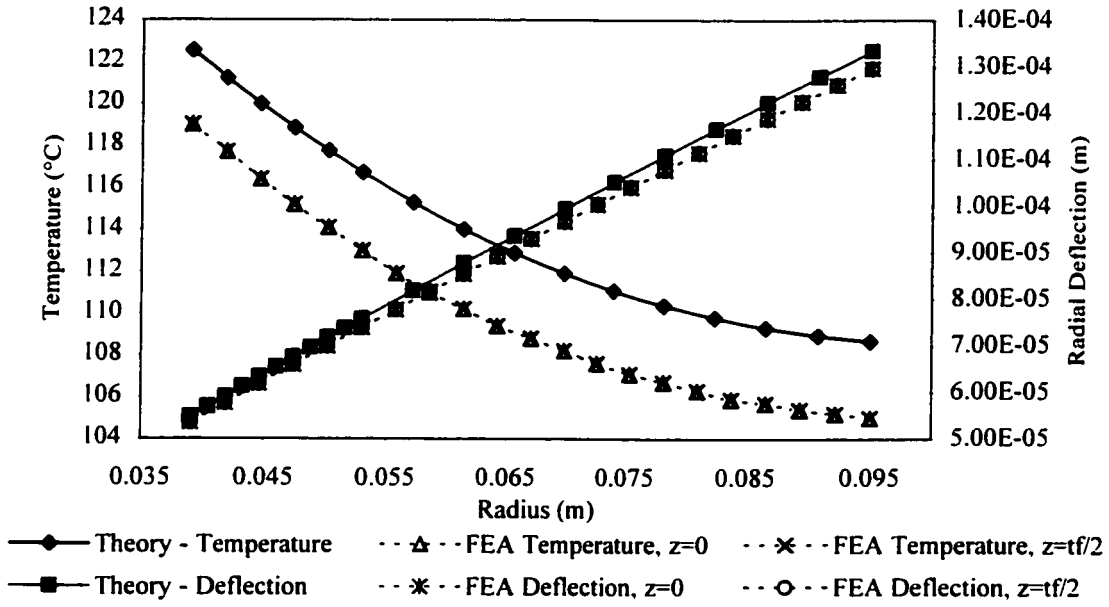

Figure 2.7 – Model FR1-A results (n=14)

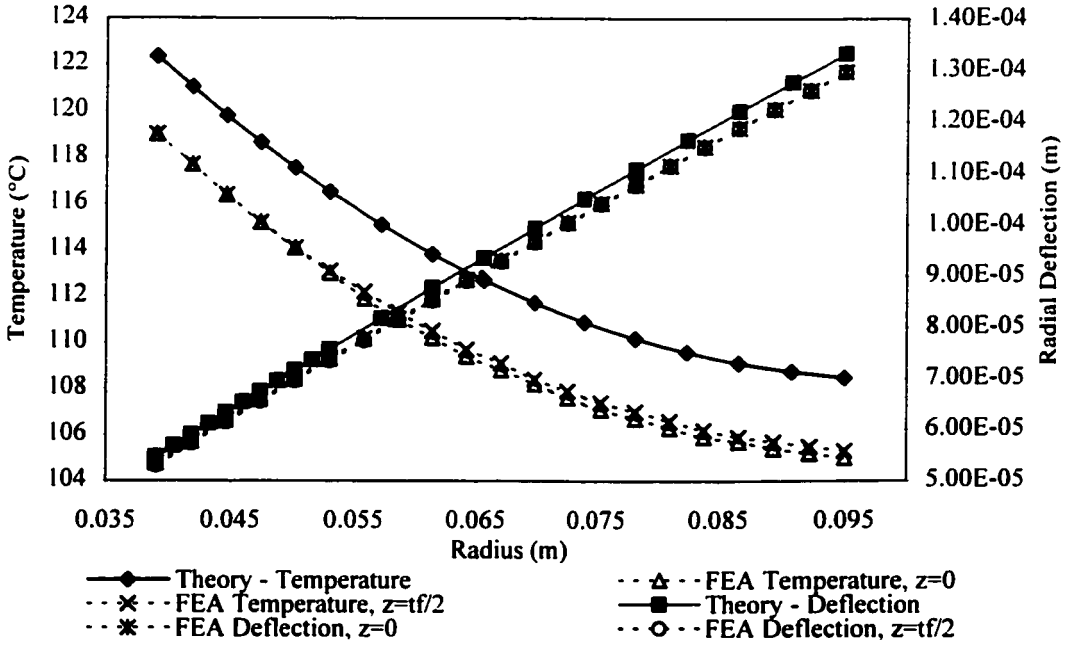

Figure 2.8 – Model FR1-A results (n=10)

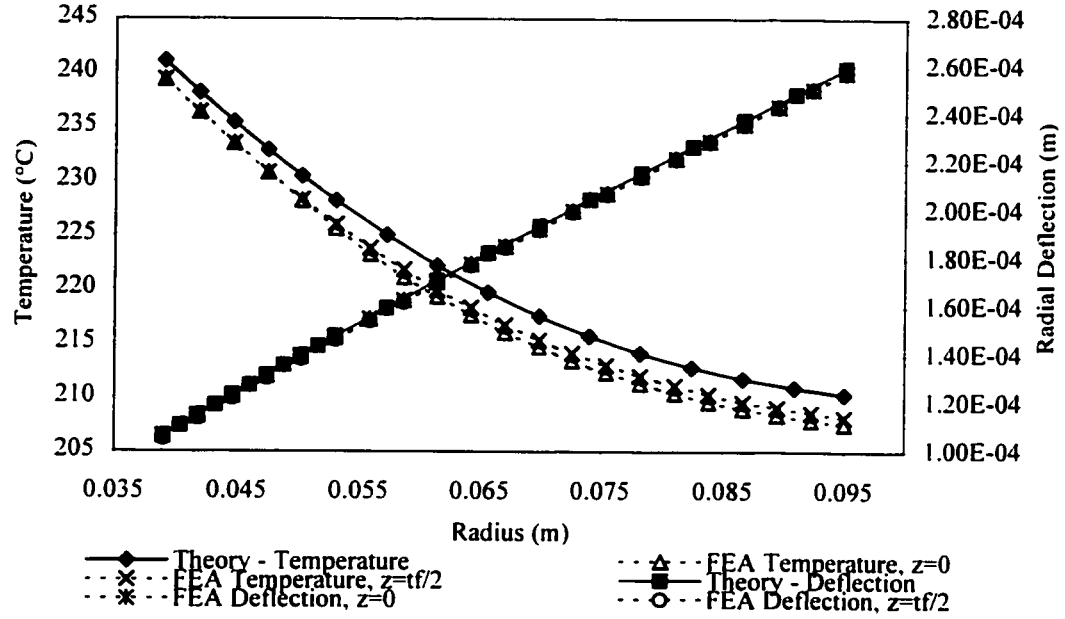

Figure 2.9 – Model FR1-B results (n=10)

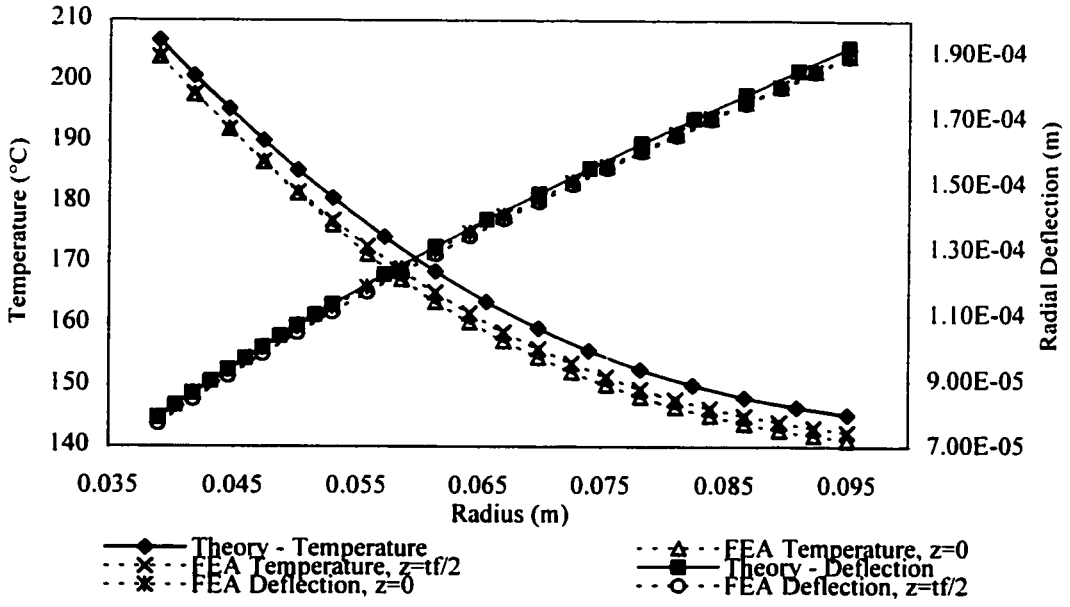

Figure 2.10 – Model FR1-C results (n=10)

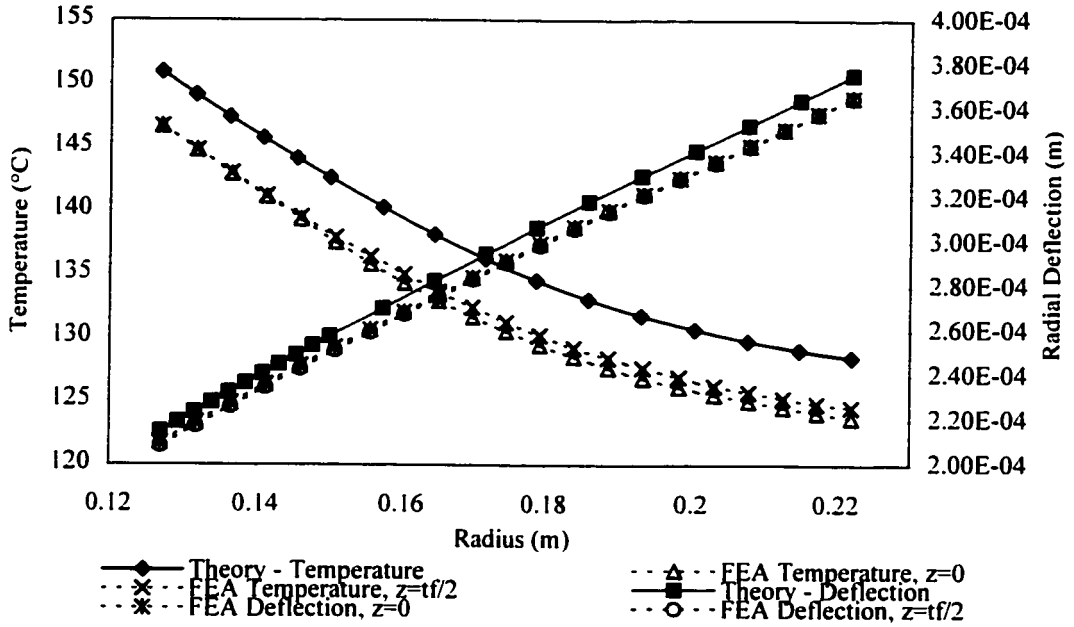

Figure 2.11 – Model FR2-A results (n=10)

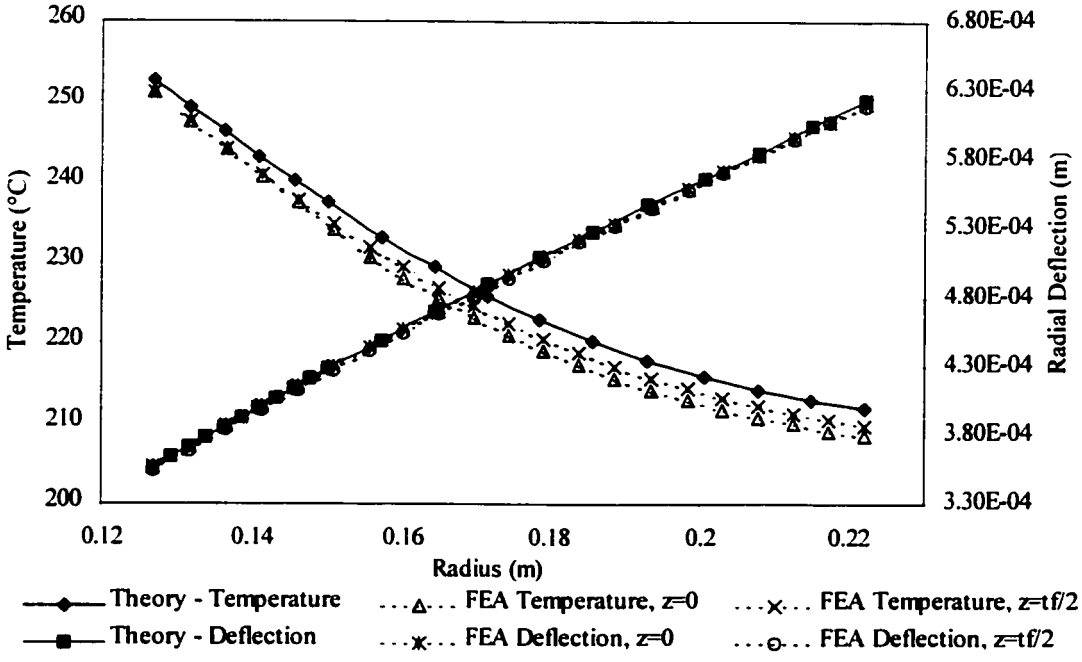

Figure 2.12 – Model FR2-B results (n=10)

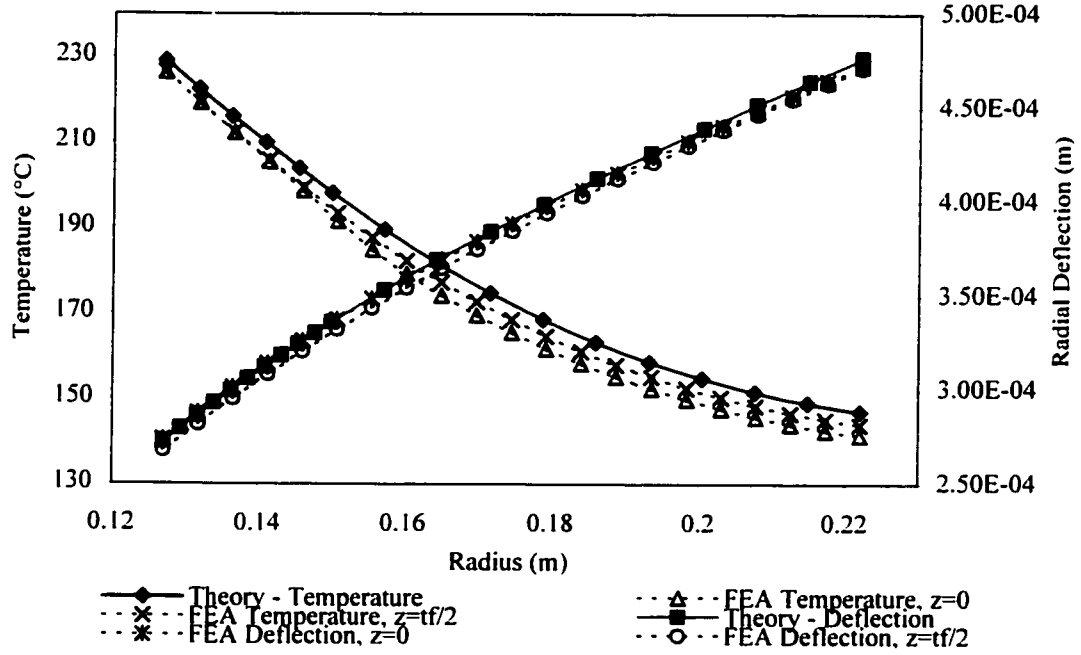

Figure 2.13 – Model FR2-C results (n=10)

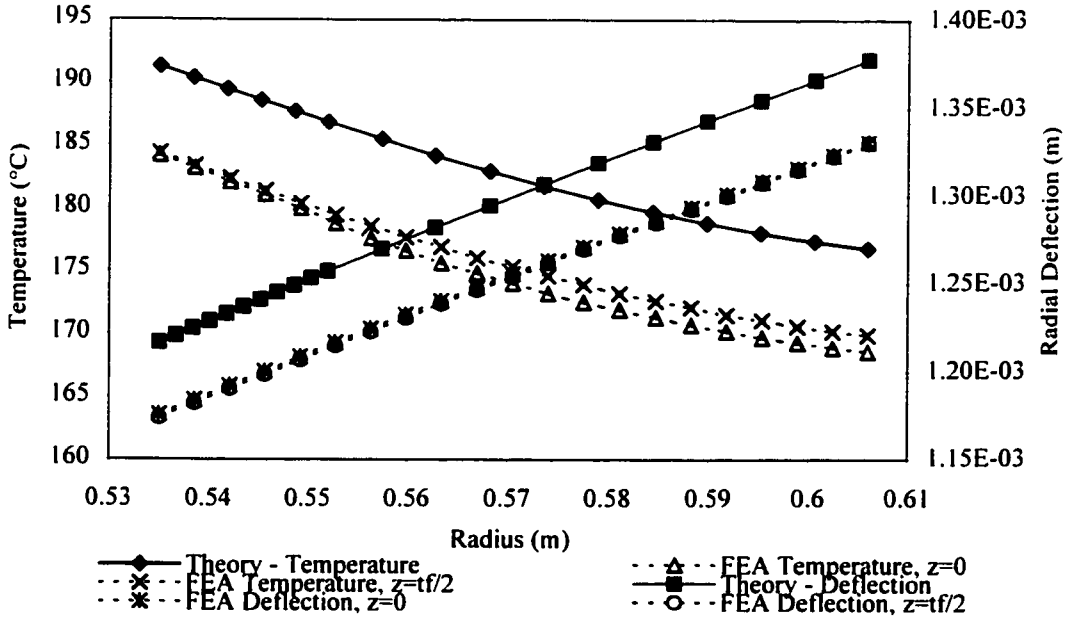

Figure 2.14 – Model FR3-A results (n=10)

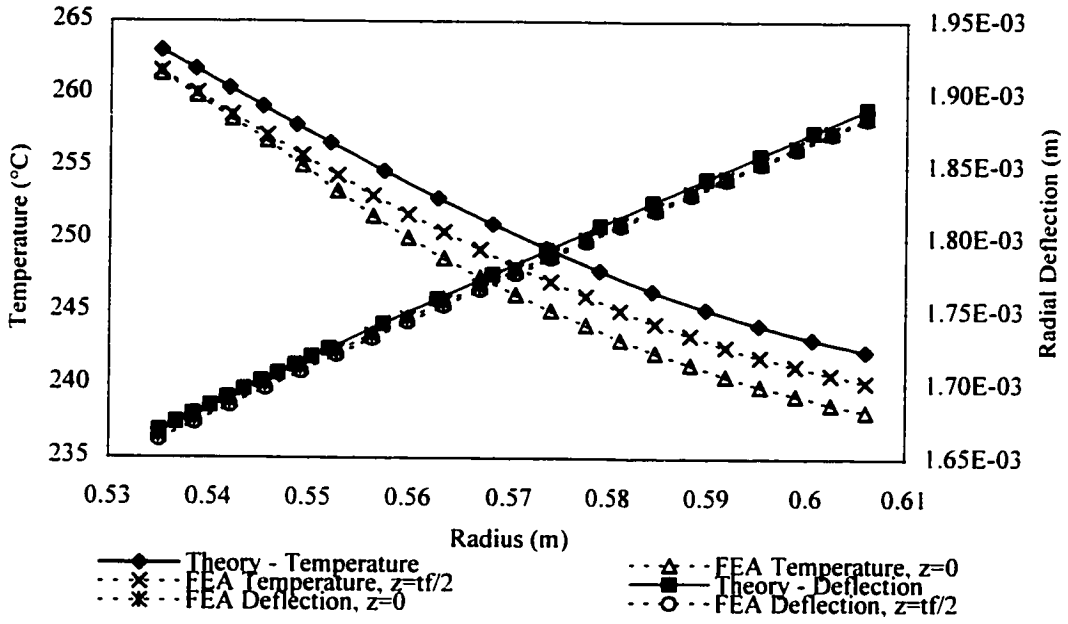

Figure 2.15 – Model FR3-B results (n=10)

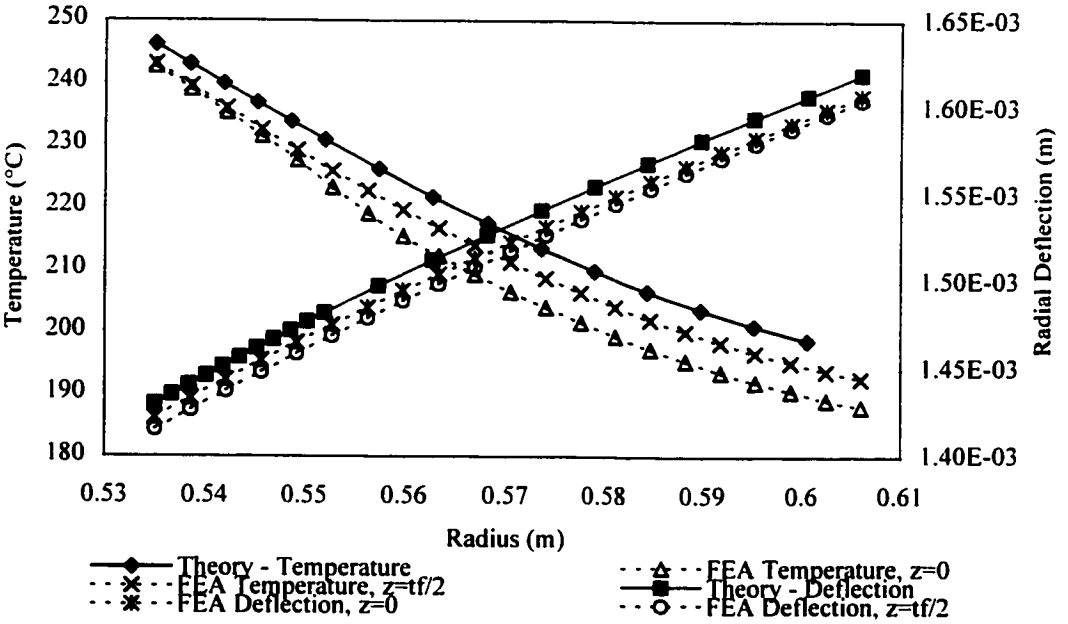

Figure 2.16 – Model FR3-C results (n=10)

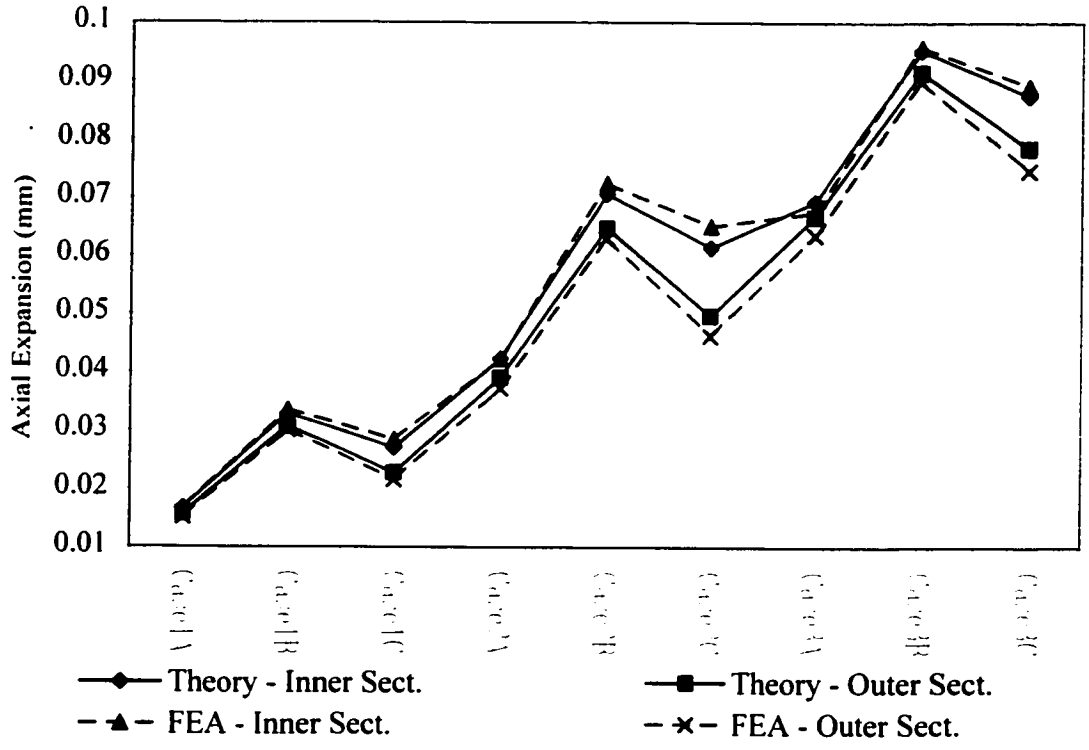

Figure 2.17 – Axial expansion comparison, all models

By comparison of Figure 2.7, for which 14 roots were used in the Bessels calculation, and Figure 2.8, for which 10 roots were used, it can be seen that the plotted curves are identical. It can therefore be concluded ten roots are sufficient for accurate calculation of the temperature gradient. Thus all further calculations were performed using ten roots.

2.2.2 Comparison with laboratory results

Due to the fact that theoretical work on flange thermal gradients had not been previously performed it was necessary to conduct laboratory experimentation to verify that the theoretical equations and assumptions were accurate. This required the measurement of the temperature profile in a flange during heating by an internal heat source.

In addition to confirming the equation accuracy the experiments also examined several other important factors, as listed below:

- Measurement of the external film heat transfer coefficient (h_{os}).
- Confirmation of the philosophy adopted for determining the effect of the gap between the mating flanges.
- Confirmation of the philosophy for heat flow into the bolt.
- Determination of the bolt/flange interface heat transfer coefficient (h_{cb}) with relation to bolt load.
- Measurement of the effect of flange orientation on the external film heat transfer coefficient.

2.2.2.1 Experiment description

The test set-up was essentially identical to the standard Tightness Testing Research Laboratory (TTRL) - Hot Blow Out Test (HOBT) rig developed by TTRL for the PTFE qualification project (Derenne et. al., 1999). Photographs of the test assembly and of the thermocouple placement are shown in Figures 2.18 and 2.19.

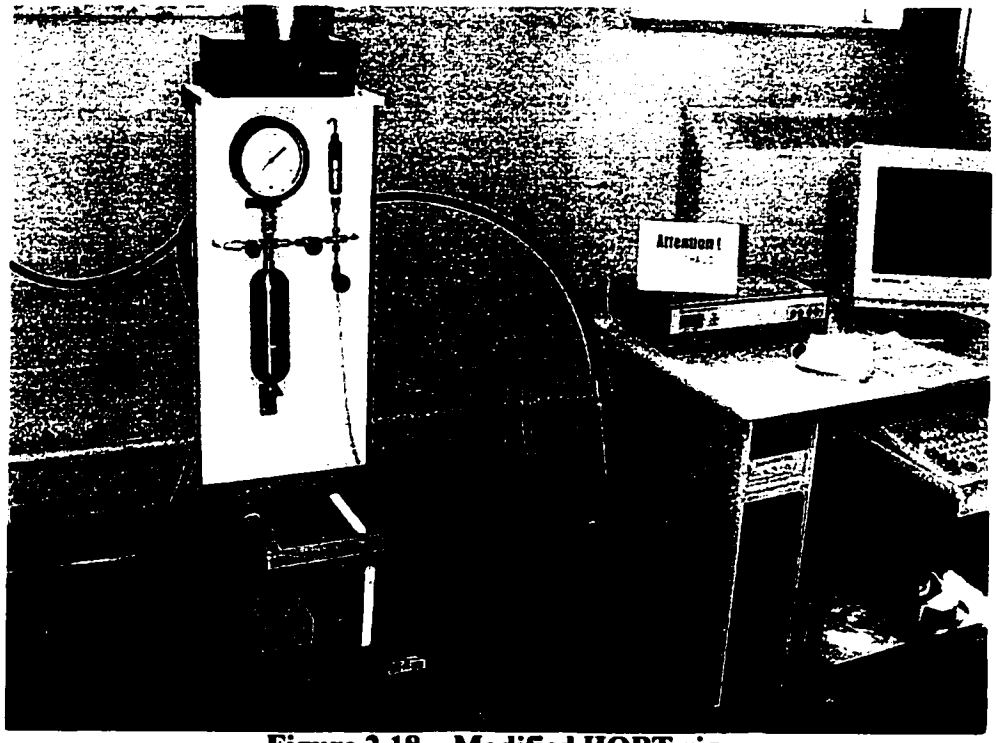

Figure 2.18 – Modified HOBT rig

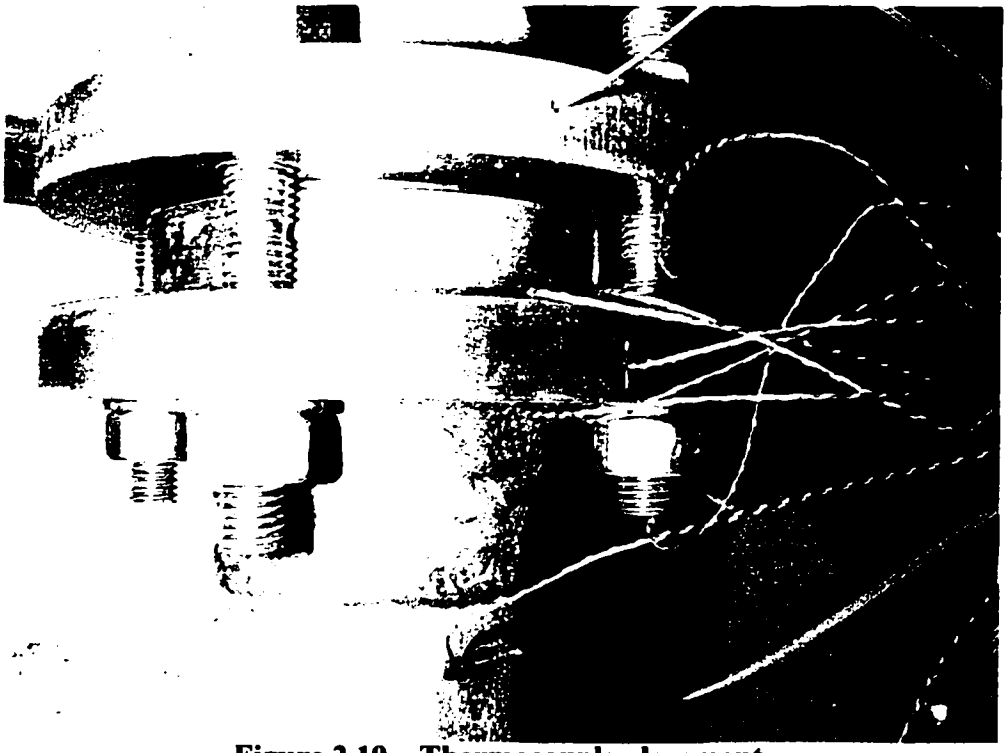

Figure 2.19 – Thermocouple placement

The modifications made to the HOBT rig were:

- The test flange used was a NPS 3 inch, cl.150 raised face welding neck flange.
- This flange was instrumented with 10 J type thermocouples, placed on the internal and external surfaces of the flange as detailed in Figure 2.20.
- All thermal insulation was removed from the test rig.
- During some tests steel spacers were inserted between the flanges to increase the gap. Longer studbolts were used during this phase of the experimentation.
- A constant pressure of approximately 350 kPa of Helium was maintained in the test rig during testing, in an attempt to ensure as high as possible heat transfer rate from the heater to the flange.

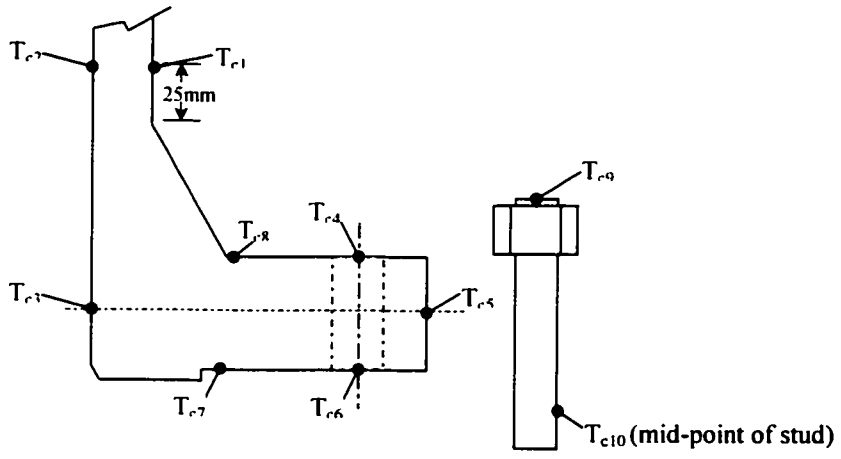

Figure 2.20 – 3" cl.150 thermocouple placement.

These modifications allowed the measurement of the thermal gradients in the flange and shell during an increase, steady state and a decrease in internal temperature. Other than these modifications the HOBT rig was configured, assembled and tests were conducted as per the standard HOBT test procedure. In total 21 tests on this unit were conducted, with changes in the flange orientation, bolt load or gap between the flanges as outlined in Table 2.2.

Table 2.2 – NPS 3 inch, cl.150 modified HOBT test cases

No.	Orient.	Gap (d) (mm)	Temp. (°C)	Bolt T. (N.m)	Washer Used
1	Vertical	4.9	325	100	No
2	Vertical	4.9	325	50	No
3	Vertical	42.1	325	50	Yes
4	Vertical	42.1	325	50	Yes
5	Vertical	42.1	325	100	Yes
6	H.-180°	29.3	325	100	Yes
7	H.-0°	29.3	325	100	Yes
8	H.-90°	29.3	325	100	Yes
9	Vertical	29.3	325	100	Yes
10	Vertical	29.3	325	100	Yes
11	Vertical	17.9	325	100	Yes
12	Vertical	17.9	325	100	Yes
13	Vertical	11.8	426	100	Yes
14	Vertical	11.8	325	100	Yes
15	Vertical	11.8	250	100	Yes
16	Vertical	4.9	426	100	Yes
17	Vertical	4.9	325	100	Yes
18	Vertical	4.9	250	100	Yes
19	Vertical	4.9	426	100	Yes
20	Vertical	4.9	325	100	Yes
21	Vertical	4.9	250	100	Yes

The tests were generally conducted with the rig in the vertical position and with the instrumented flange in the upper flange position. For Test 6 the rig was placed in the horizontal position with the thermocouples at the 180° (bottom) orientation. Tests 7 and

8 were also conducted in the horizontal position, but with the thermocouples in the 0° (top) and 90° (side) orientations respectively. Hardened washers were used under both nuts, except for Tests 1 and 2, when no washers were used at all. In all tests a 2.2mm thick metal-insert, graphite gasket was used.

2.2.2.2 Experimental results

Examples of the results for this experimentation are presented in Figures 2.21a to 2.22b. These figures demonstrate good agreement between the theoretical calculations and the obtained experimental results. Unfortunately, however, the internal heat transfer from the heating core to the flange was not constant. This was primarily due to the fact that during assembly of the test rig, it was not possible to exactly centre the flange over the heating core, which lead to an uneven gap between the core and flange resulting in a variable heat transfer. Additionally, the exact gas composition and therefore heat transfer rate could not be accurately controlled, as it was not possible to bleed the system prior to pressurisation.

In order to compensate for the variability of the internal heat transfer coefficient (h_i) the value used in the theoretical calculations was adjusted until the best fit with the recorded temperature data points for both the shell and flange were obtained. This ensured that the adjustment to the value was accurate, as one variable was being adjusted until two conditions were satisfied.

The accuracy and repeatability of the results is extremely good by comparison with the theoretical results. It can be seen from Figure 2.23 that the difference between the theory and the flange temperature readings does not exceed ±1.0% of the measured value for all 21 tests. This is incredible agreement, considering that the error of a J thermocouple is in the order of ±2.2°C (Omega, 1995) which is ±1% of the measured value in this case.

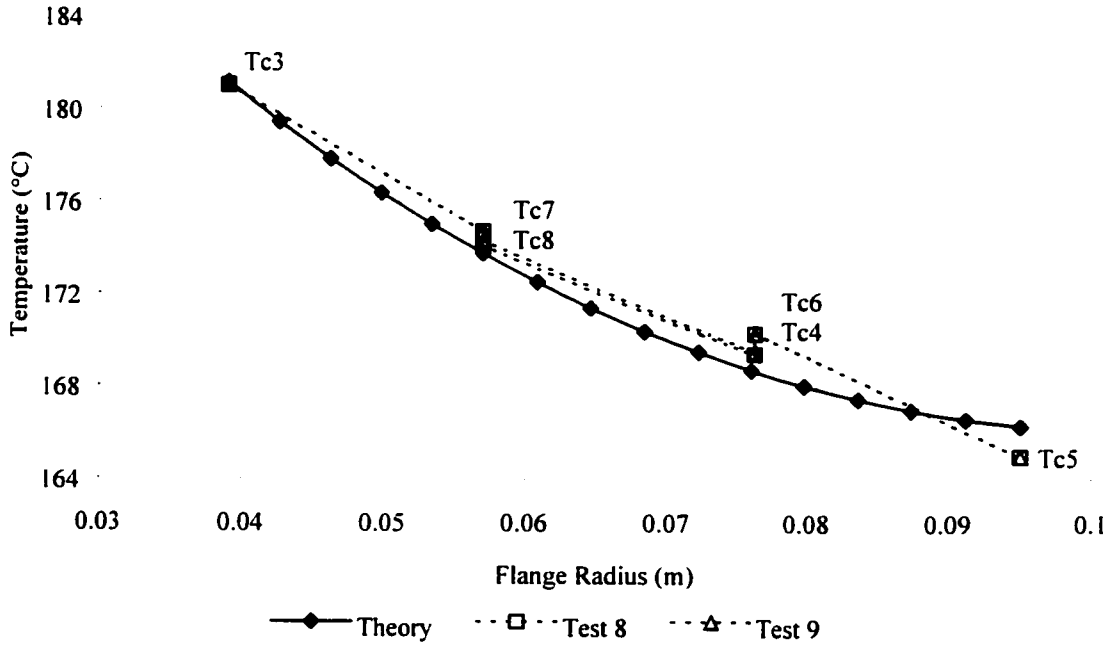

Figure 2.21a – Results of Tests 8 and 9 (flange profile)

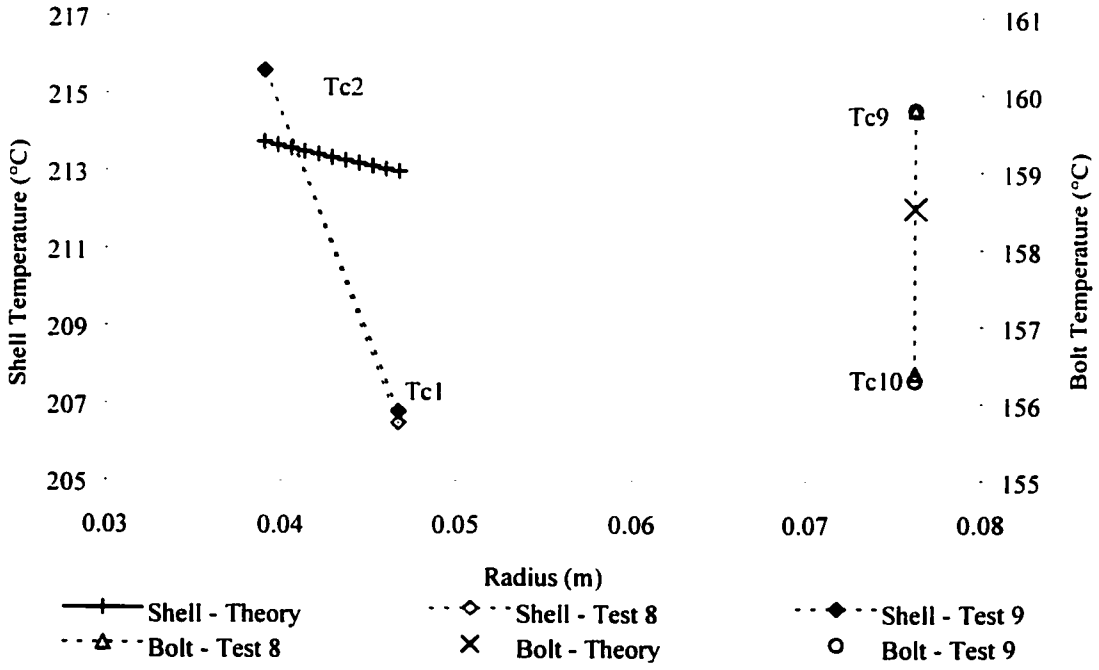

Figure 2.21b – Results of Tests 8 and 9 (shell & bolt)

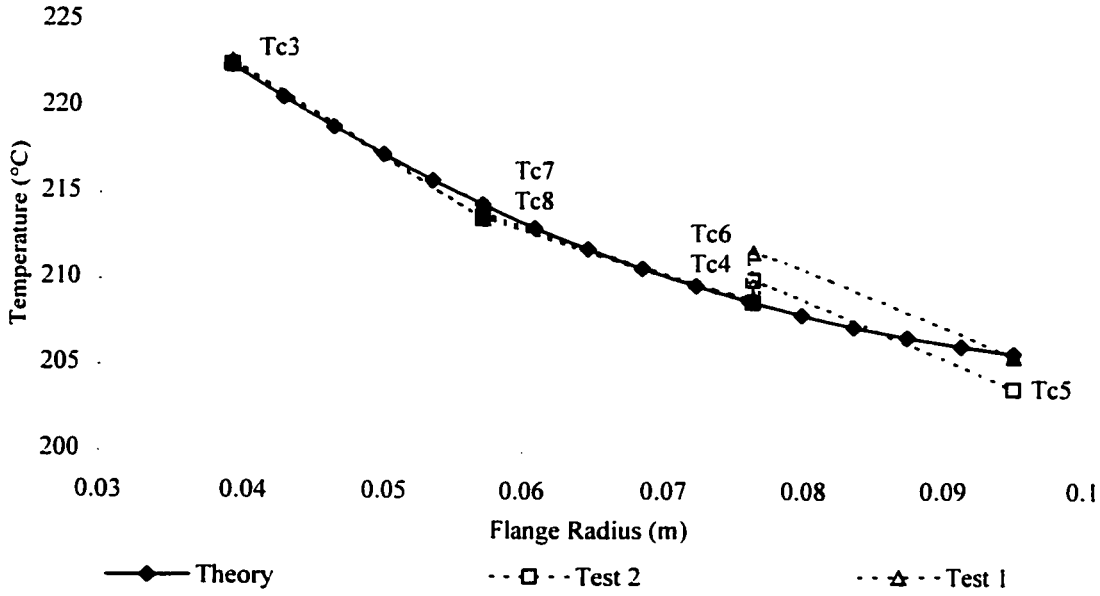

Figure 2.22a – Results of Tests 1 and 2 (flange profile)

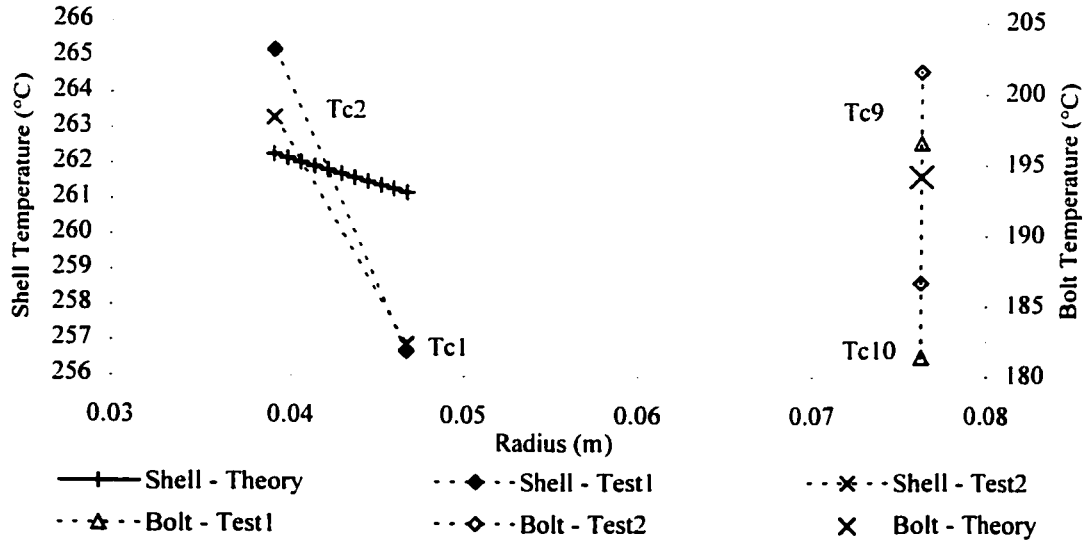

Figure 2.22b – Results of Tests 1 and 2 (shell & bolt)

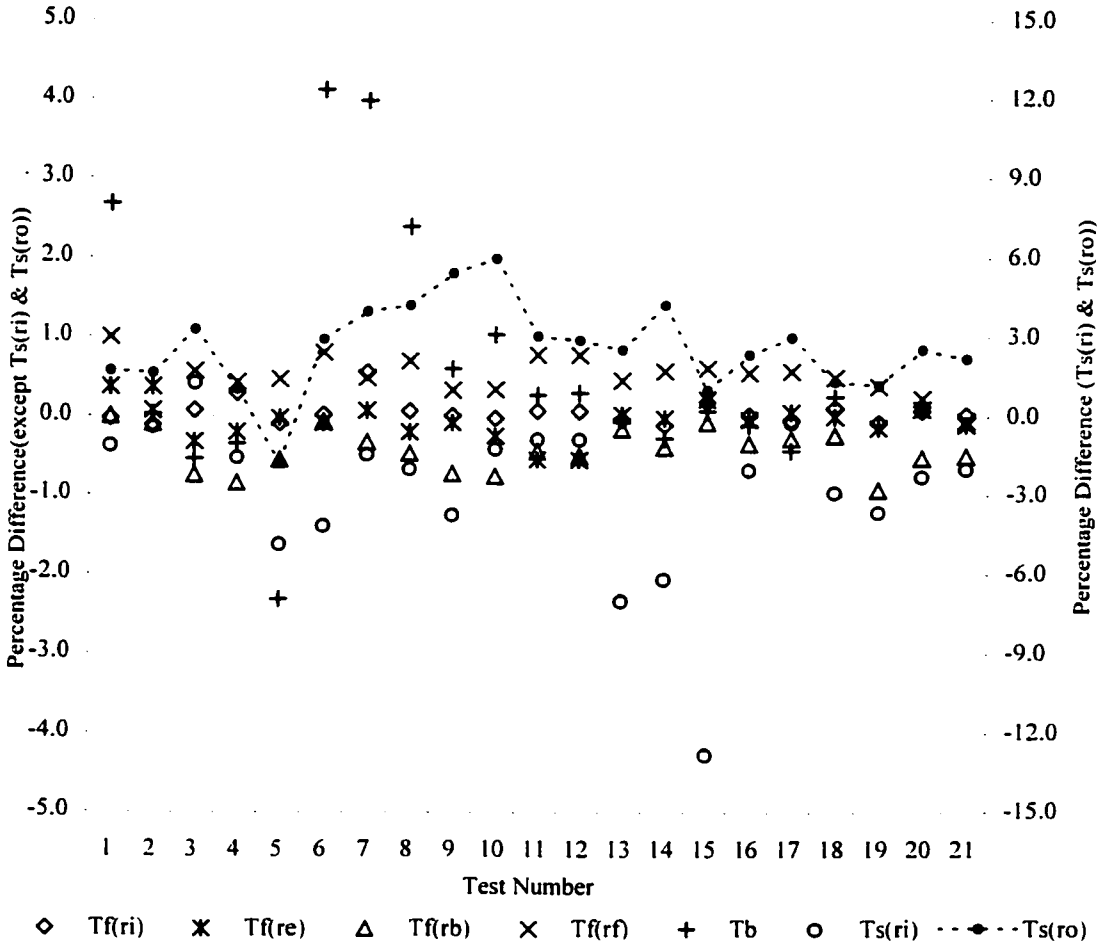

Figure 2.23 – Comparison of theory and experimentation (all tests)

The values for bolt temperature have a slightly higher difference, however in all cases it remains below 5%, which again is exceptionally good.

The shell temperature estimation was affected by the thermal interaction between the shell and the flange. The results detailed in Figure 2.23 show that in general the theory was within ±5% of the measured values. However on one occasion the difference was as high as 12%, which is most likely due to measurement errors in reading the shell temperature. In all cases the gradient through the shell wall as predicted by the theory is much lower than the measured gradient. This is thought to be due to the fact that the internal thermocouple on the shell wall was extremely close to the heating element (as evidenced by damage to the thermocouple insulation from the heating element). Thus causing an incorrect higher reading. However, as the gradient through the shell is not important in determining the mechanical interaction. As such this was not considered a problem that required further investigation.

The values also illustrate that the method of dealing with changing the gap between the flanges appears to be necessary. Without making this modification to the effective thickness, the calculated external film heat transfer coefficient (h_{os}) would be as high as 50% greater than the actual value. Hence it is clearly necessary to include the modification of the effective thickness with proportion to the gap in the calculation. Due to the fact that there appears to be no correlation between the changing gap and the obtained values of the external film heat transfer coefficient (h_{os}) it is therefore concluded that the suggested method of relating the effective thickness to the gap is sufficiently accurate.

Table 2.3 – Calculated external heat transfer coefficient values

est	1	2	3	4	5	6	7	8	9	10	11	12	13	14	15	16	17	18	19	20	21
h_{os}	25	25	27	19	19	21	21	20	20	20	22	22	27	24	23	28	26	23	26	23	22

Average h_{os} value = 23 W/(m².°C)
Standard Deviation = 2.8 W/(m².°C)
97.5% confidence interval = (21.7, 24.3) W/(m².°C)

The external film heat transfer coefficient (h_{os}) was calculated for each test by matching the theoretically calculated temperature profile and relation between the shell and flange temperatures with the experimental values. The calculated values are listed in Table 2.3:

The results are repeatable with a low confidence interval. The differences in values are most likely to be due to measurement and estimation inaccuracies. However another important aspect is the difference in the laboratory air-conditioning. During the period of the tests the laboratory was maintained at a constant temperature of 21.5 to 22°C, whilst the outside temperature varied from around 30°C to 19°C. Thus the air-conditioner operated at different levels during the different tests, leading to changing wind velocities around the test rig. This would have had an effect on the transfer coefficient.

There did not appear to be a difference in the external heat transfer coefficient (h_{os}) with relation to the changes in temperature or different orientations tested during this experimentation. The obtained value of around 23 W/(m².°C) is in good agreement with values appearing in earlier papers. Kern (1950) lists values of 28-39 W/(m².°C) (5-6.5 btu/(hr.ft².°F) for a temperature range of 500-700 °F) for heat transfer by convection and radiation from horizontal pipes in air. Codegone (1951) lists values of 8 to 29 W/(m².°C) for a heat transfer coefficient from a heated 32mm diameter pipe to an internal flow of air. Bickford et. al. (1989) utilised a value of 14.2 W/(m².°C) (2.5 Btu/(hr.ft².°F)) in their analysis of a large diameter reboiler flange.

A bolt contact coefficient of 3000 W/(m².°C) was used throughout the calculations and, as can be seen in Figure 2.23, the correlation between measured values and the theoretically calculated values is very good. However, for Tests 6, 7 and 8 the bolt temperature is over-estimated by the theory by 2.4% to 4.1%. These are the tests conducted in the horizontal position. It is therefore plausible to conclude that the heat loss from the bolts was higher in the horizontal position. However the effect is limited, less than 5%, and the value will be confirmed further in subsequent experimentation. It was therefore concluded that additional experimentation and theory to cover this effect

was not warranted. Changing the bolt load, within the given values, and removing the washers did not appear to affect the bolt temperature. It is thus reasonable to conclude that, for the normal operational service of a bolt in a pipe or exchanger joint, the given calculations and heat transfer coefficient are sufficiently accurate.

The obtained bolt contact heat transfer coefficient is in reasonable agreement with the overall magnitude of values appearing in earlier literature. However, the comparison between the literature and the obtained results is not completely accurate due to the fact that the values quoted in the literature are for plate-plate contact and for different materials to those used in the experimentation. Additionally a lubricant is used on the bolt and nuts when assembling a flange joint. These factors may alter the comparative conductance value. Nonetheless, it would be expected that the value obtained should at least be of the same order as those listed in the literature. Comparisons were made with the lower values of roughness and higher interfacial pressure quoted in the literature. This is due to the fact that with the tightening of a nut to the load values used for flange joints there is localised yielding at the interface. Hence the roughness is low and the interface pressure is high.

Ozisik (1985) quotes a value of 3,000 to 4,000 W/(m^2.°C) (roughness = 2.54μm) and 10,000 to 12,000 W/(m^2.°C) (roughness = 0.76μm) for contact between two stainless steel plates at temperatures between 93°C and 204°C. Mittlebach (1992) presents a good comparison with the research of others and indicates values between 5,000 W/(m^2.°C) and 20,000 W/(m^2.°C) for contact between aluminium plates. Krylov et. al. (1986) tests stainless steel interfacial contact with interfacial pressures in excess of the yield point of the material. The listed values are from 6,200 W/(m^2.°C) to 67,000 W/(m^2.°C) for interfacial pressures below yield and up to 82,660 W/(m^2.°C) for pressures above yield (the coefficient increases with increasing pressure). The obtained value would thus seem lower than perhaps may be expected. However, the additional resistance provided by the lubricant and also the fact that the bolt to flange path contains two interfaces (one at the

nut/flange interface and the other at the nut/bolt thread interface) may easily explain this difference.

2.2.3 Comparison with site data

The laboratory experimentation performed in Section 2.2.2 served to confirm the accuracy of the equations and to establish values for the external heat transfer coefficient (h_{os}) and the bolt/flange interface transfer coefficient (h_{cb}). However, this only confirms the accuracy of the equations for small diameter carbon steel flanges in a laboratory environment. It was thus necessary to examine the thermal profile of larger diameter flanges and also flanges manufactured from different materials, in an industrial environment, to further verify the accuracy of the theory.

To achieve this verification a series of temperature measurements were taken from flanges operating at the Chevron El Segundo refinery. All flanges were located on heat exchangers operating in the coker and crude unit of the refinery (Figures 2.24 and 2.25).

2.2.3.1 Test procedure description

The temperature of a range of flanges was measured at the shell, the base of the hub, the bolt pitch circle diameter, the outer diameter of the flange, the nut and the bolt head. The measurements were taken using a Raytek ST4L infrared temperature probe. The listed accuracy of this instrument is ±2% of the reading or ±2°C, whichever is greater. In addition to this error however, the emissivity of the material being measured must be entered for this accuracy to be achieved. A value of 0.9 was determined for the flanges being measured by comparison of painted areas and bare steel areas as per the procedure listed in the Raytek manual. In general, for the outer regions of the flange and stud bolts and nuts the reading was taken at a distance of only 50mm, hence the sampling diameter of the reading was less than 10mm. However for the hub reading and shell reading the

Figure 2.24 – Coker unit exchangers

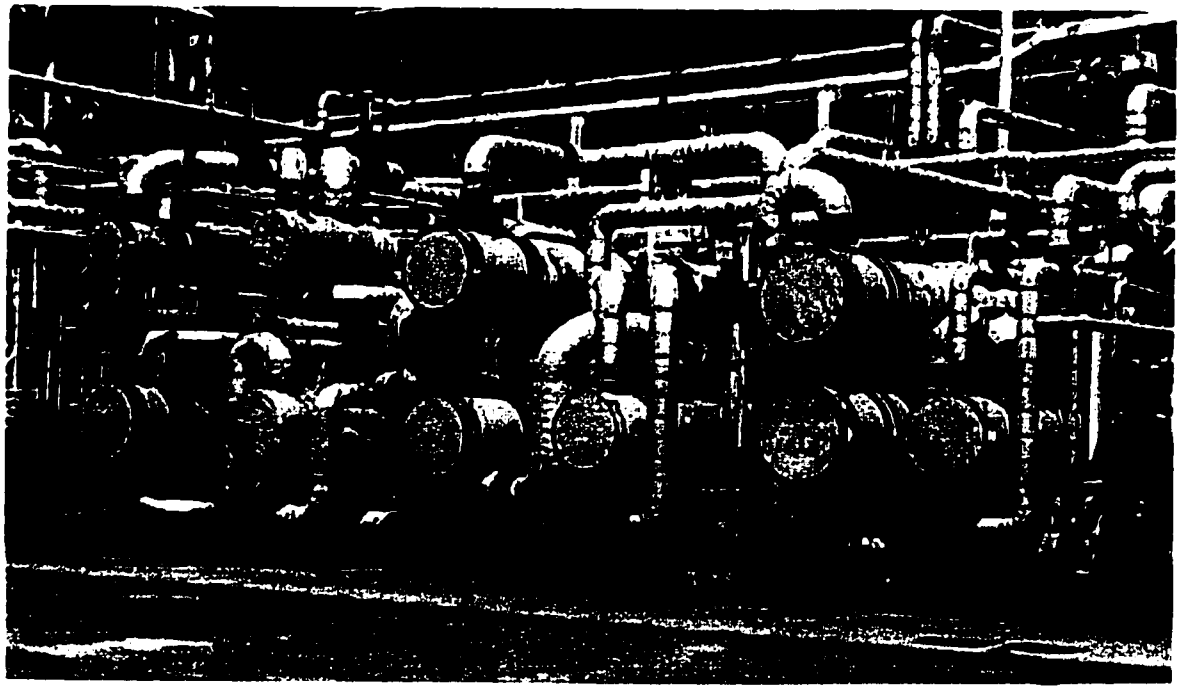

Figure 2.25 – Crude unit exchangers

distance was greater, around 150mm, due to space constraints. The sampling diameter is around 20mm for this distance.

The process operating conditions for the exchangers were taken from the refinery process control unit. Unfortunately the accuracy of this system in measurement of the process temperatures could not be assured as better than ±10%. This is due to the fact that the temperature transmitter was often not located next to the exchanger, but on piping several meters away or on the first exchanger of a bank of two or three, of which the measured exchanger was the last unit.

Thus, as is normal with site measured values due to the higher number of variables, the error involved in the readings was in excess of ±10%. However, it is the trend of the data and in particular the relationship between the flange, bolt and shell temperatures that are particularly important to this study. This is because it is the difference in the temperatures of the joint components that creates the driving force for mechanical deformation, rather than the overall magnitude.

The measurements were compared with both the theoretical method and finite element method. For the theoretical calculations the fluid properties were taken from the heat exchanger design datasheets. The internal film transfer coefficient (h_i) was calculated in accordance with Equation 2.52, taken from Kern (1950) for turbulent flow in a pipe. The flange details, operating temperature and calculated film coefficient are detailed in Table 2.4.

$$h_i = \frac{k}{2 \cdot r_i} \cdot 0.027 \cdot (R_e)^{0.8} \cdot (P_r)^{\frac{1}{3}} \cdot \left(\frac{\mu}{\mu_w}\right)^{0.14} \qquad 2.52$$

The size of the flange ranges from NPS 150mm (6 inch) class 300 ASME B16.5 flanges to 1m (40 inch) diameter heat exchanger flanges. The material varies from Carbon-Silicon Steel (ASTM A-105 material, as per the previous section) to 2% Chromium-

Table 2.4 – Site data joint details

Ident.	Flange	I.D. (m)	Material	k_s	Fluid	Fluid Temp.	w (g/sec)	h_i (W/m².°C)
E506Cin	6" cl.300 RF WN	0.1524	SA-105	47	Sponge Oil	176°C [1,4]	6,906	633
E506Cout	6" cl.300 RF WN	0.1524	SA-105	47	Sponge Oil	116°C [1,4]	6,906	633
E506Sin	6" cl.300 RF WN	0.1524	SA-105	47	Rich Sponge Oil	68°C [2,5]	3,958	373
E506SCF	29"ID, 35" OD WN	0.740	SA-105	47	Rich Sponge Oil	110°C [2,5]	3,958	407
E506SCC	29"ID, 35" OD WN	0.740	SA-105	47	Rich Sponge Oil	110°C [2,5]	3,958	407
E512Cin	10" cl.300 RF WN	0.254	SA-105	47	Heavy Naptha	199°C	18,727	670
E512Cout	10" cl.300 RF WN	0.254	SA-105	47	Heavy Naptha	171°C [3,6]	18,727	597
E512SCF	35"ID,41.4"OD WN	0.889	SA-105	47	Light Gas Oil	160°C [3,6]	9,223	498
E512SCC	35"ID,41.4"OD WN	0.889	SA-105	47	Light Gas Oil	160°C [3,6]	9,223	498
E515Cin	10" cl.300 RF WN	0.254	SA-182 GR5	33	Heavy Gas Oil	271°C	17,557	431
E515Sin	10" cl.300 RF WN	0.254	SA-105	47	Heavy Gas Oil	206°C	9,015	253
E535Cin	10" cl.300 RF WN	0.254	SA-182 GR5	33	Heavy Gas Oil	288°C [7]	18,727	454
E541Cout	10" cl.300 RF WN	0.254	SA-105	47	Heavy Gas Oil	188°C	31,499*	688
E1109Cout	6" cl.300 RF WN	0.1524	SA-105	47	Heavy Gas Oil	227°C	4,492	363
E1110Cin	12" cl.600 RF WN	0.3048	SA-105	47	A.L. Crude	210°C	53,192	669
E1111Cout	10" cl.300 RF WN	0.254	SA-105	47	Atm. Bot. C R	313°C	10,635	316
E1165Cin	18" cl.600 RF WN	0.4318	SA-182 GR5	33	A.L. Crude	284°C	26,178	230

* = Estimated

[1] = Estimated from API 40 Hydrocarbon from TEMA (1991)

[2] = Estimated from API 50 Hydrocarbon from TEMA (1991)

[3] = Estimated from API 30 Hydrocarbon from TEMA (1991)

[4] = Estimated from a 213°C inlet to Exchanger A, and outlet from B estimated at 107°F from Datasheet

[5] = Estimated from a 160°C outlet to Exchanger A, and inlet from B estimated at 68°C from Datasheet

[6] = Estimated from a 192°C inlet to Exchanger and from Datasheet information

[7] = Estimated from a 329°C inlet to Exchanger A, and outlet from B at 482°F from Datasheet

[8] = Calculated from area between floating head cover outside diameter and flange internal diameter

E.... = Heat Exchanger Identification Number

...Cout, ...Cin = Outlet from, Inlet to Exchanger Channel

...Sout, ...Sin = Outlet from, Inlet to Exchanger Shell

...SCF, ...SCC = Shell Cover Flange - Shell Side, cover Side

0.5% Molybdenum Steel (ASTM A182-GrF5 material, k_f = 0.033 W/(m.°C), α_f = $1.25x10^{-5}$ m/m/°C, E_f = 190,000 MPa, ASME, 1998a).

A FEA model was constructed for the E512Cin and E506Sin flanges for comparison with the theoretical results. A plot of the FEA models are shown in Figures 2.26 and 2.27 respectively.

2.2.3.2 Site data comparison

A comparison between the recorded temperatures and theoretically calculated temperatures was performed. Figures 2.28a to 2.29b give a comparison between the measurements, the results from the analytic equations and the FEA results. The previously determined values for heat transfer coefficients (h_{os} = 23 W/(m².°C) and h_{cb} = 3000 W/(m².°C)) were used in all FEA and analytical calculations. As expected, due to the greater amount of variables involved in taking the site data, the agreement between the theory and measured values is not as close as the laboratory experimentation.

The slope of the measured temperatures appears to be much higher for these flanges, however this is due to the previously mentioned fact that when measuring the temperature at the hub base the sample area was around 20mm diameter. From the outer surface profile of the FEA results in Figure 2.28a it can be seen that by taking a point 20mm higher than the hub base the indicated temperature will be 2.8°C higher than the hub base. This means that due to the sampling method the hub base point will always indicate a higher value than the actual value.

This problem is evident in the results and appears as the measured values for $T_f(r_e)$ being around 15% higher than the theoretically calculated values (refer to Figure 2.30). When the values of $T_f(r_e)$ are not included, due to the aforementioned error, the accuracy of the results becomes quite good. For the flange temperatures the theoretically calculated values are all within ±5% of the measured values. This is thought to be excellent

agreement, given the possible sources of error associated with the site data measurement. The theoretically calculated values for bolt and shell temperatures were within ±10% of the measured values. This higher error is thought to be primarily due to the additional difficulty involved in taking these measurements. In comparison with the flange measurements, which were highly repeatable in different areas of the flanges, the shell and bolt temperatures were less repeatable, with a range of ±5% of the reading between the bolts and between different locations on the shell being evident.

Additionally it can be seen that there does not appear to be a trend in the data with respect to the size of the flange or to the material of the flange. It can therefore be stated that the outlined theory appears sufficient in accounting for these two factors, in the size and material range that was tested. In general, given the levels of inaccuracy involved in the temperature measurement of both the joint components and the fluid flow, the theoretical results give good agreement with the site measurements, thus further verifying the accuracy of the established theory.

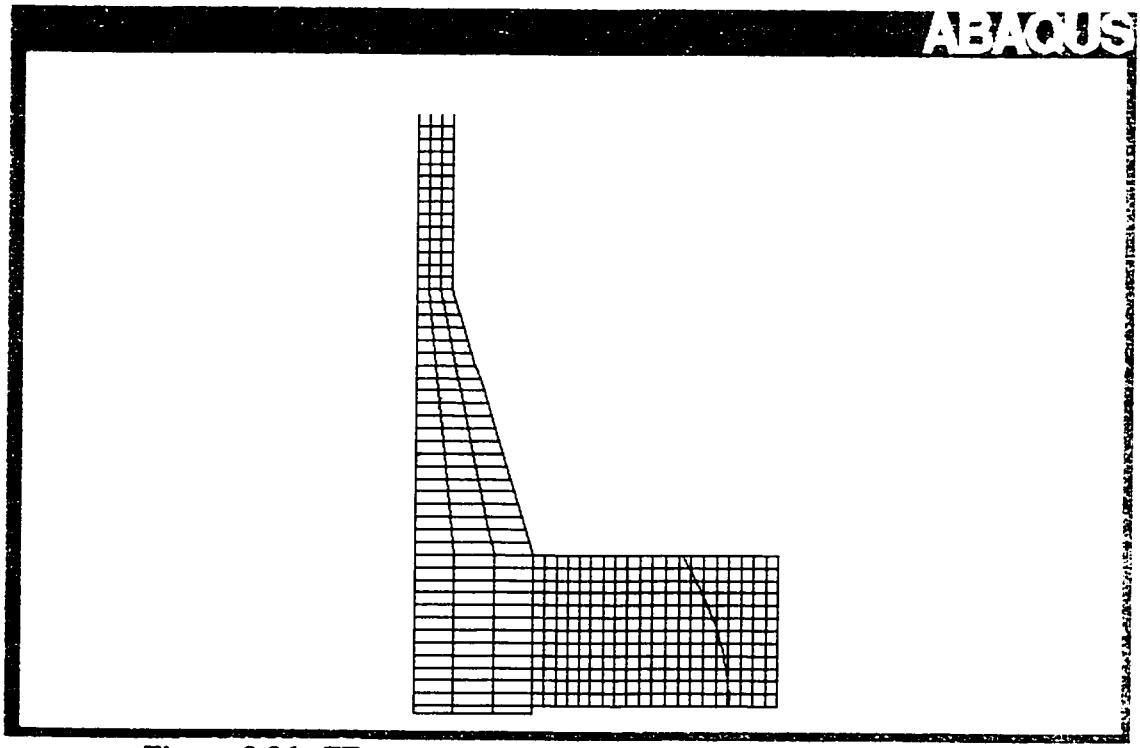

Figure 2.26– FEA model of the 10 in. cl.300 RF WN (E512Cin)

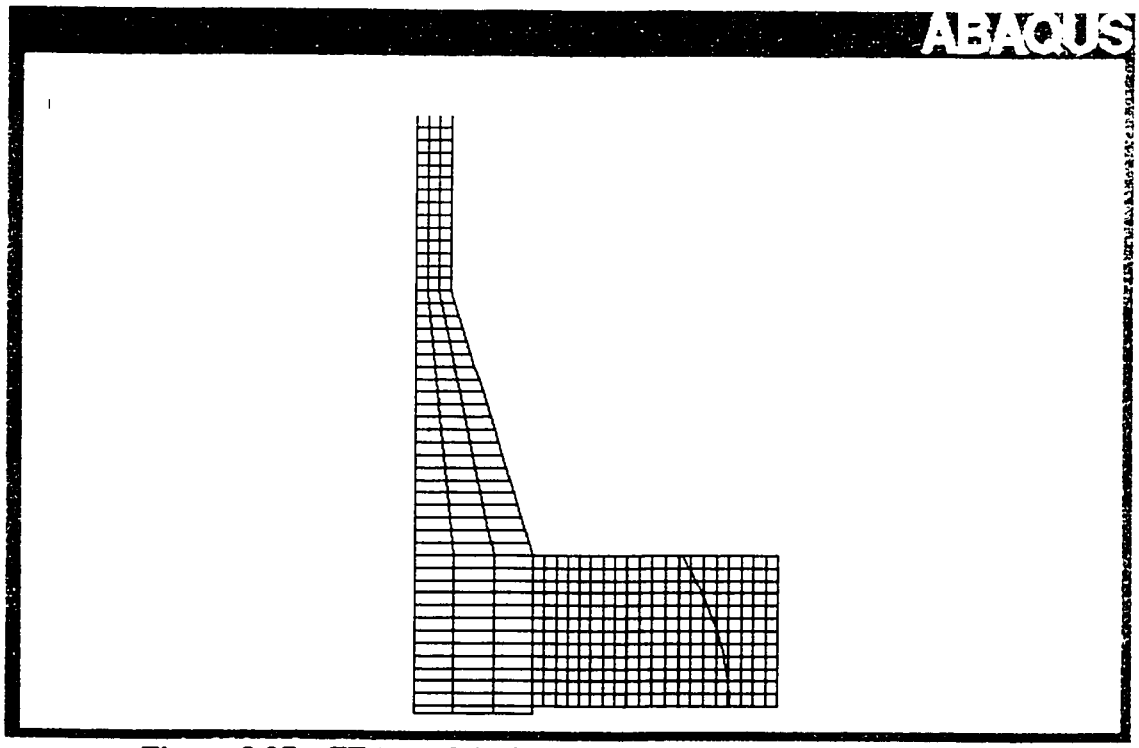

Figure 2.27 – FEA model of the 6 in. cl.300 RF WN (E506Sout)

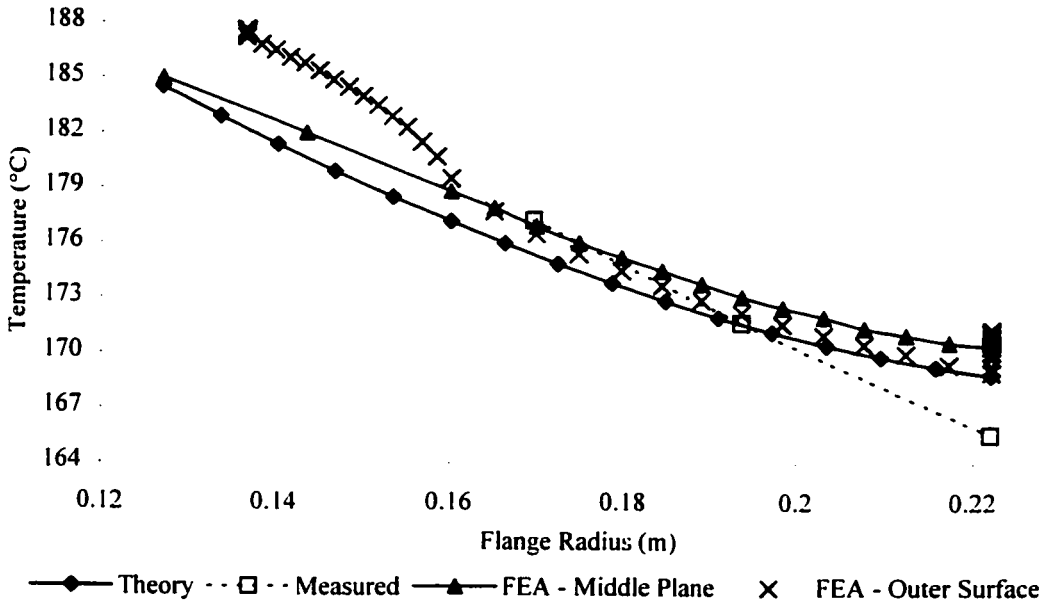

Figure 2.28a – Results for E512Cin (flange profile)

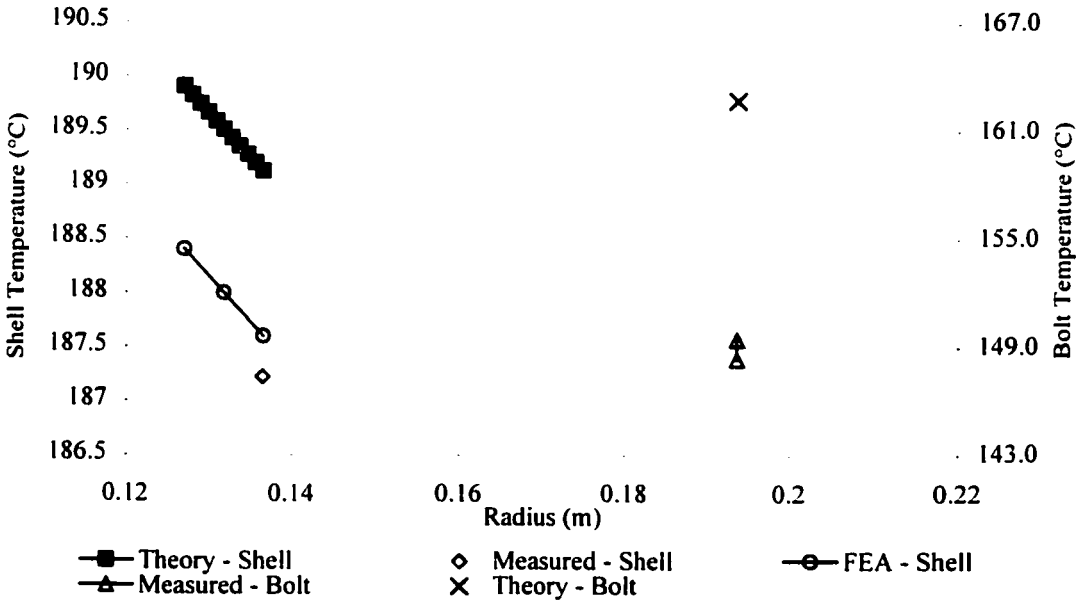

Figure 2.28b – Results for E512Cin (shell & bolt)

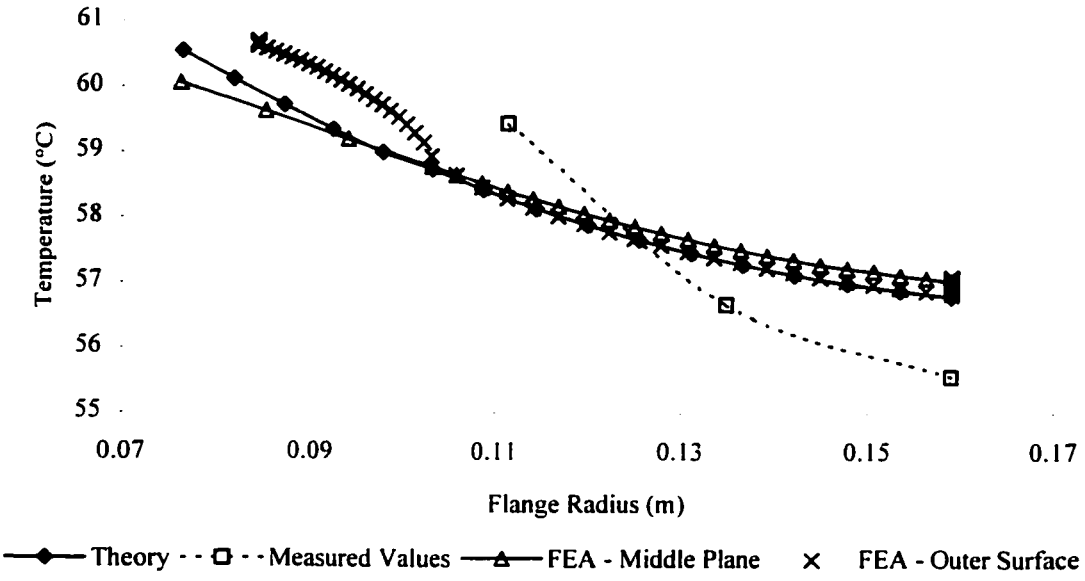

Figure 2.29a – Results for E506Sout (flange profile)

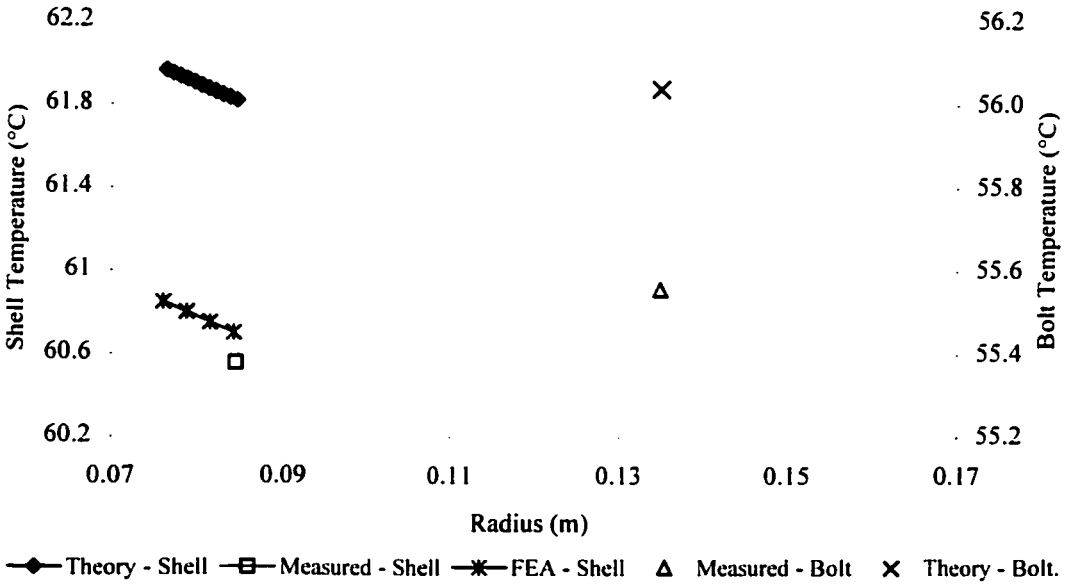

Figure 2.29b – Results for E506Sout (shell & bolt)

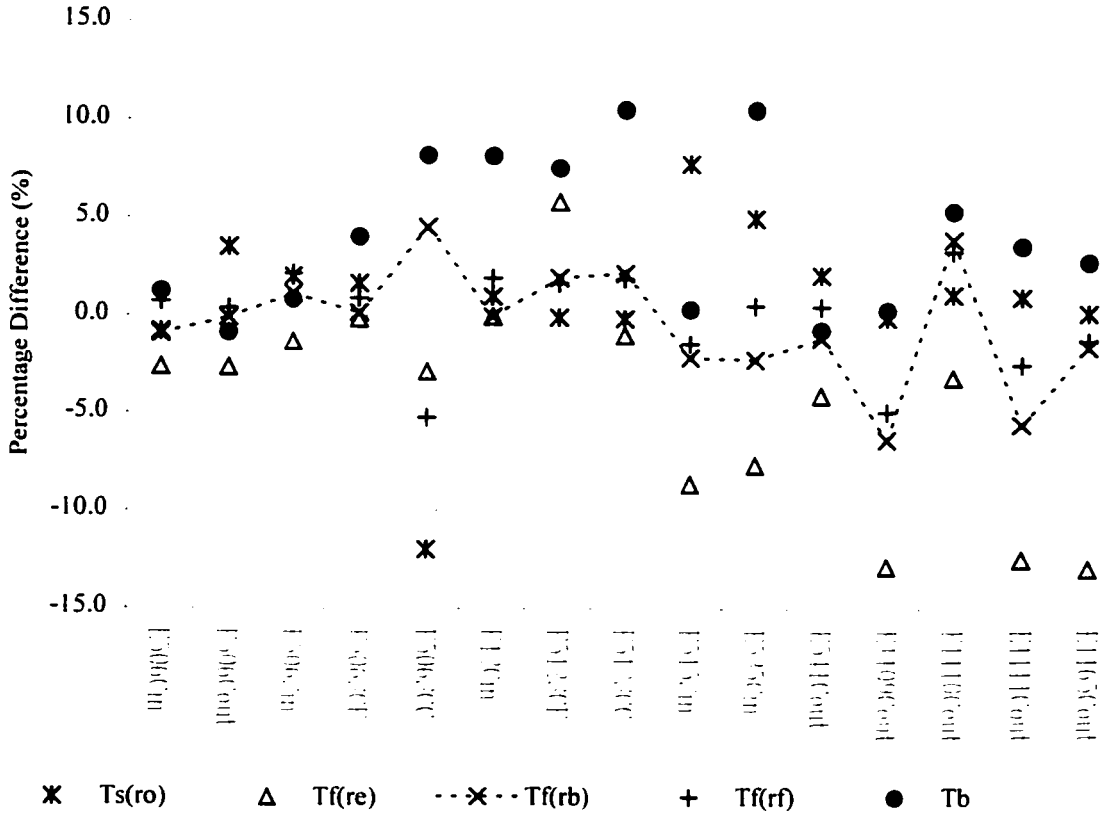

Figure 2.30 – Comparison of theory and site measured temperatures (all flanges)

CHAPTER 3

STEADY STATE MECHANICAL INTERACTION ANALYSIS

3.1 Analytic method

Due to the fact that the flange ring acts, essentially, as a cooling fin for the vessel shell, there is a thermal gradient in both the axial and radial directions, as can be seen in Figure 3.1. In order to accurately model the resulting flange deflection by analytical methods, one would need to examine the effect of the thermal gradients in all directions by using suitable axisymmetric thermoelastic analysis, such as that presented in Parkus (1976).

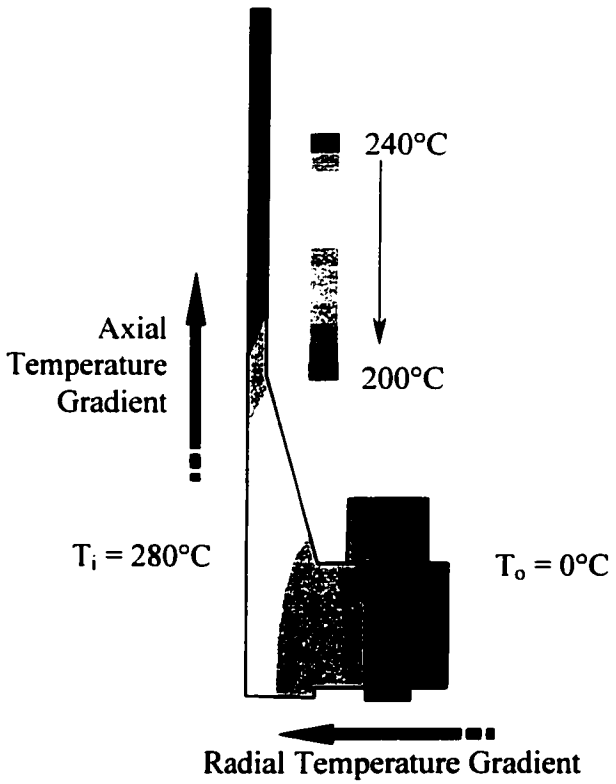

Figure 3.1 – Typical flange temperature profile

However, this creates an excessively complex elastic analysis and also necessitates an extremely complex thermal analysis. Such analysis would be unworkable in a flange design situation. It is possible, however, to create a simplified analysis which examines only the gross thermal deformations of the components and which still gives a sufficiently accurate solution. The three basic gross component deformations due to the thermal gradients are as listed below and further explained in Figure 3.2:

1. Differential axial expansion of the components due to the radial temperature gradient. These relative expansions are calculated using the equations presented previously in Section 2.1.
2. Differential radial expansion of the vessel wall and hub versus the flange ring. This differential expansion is caused by the axial temperature gradient and induces a rotation of the flange ring. It may be approximated as an equivalent pressure loading, calculated per Equation 2.30.
3. Differential radial expansion of the hub versus the flange ring, caused by the radial temperature gradient in the flange ring. The decreasing radial temperature gradient in the flange ring constricts the radial expansion of the inner section of the flange ring, relative to the hub. This causes a resulting shear force and moment at the flange/hub interface, consequential rotation of the flange and therefore a decrease in the bolt load.

The thermal deformations discussed above in Items 1 and 2 may be directly incorporated into the existing joint interaction equations. However, the differential expansion between the hub and flange requires additional calculations to determine the influence of the deflections. The differential radial expansion between the hub and flange ring imparts a moment and shear force onto the flange ring, which causes rotation of the ring and subsequent bolt load loss. The amount of rotation is proportional to the differential expansion and also to the relative rigidities of the flange ring and the hub section.

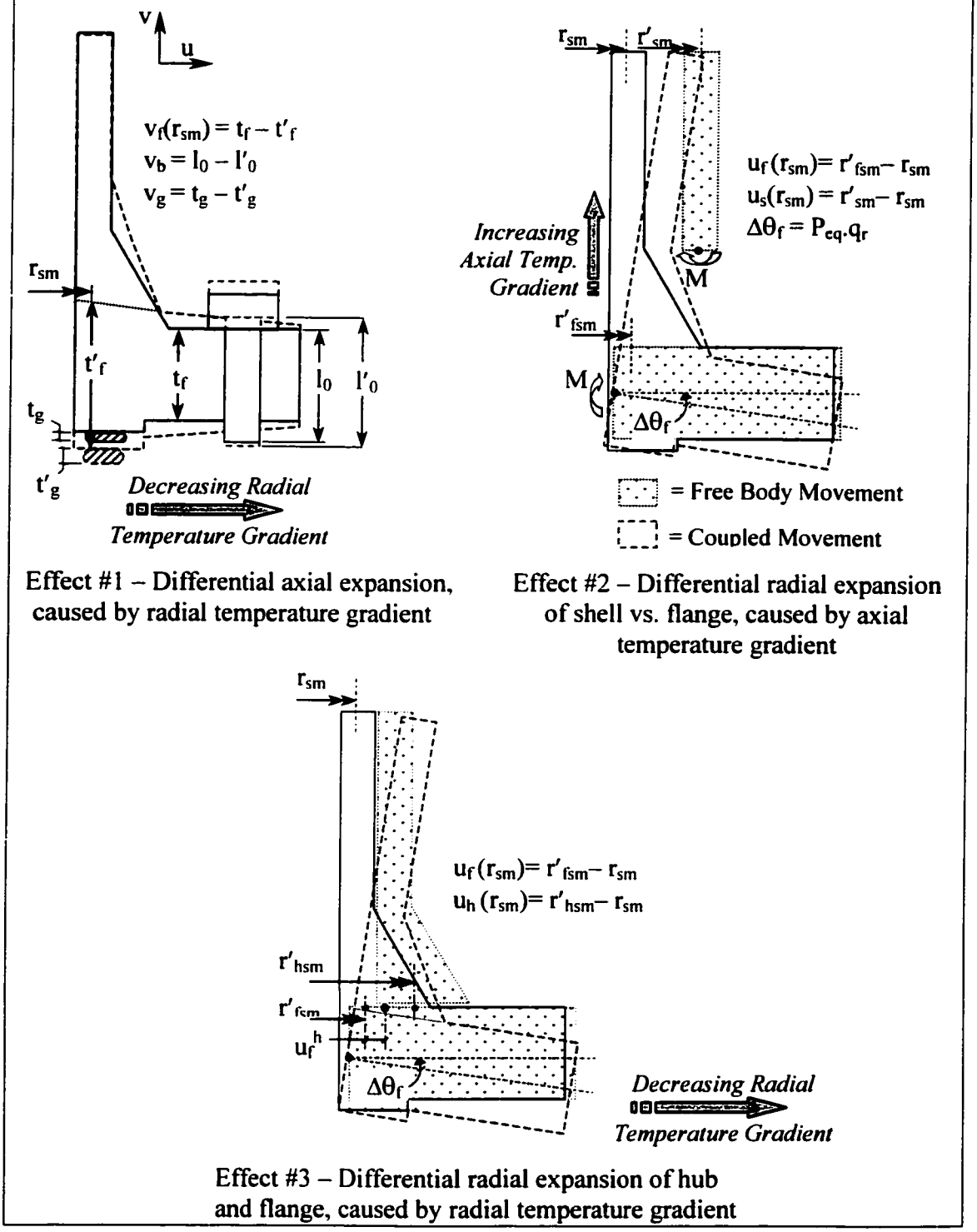

Effect #1 – Differential axial expansion, caused by radial temperature gradient

Effect #2 – Differential radial expansion of shell vs. flange, caused by axial temperature gradient

Effect #3 – Differential radial expansion of hub and flange, caused by radial temperature gradient

Figure 3.2 – Mechanical effects of joint temperature distribution

The radial deflection of the flange ring at the middle radius of the shell ($u_f(r_{sm})$) is determined using Equation 2.28. The hub is then assumed to be at a uniform temperature equal to the flange ring temperature and the following thin cylinder equation is used to determine what the approximate free expansion of the hub would be at the middle radius of the shell.

$$u_h(r_{sm}) = \alpha_f \cdot T_f(r_{sm}) \cdot r_{sm} \qquad 3.1$$

The hub is assumed to be a semi-infinite hollow cylinder of wall thickness proportional to the shell thickness and the hub thickness, modified with respect to the hub height, as defined by Lake, et. al. (1957).

If $h_0 < (B\ g_0)^{1/2}$ then

$$t_h = t_s + \frac{h_0}{\sqrt{2Bg_0}}(g_1 - t_s) \qquad 3.2a$$

Otherwise if $h_0 \geq (B\ g_0)^{1/2}$ then

$$t_h = 0.5(g_1 + t_s) \qquad 3.2b$$

The relative rigidity of the combined hub and shell, with respect to resisting the shear and moment applied to it by the flange ring, may be determined from equations for a distributed radial force and an end moment acting on a semi-infinite hollow cylinder from Timoshenko(1940). The effect of the shear and moment on the flange ring may be determined by using the equations outlined in Waters et. al.(1949). The flange is therefore separated into two components, flange ring and the hub/shell, and the force and moment balance diagram is defined as in Figure 3.3.

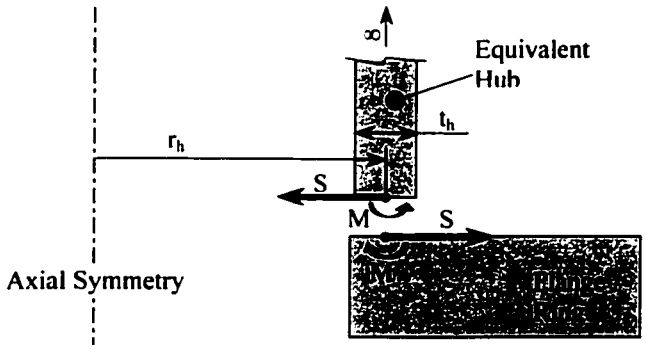

Figure 3.3 – Force and moment balance diagram

Thus, in accordance with the directions defined in Figure 3.3, the equations for radial and rotational deflection can be defined as below for each of the components.

1) Hub/Shell:

$$u_h = (\beta M - S)/2\beta^3 D + u_h(r_{sm}) \tag{3.3}$$

$$\theta_h = (S - 2\beta M)/2\beta^2 D \tag{3.4}$$

where:

$$\beta^4 = 3(1 - \nu_s^2)/(r_h t_h)^2 \tag{3.5}$$

$$D = (E_f t_h^3)/(12(1 - \nu_s^2)) \tag{3.6}$$

2) Flange Ring

$$u_f = \frac{3B\zeta}{E_f t_f^2} M + \frac{B\zeta}{E_f t_f} S + u_f(r_{sm}) \tag{3.7}$$

$$\theta_f = \frac{6B\zeta}{E_f t_f^3} M + \frac{3B\zeta}{E_f t_f^2} S \tag{3.8}$$

where:

$$\zeta = \frac{K^2(1 + \nu_f) + (1 - \nu_f)}{(K^2 - 1)} \tag{3.9}$$

From the component displacement and rotation conditions at the interface, we know the following:

$$u_f = u_h \tag{3.10}$$

and

$$\theta_f = \theta_h \tag{3.11}$$

Therefore it is possible to solve Equations 3.3, 3.4, 3.8 and 3.9 simultaneously and find the following relationships:

$$S = \frac{(u_h(r_{sm}) - u_f(r_{sm}))}{\left(\frac{B\zeta}{E_f t_f} + \frac{1}{2\beta^3 D} - \left(\frac{1}{2\beta^2 D} - \frac{3B\zeta}{E_f t_f^2}\right)^2 \Big/ \left(\frac{6B\zeta}{E_f t_f^3} + \frac{1}{\beta D}\right)\right)}$$

3.12

$$M = \frac{S\left(\frac{1}{2\beta^2 D} - \frac{3B\zeta}{E_f t_f^2}\right)}{\left(\frac{6B\zeta}{E_f t_f^3} + \frac{1}{\beta D}\right)}$$

3.13

Substituting these values for S and M into Equation 3.8 the rotation of the flange ring, due to Effect #3, is obtained. The final axial deflection of the flange ring at the bolt circle may then be determined from geometry, assuming that the flange ring remains undeformed and rotates around the mid-plane of the section:

$$v_f^h = \theta_f h_g$$

3.14

The resulting axial displacement of the flange at the bolt circle (v_f^h) determined in Equation 3.14 can therefore be incorporated into the joint interaction equations in the same way as the component axial expansions calculated in Section 2.1.

The presented analysis of the elastic interaction follows the original work from Waters et.al.(1949) and therefore makes the same assumptions as the analysis of Waters. Additionally, the following assumptions were made to facilitate simplification of the thermoelastic analysis:

a) That the axial temperature gradient along the vessel shell can be approximated by a distributed force (equivalent pressure) acting on the vessel wall. This approximation

is made possible due to the fact that the deformed shape generated by the thermal expansion is similar to that caused by internal pressure, as the two are directly dependent on the thickness of the vessel wall.

b) That the thermal gradients are axisymmetric in nature and, additionally, the thermal gradients within the individual joint components in the radial and axial directions may be neglected, as their effect is proportionally much smaller than the effects of the gross thermal deformations of the components.

c) For the calculation of the effect of the differential radial expansion of the hub versus the flange ring, the hub may be assumed to be at a uniform temperature equal to the temperature of the flange ring at the middle radius of the shell.

d) That the effect of the flange raised face in balancing the rotation of the flange caused by the differential radial expansion of the hub/flange may be neglected.

e) That the expansion of the bolt may be calculated using the length of the bolt between the two outer flange faces prior to loading the bolt. The actual distance would be the length between the flange faces in the loaded state (including gasket deflection and flange rotation due to the initial bolt preload). However, this necessitates knowledge of the level of flange deflection prior to performing the calculation, which is not always possible.

Assumption b), may not necessarily be conservative, as the axial gradient within the flange ring may induce flange rotation. However, the remaining assumptions are all conservative, indicating that the obtained change in bolt load using the outlined analytical method should generally predict an accurate or lower level of bolt stress than would actually occur.

The theory outlined in this paper is a continuation of the work presented in Wesstrom et.al. (1951). The calculated thermal deflections are added into the mechanical interaction equations and the theory developed in a similar manner to the original paper. The modified basic equations are listed below, along with the corresponding numerical

reference from the original Westrom et.al. (1951) paper. The nomenclature used follows that of the original paper, with additional terms defined as required.

The approach of the original paper was to determine the component compliances and component deflections and then, from this, the resulting component forces. When thermal deflections are included, the component deflection equations become as below (ref. Westrom et.al. (1951) – Equation 3.14) in Equation 3.15. The locations of these dimensional terms on the joint are detailed in Figure 3.4.

$$\left.\begin{array}{lll} l_2 = l_0 + q_b \cdot W_2 + v_b & ; & l_1 = l_0 + q_b \cdot W_1 \\ v_2 = v_0 + q_g \cdot H_{G2} + v_g & ; & v_1 = v_0 + q_g \cdot W_1 \\ \delta_2 = q_f \cdot M_2 \cdot h_G + v_f + v_f^h + h_G \cdot q_r \cdot (P + P_{eq}) & ; & \delta_1 = q_f \cdot M_1 \cdot h_G \end{array}\right\} \quad 3.15$$

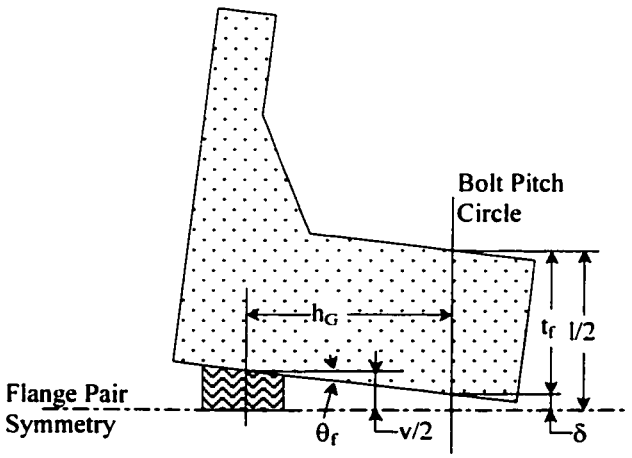

Figure 3.4 – Mechanical interaction diagram

Note that the last term of δ_2 accounts for the effect of shell/flange differential radial expansion as defined by Rodabaugh in the discussion section of Wesstrom et.al. (1951). These equations may then be developed. by summation of the above listed displacements and substitution of the previously defined loads as outlined in Equations 3.16 and 3.17.

$$l_2 - l_1 = v_2 - v_1 + 2(\delta_2 - \delta_1) \tag{3.16}$$

$$q_b(W_2 - W_1) = q_g(H_{G2} - W_1) + 2\left(q_f(M_2 - M_1)h_G + v_f + v_f^h + h_G q_r(P + P_{eq})\right) + v_g - v_b \tag{3.17}$$

The expression for M_1 and M_2 terms (flange ring moments) can be found in Wesstrom (1951). Once the terms are collected the final equation for identical flanges with respect to the effect of pressure and temperature on the bolt load (original paper Equations 20 and 53) can be determined as below in Equations 3.18 to 3.20:

$$W_2 = W_1 + \alpha_p \cdot P + \left(2 \cdot \left(v_f + v_f^h\right) + v_g - v_b - 2q_r h_G P_{eq}\right)/Q \tag{3.18}$$

where:

$$\alpha_p = \frac{\pi \cdot h_G}{4 \cdot Q}\left[\frac{q_g}{h_G}G^2 - 2 \cdot q_f\left(G^2(h_T - h_G) + B^2(h_D - h_T)\right) - \frac{8 \cdot q_r}{\pi}\right] \tag{3.19}$$

and

$$Q = \left(2q_f h_G{}^2 + q_b + q_g\right) \tag{3.20}$$

From Equation 3.18 the resulting bolt and gasket stresses may be determined and therefore the steady state effects of both pressure and temperature on the joint operation are fully defined.

3.2 Analysis verification

The analytical method was verified by comparison with finite element analysis and also by comparison with bolt stress measurements from an operational heat exchanger joint.

3.2.1 Finite element method

The finite element analysis was performed using the ABAQUS general finite element analysis program (ABAQUS, 1999). An axisymmetric model of 4 different flange types, a standard ASME NPS 14 inch class 150 RFWN flange, a standard ASME NPS 16 inch class 600 RFWN flange and two heat exchanger type flanges (37 inch and 24 inch shell diameters) were constructed. The dimensions of the two heat exchanger type flanges are detailed in Figures 3.5 and 3.6. The models used 4 node axisymmetric elements (CAX4) for the flange and tubesheet (where applicable) and plane strain elements (CPS4) to model the bolts. The gasket elements used were 4 node gasket elements, with thickness direction behaviour only, (GKAX4N) from the ABAQUS program. These elements allow accurate modelling of the non-linear elastic properties of the gasket. The bolt/flange and gasket/flange interfaces were modelled as contact surfaces with rough friction preventing relative movement. The bolt hole area had modified elastic properties to reflect the reduction of rigidity due to the presence of the bolt holes, in accordance with the philosophy for treating the residual strength of perforated plates in ASME (1998b).

The analysis was completed as an uncoupled temperature/deflection calculation, due to the fact that the ABAQUS gasket elements cannot be included in a coupled temperature/deflection analysis. The nodal temperatures were determined by using a modified model, with axisymmetric elements in place of the gasket and bolt elements. The heat transfer film coefficients on the bolt surfaces were reduced to represent the actual heat transfer surface area, as opposed to the larger modelled axisymmetric surface

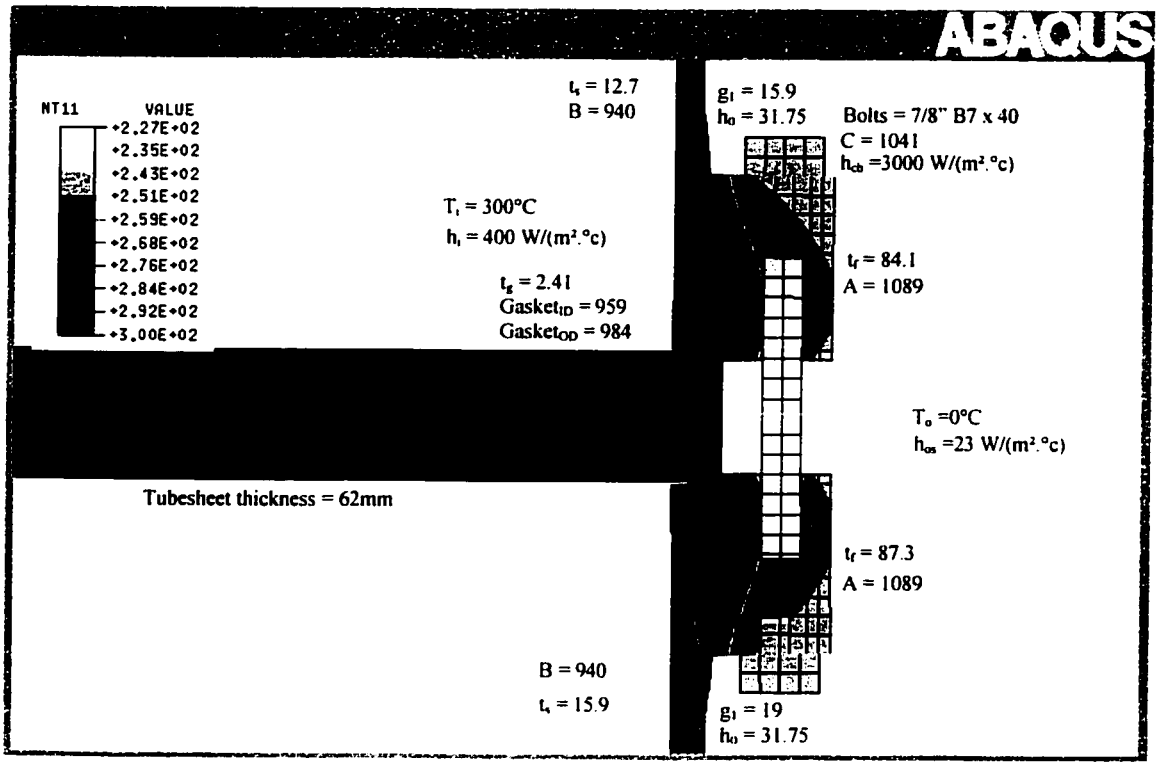

Figure 3.5 – 37" Flange FEA model: temperature distribution

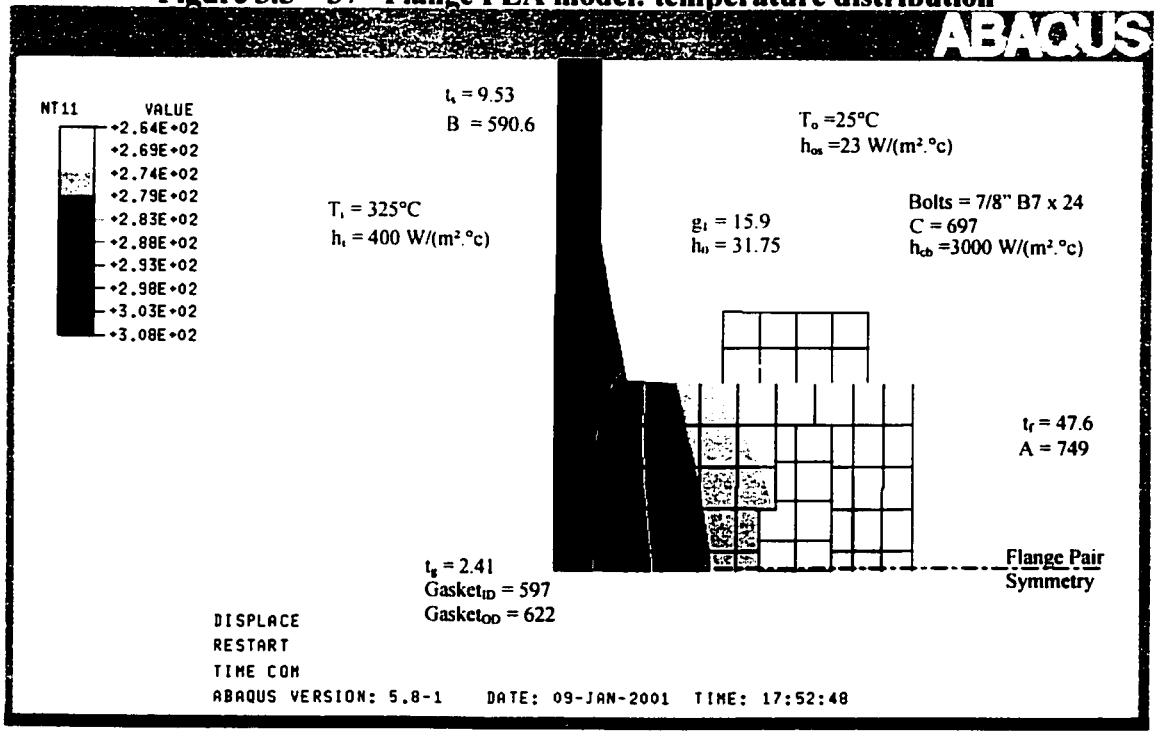

Figure 3.6 – 24" Flange FEA model: temperature distribution

area. A steady state thermal analysis was run and the nodal temperatures were stored, in order to be used later as a load input into the deflection analysis.

A second unmodified model was then run in two loading steps. Initial bolt loading was applied, using the ABAQUS "*Pretension" command. The nodal temperature loading was then input from the previous thermal analysis. In this way the overall changes in bolt and gasket stress levels were determined and could be compared to the values obtained using the analytical method. In all cases the gasket thermal and elastic properties used were those of a corrugated metal, graphite filled gasket as outlined in Appendix A.

The flanges were analysed with a temperature gradient (inside to outside) of 300°C and internal and external film coefficients of 400 W/(m².°C) and 23W/(m².°C) respectively. The material types were taken as ASTM A105 for the flange material and ASTM A193-B7 for the bolt material. The mechanical and thermal properties were obtained for these materials from ASME (1998a), for the temperature range 0-300°C. The obtained average bolt stress changes resulting from the temperature loading for both methods are presented in Table 3.1.

Table 3.1 – Analytical and FEA results comparison

Flange	ΔBolt Stress (MPa) : Analysis vs. [FEA]			
	Effect #1	Effect #2	Effect #3	Total
14" cl. 150	15 [14]	-4	-37 [-35]	-26 [-21]
16" cl. 600	17 [13]	-2.8	-20 [-16]	-7 [-4]
37" Heat Ex.	28 [25]	-0.8	-9 [-8]	18 [17]
24" Heat Ex.	3.9 [4]	-2.3	-14 [-17]	-12.4 [-13]

From the tabulated values it is apparent that the analytical results are an accurate match with the finite element results. There are minor differences between the two methods, primarily due to the assumptions made in the analytical method regarding the simplification of the component temperature gradients. Additionally, the values obtained for Effect #2 are uniformly small for all of the flanges analysed. This indicates that it

may be acceptable to neglect Effect #2 and omit it from the analysis of the effects of steady state temperature on the operational stresses in a flange joint.

3.2.2 Site measurement

The bolt stresses and joint component temperatures on a single pass reboiler tubesheet flange (Figure 3.7) operating in the Chevron El Segundo refinery were taken over the period of one year. The dimensions of this joint are the same as the FEA model detailed in Figure 3.5. The data was taken after almost a year of operation, so the changes in bolt load due to such factors as gasket relaxation were minimal and it could safely be assumed that all changes measured were due solely to joint component interaction caused by temperature fluctuations.

The bolt load measurements and joint component temperatures were recorded every 30 minutes, using standard "k" type thermocouples and 4 Omegadyne TH-DL11 load cells (Figure 3.8). The load cells were previously calibrated against a certified load cell on a hydraulic press. A sample of the results obtained, for a 24 hour period, are presented in Figure 3.9. The period of time graphed includes a system start-up, where the exchanger was put on line, as is evidenced by the sharp increase in temperature at around 21:30 hours.

This graph clearly demonstrates that there are two effects of temperature on joint operation; steady state changes of bolt load and also dynamic changes of bolt load due to the thermal "impact" of a rapid fluctuation in temperature. This section does not cover the latter effect, as it deals only with a change in steady state temperature.

Figure 3.7 - Operational 37" reboiler

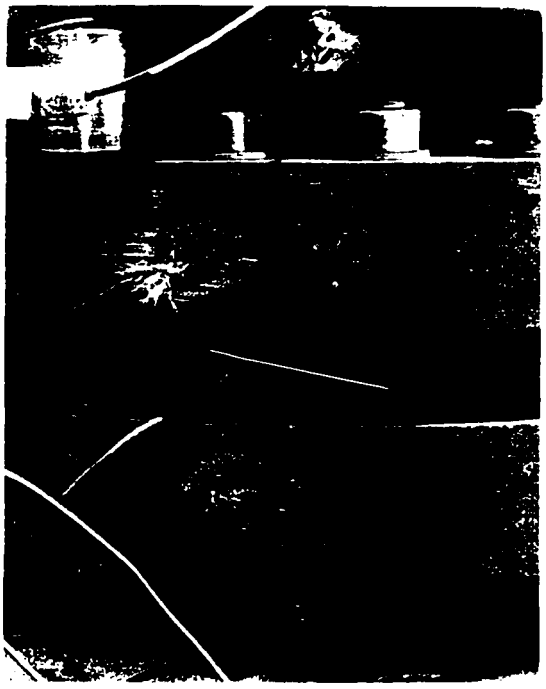

Figure 3.8 - Load cell and thermocouple placement

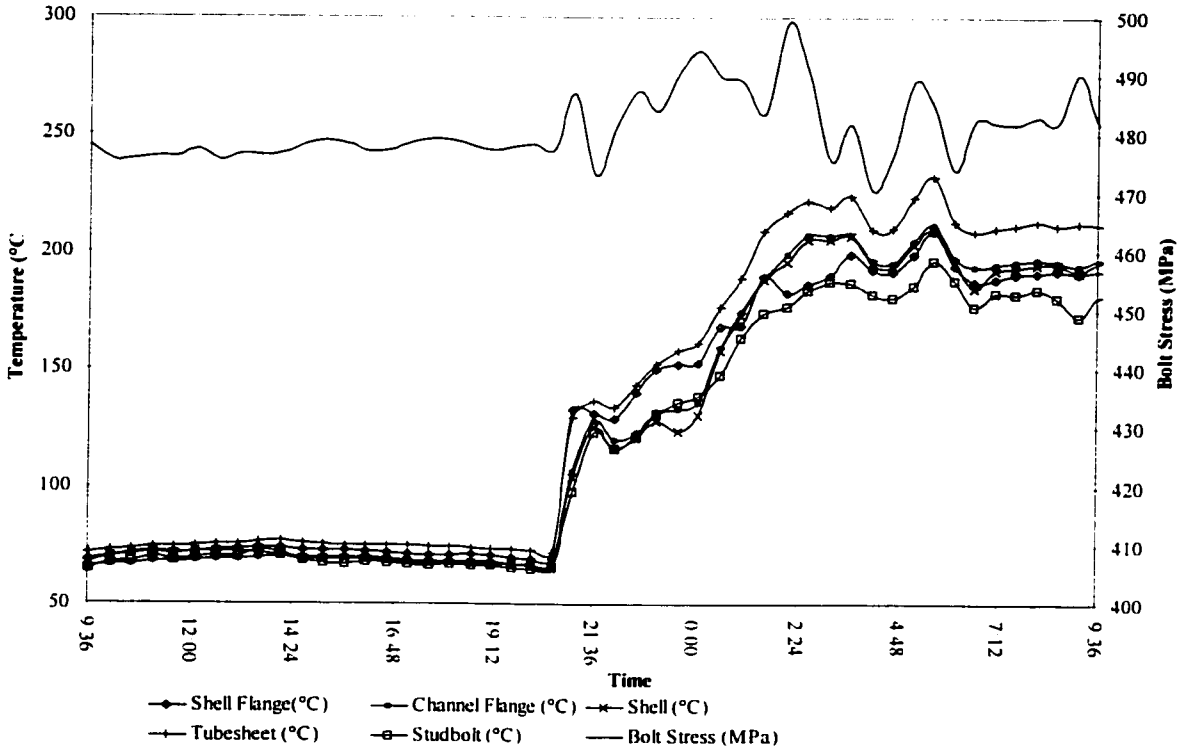

Figure 3.9 –Bolt stresses from the 37" reboiler tubesheet joint

In order to eliminate the dynamic effects, the bolt load was averaged between the times of 12:00 hours to 18:00 hours and also 6:00 hours to 9:36 hours. By comparison of these periods, which are the closest to "steady-state" that were obtained, it was determined that the bolt stress increased by 5.2MPa due to a temperature increase of 110°C. This compares favourably to the value of 5.9MPa predicted by FEA and 6.2MPa predicted by the analytical method for a temperature increase of this magnitude. This is considered good agreement of the results when compared to site collected data.

CHAPTER 4

TRANSIENT THERMAL ANALYSIS

4.1 Analysis method

Due to the complex geometry of the flange joint, it is not possible to develop a simple analytical method to determine the response of the joint to an internal fluid temperature transient. This sort of calculation can be performed using Finite Element Analysis (FEA), however the goal of the project is to develop guidelines which may be incorporated into a design methodology and are not open to incorrect interpretation, as is FEA. The focus of the analysis will therefore be to develop a graphical approach that may be used to determine the time taken for the bolt load to reach critical values during the temperature transient. The temperature of the flange ring, shell and bolts at that time will then be determined and the mechanical interaction analysis performed at each of these critical points, as steady state cases.

The effect of an increasing thermal transient on the bolt and gasket stresses in a joint will vary, depending on flange geometry and the heat transfer properties. However, for all flanges, the mass, and therefore thermal inertia, of the flange ring is much higher than that of the vessel shell. There is therefore a subsequent lag between the increase in shell temperature and the increase in flange ring and bolt temperature. This has two effects; initially the shell is at a much higher temperature and therefore Effects #2 and #3 from Section 3.1 are dominant. This means that there is a subsequent initial loss in bolt load as the flange is heated. However, as the inner section of the flange ring becomes hotter, while the bolts remain cooler, the axial expansion effect (Effect #1) becomes dominant

and the bolt and gasket load will increase. Both of these effects may be seen in Figure 4.1, which plots the FEA results for joint component temperatures and subsequent bolt load changes for an increasing thermal transient on a 37 inch heat exchanger flange.

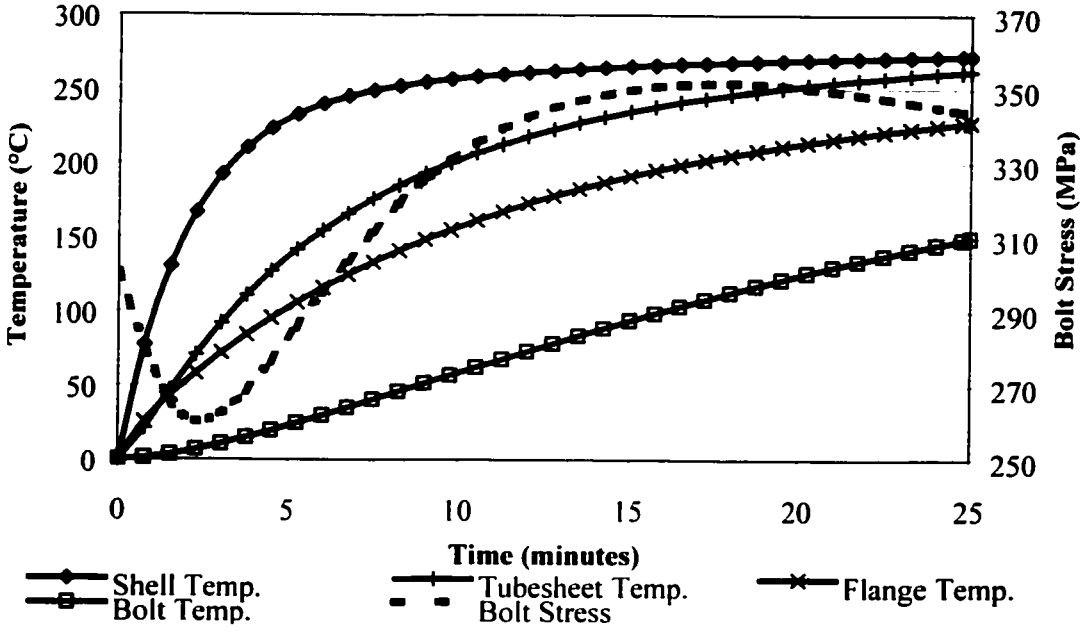

Figure 4.1 – The effects of an increasing thermal transient – 37 inch joint

The cooling cycle of the flange transient may be neglected in this analysis, as this case will always be less important than the heating cycle. This is due to the fact that the differential effects between the shell and flange ring will be reversed, leading to higher bolt forces. Additionally the bolt will always cool at the same rate or quicker than the flange, once again resulting in higher bolt forces. It is therefore more likely that joint leakage will occur during joint heating, rather than joint cooling. These effects are evident in Figure 4.2, which details the FEA results for the cooling cycle of the same 37 inch flange. It is apparent that the cooling cycle has a smaller overall effect when compared to the heating cycle. The developed analysis thus concentrates only on the heating cycle of the flange transient.

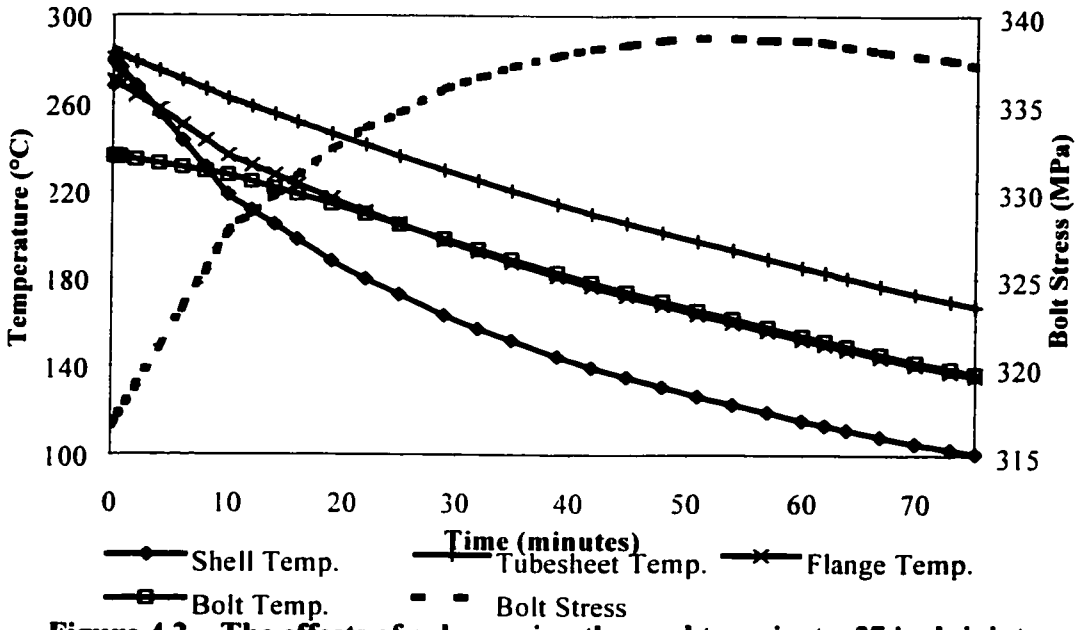

Figure 4.2 – The effects of a decreasing thermal transient – 37 inch joint

The method of analysis chosen was to solve the shell and flange ring temperature transients using the method of finite differences. A computer program was written utilising finite difference methods in the C++ programming language. This program calculated the trend of shell and ring temperature versus time for selected non-dimensional input values. The finite difference method used is fully detailed in Appendix B. The assumptions regarding heat transfer were the same as those made for the steady state case, with additional limitations placed on the heat transfer coefficients and flange ring thickness as following:

$$h_i \leq 10{,}000 \text{ W/(m}^2\text{.°C)}$$

$$h_e \leq 100 \text{ W/(m}^2\text{.°C)}$$

$$h_e/h_i \leq 0.1$$

$$t_f/r_e \geq 0.075$$

$$T_f(r_f) \geq (T_i - T_e)/10 \text{ °C}$$

The limitations placed on the internal heat transfer coefficient encompass the majority of heat transfer values which are commonly found in heat exchanger services (Butterworth,

1977). The chosen external heat transfer coefficient limits correspond to values common for the free convection regime. The limitation on the flange thickness is, once again, based on the common flange dimensions and should include all larger diameter flanges. The limitation placed on the flange temperature at the outer diameter of the flange ring ($T_f(r_f)$) is a limitation from experience of actual flange temperatures. In all measured cases of flange temperature, the flange outer diameter temperature has always exceeded 20% of the temperature difference between fluid temperature and ambient. Thus it is considered acceptable to ignore the analysis cases that fit within the geometrical and thermal constraints listed previously, but result in a flange outer diameter temperature of less than 10% of the temperature difference. The analysis constraints are therefore more accurate, and do not include excessively thin flange geometries, which would not be realistic from a mechanical strength perspective.

Multiple analysis cases were run for a selection of dimensions within the scope of the study and from these cases a series of graphs were constructed. The graphs enable the user to obtain, firstly, the time to steady state for the vessel shell and, secondly, to find the corresponding flange ring temperature, and therefore bolt temperature for that time. The graphs are based on the percentage of the steady state temperature versus time.

4.2 Shell temperature analysis

The shell was modelled as an infinite length hollow cylinder, with heat loss from the external surface and heat transfer from the internal fluid, as per the steady state case in Section 3. Using the finite difference method outlined in Appendix B, the transient temperature profile of the shell for the full range of the variables was calculated. Seven graphs were obtained from this analysis, which allow the determination of the shell temperature for any time during the transient at the inner, middle and outer diameter radial locations. The first three graphs plot the (non-dimensional) time taken to obtain 5% of the steady state (S.S.) temperature at each radial location (Figures 4.3a to 4.3c).

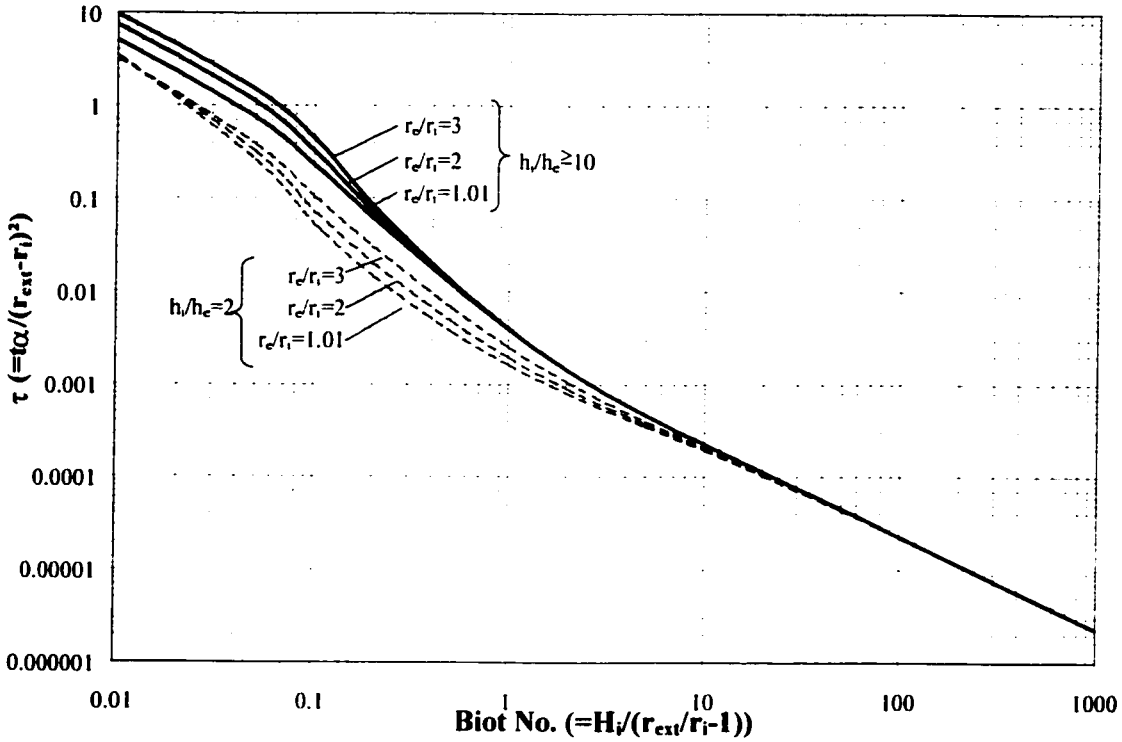

Figure 4.3a – Time taken for inner radius of cyl. to reach 5% of S.S. temperature

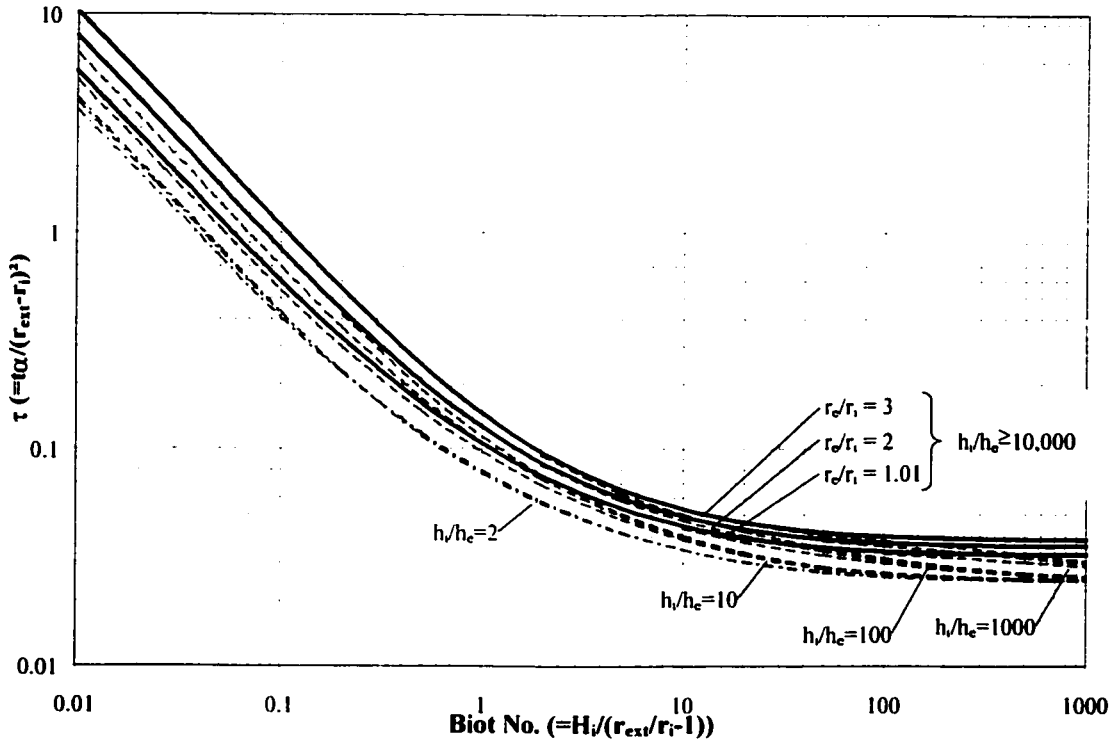

Figure 4.3b – Time taken for middle radius of cyl. to reach 5% of S.S. temperature

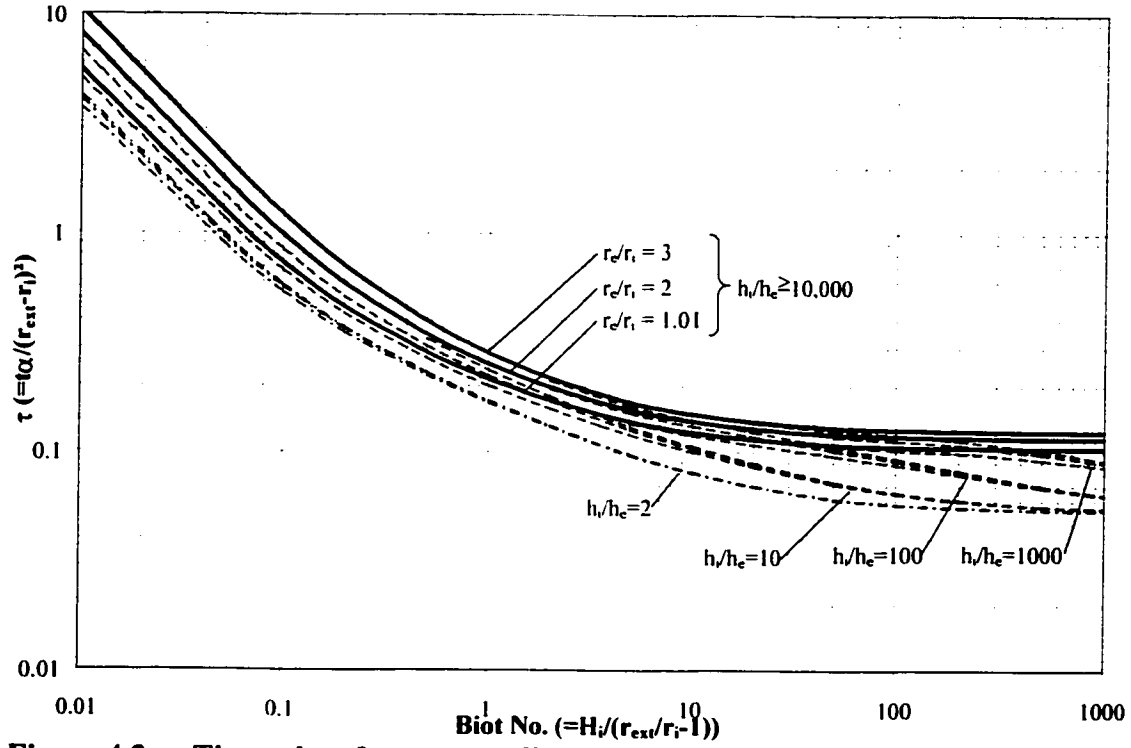

Figure 4.3c – Time taken for outer radius of cyl. to reach 5% of S.S. temperature

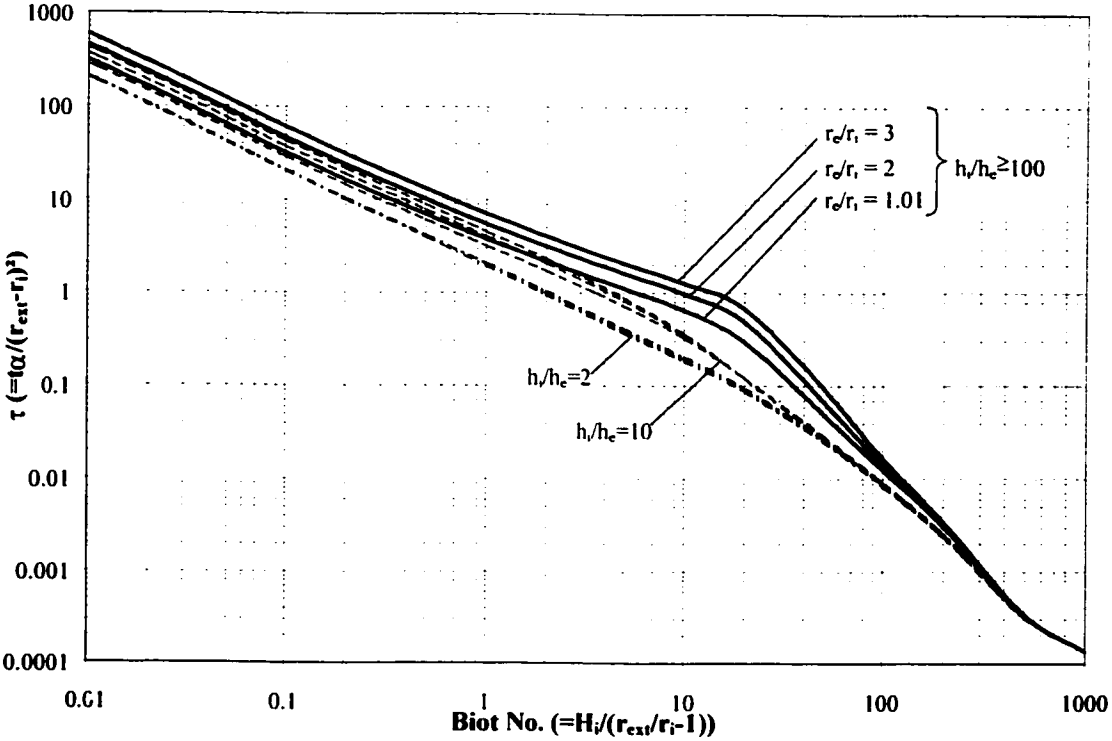

Figure 4.4a – Time taken for inner radius of cyl. to reach 95% of S.S. temperature

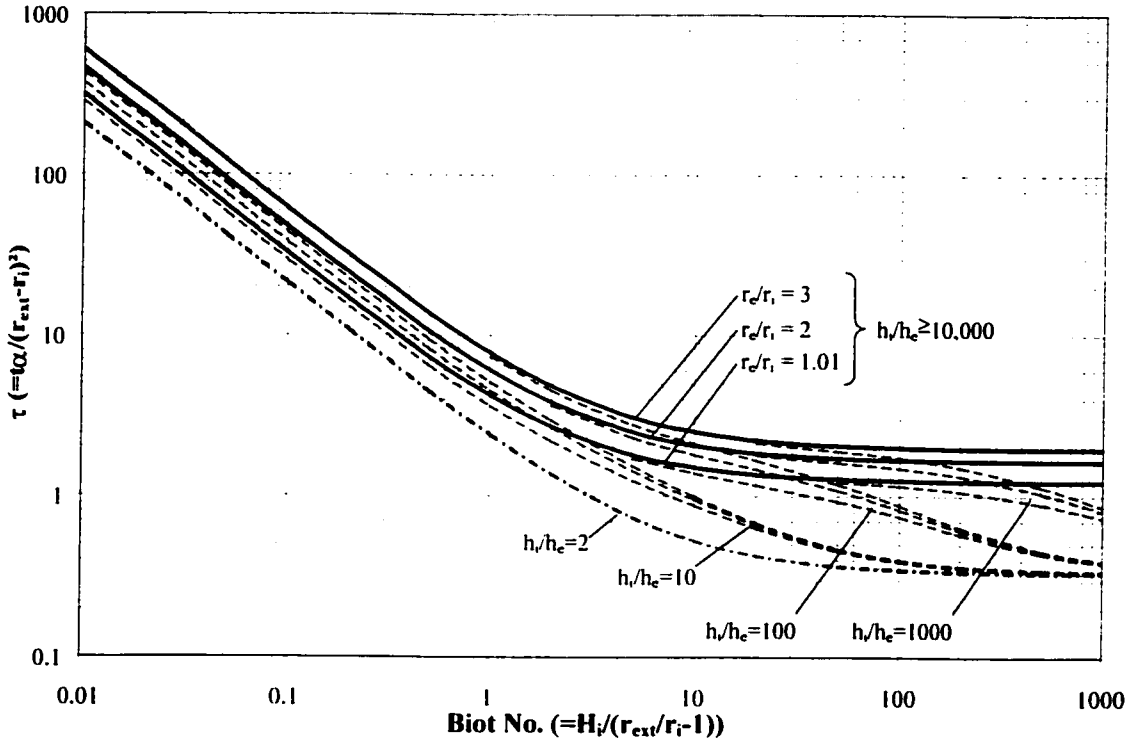

Figure 4.4b– Time taken for middle radius of cyl. to reach 95% of S.S. temperature

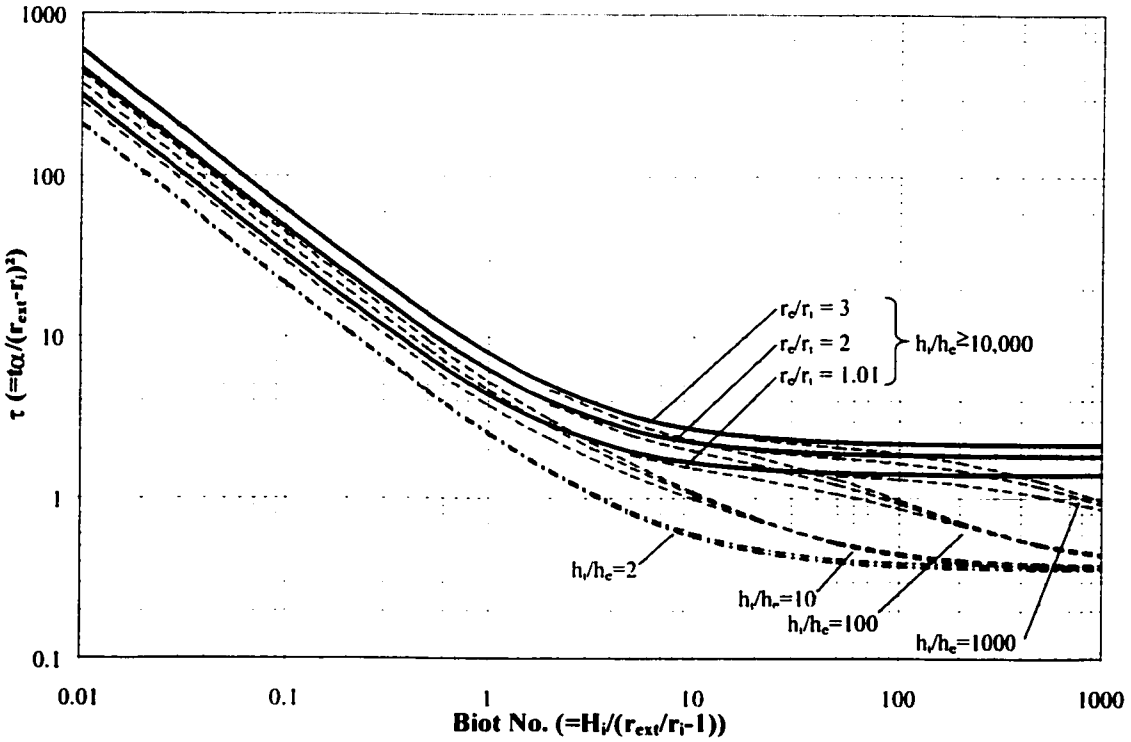

Figure 4.4c – Time taken for outer radius of cyl. to reach 95% of S.S. temperature

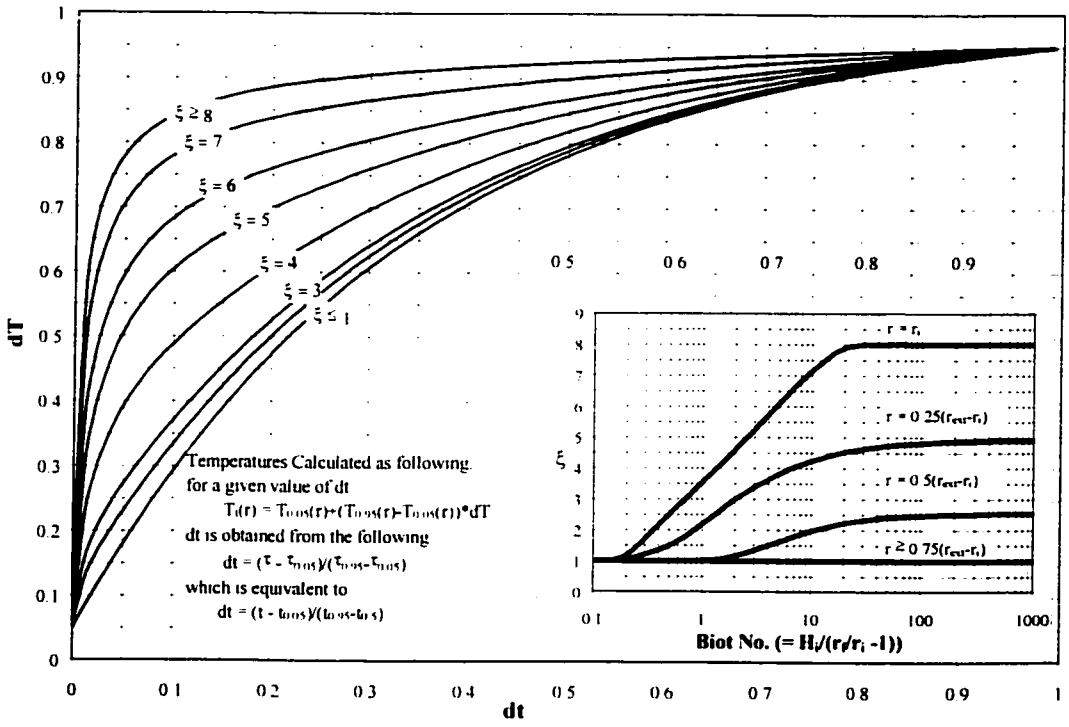

Figure 4.5 – Cylinder temperature vs. time, key graph

The second series of three graphs allow the determination of the time taken to reach 95% of the steady state temperature at each given radial location (ref. Figures 4.4a to 4.4c). The final graph (Figure 4.5) is used in conjunction with the first two series of graphs to determine the time taken for the radial point on the shell to reach any value of temperature. Conversely the temperature corresponding to a certain time may also be determined by taking the ratio of the difference between the 5% time and the given time and the difference between the 5% time and the 95% time. This graph represents a standardised temperature transient for an infinite length hollow cylinder, with the given boundary and geometrical conditions. Using these seven graphs the temperature of the shell at any one of the three radial locations, for any time during the transient, may be determined.

4.3 Flange ring temperature analysis

The flange ring was modelled as a finite length hollow cylinder, with heat gain at the inner radius surface and heat loss from the upper, lower and outer radius surfaces, as outlined previously in Section 2. The finite difference method outlined in Appendix B was then used to determine the flange ring temperature profiles across the full range of variables. Due to the geometrical limitations and the fact that the external heat transfer coefficient is always at least ten times smaller than the internal heat transfer coefficient, the finite length cylinder results do not vary greatly from the infinite length cylinder results. The ratio of the external heat transfer coefficient to the internal heat transfer coefficient (h_e/h_i) of the infinite cylinder is modified to give the same outer radius steady state temperature value as the finite length cylinder (ref. Equation 4.1). This forces the temperature profile of the infinite cylinder to closely approximate that of the finite cylinder. This approach greatly simplifies the analysis method, by eliminating the need for further graphs, since the previous infinite length cylinder graphs may therefore be used.

$$\left(\frac{H_e}{H_i}\right)^{new} = \frac{1 - T_f(r_f)}{T_f(r_f)\frac{r_e}{r_i}\left(1 + H_i \ln\left(\frac{r_e}{r_i}\right)\right)} \qquad 4.1$$

The finite length cylinder case tends towards the infinite length cylinder case as h_e and h_e/h_i become smaller and as t_f/r_e becomes larger. The greatest error in the assumption that a modified infinite length cylinder can model the finite length cylinder will therefore occur at the inverse of these conditions. Due to the additional limitation placed on the flange ring outer diameter temperature it is not possible to easily examine these limits. However, by looking at the range of cases plotted in Figures 4.6 to 4.9 it can be seen that the error is generally less than 15%.

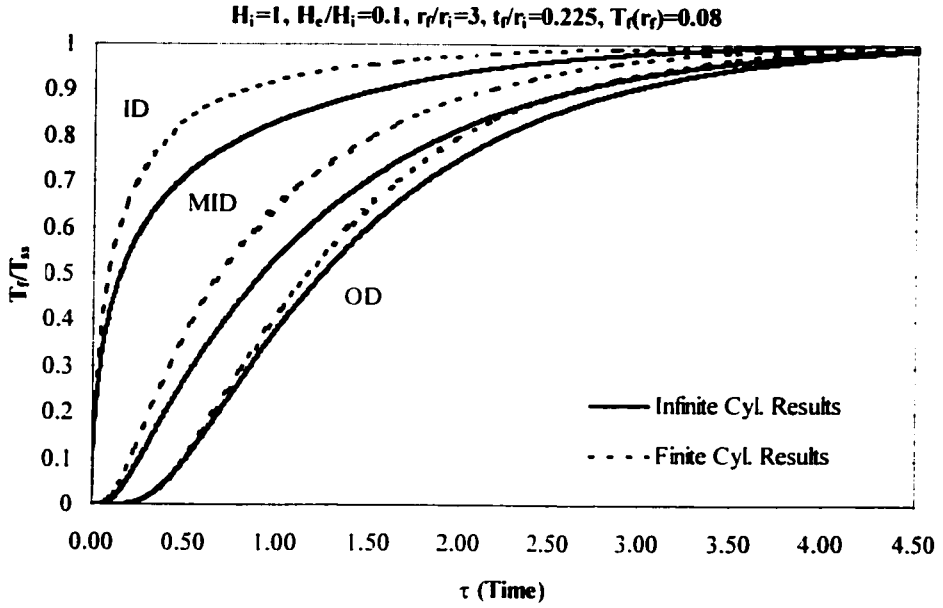

Figure 4.6 – Comparison between finite and modified infinite cylinder analysis, case of large H_e/H_i, small t_f/r_i ratio.

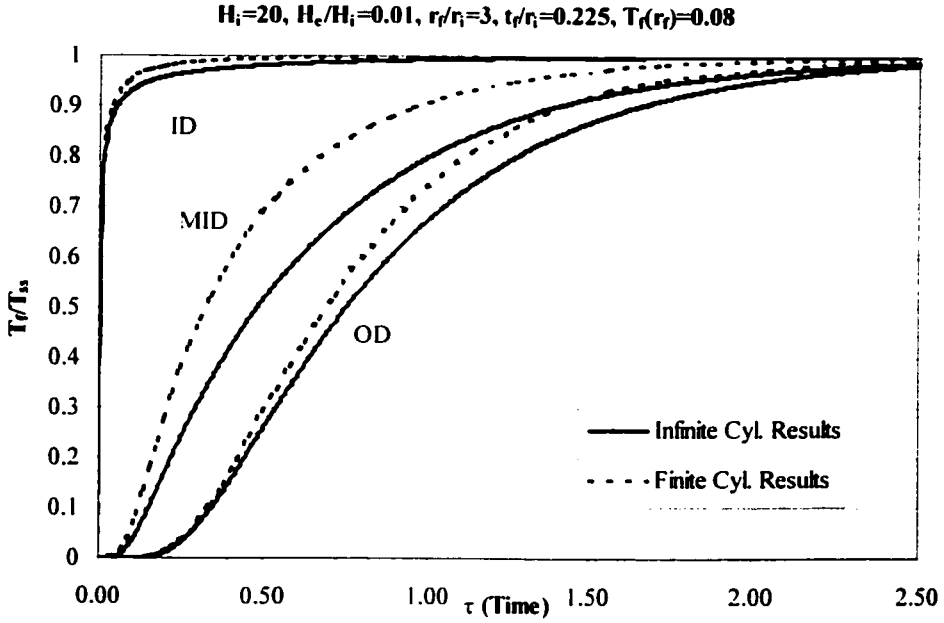

Figure 4.7 – Comparison between finite and modified infinite cylinder analysis, case of large H_i, small t_f/r_i ratio.

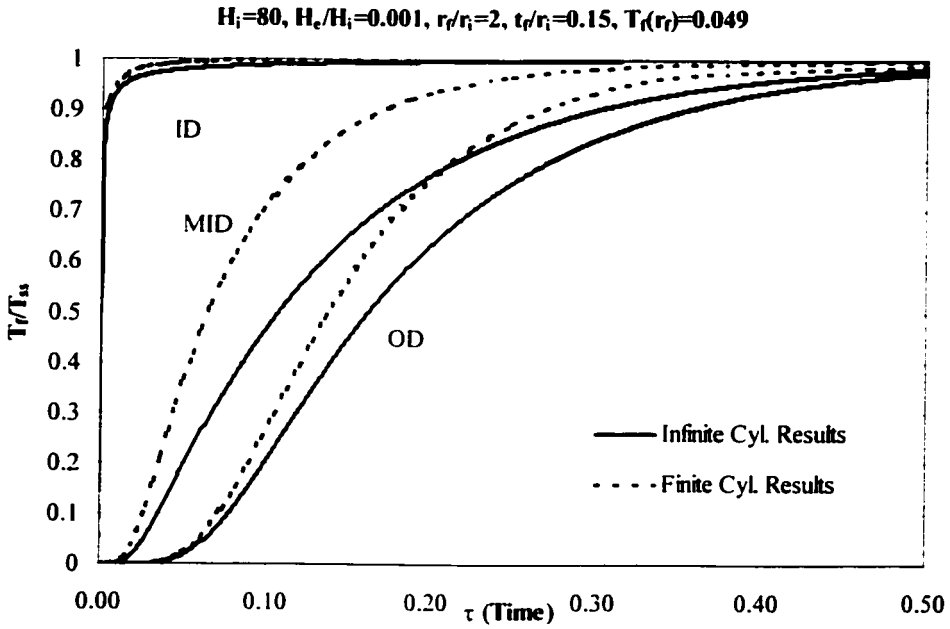

Figure 4.8 – Comparison between finite and modified infinite cylinder analysis, case of large H_i.

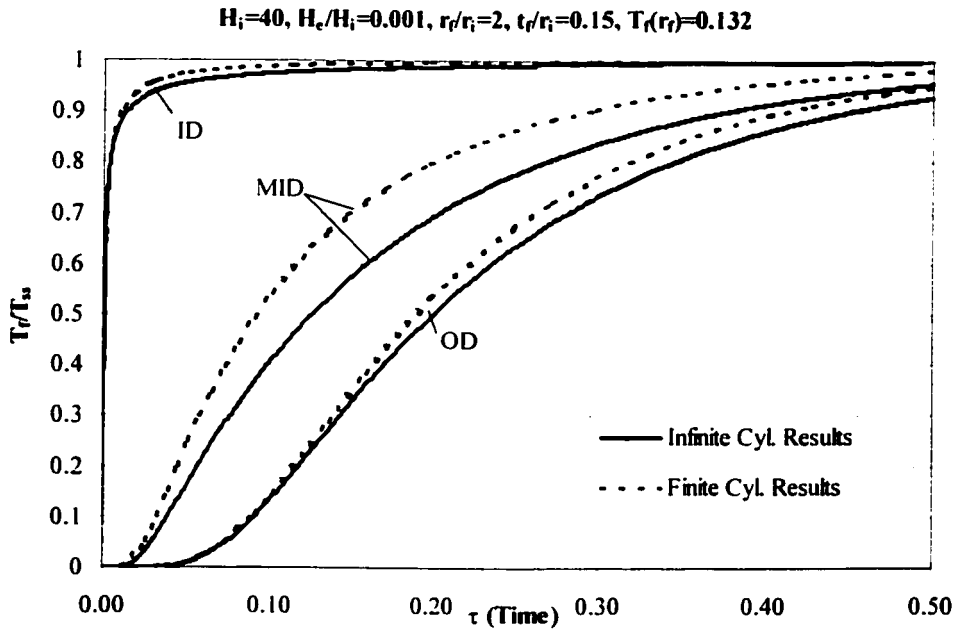

Figure 4.9 – Comparison between finite and modified infinite cylinder analysis, case of smaller H_i.

It can also be noted, by comparison of Figures 4.8 and 4.9, that the accuracy of the assumption increases very rapidly as the case moves away from the analysis limits. This indicates that the majority of cases will see a much higher accuracy of result using this method than mentioned previously. Additionally, since the flange outer diameter temperature limitation is not satisfied for the three worst cases (Figures 4.6 to 4.8), it is probably safe to say that, within the full limitations imposed previously, the error involved in using the modified infinite cylinder results will be less than 10%. This is an acceptable error level, considering the level of analysis simplification that it allows.

4.4 Bolt temperature analysis

As previously discussed for the steady state analysis, the bolt temperature will be proportional to the flange ring temperature at the bolt pitch circle. However, as there is a resistance across the flange/nut contact interface there will be an additional lag of the bolt temperature behind the flange ring temperature. This effect, of transient heat flow across contacting surfaces, can be examined using transient contact heat transfer theory (Barber et.al., 1989). However, by examining the results of such theory, it is evident that the temperature lag, due to contact effects, will be of the order of seconds. This value is around two orders of magnitude smaller than the time taken for the flange to reach steady state temperature and so may therefore be neglected. Additionally, the bolt temperature is assumed to follow the transient profile of the flange outer diameter (as opposed to the transient profile at the bolt pitch diameter). This simplifies the analysis and will also serve to counteract the error caused by neglecting the effect of the contact resistances.

However, for longer bolts there will be an additional lag between the temperature of the central portion of the bolt and the end nearest the flange surface, due to the conductive resistance along the bolt length. This effect must be accounted for within the analysis, otherwise the predicted temperature of the bolt will be much higher than actual. The simplest method for assessing this effect is to treat the bolt length as a one dimensional

lumped mass heat conduction problem. The energy balance equation may therefore be defined as per Equation 4.2.

$$\frac{4k}{L_b}\left(1-\theta_b(\tau)\right)=-\frac{\rho c\frac{\pi}{4}\varphi_b^2 L_b}{\frac{\pi}{4}\varphi_b^2}\frac{d\theta_b(\tau)}{d\tau}$$

4.2

To develop this equation it was assumed that the bolt temperature at the flange interface is 1 and that the average bolt temperature occurs at a point $L_b/4$ from this interface. The solution to this differential equation is defined in Equation 4.3, which gives a resulting factor, proportional to the bolt material properties, bolt length and also to time. The bolt temperature for any time will therefore be the bolt steady state temperature, multiplied by the flange outer diameter temperature ratio at the required time ($\theta_f(t)^{OD}$), multiplied by the factor obtained from Equation 4.3.

$$\theta_b(t)=\left(1-\exp\left(\frac{-4kt}{\rho cL_b^2}\right)\right)$$

4.3

By use of Equation 4.1, Equation 4.3 and the previous graphs for infinite length cylinders, the temperature of the shell, bolt and flange ring at any time during the transient may therefore be determined. These values may subsequently be used with the previously developed mechanical interaction equations to determine the change in bolt load due to the temperature transient.

4.5 Analysis verification

The developed graphical system for determining the shell, flange and bolt temperatures was verified by comparison to finite element analysis results. The same four flange sizes that were previously analysed in Section 3.3 were analysed using both finite element analysis and also the infinite length cylinder, finite difference based, graphical method. The node temperatures versus time, during a 300°C instantaneous increase in internal fluid temperature, were obtained for both analysis methods. These node temperatures were then plotted for comparison between the two methods. For the finite element analysis results, the bolt temperature plotted is the average temperature of the bolt nodes along the bolt length. These figures appear following (Figures 4.10 to 4.13). By comparison of the results obtained by finite element method and by the finite difference graphical method it is apparent that the agreement between the two methods is good. Additionally, the method of accounting for the time lag effects of the bolt temperature appears to be sufficient.

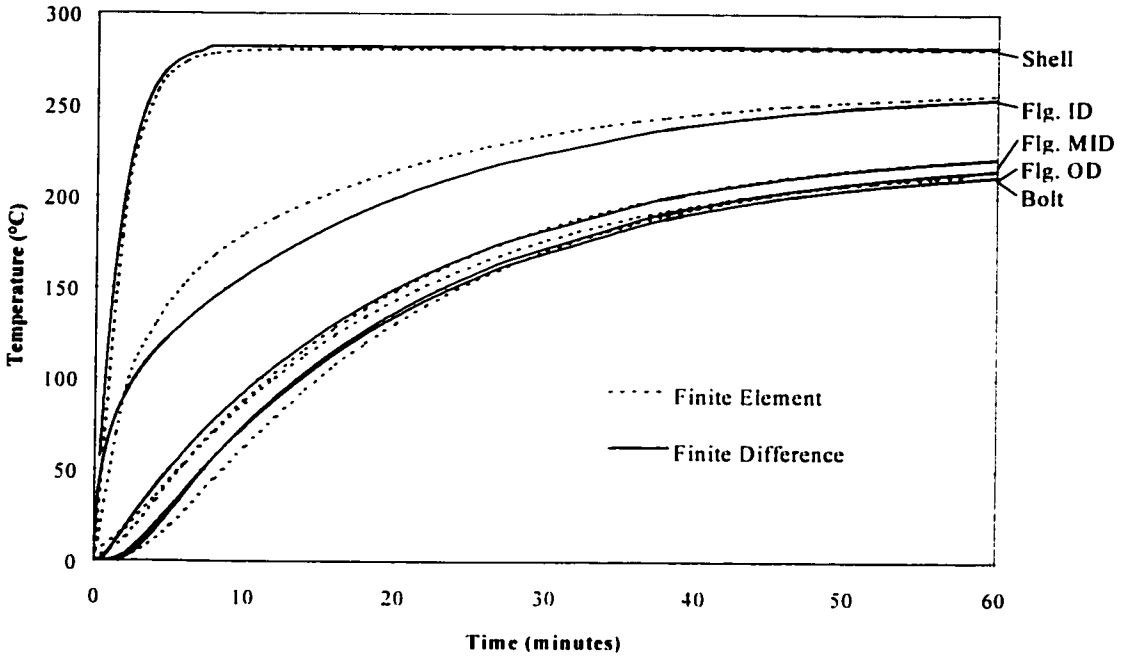

Figure 4.10 – Finite Difference vs. FEA results – 14inch class 150 RFWN

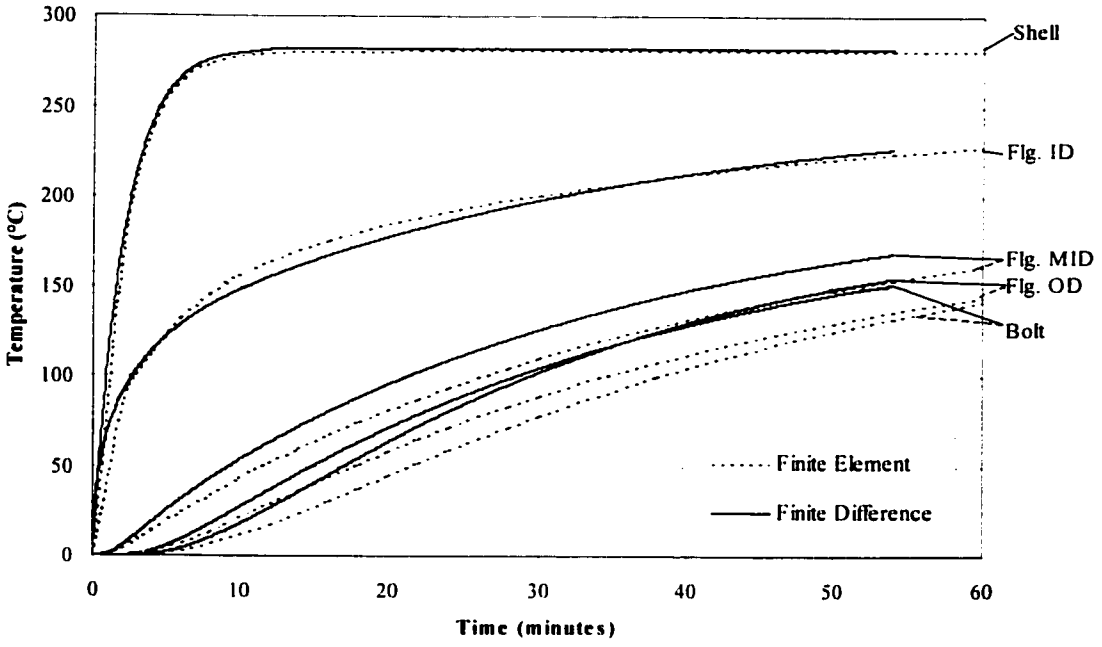

Figure 4.11 – Finite Difference vs. FEA results – 16inch class 600 RFWN

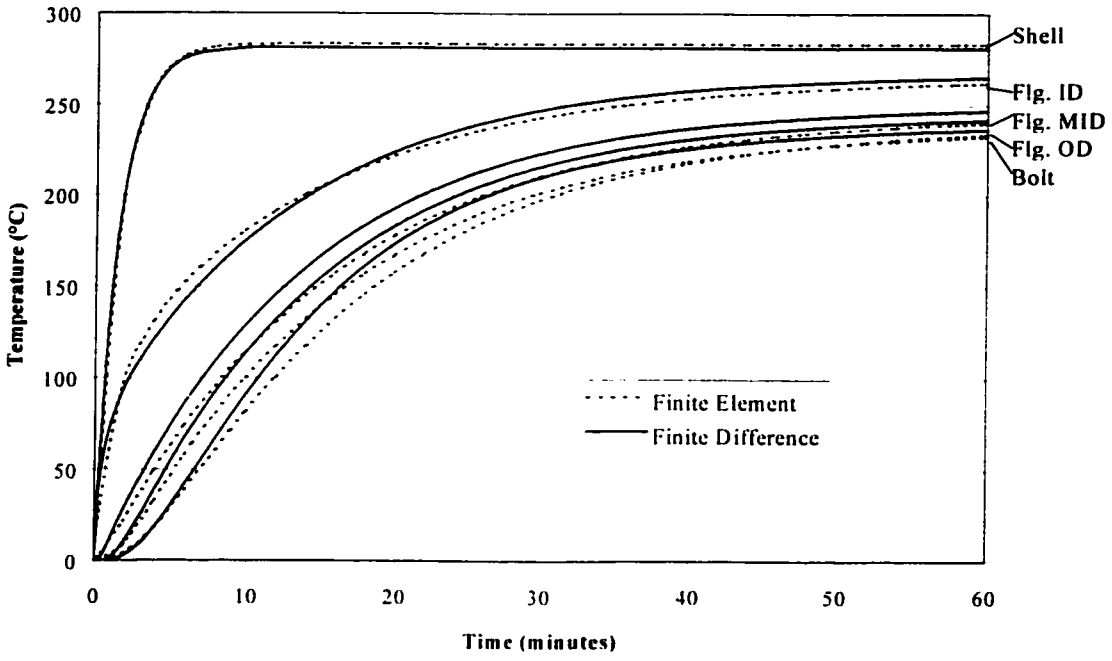

Figure 4.12 – Finite Difference vs. FEA results – 24inch heat exchanger

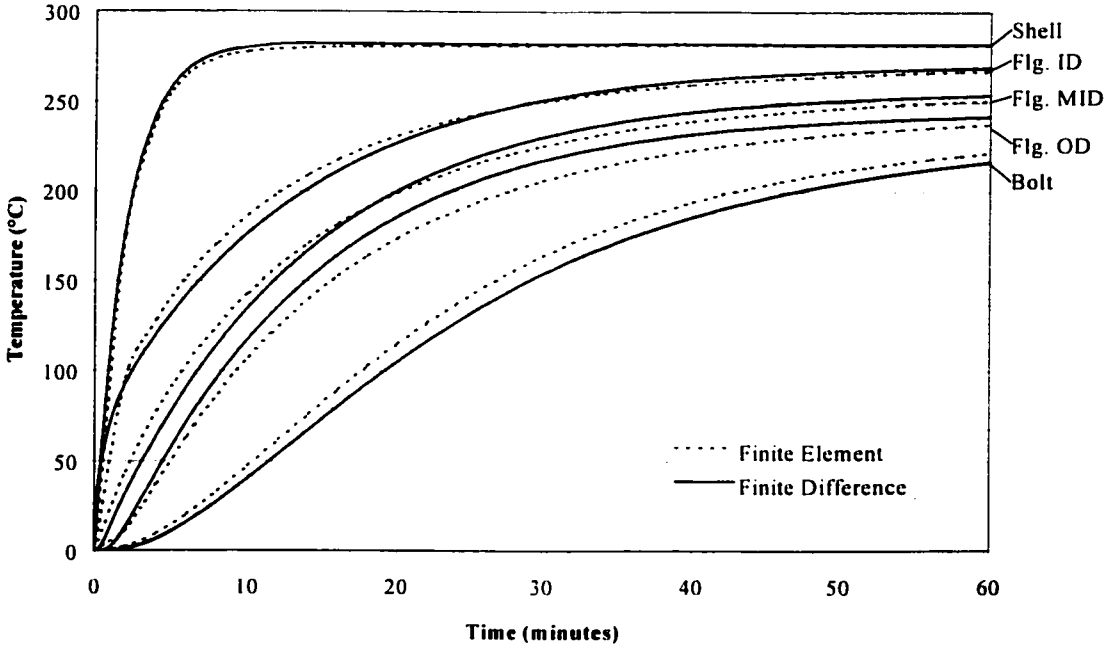

Figure 4.13 – Finite Difference vs. FEA results – 37inch heat exchanger

CHAPTER 5

TRANSIENT MECHANICAL ANALYSIS

5.1 Analysis method

The mechanical equations formulated in Section 3 are developed in this section to establish the resulting joint component interaction during the temperature transient. The most important factor in adapting these equations for the transient case is in the determination of the critical points during the transient at which to perform the mechanical analysis. As discussed in Section 3 there are three basic mechanical effects that take place during the increasing thermal transient. These three effects combine to cause both a high and a low point in the bolt load during the transient (Figure 5.1).

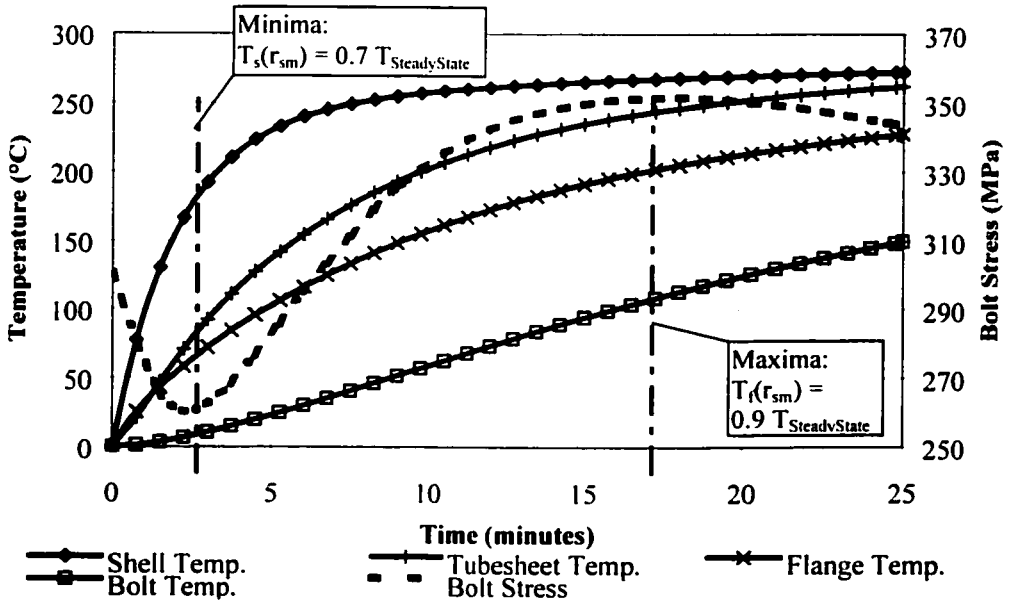

Figure 5.1 – Critical points for an increasing thermal transient – 37 inch joint

To aid in the determination of the critical temperature values, it is useful to remember which component temperatures, and therefore subsequent thermal expansions, cause each of the three mechanical effects. The driving component temperatures for each effect are detailed in Table 5.1. Additionally an example of the joint dynamics during a thermal transient is given in Figure 5.2. This graph, obtained by using FEA and finite difference methods, separates the change in bolt stress caused by each of the three mechanical effects by comparison to the component temperatures.

Table 5.1 – Driving component temperatures for each mechanical disturbance

Effect	Driving Component Temperatures	Equation
#1	Temperature difference between flange ring and bolt.	$(T^{fm} - T^{b})$
#2	Temperature difference between flange ring and shell.	$(T^{sm}-T^{fi})$
#3	Temp. difference between hub and flange outer section.	$((T^{sm}+T^{fi})/2 - T^{fm})$

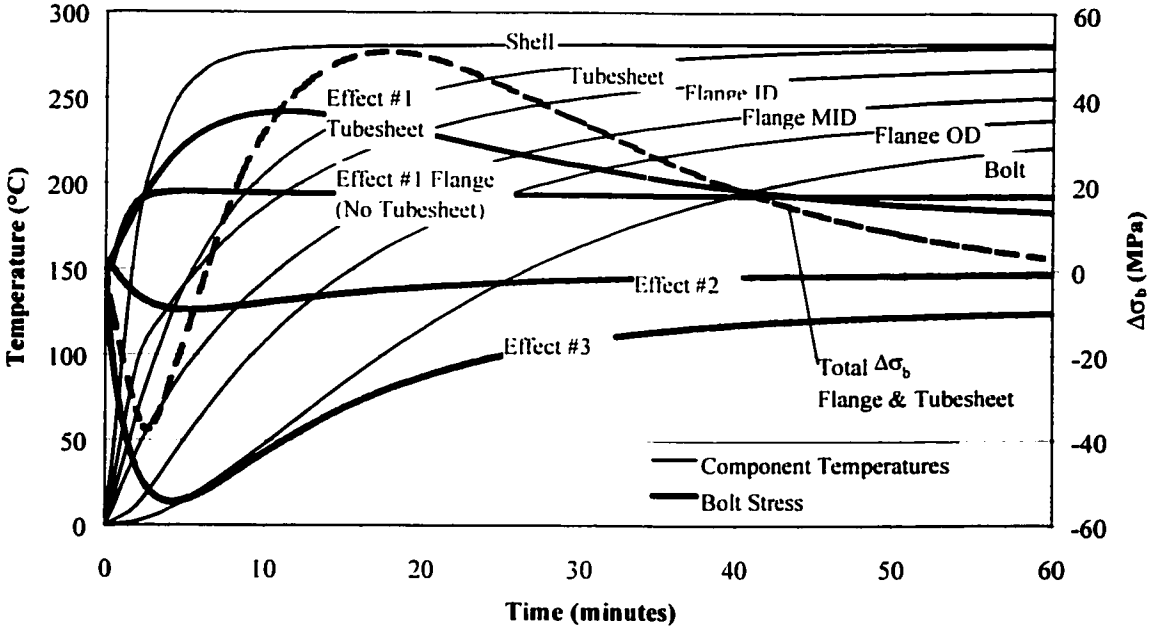

Figure 5.2 – Separation of transient thermal-mechanical effects – 37 inch joint

The minima of the bolt load curves appear to occur at the time when the shell has reached 70 - 95% of the steady state temperature. This figure depends on whether or not the joint has a tubesheet. To accurately analyse a joint with a tubesheet, the transient temperature of the tubesheet must also be determined. However, when determining the bolt load minima it is conservative to analyse the joint without the tubesheet, at the time corresponding to 95% shell temperature. This will result in a higher bolt load loss being calculated than actually occurs.

If the steady state change in bolt stress indicates an increase in bolt load then it may be advisable to examine the maxima of the bolt load curves, to ensure that the gasket is not over-stressed. This would not be necessary with most joints that do not have a tubesheet or similar spacer between the flange faces. The maxima of the bolt load curves, in a joint without a tubesheet, occur when the inner section of the flange ring has reached approximately 90 - 95% of its steady state temperature. At this point the greatest difference between the bolt temperature and the flange temperature occurs, resulting in an increase in bolt stress. If the joint contains a tubesheet, the maximum bolt load will occur at a time corresponding to when the tubesheet is at 95% of its steady state temperature. To determine this time, it is conservative to assume that the tubesheet is a lumped mass. The time taken to reach 95% of the steady state temperature may therefore be determined by Equation 5.1, adapted from Ozisik (1985).

$$t_{0.95} = \frac{-\ln(0.05)t_{ts}c\rho}{h_i} \qquad 5.1$$

In this equation the tubesheet thickness (t_{ts}) is taken as half the actual tubesheet thickness if heat transfer is occurring on both side of the tubesheet. The required component temperatures for the bolt stress analysis at the two critical points may therefore be defined as per Table 5.2.

The change in bolt stress caused by each of the effects, at the instant of analysis during the temperature transient, will be directly proportional to the ratio of the driving transient

Table 5.2 – Critical points for transient mechanical analysis

Critical Point	Component Temperature Criteria
Point #1 – Bolt Load Minima	
Shell Temperature (T^{s}_{1})	95% of Steady State Temperature. Time taken for the middle radius of the shell to reach 95% of Steady State temperature ($t^{sm}_{0.95}$) from Fig. 4.4b.
Flange Ring Inner Section Temperature (T^{fi}_{1})	Temperature from flange transient analysis curves ((Figs. 4.3a, 4.4a and 4.5)) at time ($t^{sm}_{0.95}$).
Flange Ring Outer Section Temperature (T^{fo}_{1})	Temperature from flange transient analysis curves (Figs. 4.3b, 4.4b and 4.5) at time ($t^{sm}_{0.95}$).
Bolt Temperature (T^{b}_{1})	Temperature from flange transient analysis curves (Figs. 4.3c, 4.4c and 4.5) and Eq. 4.3, at time ($t^{sm}_{0.95}$).
Point #2 – Bolt Load Maxima	**(Without Tubesheet)**
Shell Temperature (T^{s}_{2})	100% of Steady State Temperature
Flange Ring Inner Section Temperature (T^{fi}_{2})	95% of Steady State Temperature. Time taken for flange inner radius to reach this temperature ($t^{fi}_{0.95}$) from Fig 4.3a.
Flange Ring Outer Section Temperature (T^{fo}_{2})	Temperature from flange transient analysis curves (Figs. 4.3b, 4.4b and 4.5) at time ($t^{fi}_{0.95}$).
Bolt Temperature (T^{b}_{2})	Temperature from flange transient analysis curves (Figs. 4.3c, 4.4c and 4.5) and Eq. 4.3, at time ($t^{fi}_{0.95}$).
Point #2 – Bolt Load Maxima	**(With Tubesheet)**
Shell Temperature (T^{s}_{2})	100% of Steady State Temperature
Tubesheet (T^{ts}_{2})	95% of Steady State Temperature. Time for tubesheet to reach this temperature ($t^{ts}_{0.95}$) from Eq. 6.1.
Flange Ring Inner Section Temperature (T^{fi}_{2})	Temperature from flange transient analysis curves (Figs. 4.3a, 4.4a and 4.5) at time ($t^{ts}_{0.95}$).
Flange Ring Outer Section Temperature (T^{fo}_{2})	Temperature from flange transient analysis curves (Figs. 4.3b, 4.4b and 4.5) at time ($t^{ts}_{0.95}$).
Bolt Temperature (T^{b}_{2})	Temperature from flange transient analysis curves (Figs. 4.3c, 4.4c and 4.5) and Eq. 4.3, at time ($t^{ts}_{0.95}$).

temperature difference over the driving steady state temperature difference (ΔT_{SS}). This hypothesis is made because, for small bolt stress changes, the mechanical interaction may be assumed to be linear. Therefore, this gives us a series of simple equations that define the minima and maxima of the transient bolt stress. These equations are set out in Table 5.3 for each of the three cases.

Table 5.3 - Equations for the calculation of the change in transient bolt stress

Analysis Point	Component Temperature Criteria	Eq.
Point #1 – Minima		
Effect #1	$\Delta\sigma_{b1.1} = \Delta\sigma_{bSS.1}(T^{fo}_1 - T^{b}_1)/\Delta T_{SS.1}$	5.2a
Effect #2	$\Delta\sigma_{b1.2} = \Delta\sigma_{bSS.2}(T^{s}_1 - T^{fi}_1)/\Delta T_{SS.2}$	5.2b
Effect #3	$\Delta\sigma_{b1.3} = \Delta\sigma_{bSS.3}((T^{fi}_1+T^{s}_1)/2 - T^{fm}_1)/\Delta T_{SS.3}$	5.2c
Total	$\Delta\sigma_{b1} = \Delta\sigma_{b1.1} + \Delta\sigma_{b1.2} + \Delta\sigma_{b1.3}$	5.2d
Point #2 – Maxima	**(No Tubesheet)**	
Effect #1	$\Delta\sigma_{b2.1} = \Delta\sigma_{bSS.1}(T^{fo}_2 - T^{b}_2)/\Delta T_{SS.1}$	5.3a
Effect #2	$\Delta\sigma_{b2.2} = \Delta\sigma_{bSS.2}(T^{s}_2 - T^{fi}_2)/\Delta T_{SS.2}$	5.3b
Effect #3	$\Delta\sigma_{b2.3} = \Delta\sigma_{bSS.3}((T^{fi}_2+T^{s}_2)/2 - T^{fm}_2)/\Delta T_{SS.3}$	5.3c
Total	$\Delta\sigma_{b2} = \Delta\sigma_{b2.1} + \Delta\sigma_{b2.2} + \Delta\sigma_{b2.3}$	5.3d
Point #2 – Maxima	**(Including Tubesheet)**	
Effect #1	$\Delta\sigma_{b2.1} = \Delta\sigma_{bSS.1}((T^{fo}_2 - T^{b}_2)+(T^{ts}_2 - T^{b}_2))/\Delta T_{SS.1}$	5.4a
Effect #2	$\Delta\sigma_{b2.2} = \Delta\sigma_{bSS.2}(T^{s}_2 - T^{fi}_2)/\Delta T_{SS.2}$	5.4b
Effect #3	$\Delta\sigma_{b2.3} = \Delta\sigma_{bSS.3}((T^{fi}_2+T^{s}_2)/2 - T^{fm}_2)/\Delta T_{SS.3}$	5.4c
Total	$\Delta\sigma_{b2} = \Delta\sigma_{b2.1} + \Delta\sigma_{b2.2} + \Delta\sigma_{b2.3}$	5.4d

The terms $\Delta T_{SS.n}$ and $\Delta\sigma_{bSS.n}$ in the Equations 5.2a to 5.4c are from the calculations performed in Sections 2 and 3 and are the temperature difference used in the calculation and resulting change in bolt stress for the applicable mechanical effect (n) respectively. The steady state temperature difference for Effect #3 is approximated as the flange ring middle radius temperature minus the flange ring inner radius temperature.

5.2 Method validation

5.2.1 Comparison with finite element analysis

The change in bolt stress during the same temperature transients analysed in Section 4 were obtained from the finite element models by performing an uncoupled thermal-mechanical analysis. The nodal temperatures were input as nodal loading in discrete time steps during the transient. This allowed the plotting of both the component temperature values and also the resulting bolt stress change with time. By using the Finite Difference calculation method for an infinite length hollow cylinder outlined in Appendix B and Section 4, it was also possible to construct comparative curves for the Finite Difference method. The Finite Difference bolt load curves were calculated using the assumptions listed previously in this section.

Additionally the graphical method outlined in this section was also used to determine the bolt load curve minima and, if applicable, maxima. These calculated values are listed in Table 5.4, with the working and intermediate values detailed in Appendix D. The graphical comparisons of the Finite Difference Method and the Finite Element Method are outlined, for the four flanges that were analysed, in Figures 5.3 to 5.6. From both of these comparisons it can be seen that the agreement between these two analysis methods is very good. The assumptions for the time taken to reach the "worst-case" bolt stress also appear to eliminate some inaccuracies in the finite difference method bolt stress values during the early stages of the transient (as can be seen in Figure 5.4).

Table 5.4 – Results summary for graphical analysis method

	14" cl. 150	16" cl. 600	24" Heat Exch.	37" Heat Exch.
$\Delta\sigma_{b1}$ (MPa)	-112	-48	-83	-44
$\Delta\sigma_{b2}$ (MPa)	-26	-16	-12	63

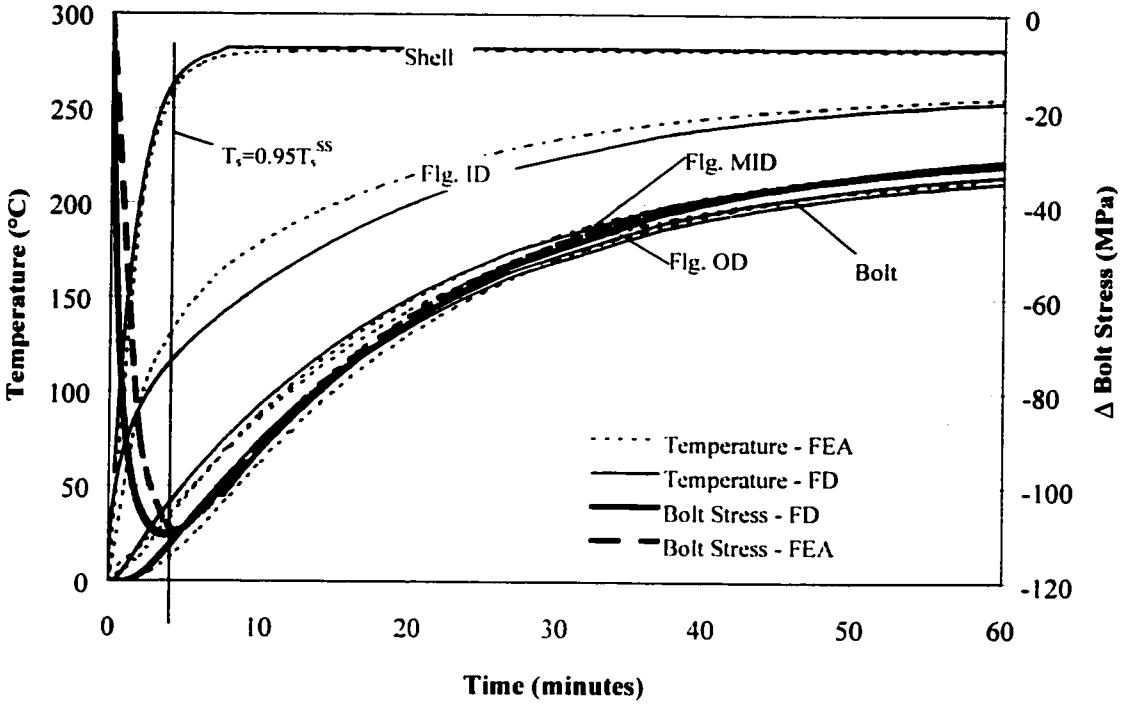

Figure 5.3 – Finite element vs. finite difference comparison – 14" cl. 150 RFWN

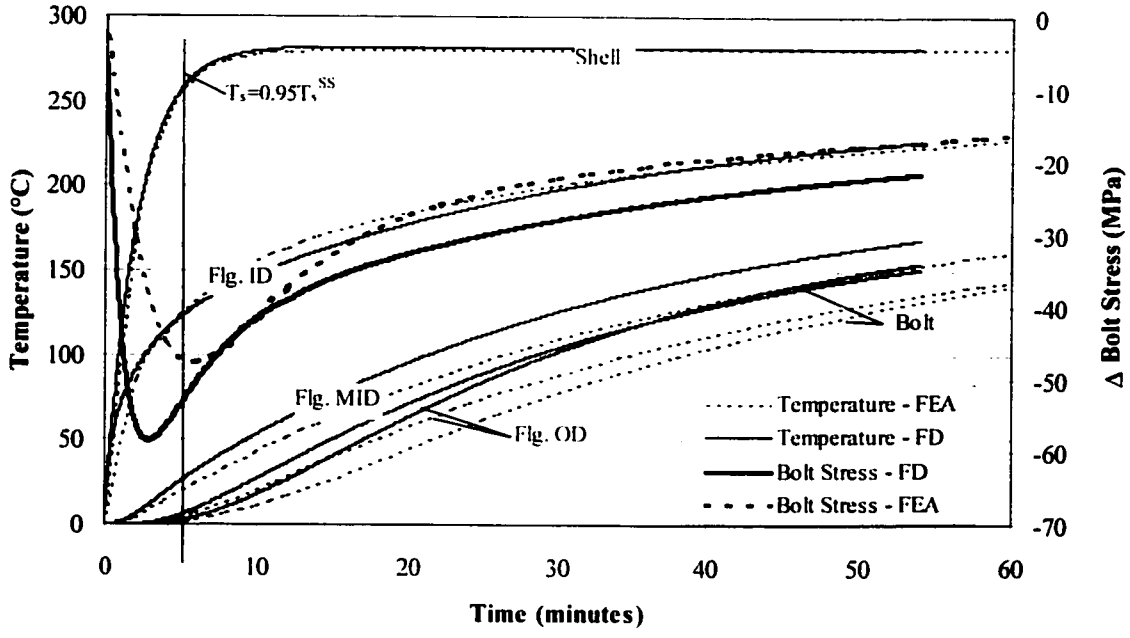

Figure 5.4 – finite element vs. finite difference comparison – 16" cl. 600 RFWN

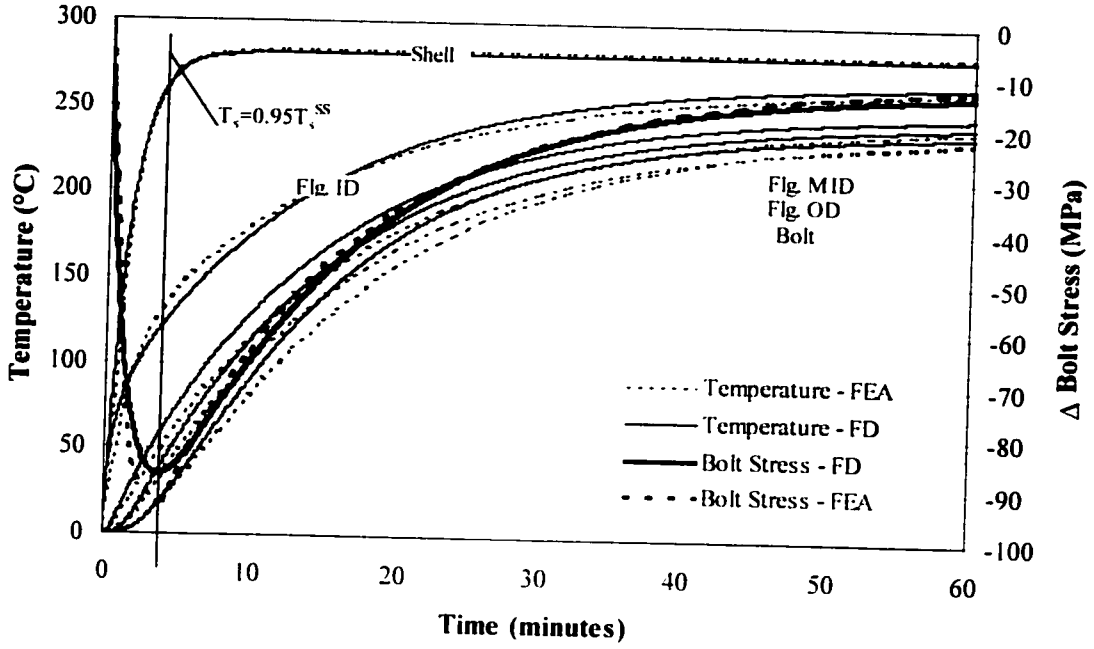

Figure 5.5 – Finite element vs. finite difference comparison – 24" heat exchanger

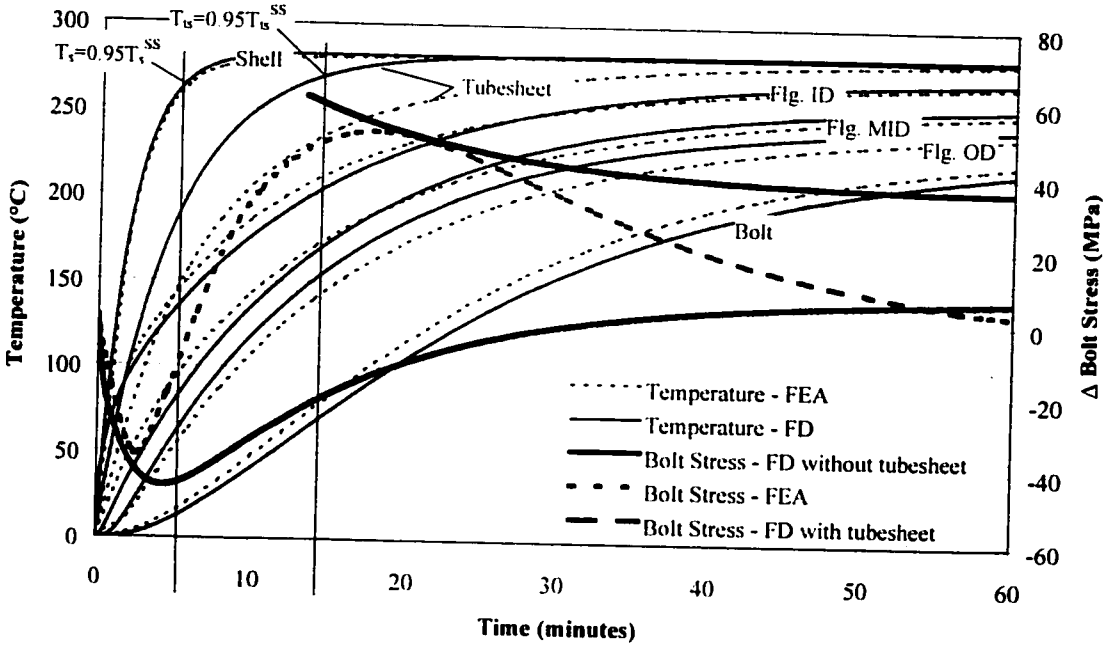

Figure 5.6 – Finite element vs. finite difference comparison – 37" heat exchanger

5.2.2 Verification with site data

It is possible, using the previously outlined methods, to compute the change in bolt stress that would be expected during an ideal, or theoretical, heat exchanger start-up. However, there are many variables that might influence whether or not the calculated value was relevant to the actual changes in bolt stress that occur during heat exchanger operation. These variables include factors such as the assumption of constant fluid temperature and heat transfer coefficient. In reality the internal fluid will probably pass through a long piping system and other vessels prior to the heat exchanger and therefore the fluid temperature would fluctuate during start up. Additionally, the fluid flow rate will also probably vary during the start-up process.

However, by using the ideal condition to perform the calculation, we are attempting to set an upper and lower limit on the changes in bolt stress that occur during a temperature transient. Therefore, it does not matter if all the process variables are not fully modelled, as long as the indicated result is conservative, but not excessively conservative. The joint designer requires an overall feel for the effects of temperature, rather than an exact figure, given the inaccuracies involved in joint assembly and in the calculation of the required gasket sealing stress.

The values that were previously calculated in this section for the amount of bolt load loss during thermal transient seem high. From Table 5.3 it can be seen that two of the flanges indicated around 100MPa bolt load loss. This figure is equivalent to around 20% to 40% of initial bolt assembly loads commonly used, which is a very high proportion. It is a concern that this value may be excessively conservative and therefore not relevant to the actual flange design.

However, to examine this concern, the theoretical results for the 37 inch heat exchanger were compared to site measured bolt load data that was collected during normal heat exchanger operation (Figure 5.7). From the bolt load measurements it can be seen that

the maximum single increase in bolt load occurred during unit start-up and was of the order of 50MPa. Additionally there are continual bolt load fluctuations during heat exchanger operation of around 40MPa. These site measured bolt stress values compare very well with the predicted bolt load increase of 63Mpa and –45MPa during unit start-up. It can therefore be seen that the theoretical values are certainly not excessively conservative. Additionally, it would seem that the analysis of the flange under ideal start-up conditions seems to give a good indication as to the actual operational changes in bolt load, even though there are other factors, such as uneven flange pair heating, occurring in reality. Indeed, it can be noted that small variations in temperature after start-up have caused significant changes in bolt stress. This is due to variations in the process conditions, which cause uneven flange pair heating.

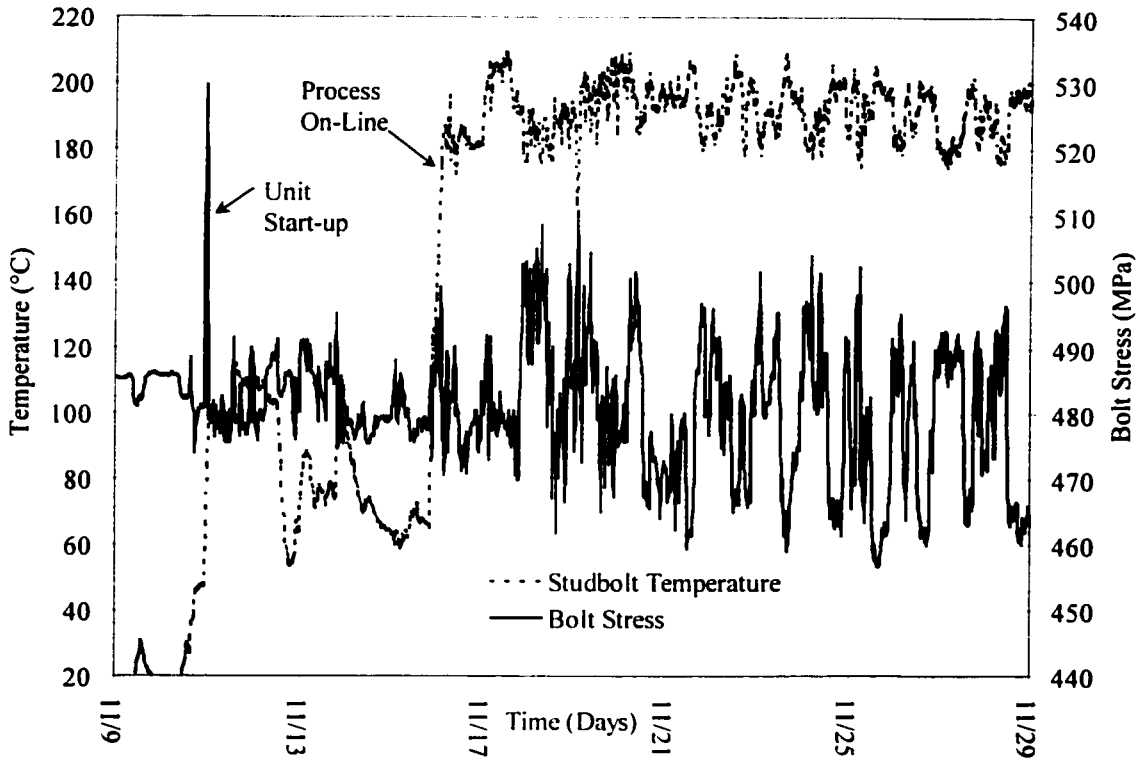

Figure 5.7 – Site measured operational bolt load data – 37" heat exchanger

CHAPTER 6

PRINCIPAL LABORATORY EXPERIMENTATION

6.1 Overview of experimental rig

In order to examine the overall validity of the developed analysis methodology it was necessary to construct a special experimental test rig to study the effects of temperature on bolted joints. Existing test rigs were not suitable, due to the fact that the movement generated by a temperature transient increases with increasing flange diameter. Additionally the flange heating should model, as closely as possible, the heating seen in an actual heat exchanger. Such a large diameter, internally heated test rig has never before been utilised to study this type of effect in documented laboratory experimentation.

A 24inch internal diameter pressure vessel was constructed (refer to Figure 6.1). The flanges were designed to the ASME VIII (1998b) pressure vessel design code in a configuration similar to heat exchanger flanges. The vessel is heated internally by electrical tube heaters. The heaters are electronically controlled, so that the heating rate may be varied and the steady state temperature held constant. The vessel joint is fully instrumented, allowing the monitoring of flange temperature, bolt load and flange deflection at two points.

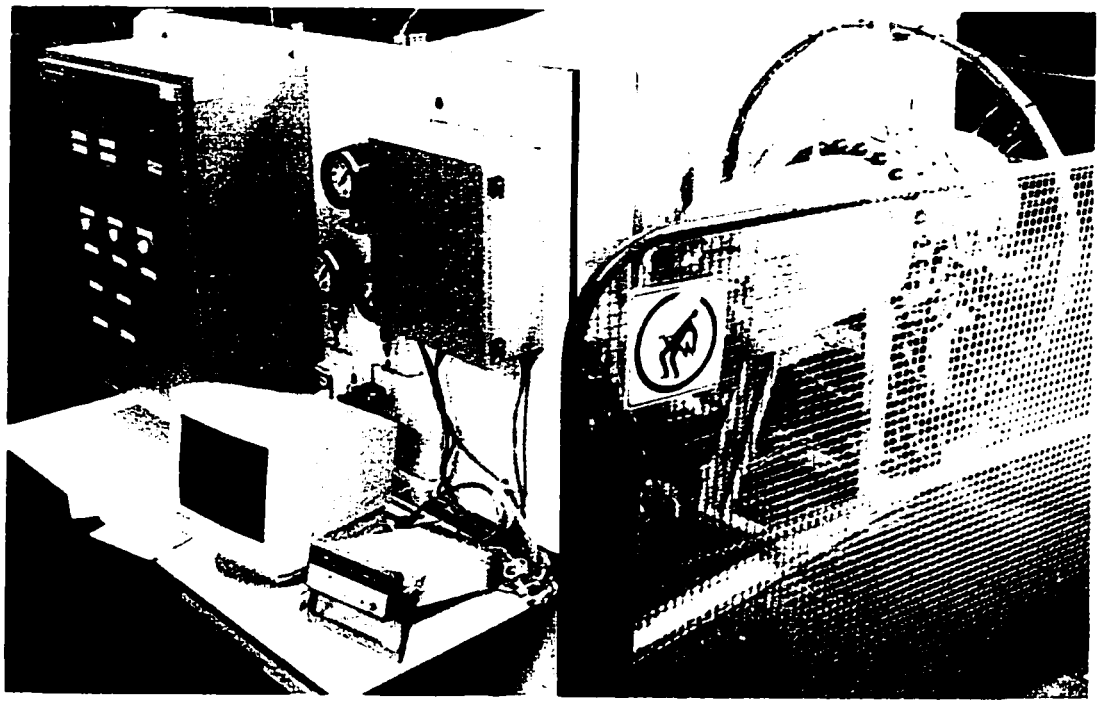

Figure 6.1 – Project test rig

The testing consisted of cycling the temperature of the joint and recording the flange temperatures, deflections and the bolt loads during the cycle. This data was then compared to the analytic methods to verify their accuracy. This therefore provides the necessary verification of the developed analytic techniques and confirms their validity for use in analysing the effects of temperature on flange sealing.

6.2 Description of the experimental rig

6.2.1 Test vessel

The test vessel was constructed from 24 inch standard wall thickness ASTM A106B pipe. The specially designed flanges (ref. Figure 6.2) were forged in ASTM A266-Gr4 and butt welded to the vessel shell. The flange configuration allowed a metal spacer to be inserted between the two flanges, in order to simulate a tubesheet joint. This means that there are two possible configurations for the joint; without tubesheet (1 gasket) and with tubesheet (2 gaskets). The flange facing surface finish was machined with concentric grooves to a 125AARH surface finish.

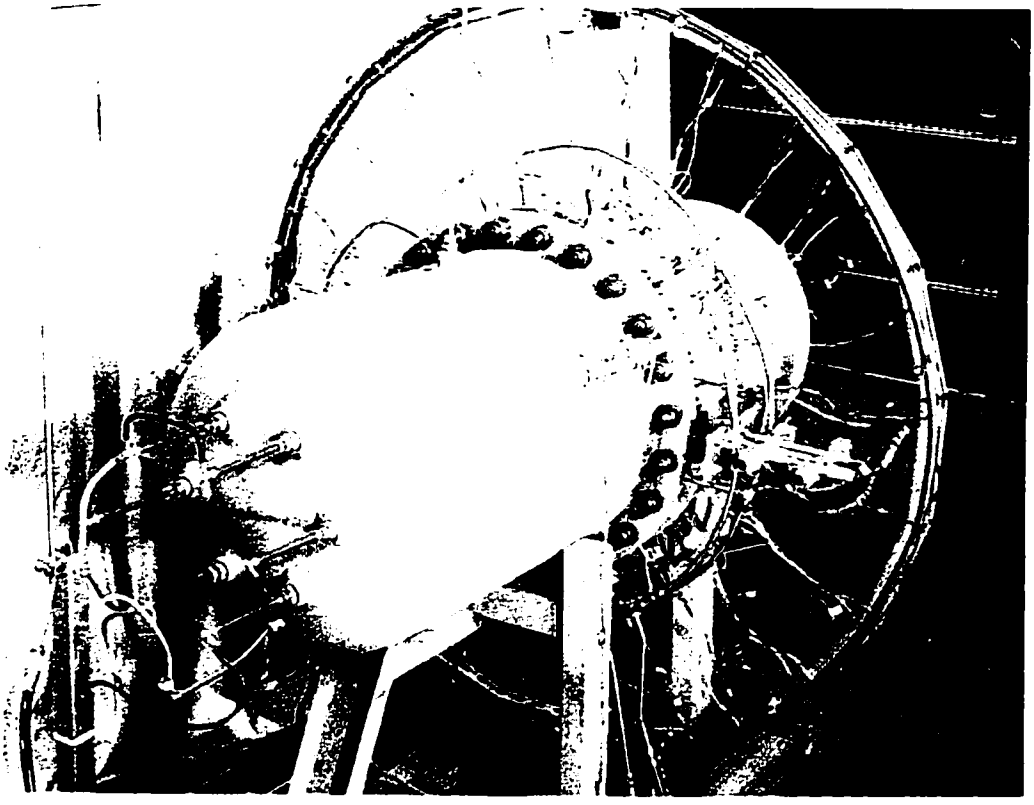

Figure 6.2 –Test rig vessel

6.2.2 Heating system

The vessel was internally heated using electrical tube heaters (ref. Figures 6.3 and 6.4). The heaters were controlled by an electronic control system (ref. Figure 6.5), so that the rate of the temperature transient could be modified and the steady state element temperature could be maintained to within ±5°C. The heater elements have a maximum operational temperature of 775°C, however the vessel flange obtained the desired maximum steady state temperature of 300°C with an element temperature of 480°C. The element temperature was therefore ramped from ambient to 480°C in either 10 minutes or 30 minutes.

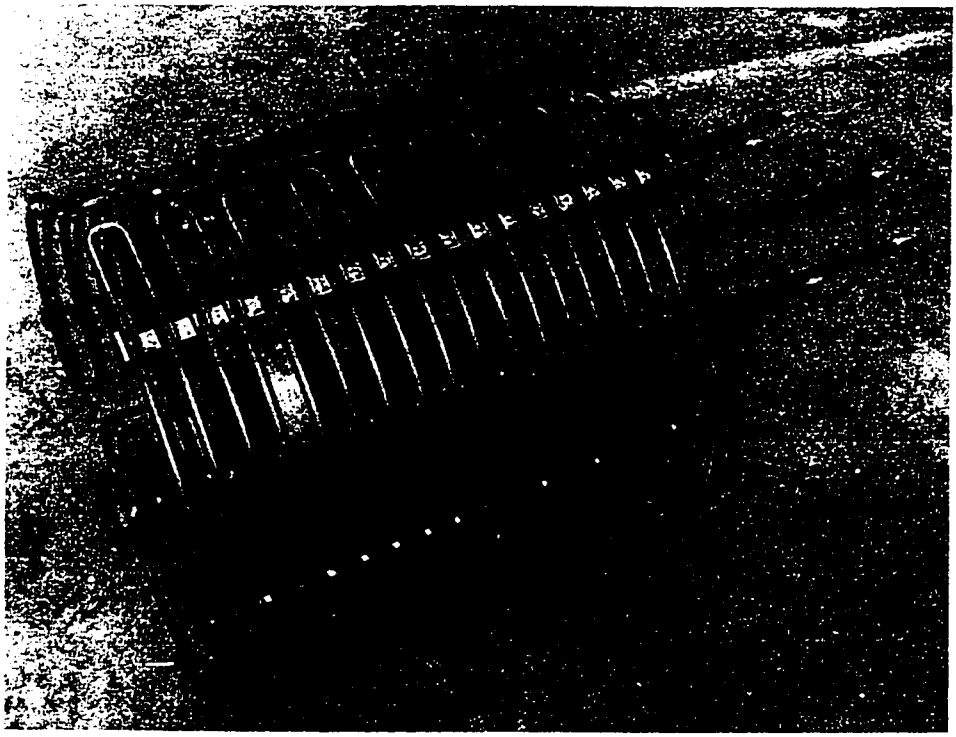

Figure 6.3 – Test rig heater elements

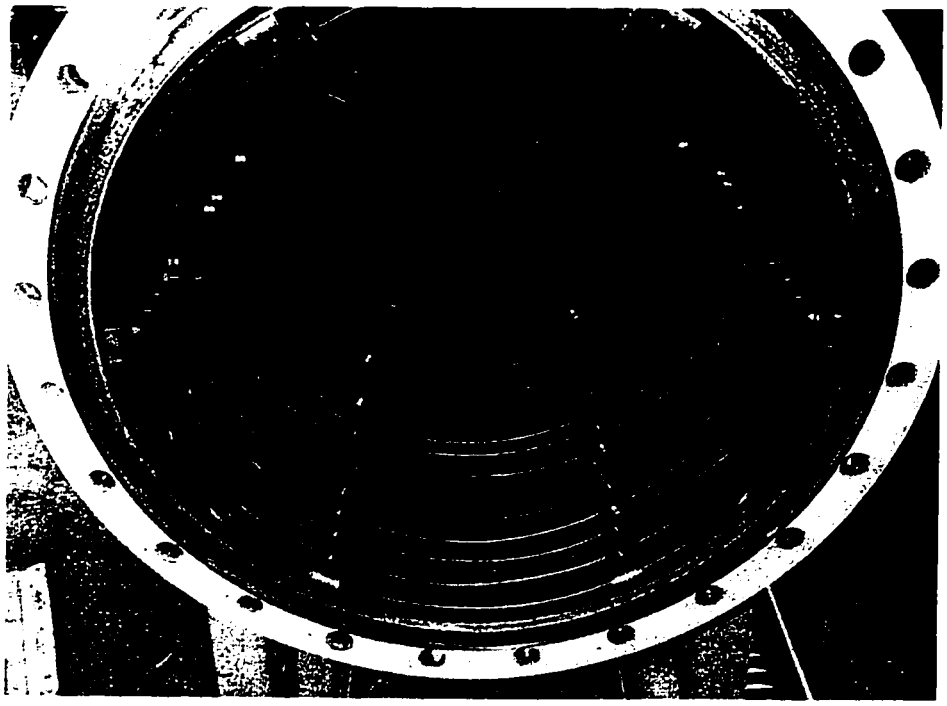

Figure 6.4 – Installed heater elements

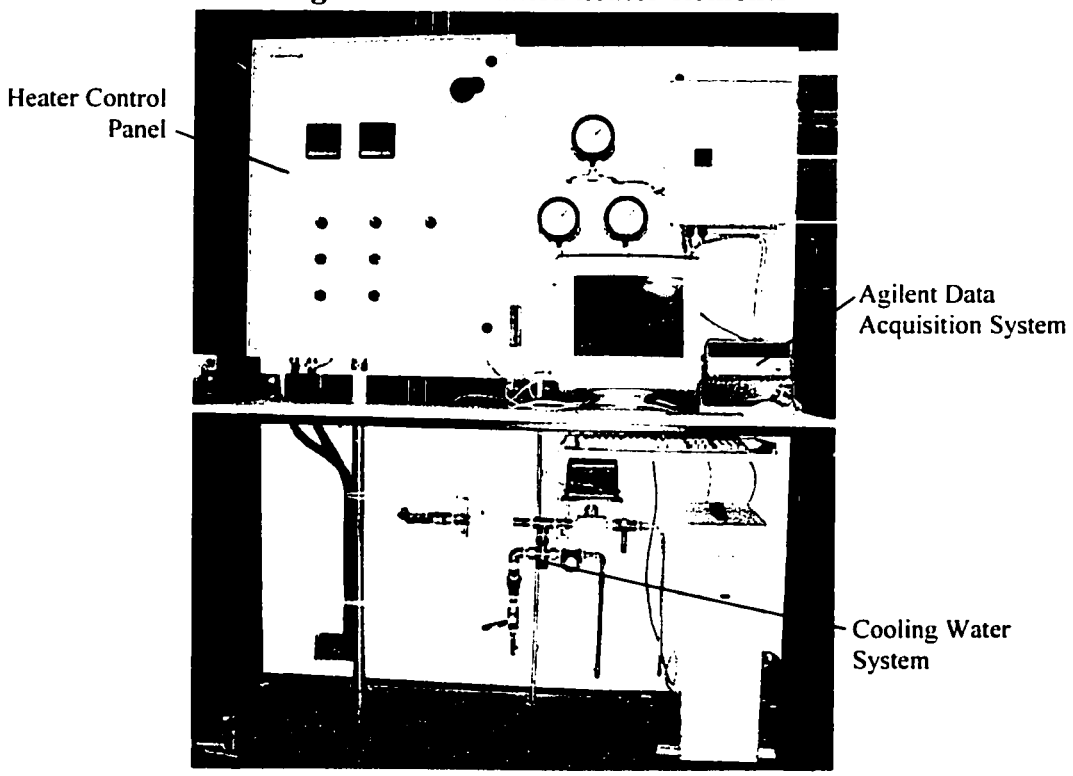

Figure 6.5– Test rig control panel

6.2.3 Data acquisition system

The instrument data was collected using an Agilent 34970A Data Acquisition system, fitted with three 20 channel 2-wire HP 34901A multiplexer cards (ref. Figure 6.5). There were therefore 60 available channels of data collection in total. The collected data was downloaded into a spreadsheet using the Agilent Benchlink software. The data was acquired at 5.5 digits and 18 bits, giving an acquisition resolution for the bolt loads in excess of 0.01MPa.

The signals were zeroed and automatically scaled within the data acquisition system. The calibration data was obtained during the individual instrument calibration processes (outlined in following sections). The data acquisition unit also has an in-built reference thermocouple junction, thus allowing referencing of the thermocouple signals to this value, eliminating voltage fluctuation effects.

6.2.4 Temperature measurement system

The vessel, flange and bolt temperatures were all recorded using 24gauge K-type thermocouples. The listed accuracy for such thermocouples is ±2.2°C (Omega, 1995). The thermocouples were spot-welded to the measurement point, to ensure the measured temperature was accurate and the thermocouple response was rapid (ref. Figure 6.6).

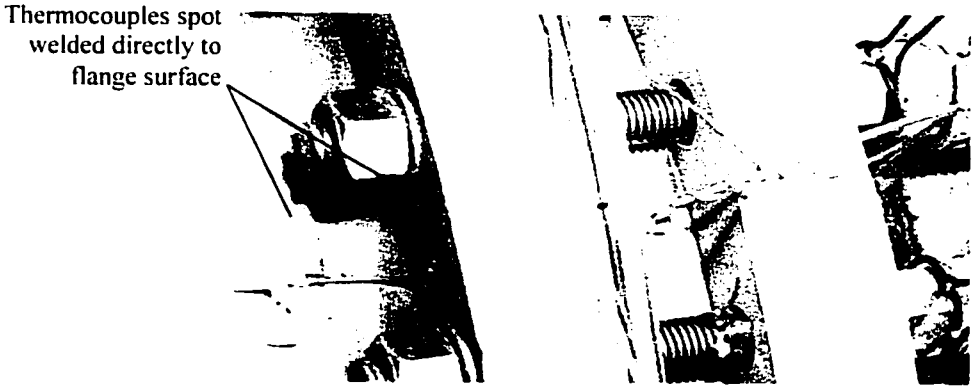

Figure 6.6 – Thermocouple arrangement

6.2.5 Bolt stress measurement system

The most important aspect of the experimental rig was the bolt instrumentation. Due to the relatively high temperatures (>300°C) it is not possible to use standard measurement methods, such as strain gauges, with an acceptable level of repeatability. Special bolt gauges, which were externally cooled, were fabricated (ref. Figures 6.7 to 6.9). The gauges were constructed using partially fired Aluminium-Silica ceramic and a full-bridge strain gauged cantilever beam. The bolt stretch, or relative displacement between the ends, is transmitted using a central pin inserted along the bolt length and welded at one end. As the bolt stress increased, the subsequent bolt stretch is measured as a movement of the cantilever beam due to the relative displacement of the bolt ends. Each bolt was individually calibrated, for both output signal versus bolt stress and also for output signal versus bolt temperature. An explanation of the calibration process and the resulting calibration sheets are included in Appendix D.

Neglecting the signal offset effects due to temperature, the calibration of the bolt gauges indicated that the gauge reading accuracy was generally better than ±10MPa (4% of full scale reading). More importantly however, when zero offset effects are neglected the accuracy improves, in general, to better than ±1MPa (0.4% of full scale). These accuracy figures mean that the joint assembly load can be determined to within ±10MPa and subsequent changes in bolt load can be determined to within ±1MPa.

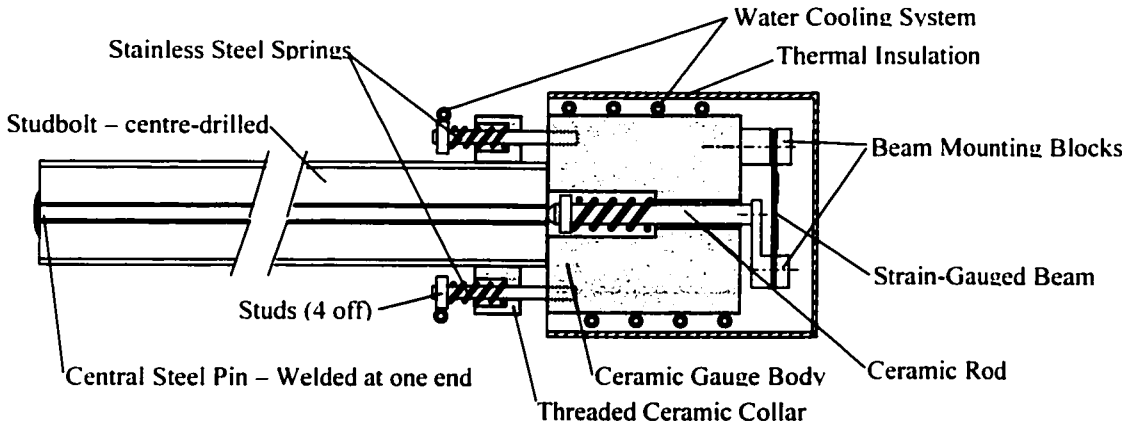

Figure 6.7 - Bolt gauge configuration

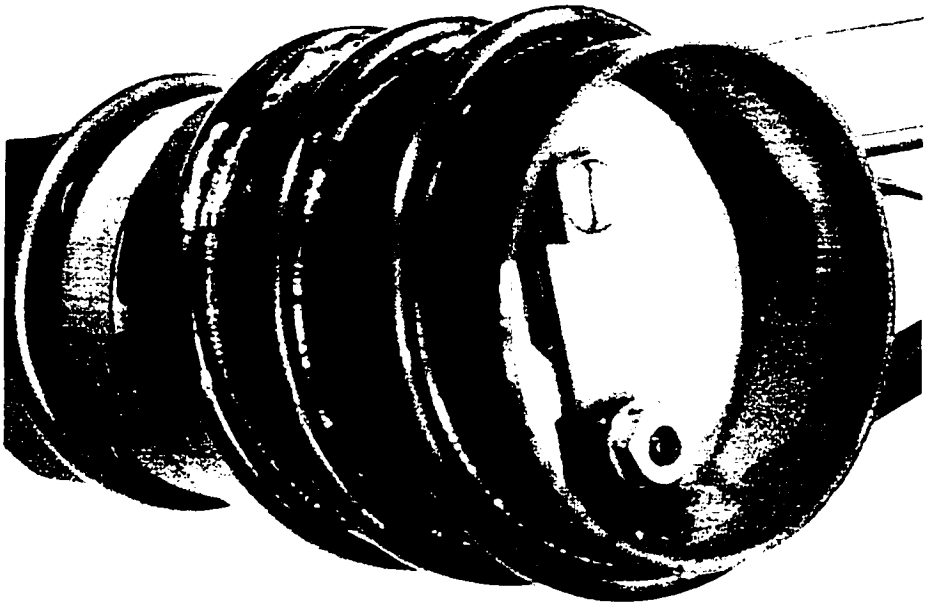

Figure 6.8 - Bolt gauge – view of strain gauged beam

Figure 6.9 - Bolt gauge – installed view

In addition to the gauge errors there is also an inaccuracy associated with the differential heating of the bolt and bolt gauge components. This leads to differential expansion of the components, which results in an erroneous gauge reading. However, since the gauge is maintained at a reasonably constant temperature and the material has a low coefficient of thermal expansion, this effect is generally limited to less than 10MPa variation in gauge reading for the temperature transients used in this testing. The variation in gauge output signal versus temperature is accounted for in the experimentation by modifying the measured bolt stress data during heat up and cool down of the rig, against the measured bolt temperature. The standardised calibration data for this correction is outlined in Appendix D. Due to the variability of this effect the previously listed ±1MPa accuracy decreases to around ±3MPa during temperature transients. However, the accuracy should be higher for the average bolt stress, as the errors on the 24 bolts will tend to cancel each other out, to a certain extent.

6.2.6 Flange deflection measurement system

The flange rotation was monitored using two or four Linear Variable Differential Transducers (LVDTs), depending on whether the tubesheet was fitted, at two opposing locations on the flange (ref. Figure 6.10). The LVDTs were mounted on 12.7mm diameter fully-fired ceramic rods. The rods and LVDT mounting system were water cooled to minimise thermal expansion effects. The LVDTs and upper mounting system were shielded from the effects of heat radiation by a water-cooled aluminium plate (ref. Figures 6.11 to 6.13).

The mounting system (ref. Figure 6.11) was designed so that the displacement of the flanges, relative to each other, in the axial direction could be measured at two radial distances. From these measurements the relative axial deflection and flange rotation were calculated. The results of the calibration of the LVDTs can be found in Appendix E.

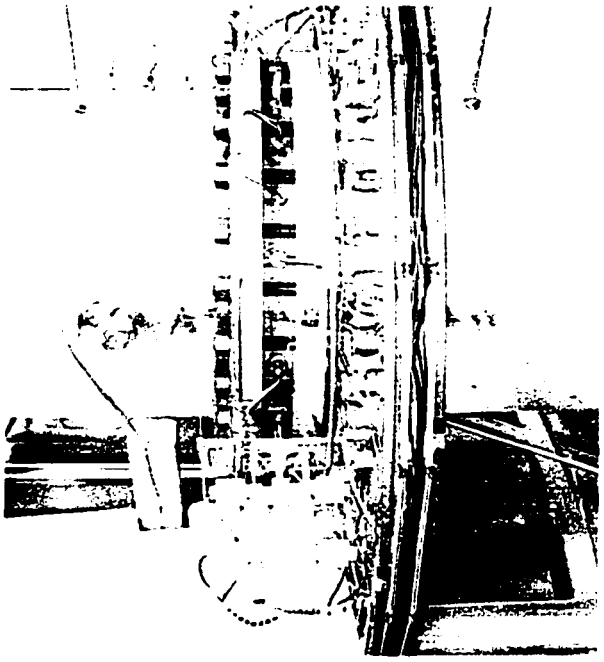

Figure 6.10 - LVDT mounting location

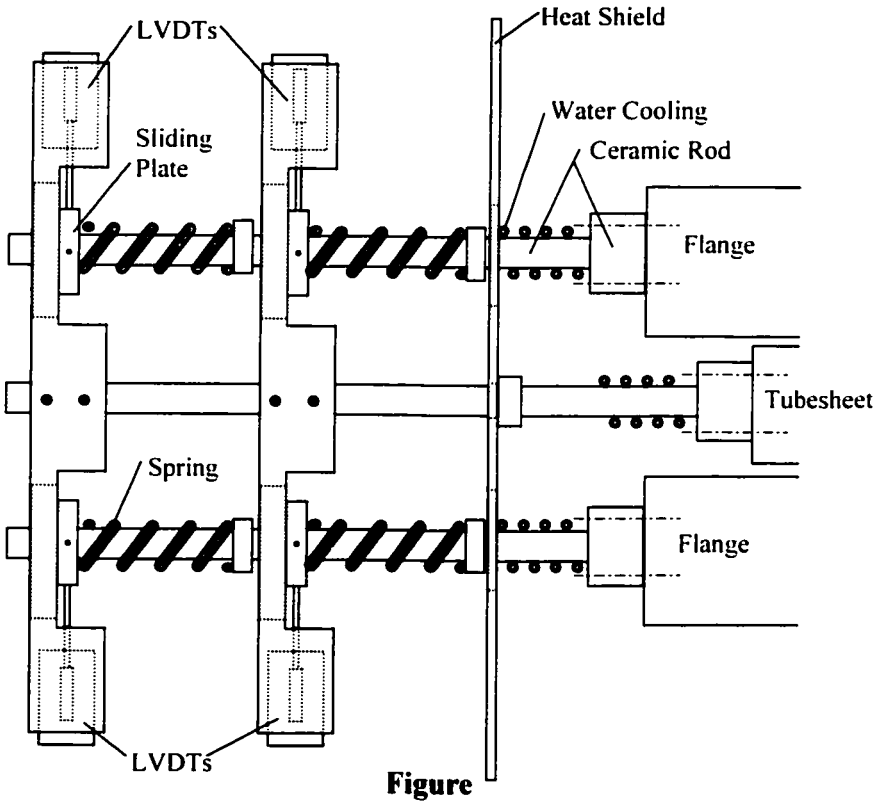

Figure 6.11 - LVDT general arrangement

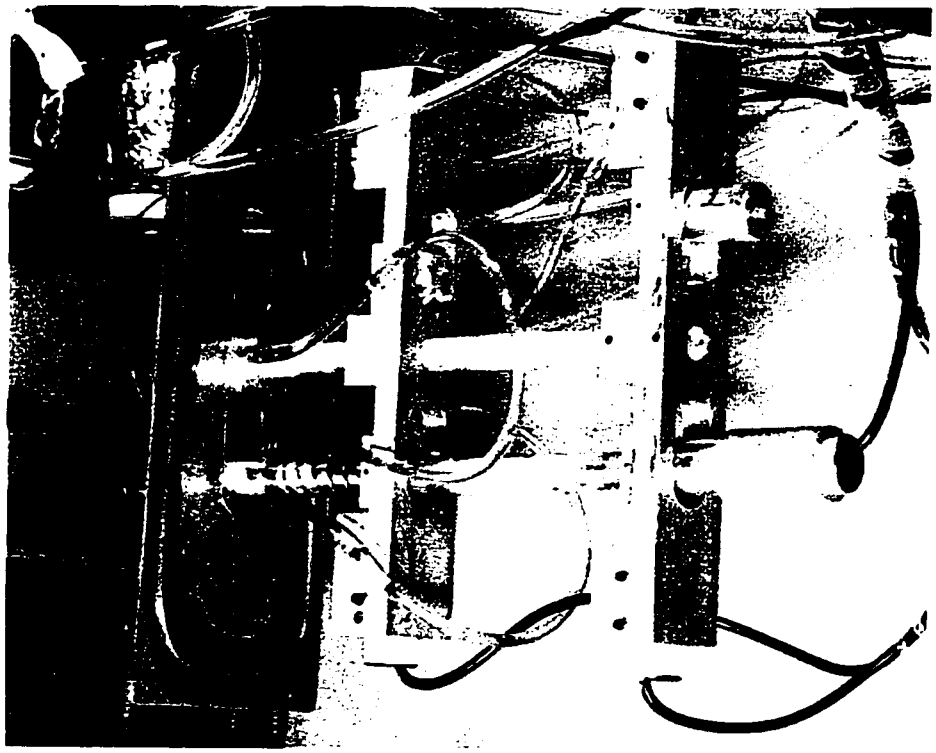

Figure 6.12 - LVDT set-up, without tubesheet

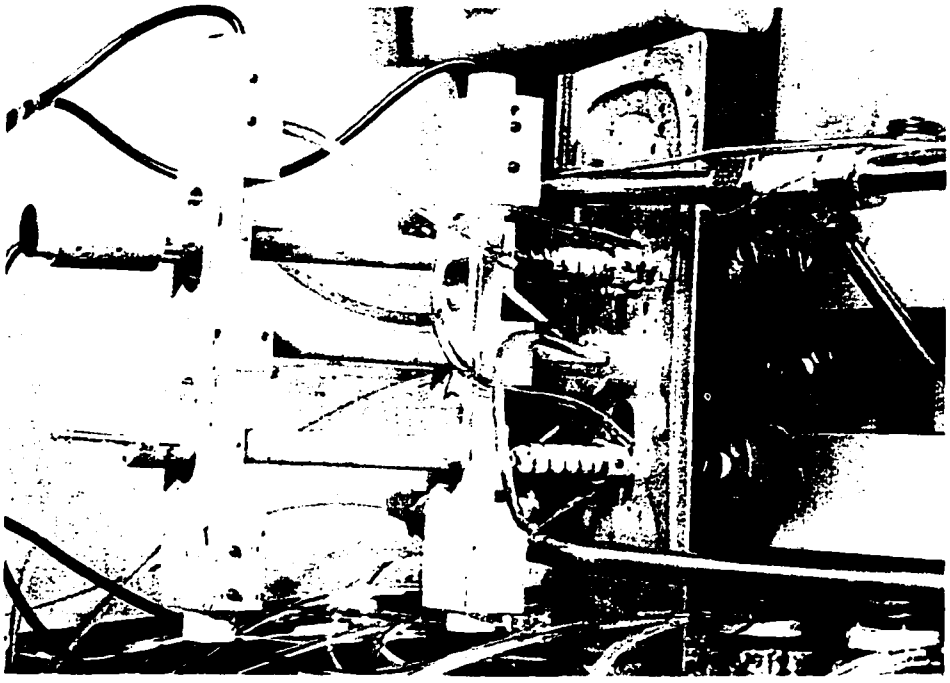

Figure 6.13 - LVDT set-up, with tubesheet

6.3 Test procedure

The test procedure used was as outlined following:

1. The bolt and LVDT cooling system was started and left to stabilise for 30mins.
2. The bolt and LVDT readings were zeroed in the data acquisition system.
3. The joint was then assembled to a nominal bolt stress.
4. The data acquisition system was then set to record all data at a rate of one reading every two minutes.
5. The rig was then left for several hours, to allow for initial room temperature gasket relaxation.
6. The heater was started, with a heating rate of either 48°C/min or 16°C/min. After this initial heating ramp, the heater control held the heater element temperature at a constant 480 ± 5°C for the period of the test.
7. The heater would then be stopped and the vessel was allowed to cool.
8. The rig was then either disassembled or another test was run.
9. The collected data was adjusted for the variation in bolt gauge reading with temperature.

Table 6.1 – Test configurations

Test	Heat Rate °C / min	Initial σ_b (MPa)	Tubesheet	Gasket Type
1a	48	250	No	CORR (a)
2a	48	150	No	CORR (b)
2b	48	from 2a	No	from 2a
3a	48	250	No	CORR (b)
3b	48	from 3a	No	from 3a
3c	16	from 3b	No	from 3b
4a	48	300	Yes	CORR (a)
5	48	Zero	No	CORR (a)
6a/b	48	Zero	Yes	CORR (a)

A total of 10 test runs were performed on the test rig. The runs are identified, with the applicable test variations, in Table 6.1. The gasket type used in each test was a corrugated metal gasket with graphite filler on each side. The gasket nominal initial thickness was 2.4 mm. There were two different gasket manufacturers used during the testing, (a) and (b). All tests, except for Tests 4a, 6a and 6b, were run without the tubesheet fitted in the joint.

6.4 Test results

6.4.1 Overall joint behaviour

The results for joint component temperature versus average bolt load for each of the tests are graphed in Figures 6.14 to 6.17. The repeatability of the tests is evident from the similarity of the graphs. There are certain aspects that can be noted from these graphs. The first is the initial relaxation of the gasket, which occurs predominantly during the first thermal cycle. From Figures 6.15 and 6.16 it can be seen that the average loss in gasket stress for the type (b) gasket is around 25MPa, with the majority of this relaxation occurring in the first cycle. The type (a) gasket relaxed more, with an average reduction in stress of around 35MPa during the test. It is interesting to note that the total loss in gasket load during Test 4a, which was performed with a tubesheet and therefore two gaskets, was slightly less than twice the loss measured in Test 1a, as would be expected (due to the relatively lower bolt rigidity when the tubesheet is fitted).

The second aspect that should be noted from these graphs is the difference between the shell inner diameter temperature and the shell outer diameter temperature. For each test the difference is in the order of 50°C. Such a temperature difference across a thin walled cylinder is not possible. It is evidence of erroneous measurement in either, or both, of these two readings. It is likely that the shell inner diameter reading is elevated from the actual temperature due to the proximity of the heating elements to the thermocouple. The incident heat radiation from the heating elements would artificially elevate the

thermocouple reading. Conversely, for the outer diameter thermocouple, the thermocouples on the shell were located close to the welded couplings used as entry points for the internal thermocouples. These couplings acted as local pin-type fins and therefore resulted in a lower reading compared with the shell average.

In addition to these two effects is the fact that the distribution of the temperature on the inner diameter will not be uniform, as assumed in the analysis. In reality the heat transfer from the heater elements would result in a much higher temperature in the vicinity of the elements, than in the space between two elements. However, an error in the component temperature does not correspond to an equal error in the magnitude of the bolt load, as will be demonstrated later in this section. It is therefore acceptable to assume that the actual average shell wall temperature lies somewhere between the two measured values, for purposes of bolt stress calculation and comparison with the analytical calculations.

In general, the graphs demonstrate good agreement with the predictions of the analytical theory. The bolt load decreases dramatically during the initial stages of heating and then slowly increases as the joint component temperatures reach steady state. Additionally, the bolt stress initially increases and then decreases during the joint cooling cycle. As predicted by the theory, this effect is much lower than that of the heating cycle. The maximum change in bolt stress was, on average, almost two times larger during the heating cycle than the cooling cycle. The smaller magnitude of the cooling cycle, together with the gasket relaxation which occurs during the initial thermal cycle, mean that the gasket stress will never exceed the initial assembly stress during cooling. It is therefore confirmed that the effects of the cooling cycle may be neglected.

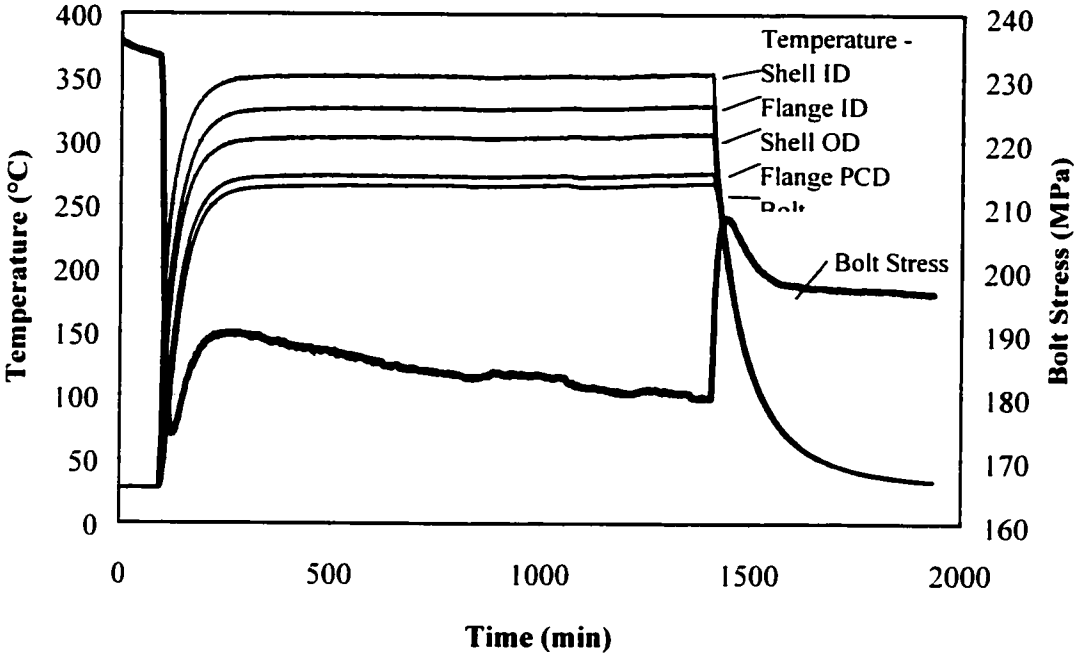

Figure 6.14 – Overall test results – Test 1

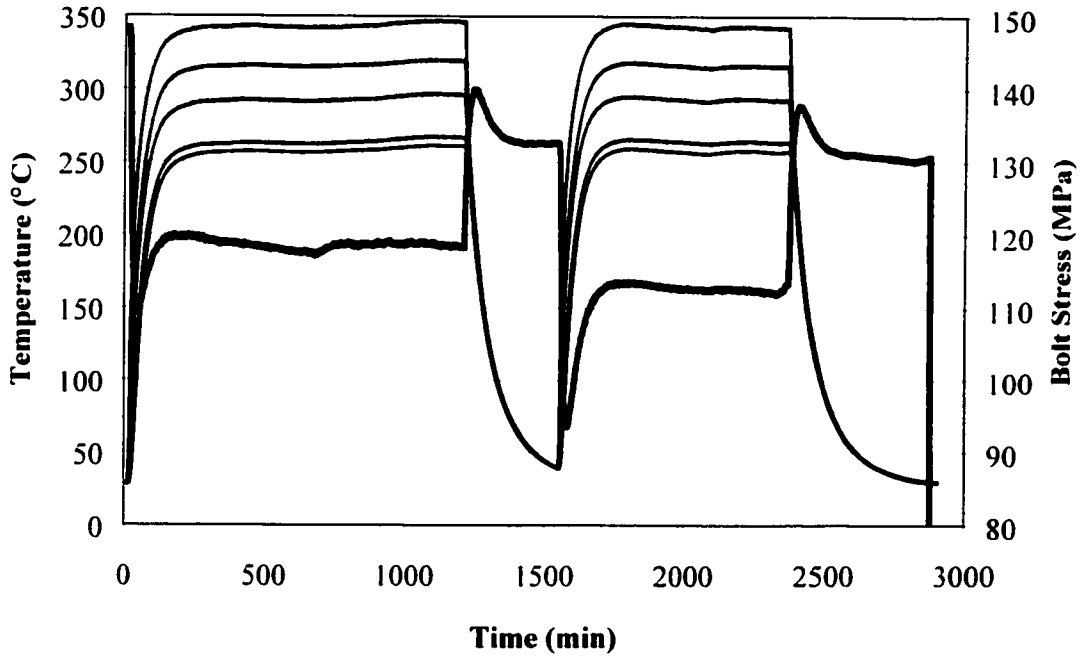

Figure 6.15 – Overall test results – Test 2

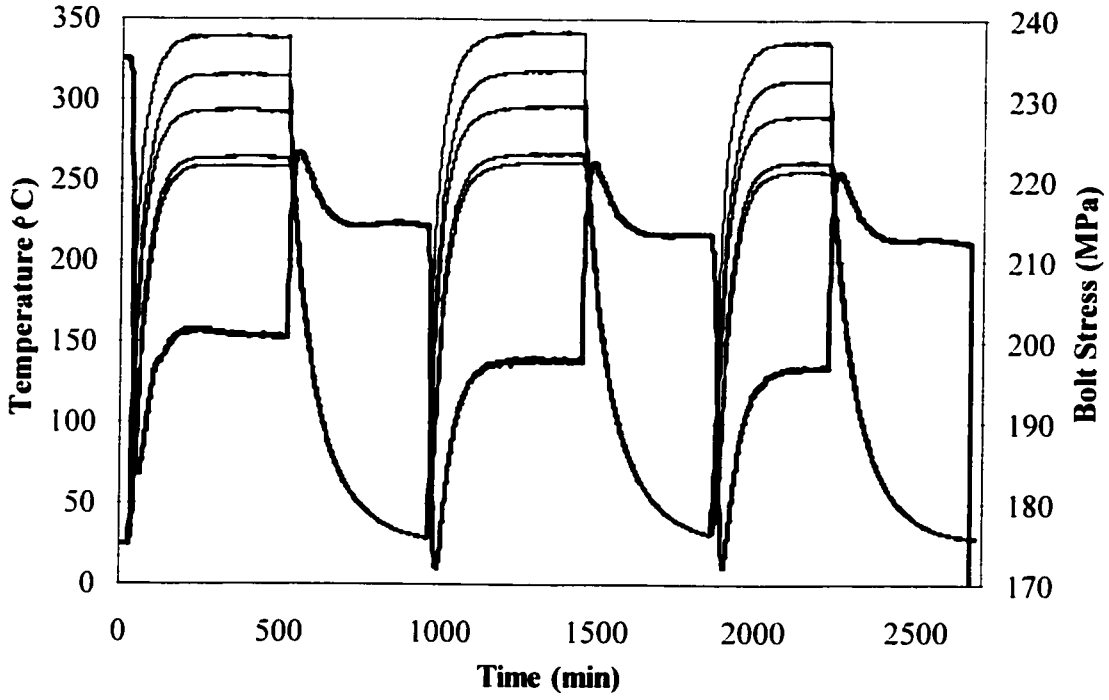

Figure 6.16 – Overall test results – Test 3

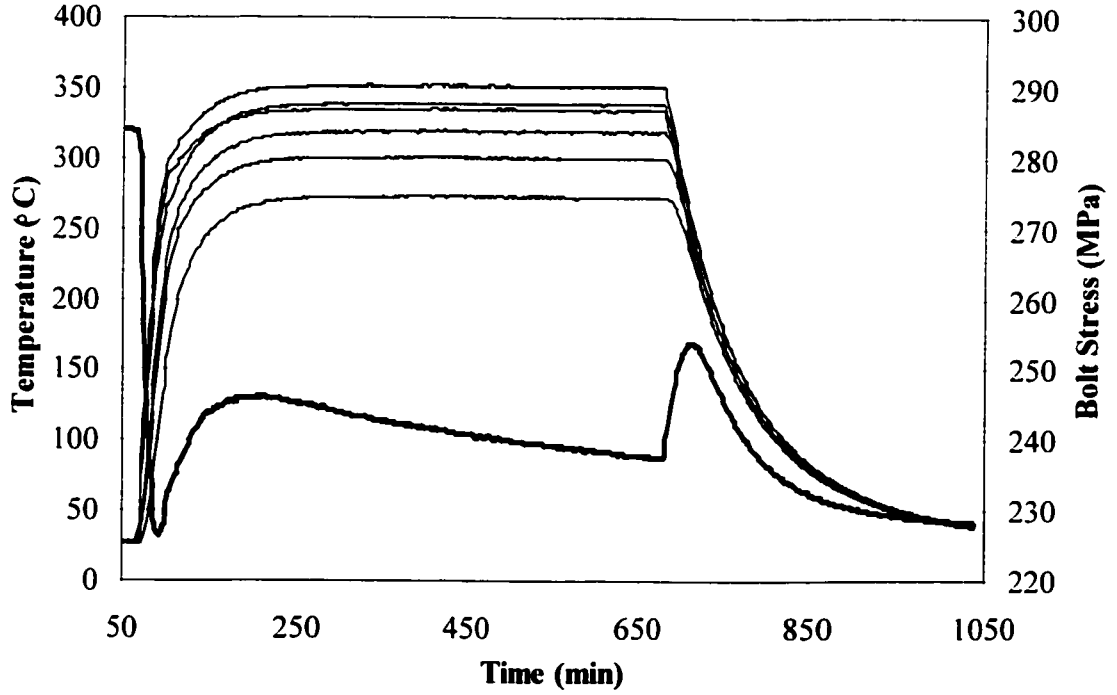

Figure 6.17 – Overall test results – Test 4

6.4.2 Heat transfer behaviour

By examining the steady state temperatures of the joint components it is possible to determine the approximate internal heat transfer coefficient from the heaters to the test vessel. The measured shell and flange temperature profiles indicate an internal heat transfer coefficient of only 47 W/(m².°C). Unfortunately this internal heat transfer coefficient for the electrical heater system is much lower than the values that would be expected in common heat exchanger operation (10,000 W/(m².°C) > h_i > 200 W/(m².°C)) (Butterworth, 1977). Even though the total heater power is 60 kW, it would appear that this could not match the thermal inertia of a hot fluid.

There is also a secondary effect caused by the small thermal inertia of the heater elements, as compared to an internal fluid. The analysis assumes that the fluid is at a constant temperature, or ramps to a constant temperature at a constant rate. However, the heater elements ramp to the constant temperature at a constant heat flux (60kW or lower, depending on heating rate). The heater element temperature is then held constant. As a result, this means that the heat transfer is not the same for the shell when compared to the flange during the thermal transient, due to the lower thermal inertia of the shell.

By modifying the shell internal heat transfer coefficient during the heating transient in the finite element analysis it was possible to obtain a similar temperature profile to the experimental results. This enabled the direct comparison of the finite element bolt stresses during the temperature transient to the experimental values. The analytical theory could not be to easily extend to encompass this change in heat transfer coefficient. However, since the analytical theory had previously been shown to compare very well with the finite element model, it was considered sufficient to show good agreement between the experimental results and the finite element model to verify both analytical approaches.

The finite element model was run during the transient with a constant internal heat transfer coefficient on the flange inner diameter of 47 W/(m².°C). The corresponding internal temperature was ramped from 0 to 455°C (480°C minus ambient) in 10 minutes. The shell internal heat transfer coefficient was held constant at 47 W/(m².°C). However, the corresponding internal temperature was modified during the transient. The temperature was ramped to 345°C in the first 10 minutes. It was then ramped to 455°C over the next 65 minutes. This gave a similar temperature profile for all the joint components to the experimentally measured values, as can be seen in Figure 6.19.

6.4.3 Heating cycle bolt stress behaviour

The steady state change in bolt stress due to the increase in joint temperature from ambient to 300°C is a reduction, on average, of 15MPa (ref. Figures 6.13 to 6.17). This compares well with the predictions of both the finite element analysis and the analytical method, which predict a bolt load loss of 18MPa and 13MPa respectively. The difference between the two analytical methods is due to the fact that the FEA solution predicts a higher bolt temperature than the analytical solution, hence the reduction in gasket stress is greater.

Some of the results for the change in temperature and bolt stress during the heating cycle are graphed in Figures 6.18 to 6.20. Figure 6.19 shows the FEA results superimposed on the measurements taken during Test 2b. The agreement between the experimental results and the FEA, both in magnitude of bolt stress reduction and in the shape of the transient curve, is very good. The minor differences between the experimental temperatures and the FEA model temperatures during the transient can be seen to have a very small effect on the difference between the corresponding bolt load curves.

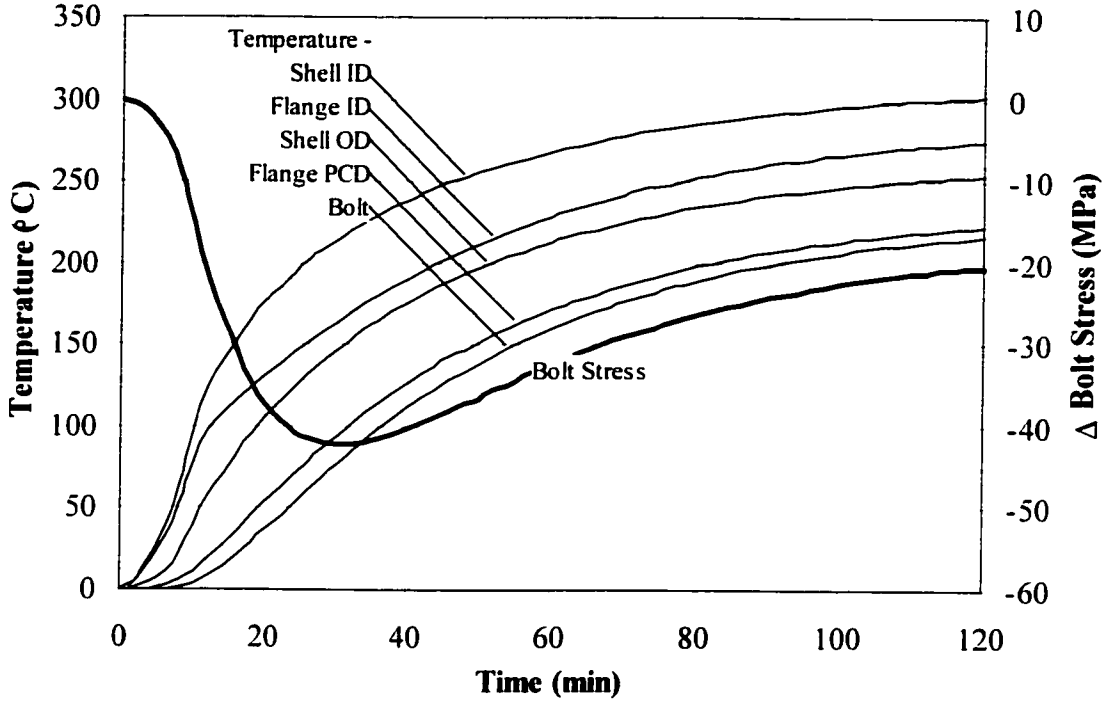

Figure 6.18 – Joint heating cycle behaviour – Test 3b

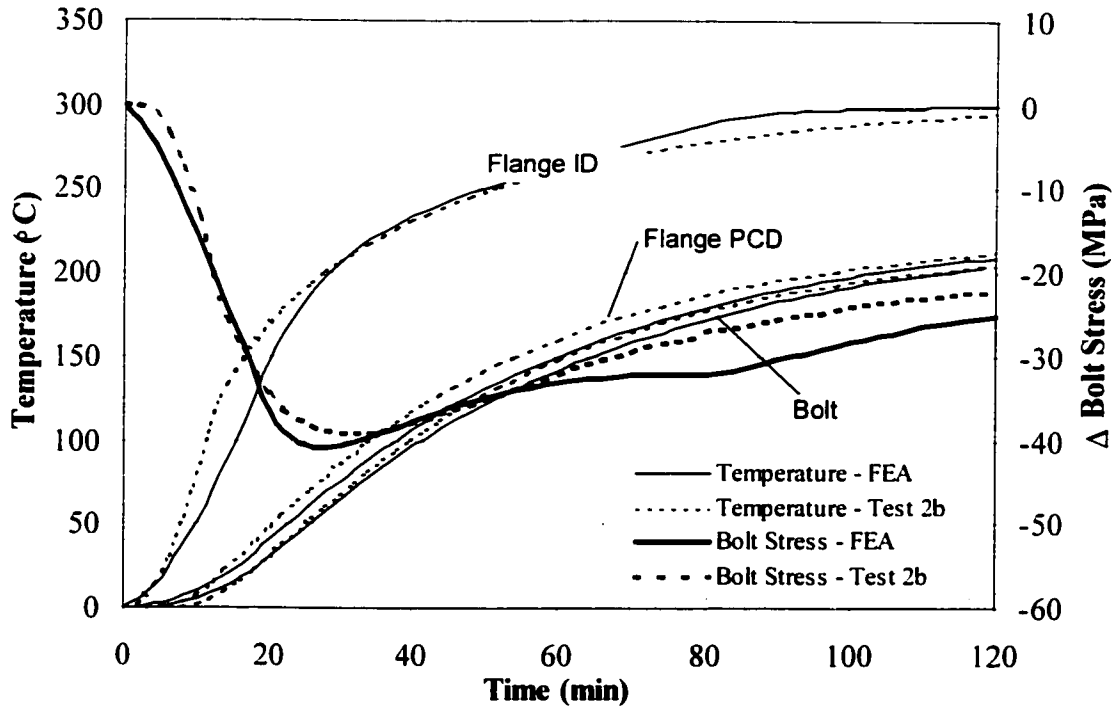

Figure 6.19 – Joint heating cycle behaviour – Test 2b and FEA

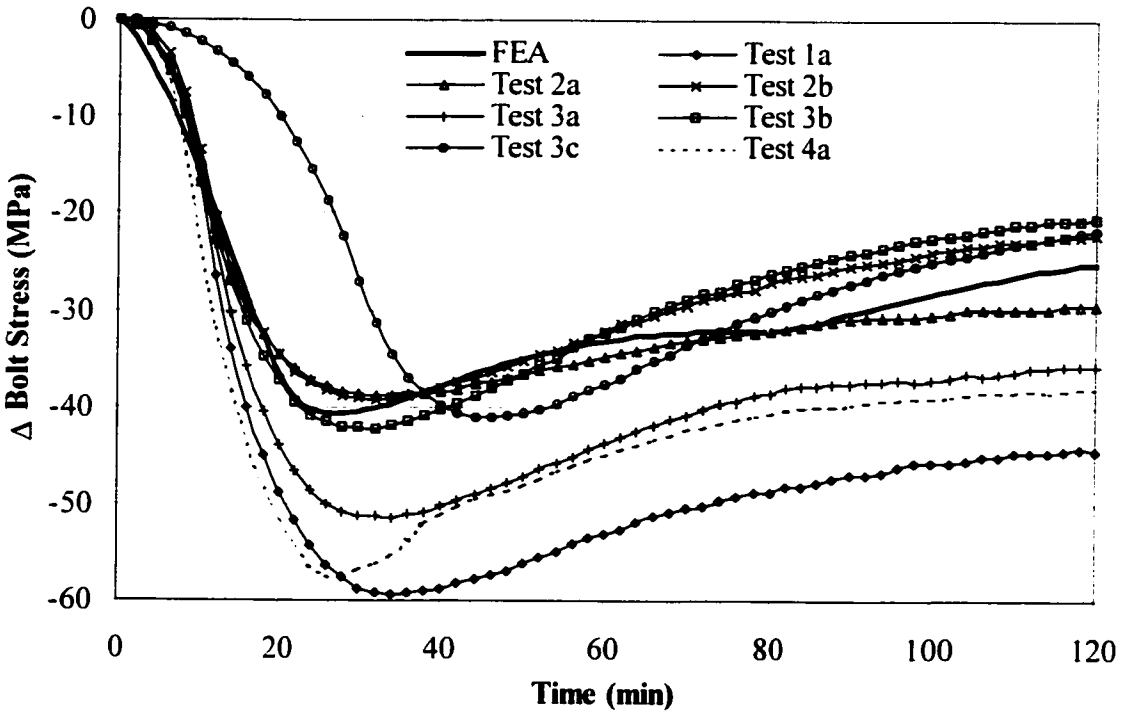

Figure 6.20 – Heating cycle bolt stress – all tests and FEA

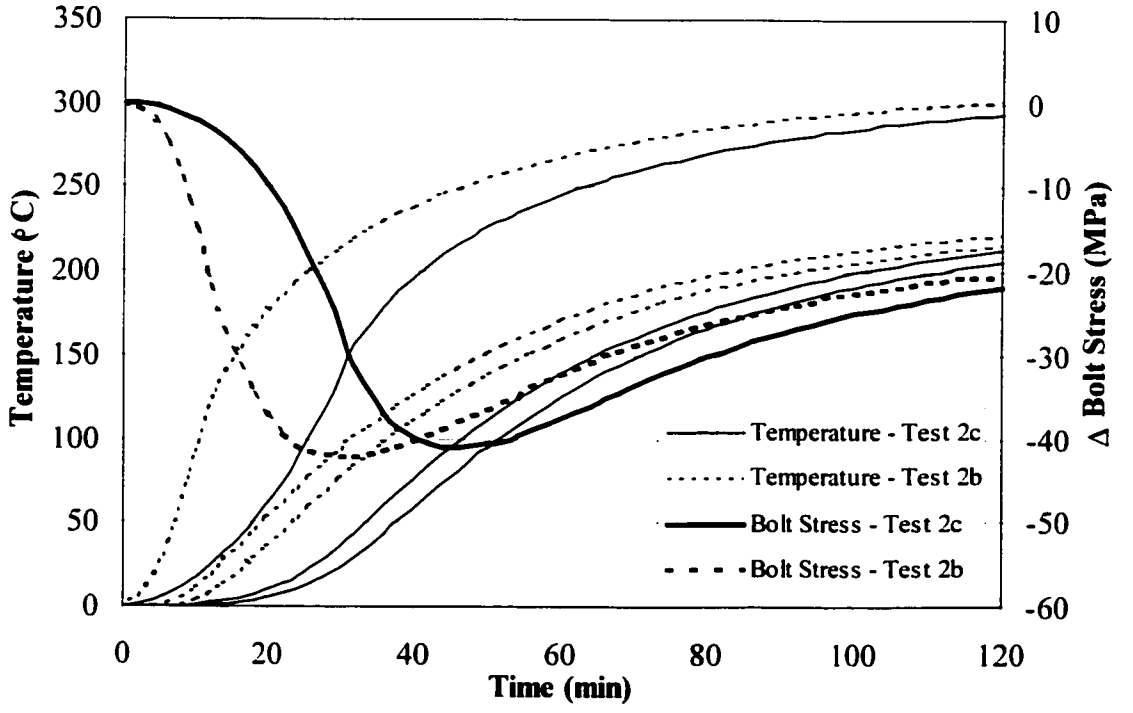

Figure 6.21 – Joint heating cycle behaviour comparison – Tests 2b and 2c

Figure 6.20 graphs all of the measured bolt stress variations versus the FEA results. As can be seen, the agreement between the FEA and experimental results is excellent and the experimental results are obviously highly repeatable. The only variation in result occurs when there is a change in test configuration, such as a modified heating rate (Test 3c), the addition of the tubesheet (Test 4a), or for the first run on the type (a) gaskets (Tests 1a and 4a). The relaxation that occurs during the first thermal cycle is evident in this graph as an offset of the bolt load. However, even though the magnitude of bolt load loss is greater, it is still evident that the overall shape of the curve is the same.

6.4.4 The effect of heating rate

Figure 6.21 shows a comparison of Tests 2b, with a 48°C/min heating rate, and Test 2c, with a 16°C/min heating rate. As would be expected, the slope of the bolt transient is lower for Test 2c. However, the most important aspect is that there is very little variation in the overall magnitude of the bolt load change. The maximum losses in bolt load are effectively identical, considering the possible errors involved in measurement, even though the heating rate is three times slower.

This result is in good agreement with the FEA results, which were run for a constant 47W/(m².°C) internal heat transfer coefficient case (ref. Fig 6.22). The very small variation in bolt stress between the different heating rates is influenced by the low internal heat transfer coefficient. However, by comparison of FEA results for a higher internal heat transfer coefficient (400W/(m².°C)) and varying heating rates (ref. Figure 6.23), it can be seen that the change in the bolt stress variation is still of the same magnitude. This indicates that, within reasonable limits, the heating rate can be ignored. Additionally, assuming an instantaneous heating rate results in the calculation of conservative values of the bolt stress variation and avoids problems associated with defining the actual fluid temperature variation and internal heat transfer coefficient.

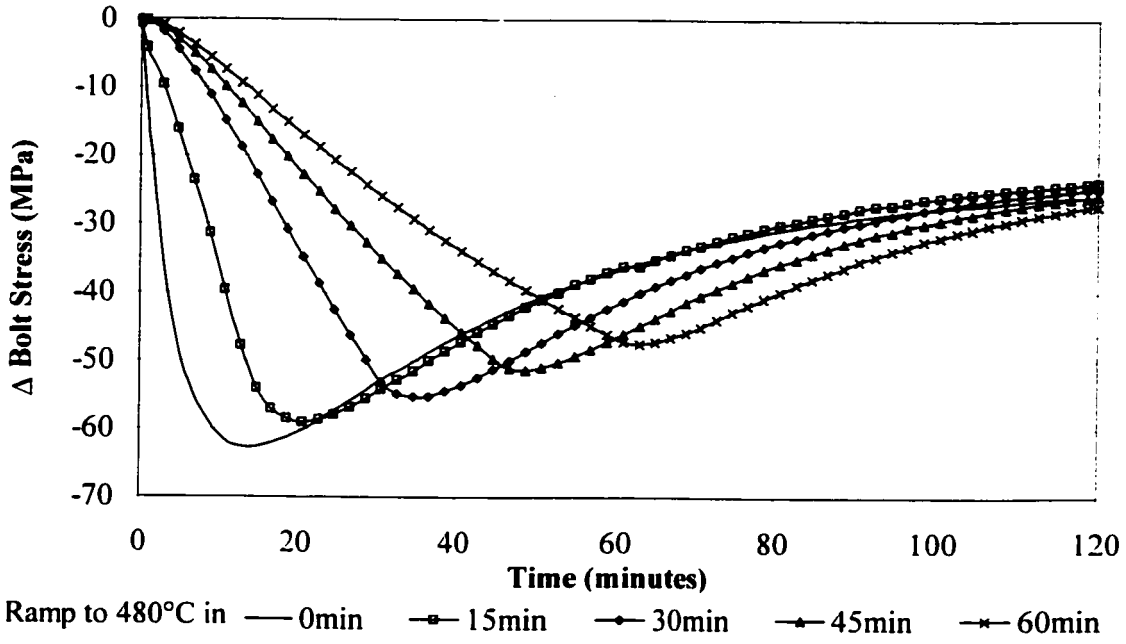

Figure 6.22 – FEA results for varying heating rates (h_i = 47W/(m².°C))

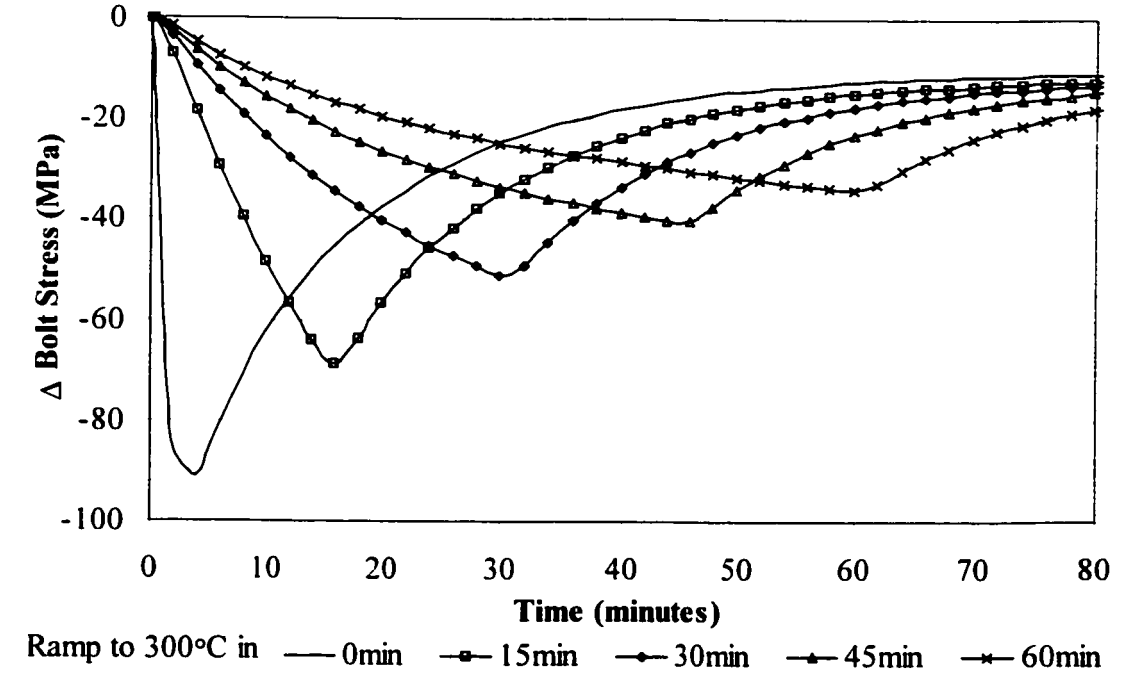

Figure 6.23 – FEA results for varying heating rates (h_i = 400W/(m².°C))

This is particularly important from a practical aspect, as it would be very difficult to define the heating rate of an operational exchanger. It would also be impractical to specify the heating rate during design, as the exchanger will be operated to maximise production, rather than minimise the chances of leakage. Additionally, there would always be a chance of higher heating rates during plant upset conditions that could not be foreseen. Therefore, the most robust design process would be to analyse the joint as if the internal fluid temperature was applied instantaneously, as previously assumed in the proposed analysis.

6.4.5 The effect of the tubesheet

In heat exchanger joints the tubesheet plays a important part in the transient behaviour of the joint due to the fact that it has a large heat transfer surface and therefore responds to the thermal transient very quickly. However, the test rig tubesheet is not specifically heated by the electric heaters and so the heating rate of the tubesheet is similar to the flanges. This means that the tubesheet had little effect on the obtained results, as can be seen in the comparison of bolt loads for all tests in Figure 6.20. There was therefore little reason to perform comparison of the analytical results with the bolt load curve of Test 4a.

6.4.6 Heating cycle flange deflection

In addition to measuring the change in bolt load during the temperature transient, the flange rotation was also measured by the LVDT system. This allowed comparison with the analytically predicted results to ensure that the amount of flange rotation occurring due to the mechanical Effects #2 and #3 was actually happening. It should be noted, however, that the amount of the rotation being measured during the transient, for a fully assembled joint, is only in the order of 0.02°. The readings are therefore very susceptible

to measurement error, particularly during thermal cycles. It is, consequently, difficult to compare the flange rotation during thermal cycles if the flange is fully assembled.

However, if the bolts are not tightened, then the flange rotation predicted by theory increases to around 0.14°. It is this rotation of the flange, due to the internal temperature gradient, that causes the reduction in bolt load due to the mechanical Effects #2 and #3. It is therefore highly useful to examine the thermally driven flange rotation when the joint is assembled, but the bolts are not tightened (ref. Figure 6.24). From this graph it is evident that the theoretically predicted rotation is a good match for the experimental results. There appears to be a certain amount of thermally driven error that affects the LVDT measurements. This error has the effect of increasing the rotation reading in the order of 0.02° to 0.04°, depending on position during the transient.

However, the trend and change in value are still very similar for all tests by comparison to the FEA results. Tests 6a and 6b had slightly improved readings from Test 5, this is due to minor modifications made to the LVDT set-up. These modifications involved the insertion of very thin shim stock into the system to eliminate some of the radial clearances between the sliding pads and the ceramic rods. It is therefore evident that this free-play in the system is a cause of some of the thermally driven inaccuracy. It should be noted, when examining these results, that the degree of rotation being measured is very small. The error in one LVDT measurement corresponding to a rotation measurement error of 0.04° would only be of the order of 80 μm (which is approximately the diameter of human hair).

To determine whether or not this thermally driven error is repeatable it is useful to examine the flange rotation results for the fully assembled test, by comparison to the analytical predictions. The results of Test 1a, for both left and right side LVDTs, are graphed by comparison to the FEA results in Figure 6.25. It can be seen that there is a discrepancy between the initial flange rotation on the two sides of the joint. This is due

either to initial misalignment of the joint during assembly, when the LVDTs were zeroed, or uneven free-play in the two LVDT arrangements.

It can also be noted that the initial flange rotation appears to be only 70% to 90% of the value expected by both the FEA model and the analytical method. However, both of the previously mentioned sources of error would also have caused the overall reading of flange rotation to be lower. It would therefore appear likely to be inaccuracy in the LVDT system that causes this discrepancy between the theory and experimentation. This level of error was also repeatable in subsequent tests, although in some instances the indicated rotation was up to 95% of the predicted analytical value.

Additionally, the experimental values appear to change by as much as twice the predicted theoretical value during the temperature transient. However, the magnitude and form of the error appear to identically match the error found in the previous, unassembled test. It can be seen, by comparison of several test runs (ref. Figure 6.26), that the results, and therefore the error, are repeatable. This reinforces the likelihood that this difference in value is probably due to a repeatable experimental error, especially considering the fact that agreement between the FEA and the experimental bolt stress values was so good.

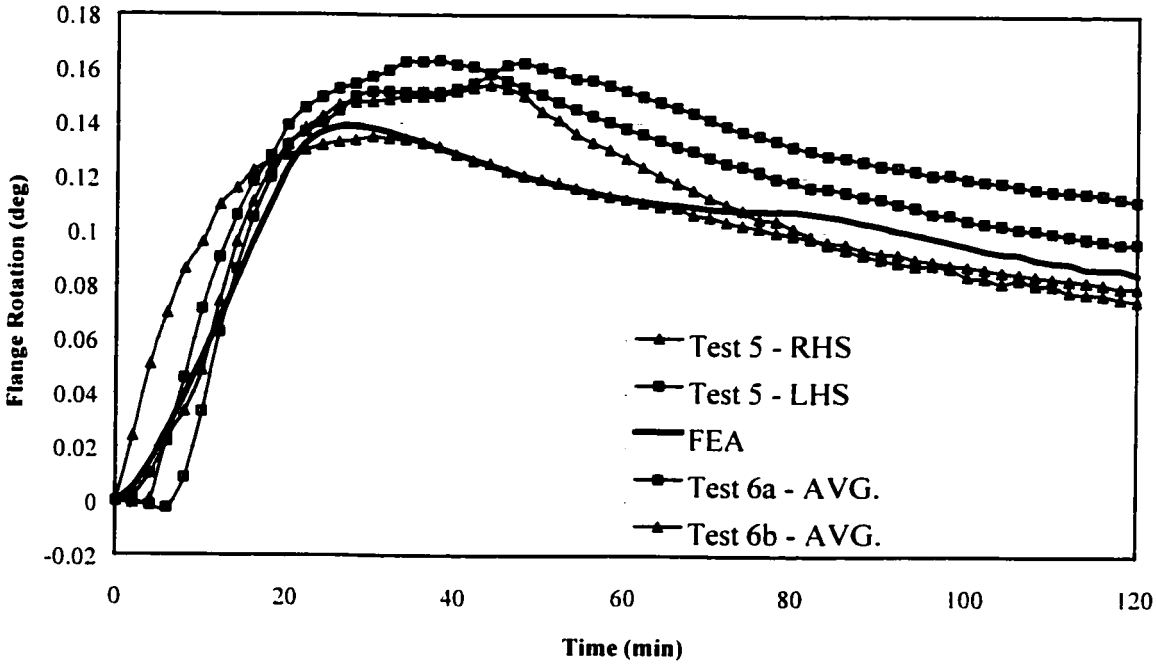

Figure 6.24 – Experimental flange rotation versus FEA – Tests 5 & 6.

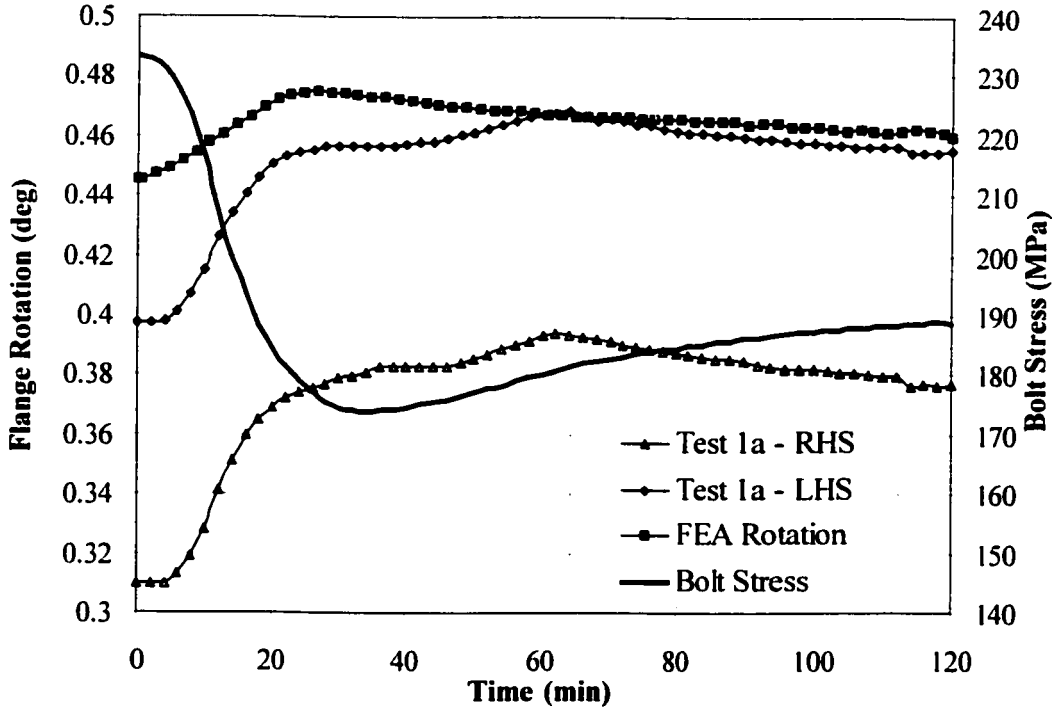

Figure 6.25 – Experimental flange rotation versus FEA – Test 1a

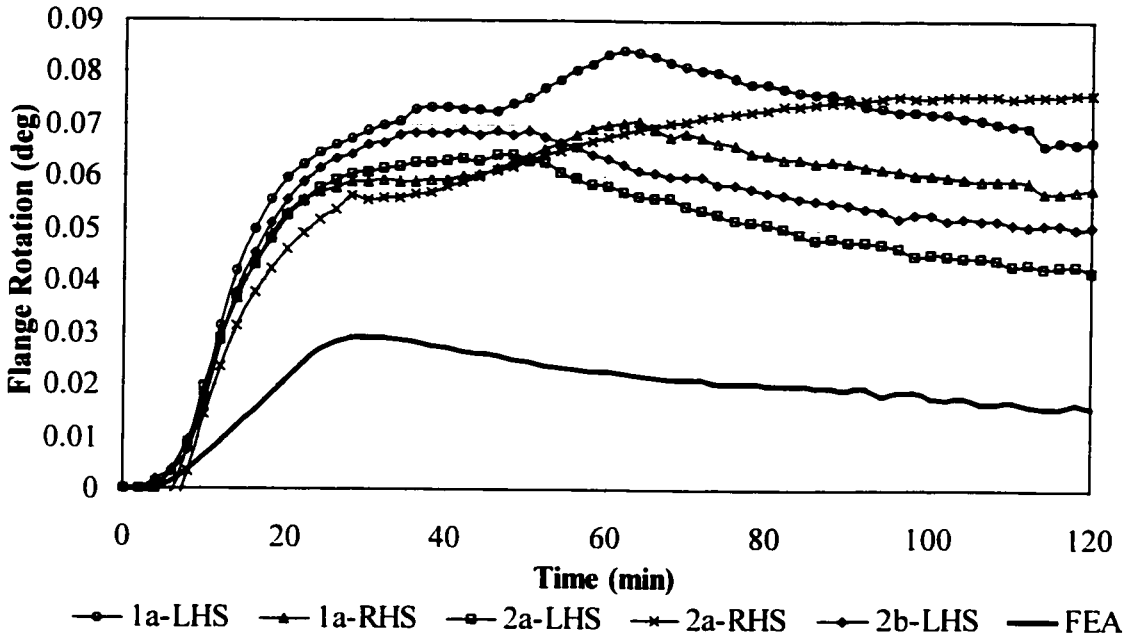

Figure 6.26 – Experimental flange rotation versus FEA – Tests 1 and 2.

CHAPTER 7

ANALYSIS SUMMARY

7.1 Summary of developed methodology

In order to analyse the effects of temperature on joint operation the joint designer must consider two main areas:

- The effects of temperature on the flange deflection
- The effects of temperature on the gasket stress

In order to analyse these two areas the first step is to determine the joint component steady state operational temperatures for the design service. This is done using Equations 2.1 to 2.8 (shell), 2.16 to 2.24 (flange ring) and 2.45 to 2.50 (bolt). Once the steady state temperatures are determined then it is relatively easy to use Equations 2.9 (shell) and 2.28 (flange ring) to assess the radial expansion of the flange. This is an important aspect, especially if the two mating flanges are operating at different temperatures. The differential radial expansion may in fact physically destroy the gasket, depending on the individual gasket construction.

The individual component axial expansions are determined using Equation 2.26, for the axial expansion occurring in the flange ring at both the inner section and at the bolt pitch circle. Then Equation 2.51 is used to determine the bolt axial expansion. Additionally the equivalent pressure due to the differentially higher expansion of the shell must be determined using Equation 2.30. The steady state mechanical interaction analysis can then be performed, using Equations 3.1 to 3.13 and 3.18.

The transient temperature effects may then be determined using the procedure outlined in Tables 5.2 and 5.3, Figures 4.3a to 4.5 and Equations 4.3 and 5.1. This allows the maximum reduction in bolt stress to be determined. By assessment of the flange rotation, the maximum rotational deflection of the flange may be determined. This deflection is important as excessive rotation of the flange may in fact lead to gasket leakage, due to a reduced gasket sealing surface area being utilised. For certain joint configurations it may also be necessary to examine the maximum increase in bolt load that occurs during the thermal transient. This is only important, however, if the gasket is susceptible to damage due to over-stress.

7.2 Future work

The presented analytical method addresses only symmetrical flange pairs that are evenly heated. There is a large proportion of flanged joints that are not covered by this simplification. However, the analysis provides the basis for future extensions to allow for additional analysis steps, to account for such effects as:

- Non-symmetrical flange pairs
- Uneven flange heating (circumferential gradients)
- The effects of joint component creep
- Non-standard flange constructions
- Optimisation of flange geometry for transients

Additionally, for inclusion in current design procedures, the methodology requires simplification. Guidelines as to which joint designs would require analysis of the effects of temperature must also be developed, so that the designer knows when this additional analysis must be performed. The majority of the complex equations for determination of the temperature profile for the flange ring may be incorporated into a graphical approach, thus eliminating the necessity of the use of Bessel functions. Similarly, some

sections of the mechanical interaction equations may also be developed into a graphical approach, such that the complexity of the analysis is reduced. In this way the method of analysing the temperature effects will be similar to current pressure vessel design codes, which use a combination of simple equations and graphs in the design of pressure vessels.

CONCLUSION

The developed methodology allows the pressure vessel flanged joint designer to consider the effects of temperature during joint design. It has been demonstrated that the developed analysis methods can be accurately applied to the determination of the joint component deflections and stresses during both steady state operation and thermal transients. The methodology provides an analytical basis for the analysis of the effects of temperature on joint operation. The developed analysis may easily be extended to cover all existing configurations of pressure vessel and piping flanged joints.

In addition, the analytical and graphical solutions are more robust and, if automated, much faster to use than current analysis methods, such as Finite Element Analysis. The operational factors determined during the study, such as actual heat transfer coefficients, are also necessary when using Finite Element Analysis. These factors were not available in published literature, prior to the work performed during this study. The experimental work provides a solid basis against which realistic assessment of any analysis technique for the effect of temperature on flanged joint operation may be performed.

Furthermore, it has been demonstrated that, for certain joint configurations, the effects of temperature on joint sealing may be far greater than the effects of pressure. The frequency of joint leakage in heat exchanger operation also supports the fact that it is necessary to include an assessment of the effects of temperature on joint leakage in joint design. This study has therefore provided an important development in the prevention of the detrimental effects of heat exchanger joint leakage, which include increased operational costs, loss of life and environmental impact.

REFERENCES

ABAQUS. (1999). ABAQUS Standard Manual, Version 5.8.1. Abaqus.

ANDRESSO, S., FLESCH, B., BOUCHE, D. (1985). Parameters governing mechanical and thermal behavior of the bolted flange simplified method. Proceedings of the ASME PVP conference, New Orleans, Louisiana, 129-135

ANDRESSO, S. (1984). Calculation of the Initial load of a closure tightening taking into account the deformation of the parts submitted to pressure. Proceedings of the 5th international conference on pressure vessel technology, San Francisco

ANON. (1942). Gasket Materials and Contact Facings. Mechanical Engineering, 64, n.2, 146-149

ASME. (1998a) ASME II, Part D, Boiler and Pressure Vessel Code. American Society of Mechanical Engineers, NY

ASME. (1998b) ASME VIII, Div 2, Boiler and Pressure Vessel Code. American Society of Mechanical Engineers, NY

BAILEY, R.W. (1937). Flanged pipe joints for high pressures and temperatures. Engineering, 144, 364-365, 419-421, 490-492, 538-539, 615-617, 674-676

BAKKER, A., SPAAS, H.A.C.M. (1977). A computational procedure for the stress and deformation analysis of high-pressure vessel flanges. International Journal of Pressure Vessels and Piping, 5, 122

BARBER, J.R., AMMAR, F.B., GEORGIADIS, H.G., (1989). Conductive heat exchange between bodies which are in contact for a very short period of time. Collected Papers in Heat Transfer, ASME HTD, 123, 101-106

BARTONICEK, J., KOCKELMANN, H. (1995). Characteristics for spiral wound gaskets in flanged joints with metaltometal contact. Proceedings of the 1995 Joint ASME/JSME Pressure Vessels and Piping Conference, 305, Honolulu, HI, USA, 83-96

BAZERGUI, A. (1977). Compressibility and Compliance of Spiral Wound Gaskets. Proceedings of the 3rd international conference on pressure vessel technology, 1, 181-189

BAZERGUI, A. (1984a). Short term creep and relaxation behaviour of gaskets. Welding Research Council Bulletin, n.294, 9-22

BAZERGUI, A., MARCHAND, L., RAUT, H.D. (1984b). Development of a production test procedure for Gaskets. Welding Research Council Bulletin, n.309, 1-39

BAZERGUI, A. MARCHAND, L. (1988a). Development of tightness test procedures for gaskets in elevated temperature service. Welding Research Council Bulletin, n.339

BAZERGUI, A., PAYNE, J.R. (1988b). On elevated temperature behaviour of gaskets. Proceedings of the 6th international conference on pressure vessel technology, Beijing, China

BAZERGUI, A., WINTER, J.R. (1989). Room temperature and elevated temperature tests of a metal corrugated gasket with flexible graphite fill. Proceedings of the 1989 ASME Pressure Vessels and Piping Conference, 158, Honolulu, HI, USA, 33-40

BERBEE, JAN A. (1998). Users view on the application of grooved metal gaskets. Proceedings of the 1998 ASME/JSME Joint Pressure Vessels and Piping Conference, 368, San Diego, CA, USA, 259-274

BERNARD, H.J. (1963). Flange Theory and the revised Standard BS.10: 1962 flanges and bolting for pipes, valves and fittings. Proceedings of IMechE, 178, Institute of Mechanical Engineers, London, 107-131

BICKFORD, J H. HAYASHI, K. CHANG, A T. WINTER, J R. (1989a). Preliminary evaluation of the Elevated Temperature Behavior of a bolted flanged connection. Weld Research Council Bulletin, n.341

BICKFORD, J.HM HSU, K.H., WINTER R.J. (1989b). A progress Report of the US PVRC joint task group on elevated temperature behaviour of bolted flanges. Pressure Vessel Technology, 1, Permagon Press, 249-266

BIREMBAUT, Y., BRAVO, F. (1987). Influence of high temperature on mechanical and sealing properties of flat gaskets. Proceedings of the 11th international conference on fluid sealing, BHRA, Elsevier Applied Science Publishers, 684-697

BIREMBAUT, Y., BRAVO, F., LEDAUPHIN, T. (1992). Sealing of bolted gasketed joints. Welding Research Council Bulletin, n.374, 38-50

BIREMBAUT, Y., LEDAUPHIN, T, DERENNE, M., VIGNAUD, J.C., PAYNE, J.R. (1997). Bolted Flanged Gasketed Joints Technology: Comparison of North American and European Approaches. Proceedings of the 1997 ASME Pressure Vessels and Piping Conference, 354, ASME New York NY USA, 209-244

BIREMBAUT, Y., LEDAUPHIN, T. (1994). French approach to characterize industrial gaskets based on graphite sheets. Proceedings of the 1994 Pressure Vessels and Piping Conference, 274, Minneapolis, MN, USA 91-100

BLACH, A.E, BAZERGUI, A. (1981). Method of analysis of bolted flanged connections a review. Welding Research Council Bulletin, n.271

BLACH, A.E., LIGUO, S. (1992a). Bolted Flanged Connections with Longitudinal Bending Moments: Experimental Results. Proceedings of the 1992 Pressure Vessels and Piping Conference, 255, ASME New York NY USA, 97-103

BLACH, A.E., LIGUO, S. (1992b). Bolted Flanged Connections with Longitudinal Bending Moments. Proceedings of the 1992 Pressure Vessels and Piping Conference, 235, ASME New York NY USA, p 38

BLICK, R.G. (1950). Bending Moments and Flange Design. Petroleum Refiner, Parts I-III, Feb, May and Jun

BOCHKOV, N.A., KOLESOV, V.S. (1990). Unsteady thermoelastic state of a cylinder of finite length. Soviet Applied Mechanics (English Translation of Prikladnaya Mekhanika), 26, n.6, 542-548

BOISSENOT, J.M., LACHAT, J.C. (1977). Elastoplastic flange design. Proceedings of the 3rd international conference on pressure vessel technology, 1, 215-222

BOLEY, B.A., WEINER, J.H. (1960). Theory of Thermal Stresses. John Wilery & Sons.

BOLEY, B.A., WEINER, J.H. (1960). Theory of Thermal Stresses. John Wilery & Sons

BOUZID, A., CHAABAN, A. (1994a). The influence of flange rotation on the leakage performance of bolted flanged joints. Proceedings of CAME Forum, 1, Montréal, Canada, 184-194

BOUZID, A., CHAABAN, A. (1996). Proposed method for evaluating relaxation in bolted flanged connections. Proceedings of the 1996 ASME Pressure Vessels and Piping Conference, 2, Montreal, Canada, 123-132

BOUZID, A., CHAABAN, A. (1997). Accurate method of evaluating relaxation in bolted flanged connections. Journal of Pressure Vessel Technology, Transactions of the ASME, 119, n.1, 10-17

BOUZID, A., CHAABAN, A., BAZERGUI, A. (1994b). Effect of gasket creep relaxation on the leakage tightness of bolted flanged joints. Proceedings of the 1994 Pressure Vessels and Piping Conference, 286, Minneapolis, MN, USA, 155-163

BOUZID, A.H. (1994c). Analysis of bolted flanged gasketed joints. PhD thesis, Ecole Polytechnique de Montréal, Canada.

BOUZID, A-H., DERENNE, M., CHAARANI, A. (1998). Tightness prediction of bolted flanged connections subjected to external bending moments. Proceedings of the 1998 ASME/JSME Joint Pressure Vessels and Piping Conference, 367, San Diego, CA, USA, 61-67

BOUZID, A., DERENNE, M., MARCHAND, L., PAYNE, J.R. (2001). "In-service Temperature Characterisation of PTFE-Based Gaskets", For future publication in the Journal of Testing and Evaluation.

BRADLEY, T.L., LARDNER, T.J., MIKIC, B.B. (1971). Bolted Joint Interface Pressure for thermal contact resistance. Transactions of ASME, Series E, 38, n.2, 5-42

BROWN, W. (1993). Design and Behaviour of Bolted Joints. Proceedings of the 3rd international symposium on fluid sealing of static gasketed joints, Biarritz, France, 111-121

BSI. (1969). A review of present methods for design of bolted flanges for pressure vessels. British Standards Institute publication n. PD6438

BUSHNELL, D. (1984). Computerised analysis of shells governing equations. Computers and Structure, 18, 471-535

BUTTERWORTH, D. (1977). Introduction to Heat Transfer, Oxford University Press

C.H. KENT. (1932). Thermal Stresses in Spheres and Cylinders. Transactions of ASME, 54, 185-196

CARLSON, I.H., BLACK, W.S. (1951). Joints for High Pressure, High Temperature Piping. Transactions of ASME, 73, n.3, 237-246

CARSLAW, H.S., JAEGER, J.C. (1959). Conduction of Heat in Solids. 2nd edition, Oxford at the Clarendon Press, U.K.

CARTRAUD, P., WIELGOSZ, C. (1994). Numerical modelling of the elastoplastic behaviour of a gasket material. Proceedings of the 1994 4th International Workshop on Computational Modelling of the Mechanical Behaviour of Materials, 5, n.13, Elsevier Science B.V. Amsterdam Netherlands, 75-81

CASCALES, D.H., MILITELLO, C., MIHALL, W.J. (1987a). An accurate simple model to evaluate integral flange rotation. International Journal of Pressure Vessels and Piping, 30, 151-159

CASCALES, D.H., MILITELLO, C., MIHALL, W.J. (1987b). Bolted Flange Joint Leakage Analysis with nonlinear gasket behaviour. International Journal of Pressure Vessels and Piping, 30, 205-215

CHAO, R.C. (1998). Behaviour of Bolted Flanges at Elevated Temperature program overview. Proceedings of the 1985 pressure vessels and pipng conference, 98.2, 117-123

CHEN, L.S., CHU, H.S. (1991). Transient thermoelastic problem of ring stiffened hollow cylinder heated by a moving line source. Journal of Thermal Stresses, 14, n.2, 105-119

CHEN, P. Y. P. (1989). Transient thermal stresses in a finite cylinder of nonuniform cross section. Journal of Thermal Stresses, 12, n.4, 451-463

CODEGONE, C. (1951). The Air Convection Coefficient in Pipes from 400° to 700°C. General Discussion on Heat Transfer, The Institute of Mechanical Engineers, London. 183-184.

DAHL, O.G.C. (1924). Temperature and Stress Distribution in Hollow Cylinders. Transactions of ASME

DERENNE, M, MARCHAND, L, PAYNE, J. (1996a). Characterisation Behaviour of Flexible Graphite Sheet Gasket Materials. Proceedings of the 1996 ASME Pressure Vessels and Piping Conference, 1, Montreal, Canada, 125-146

DERENNE, M. MARCHAND, L., PAYNE, J. R. (1996b). Characterization behaviour of flexible graphite sheet gasket materials. Fatigue/Fracture, NDE, Materials and Manufacturing Proceedings of the International Conference on Pressure Vessel Technology, 1, ASME, New York, NY, USA, 125-146.

DERENNE, M., MARCHAND, L., PAYNE J.R. (1999), Summary Report on the PTFE Gasket Qualification Project. WRC Bulletin under publication. Welding research Council, New York.

DERENNE, M., MARCHAND, L., PAYNE, J.R, BAZERGUI, A. (1994b). Elevated temperature testing of gaskets for bolted flanged joints. Welding Research Council Bulletin, n.391, New York NY USA.1-37

DERENNE, M., MARCHAND, L., PAYNE, J.R. (1997a). Summary Report on the PTFE Gasket Qualification Project. Report Submitted to the PVRC subcommittee, November 1997

DERENNE, M., MARCHAND, L., PAYNE, J.R. (1997b). Elevated temperature characterization of flexible graphite sheet materials for bolted flanged joints. Welding Research Council Bulletin, n.419, 1-86

DERENNE, M., PAYNE, J.R., MARCHAND, L. (1994a). Gasket Performance Characterisation for Bolted Flanged Connections. Report submitted to the PVRC subcommittee, October 1994

DONALD, M.B., SALOMON, J.M. (1959a). Behaviour of Compressed Asbestos Fibre gaskets in Narrow Faced, Bolted Joints. Proceedings of IMechE, 173, n.17, Institute of Mechanical Engineers, London, 459-468

DONALD, M.B., SALOMON, S.M., SALOMON, J.M. (1959b). The Behaviour of Narrow Faced, Bolted, Flanged Joints Under the Influence of Internal Pressure. Proceedings of IMechE, 173, n.17, Institute of Mechanical Engineers, London, 459-464

DOWNEY, ST.C, DRAPER, J.H.M. (1964). Paper on thermal loading and creep in structures and components. Proceedings of IMechE

DUDLEY, W.M. (1961). Deflection of Heat Exchanger Flanged Joints as affected by Barrelling and Warping. Transactions of ASME, Series B, 83, n.4, 460-466

DUNCAN, J.P. (1956). Rational design of stayed tubeplates. Engineering, 459-463, 525-528

DUNCAN, J.P., UPFOLD, R.W. (1963). Equivalent elastic properties of perforated bars and plates. Journal of Mechanical Engineering Science, 5, n.1, 53-65

FARNAM, R.G. (1951). Studies of Relaxation Characteristics of nonmetallic gasket material. India Rubber World, 123, n.6, 679-682

FESSLER, H., MUSSON, J.K. (1972). Tests of some taper hub flanges with narrow gaskets. Journal of Mechanical Engineering Science, 14, n.2, 98-106

FESSLER, H., SWANNELL, J.H. (1974). Prediction of the creep behaviour of a flanged joint. Proceedings of the conference on creep behaviour of piping, ImechE, 39-49

FLETCHER, L.S., PETERSON, G.P., MADHUSUDANA, C.V., GROLL, E. (1989). Heat transfer through bolted and riveted joints. ASME HTD Papers in Heat Transfer 1989: Presented at the Winter Meeting of the ASME Dec 10-15 1989, 123, San Francisco, CA, USA, 107-115

FUKUOKA, T., TAKAKI, T. (1998a). Three dimensional finite element analysis of pipe flange effects of flange interface geometry. Proceedings of the 1998 ASME/JSME Joint Pressure Vessels and Piping Conference, 367, San Diego, CA, USA, 125-131

GALISHIN, A.Z., ISCHENKO, D.A., MERZLYAKOV, V.A., SAVCHENKO, V.G. (1991). Applicability of the kirchhofflove hypotheses to analysis of the

thermoelastoplastic state of cylindrical shells. Soviet Applied Mechanics (English Translation of Prikladnaya Mekhanika), 27, n.2, 167-171

GALISHIN, A.Z., MERZLYAKOV, V.A., SKOSARENKO, YU.V. (1991). Applicability of different approaches to the determination of the axisymmetric stress strain state of cylindrical shells reinforced by annular ribs. Soviet Applied Mechanics (English Translation of Prikladnaya Mekhanika), 26, n.10, 961-965

GARDNER, K.A. (1952). Heat Exchanger tubesheet design 2 - fixed tubesheets. Journal of Applied Mechanics, 159-166

GHONEIM, G. ABDEL, HAVERTY, K.G. (1990). Capabilities of API flanges under combined pressure, tension and bending moment. ASME EnergySources Technology Conference and Exhibition, New Orleans, LA, USA

GOLDBERG, J.E. (1953). Axisymmetric Flexural Temperature Stresses of Circular Plates. Journal of Applied Mechanics, 257-260

GOODIER, J.N. (1957). Thermal stress. Journal of Applied Mechanics, 24, 467-474

GOUGH, H.J. (1936). First report of the pipe flanges research committee. Proceedings of IMechE, 132, Institute of Mechanical Engineers, London, 201-340.

GROSSE, I.R., MITCHELL, L.D. (1990). Nonlinear axial stiffness characteristics of axisymmetric bolted joints. Journal of Mechanisms, Transmissions, and Automation in Design, 112, n.3, 442-449

HEISLER, M.P. (1947). Temperature Charts for Induction and Constant Temperature Heating. Transactions of ASME, 69, 227-236

HEISLER, M.P. (1953). Transient Thermal Stresses in Slabs and Circular Pressure Vessels. Transactions of ASME, 20, n.2, 261-269

HOLLINGER, G.L., HECHNER, J.L. (1996). The PVRC project on three dimensional stress criteria considerations for linearization of stresses. Proceedings of the 1996 ASME Pressuse Vessels and Piping Conference, 2, Montreal, Canada, 263-270

HOLMBERG, E.O., AXELSON, K. (1932). Analysis of Stresses in circular plates and rings. Transactions of ASME, 54, n.2, 13-28

HORVAY, G., CLAUSEN, J.R., SCHENECTADY, N.Y. (1954). Stresses and Deformations of Flanged Shells. Journal of Applied Mechanics, 109-116

HORVAY, G., SCHENECTADY, N.Y. (1952). Bending of honeycombs and of perforated plates. Journal of Applied Mechanics, 122-123

HOUTMAN, J.L. (1978). Elastic-Plastic Strains from Thermal Shock at a discontinuity a simplified approach. Proceedings of the ASME PVP Conference, Montreal, Canada, ASME

HWANG, D.Y., STALLINGS, J.M. (1994). Finite element analysis of bolted flange connections. Computers and Structures, 51, n.5, Pergamon Press Inc Tarrytown NY USA, 521-533

INOUE, H., UENISHI, M., SHIMOTSUMA, Y. (1986). Static stiffness of bolted joints under high bolt preload up to the plastic range. Technology Reports of Kansai University, n.28, 49-58

ITOH, S., SHIINA, Y., ITO, Y. (1992). Behavior of interface pressure distribution in a single bolt flange assembly subjected to heat flux. Journal of Engineering for Industry, Transactions of the ASME, 114, n.2, 231-236

JAEP, W.F. (1951). A design procedure for integral flanges with tapered hubs. Transactions of ASME, 73, n.5, 569-574

JAHANIAN, S. (1996). Thermoelastoplastic stress analysis of a thickwalled tube of nonlinear strain hardening. Journal of Mechanical Design, Transactions of the ASME, 118, n.3, ASME New York NY USA, 340-345

JAHANIAN,S, SABBAGHIAN,M. (1990). Thermoelastoplastic and residual stresses in a hollow cylinder with temperature dependent properties. Journal of Pressure Vessel Technology, Transactions of the ASME, 112, 85-91

JASPER, T.M, GREGERSEN, H., ZOELLNER, A.L. (1936). Strength and design of covers and flanges for pressure vessels and piping. Heating, Piping and Air Conditioning, 8, 605-608, 672-674, (1936), 9, 43-57, 109-112, 174-178 (1937)

JOHNSON, A.E., BAILEY, R.W. (1954). Third Report of pipe flanges research committee. Proceedings of IMechE, 168, n.15, Institute of Mechanical Engineers, London, 423-455

KENNY, B., MOORE, G.G., DUNCAN, J.P. (1963). Stiffness of Broad Faced Gasketted Flanged Joints. Journal of Mechanical Engineering Science

KENT, C.H. (1931). Thermal Stresses in thin walled cylinders. Transactions of ASME, 53, 167-180

KERKHOF, W.P. (1951). New Stress Calculations and Temperature Curves for Integral Flanges. Proceedings of the 3rd World Petroleum Congress, 8, 146-168

KERN, D.Q. (1950). Process Heat Transfer. McGraw-Hill Book Company.

KERN, D.Q., KRAUS, A. D. (1972). Extended surface heat transfer. McGraw Hill

KIM, T., KIM, Y., LEE, B. (1998). Finite element analysis of bolted joint assembly of nuclear power plants. Proceedings of the 1998 ASME/JSME Joint Pressure Vessels and Piping Conference, 368, San Diego, CA, USA, 185-189

KOCKELMANN, H., HAHN, R. (1990). On the behaviour of graphite flat gaskets subjected to compressive and creep relaxation loading. Proceedings of the 2nd International Symposium on Fluid Sealing, La Baule, France, 197-206

KOSYKH, N.S., NIKITIN, V.V., ZDANAVICHYUS, G.B. (1989). Investigation of heat transfer in piping fittings. Chemical and Petroleum Engineering, 25, n.34, 115-117

KOVES,W.J. (1996). Analysis of flange joints under external loads. Journal of Pressure Vessel Technology, Transactions of the ASME, 118, 59-63

KRAUS, H., ROSENKRANS, W. (1984). Creep of Bolted flange connections. Welding Research Council Bulletin, n.294, 2-8

KRYLOV, V I. KISELEV, I G. (1987). Effect on contact heat transfer on thermally stressed state of the flanged joints of a power plant pipeline valve. Thermal Engineering, 34, n.11, 630-632

KRYLOV, V.I., URUSHEV, S.V. (1986). Mathematical modeling of contact heat transfer in sectional connections of power plant piping. Thermal Engineering, 11, 640-641

KUMANO, H., SAWA, T., HIROSE, T. (1994). Mechanical behavior of bolted joints under steady heat conduction. Journal of Pressure Vessel Technology, Transactions of the ASME, 116, n.1, ASME New York NY USA, 42-48

KUMANO, H., SAWA, T., HIROSE, T., NAKAGO, Y. (1993). The Characterisitcs of a Bolted Joint under Thermal Changes. Proceedings of the 3rd international symposium on fluid sealing of static gasketed joints, Biarritz, France, 101-109

KUMANO, H., SAWA, T., NITTA, T. (1995). Characteristics of bolted joints under thermal changes. Proceedings of the 1995 Joint ASME/JSME Pressure Vessels and Piping Conference, 305, Honolulu, HI, USA 125-132

LABROW, S. (1947). Design of Flanged Joints. Proceedings of IMechE, 156, n.1, Institute of Mechanical Engineers, London, 66-73

LADOPOULOS, E.G., ZISIS, V.A., KRAVVARITIS, D. (1994). Multidimensional singular integral equations applied to three dimensional thermoelastoplastic stress analysis. Computers and Structures, 52, n.4, Pergamon Press Inc, NY USA, 781-788

LAKE, G.F., BOYD, G. (1957). Design of Bolted Flanged Joints. Proceedings of IMechE, 171, Institute of Mechanical Engineers, London, 843-872

LATTE, J., ROSSI, C. (1996). Creep and Leakage Properties of Modified PTFE. Proceedings of the 4th International Symposium on Fluid Sealing, Mandelieu La Napoule, France

LAVIOLETTE, D., NICA, A., CHABAAN, A., MARCHAND, L., ABOULFAZI, S.A. (1996). Mechanical Behaviour of pressurized bolted joints subject to external bending loads. Proceedings of the 1996 ASME Pressure Vessels and Piping Conference, 2, Montreal, ASME New York NY USA, 117-122

LEE, S., CHEN, W. (1996). Three dimensional thermoelastic contact between two plates with bolted joints. Journal of Thermal Stresses, 19, n.2, Taylor & Francis Ltd Basingstoke Engl., 123-138

LEE, S., YOVANOVICH, M.M., SONG, S., MORAN, K.P. (1993). Analysis of thermal constriction resistance in bolted joints. International Journal of Microcircuits and Electronic Packaging, 16, n.2, 125-136

LEHNHOFF, T.F., WISTEHUFF, W.E. (1996). Nonlinear effects on the stresses and deformations of bolted joints. Journal of Pressure Vessel Technology, Transactions of the ASME, 118, n.1, ASME New York NY USA, 54-58

LIN, B., NICHOLSON, D.W. (1997). Incremental finite element method for thermomechanical contact: Parts I & II. Proceedings of the 1997 ASME Pressure Vessels and Piping Conference, 356, Orlando, FL, USA

M., NISHIDA, T., YAMANAKA, Y. (1996). Gasket performance of SWG in ROTT and short term estimation at elevated temperature. Computer Technology 1996: Applications and Methodology Proceedings of the 1996 ASME Pressure Vessels and Piping Conference, 326, Montreal, Canada, 47-59

MACNEIL, J.E., BROCA. (1971). Engineering Data File Charts for transient temperature. Heating, Piping and Air Conditioning, 107-119

MADDREN, J. MARSCHALL, E. (1995). Finite element modelling of heat transfer across bolted joints. International Journal of Microelectronic Packaging Materials & Technologies, 1, n.1, 51-61.

MANTELLI, M.B.H., YOVANOVICH, M.M. (1998a). Parametric heat transfer study of bolted joints. Journal of Thermophysics and Heat Transfer, 12, n.3, Reston VA USA, 382-390

MANTELLI,M.B.H. (1998b). Compact analytical model for overall thermal resistance of bolted joints. International Journal of Heat and Mass Transfer, 41, n.10, 125-566

MARCHAND, L., BAZERGUI, A. HAHN, R. KOCKELMANN, H. (1993). The influence of the stiffness of flanges and bolts on the creep relaxation behaviour of gaskets. Proceedings of the 3rd international symposium on fluid sealing of static gasketed joints, Biarritz, France, 31-42

MARCHAND, L., DERENNE, M. (1996). Long term performance of elastomeric sheet gasket materials subjected to temperature exposure. Proceedings of the 1996 ASME Pressure Vessels and Piping Conference, 1, Montreal, Canada, 107-123

MARCHAND, L., DERENNE, M., BAZERGUI, A. (1986). Elevated temperature gasket trends. Proceedings of the 1st International Symposium on Fluid Sealing, Nantes, France, 175-184

MARINE, J. (1938). Stress and Deformation in pipe flanges subjected to creep at high temperatures. Franklin Institute Journal, 226, n.5, 645-657

MARTENS, D., PORTER, M. A. (1994). Investigation and repair of heat exchanger flange leak. Proceedings of the 1994 Pressure Vessels and Piping Conference. Part 9 (of 19), 278, Minneapolis, MN, USA, 133-143

McNEILL, D.R., BROCK, J.E. (1971). Charts for transient temperatures in pipes. Heating/Piping/Air Conditioning, November, 107-119

MILLER, K.A.G. (1953). The design of tube plates in heat exchangers. Proceedings of IMechE, 672-688

MITTELBACH,M, VOGD,C, FLETCHER,L.S. (1994). The interfacial pressure distribution and thermal conductance of bolted joints. Journal of Heat Transfer, 116, 823-828

MITTLEBACH, M., VOGD, C., FLETCHER, L.S., PETERSON, G.P. (1992). Interfacial pressure distribution and thermal conductance of bolted joints. General Papers in Heat Transfer and Heat Transfer in Hazardous Waste Processing Winter Annual Meeting of ASME, 212, Anaheim, CA, USA 9-17

MOON, P., SPENCER, D.E. (1961). Field Theory for Engineers. D. Van Nostrand Company, Princeton, New Jersey

MOROHOSHI, T., SAWA, T., MARUYAMA, K., YAMAMOTO, K. (1989). Characteristics of bolted joints subjected to external bending moments. (Analysis of the case where clamped parts are pipe flanges with gaskets by three dimensional theory of elasticity). JSME International Journal, Series 1: Solid Mechanics, Strength of Materials, 32, n.4, 477-484

MOTOSH, I.N. (1976). Determination of joint stiffness in bolted connections. Journal of Engineering for Industry, 98, 858-861

MUKOED, A.P., KHVOROSTYANYI, F.O. (1989). General solutions of orthotropic cylindrical shell equations. Soviet Applied Mechanics (English Translation of Prikladnaya Mekhanika), 24, n.9, 898-904

MURRAY, N.W., STUART, D.G. (1961). Behaviour of Large Taper Hub Flanges. Proceedings of Symposium on Pressure Vessel Research Towards Better Design, Institute of Mechanical Engineers, London, 133-147

NAGY, A. (1994). Determination of the loosening coefficient at large size welding neck flange joints. Periodica Polytechnica, Mechanical Engineering, 38, n.23, Technical Univ of Budapest, Budapest, Hungary, 179-199

NAGY, A. (1996). Determination of the gasket load drop at large size welding neck flange joints in the case of non-linear gasket model. International Journal of Pressure Vessels and Piping, 67, n.3, Elsevier Science Ltd Oxford Engl., 243-248

NAGY, A. (1997). Time dependent characteristics of gaskets at flange joints. International Journal of Pressure Vessels and Piping, 72, n.3, Elsevier Science Ltd Oxford Engl., 219-229

NAU, B.S. (1985a). Computer modelling of the sealing behaviour of gaskets in flanged joints. Proceedings of the 2nd workshop on containment integrity, , US nuclear regulatory commission, NUREG/CP0056, 433-450

NAU, B.S. (1996). Concepts Relating to Gasket Design Data. Proceedings of the 4th International Symposium on Fluid Sealing, Mandelieu La Napoule, France

NAU, B.S., WATSON, S. (1985b). Computer modelling of thermal lag effects in bolted joints. Proceedings of the ASME PVP conference 1985, New Orleans, Louis., 125-128

NERLI, G., BERTONI, G. (1974). Calculation and Experimental Determination of the Deformation of the Supporting Surface of the Gasket in a Series of High Pressure Flanges. Meccancia, 130-142

NEWMAN, A.B. (1936). Heating and Cooling Rectangular and Cylindrical Solids. Industrial and Engineering Chemistry, 28, n.5, 545-548

NISHIOKA, K., MORITA, Y., KAWASHIMA, T. (1979). Strength of integral pipe flanges (no.1 & no.2). Bulletin of JSME, 22, n.174, 1705-1718

OLSON, F.C., SCHULTZ, O.T. (1942). Temperatures in Solids during Heating or Cooling. Industrial and Engineering Chemistry, 34, n.7, 874-877

OMEGA. (1995). Omega Complete Temperature Measurement Handbook and Encyclopaedia. Omega Engineering Inc. USA

OSWEILLER, F. (1996). Utube heat exchangers a comparison of code design rules. Proceedings of the 1996 ASME Pressure Vessels and Piping Conference, 2, Montreal, ASME New York NY USA, 223-235

OZISIK, M.N. (1985). Heat Transfer, A Basic Approach Mc-Graw-Hill Book Company.

PARKUS, H. (1976). Thermoelasticity. 2nd edition, SpringerVerlag

PAYNE, J.R. (1985). PVRC Flanged Joint User's Survey. Bulletin n.306. Welding Research Council.

PRICE, J.W.H., CHANANA, A. (1996). Leakage of bolted flanged joints in high temperature pressure systems. Proceedings of the 1996 ASME Pressure Vessels and Piping Conference, 2, Montreal, Canada, ASME New York NY USA, 133-139

QU,J., WANG,P., DOU,Y., QUAN,H., SHEN,X., XIE,S., QIAO,W. (1989). Test and analysis of sealing characteristics under thermal transient on a nuclear pressure vessel model. 6th International Conference on Pressure Vessel Technology, 1, Permagon Press, 239-248

RAJU, P.R. (1980). Simplified Analysis of closure flanges under Mechanical and Thermal Loads. ASME Paper n.80C2/NE16

RENJITANG, ERDOGAN,F. (1985). Transient thermal stresses in a reinforced hollow disk or cylinder containing a radial crack. Journal of Engineering for Gas Turbines and Power, 107, 212-219

ROBERTS, I. (1950). Gaskets and Bolted Joints. Journal of Applied Mechanics, Transactions of ASME, 17, n.2, 169-179

ROSE, R.T. (1970). Flanges. The stress analysis of pressure vessels and pressure vessel components, Pergamon Press, 1970

ROSSHEIM, D.B., GEBHART, H., OLIVER, H.G. (1938). Tests of Heat Exchanger Flanges. Transactions of ASME, 60, n.4, 305-314

ROSSHEIM, D.B., MARKL, A.R.C. (1943). Gasket loading constants. Mechanical Engineering, 65, n.9, 647-648

RUSSO, E.P., CYR, W.W.ST., HERRINGTON, P.D. (1994). Thermal stresses in a partially filled horizontal vessel. Journal of Pressure Vessel Technology, Transactions of the ASME, 116, n.3, ASME New York NY USA, 302-305

SAWA, I., KUMANO, H., IWAKAWA, H. (1986). Characteristics of bolted joints with gaskets (stress analysis of a metallic flat gasket used for raised face in a cover of pressure vessel). Bulletin of the JSME, 29, n.255, 2789-2796.

SAWA, T., ASAHINA, M., ISHIHARA, T. (1998). Thermal stress analysis and the new gasket factors of pipe flange connections with spiral wound gaskets under elevated temperature. Proceedings of the 1998 ASME/JSME Joint Pressure Vessels and Piping Conference, 367, San Diego, CA, USA, ASME Fairfield NJ USA, 11-16

SAWA, T., HIGURASHI, N., HIROSE, T. (1991a). A stress analysis of a taper hub flange with a bolted flat cover. ASME PVP Vol. 217, Pressure vessel and components, ASME, 129-136

SAWA, T., HIROSE, T., KUMANO, H. (1993b). Behavior of pipe flange connection in transient temperature field. Journal of Pressure Vessel Technology, Transactions of the ASME, 115, n.2, 142-146

SAWA, T., HIROSE, T., NAKAGOMI, Y. (1996a). Behavior of a tapered hub flange with a bolted flat cover in transient temperature field. Journal of Pressure Vessel Technology, Transactions of the ASME, 118, n.1, 115-120

SAWA, T., KOTANI, K. (1996b). Thermal stress analysis of pipe flange connections with raised face gasket subjected to heat conduction. Proceedings of the 1996 ASME Pressure Vessels and Piping Conference, 326, Montréal, Canada, 103-108

SAWA, T., KUMANO, H. (1985a). On the characteristics of bolted joints with gaskets. Bulletin of the JSME, 28, 400-407

SAWA, T., KUMANO, H. (1993a). A Stress Analysis and an Evaluation of the Sealing Performance in Pipe Flange Connection with Gaskets. Proceedings of the 3rd international symposium on fluid sealing of static gasketed joints, Biarritz, France, 85-100

SAWA, T., KUMANO, H., IWAKAWA, H. (1985b). On the characteristics of bolted joints with gaskets (stress analysis of metallic gaskets with raised face interposed between pipe flanges). Bulletin of JSME, 29, n.248, 385-392

SAWA, T., KUMANO, H., MARUYAMA, H., SUZIKI, Y. (1985c). Effects of interface configurations on the characteristics of bolted joints (the case where clamped part is a cover of pressure vessel). Bulletin of JSME, 29, n.248, 377-384

SAWA, T., MARUYAMA, K. (1979a). The force ration of bolted joint (the case where clamped parts are flanges. Bulletin of JSME, 22, n.165, 420-428

SAWA, T., MOROHOSHI, T., KUMANO, H. (1979b). A new calculation method of the spring constant in a bolted connection with gasket. ASME PVP, 217, 119-128

SAWA, T., MOROHOSHI, T., YAMAMOTO, K. (1995a). Stress Analysis of Pipe Flange Connections with Gaskets Subjected to External Bending Moments. ASME Current Topics in Computational Mechanics, 305, 109-118

SAWA, T., NAKAGOMI, Y., KOTANI, K. (1995b). Axisymmetrical thermal stress analysis of pipe flange connections with metallic gaskets subjected to heat conduction. Proceedings of the 1995 Joint ASME/JSME Pressure Vessels and Piping Conference, 305, Honolulu, HI, USA ASME New York, 157-162

SAWA, T., SHIRAISHI, H. (1983). Simple method of calculate the force ratio of bolted joints (the case where clamped parts are circular flanges and pipe flanges). Bulletin of JSME , 26, n.216, 1088-1095

SAWA,T, HIGURASHI,N, AKAGAWA,H. (1991b). A stress analysis of pipe flange connections. Journal of Pressure Vessel Technology, Transactions of the ASME, 113, 497-503

SCHNEIDER, R.W., RODABAUGH, E.C. (1982). Flanges, Gaskets and Closure Systems. Pressure vessels and piping design technology, a decade of progress: ASME PVP, 1982

SCLIFFET, L. (1993). Comportement Thermomecanique des Jonctions Boulonnees. Proceedings of the 3rd international symposium on fluid sealing of static gasketed joints, Biarritz, France, 43-60

SCLIFFET, L. (1994). Thermomechanical Behaviour of Bolted Assemblies. BHRG International Conference on Valves and Actuators, Manchester

SHEVCHENKO, YU.N., MERZLYAKOV, V.A., GALISHIN, A.Z. (1991). Thermoelasticplastic stress state of shells of revolution reinforced by annular ribs. Soviet Applied Mechanics (English Translation of Prikladnaya Mekhanika), 27, n.1, 43-47

SINGH, K.P. (1979a). Study of bolted joint integrity and intertubepass leakage in Utube heat exchangers (Parts I and II). Journal of Engineering for Power, 101, 9-22

SINGH, K.P., HOLTZ, M. (1979b). Analysis of temperature induced stress in the body bolts of single pass heat exchangers. Transactions of ASME, ASME 79WA/NE7, 19

SINGH, K.P., SOLER, A. (1983). Design parameters affecting bolt load in ring type gaskets. Journal of Pressure Vessel Technology, Transactions of the ASME, 105, 11

SMITH, A.C., BRIGGS, G. (1996). Finite Element Analysis of Bolted Flange Assemblies. Proceedings of the 4th International Symposium on Fluid Sealing, Mandelieu La Napoule, France, 181-192

SMITH, C.O. (1984). Probabilistic design criteria for cylinders and spheres under thermal stresses. Journal of vibration, acoustics, stress and reliability in design, 106, ASME, 523-528

SMOLEY, E.M., KESSLER, F.J., KOTTMEYER, R.E. AND TWEED, R.G. (1963). The creep relaxation properties of a flat faced gasketed joint assembly. SAE Paper S361

SOLER, A.I. (1980). Analysis of bolted joints with nonlinear gasket behavior. Journal of Pressure Vessel Technology, Transactions of the ASME, 102, 249-256

SPAAS, H.A.C.M., LATZKO, D.G.H., BAKKER, A. (1977). High-pressure vessel flange behaviour under transient thermal loadings. Proceedings of the 3rd international conference on pressure vessel technology, 1, 293-309

STALLINGS, J.M., HWANG, D.Y. (1992). Modelling pretensions in bolted connections. Computers and Structures, 45, n.4, Pergamon Press Inc Tarrytown NY USA, 801-803

SWICK, R.H. (1977). How much pressure will that gasket take?. Machine Design, 86-89

TAPSELL, H.J. (1939). Second Report of pipe flanges research committee. Proceedings of IMechE, 141, n.5, Institute of Mechanical Engineers, London, 433-471

TEMA (1991). Standards of the Tubular Exchanger Manufacturers Association, 8th Edition, TEMA, NY

THOMPSON, J.C., SZE, Y., STREVEL, D.G., JOFRIET, J.C. (1976). The interface Boundary Conditions for Bolted Flanged Connections. Journal of Pressure Vessel Technology, 277-282

THOMSON, G. (1989). Strength and flexibility of pressurised taper hub flanged joints. Applied Solid Mechanics Conference, University of Strathclyde, Glasgow

THORN, F.C. (1949). Creep and Relaxation in compressed asbestos gaskets. ASTM Bulletin n.160, 58-61

TIMOSHENKO, S. (1940) Theory of Plates and Shells, McGraw-Hill, US

TOOTH, A.S., CHEUNG, J.S.T., ONG, L.S., NG, H.W., NADARAJAH, C. (1998). Support of horizontal vessels containing high temperature fluids a design study. Journal of Pressure Vessel Technology, Transactions of the ASME, 120, n.3, ASME Fairfield NJ USA, 232-237

TOOTH, A.S., PANAYOTTI, A., OWEN, R. (1989). Thermal behaviour of thin cylindrical shells. I. Heat transfer and harmonic analysis. International Journal of Mechanical Sciences, 31, n.9, 693-706

TOULOUKIAN, Y.S., LILEY, P.E., SAXENA, S.C. (1970). Thermal Conductivity, Nonmetallic Liquids and Gases. Thermophysical Properties of Matter, Volume 3. IFI/Plenum, New York.

TOULOUKIAN, Y.S., KIRBY, R.K., TAYLOR, R.E, LEE, T.Y.R. (1970). Thermal Expansion, Nonmetallic Solids. Thermophysical Properties of Matter, Volume 13. IFI/Plenum, New York.

TSCHIERSCH, R., BLACH, A.E. (1996). Gasket Loadings in Bolted Flanged Connections Subject to External Bending Moments. Proceedings of the 1996 ASME Pressure Vessels and Piping Conference, 1, Montreal, ASME New York NY USA, 169-182

VAN CAMPEN, D.H., DEEN, P.J., LATZKO, D.G.H. (1960). Deformation of large diameter high pressure vessel flanges. Proceedings of the 1st international conference on pressure vessel technology, Delft

VARGA, L., BARATOSY, J. (1995). Optimal pre-stressing of bolted flanges. International Journal of Pressure Vessels and Piping, 63, n.1, Elsevier Science Ltd, Oxford, 25-34

VIGNAUD, J.C., MOINEREAU, D., NOWAK, H., DIGAT, P. (1986). Comportement Mecanique des joints spirales; compression et relaxation du joint. Proceedings of the 1st International Symposium on Fluid Sealing, Nantes, France, 167-174

WATERS, E.O. (1938). Analysis of Bolted Joints at High Temperatures. Transactions of ASME, 60, 83-86

WATERS, E.O., ROSSHEIM, D.B., WESSTROM, D.B., WILLIAMS, F.S.G. (1949) Development of General Formulas for Bolted Flanges, Taylor Forge & Pipe Works, USA

WATERS, E.O., TAYLOR, J.H. (1927). The Strength of Pipe Flanges. Mechanical Engineering, 49, n.5a, 531-542

WATERS, E.O., WESSTROM, D.B., ROSSHEIM, D.B., WILLIAMS, F.S.G. (1934) Design of Bolted Flanged Connections. Mechanical Engineering, 56, n.12, 736-738

WATERS, E.O., WESSTROM, D.B., ROSSHEIM, D.B., WILLIAMS, F.S.G. (1937) Formulas for Stresses in Bolted Flanged Connect. Transactions of ASME, 59, 161-169

WESSTROM, D.B., BERGH, S.E. (1951). The effects of internal pressure on stresses and strains in bolted flange connections. Transactions of ASME, 73, n.5, 508-568

WINTER, J R. (1988). Use ultrasonic extensometer to determine the variations in the assembly bolt loads problem industrial flange. Experimental Techniques, 12, n.11, 6-11

WINTER, J. RONALD, COPPARI, LAWRENCE A. (1996). Flange thermal parameter study and gasket selection. Proceedings of the 1996 ASME Pressure Vessels and Piping Conference, 2, ASME New York NY USA, 141-174

WINTER, J.R. (1990). Gasket selection flowchart. Proceedings of the 2nd International Symposium on Fluid Sealing, La Baule, France, 267-310

WINTER, J.R., LEON, G.F. (1985). Radially inward buckling of spiral wound gaskets. Proceedings of the 1985 ASME PVP conference, New Orleans, Louisiana, 111-116

YU, YY. (1956). Rational analysis of heat exchanger tubesheet stresses. Journal of Applied Mechanics, 468-473

ZERRES, H., PEREZ, M., LEMAUVIEL, L., SCLIFFET, L. (1998). Comparison between the analysis of the mechanical behaviour of bolted joints by the Finite Elements method and by the European approach (PR EN 1591). Proceedings of the 1998 ASME/JSME Joint Pressure Vessels and Piping Conference, 367, San Diego, CA, USA, 69-73

ZIBDEH, H.S. (1990). Reliability of thermally loaded cylinders. Journal of Pressure Vessel Technology, Transactions of the ASME, 112, n.3, 303-308

APPENDIX A

GASKET THERMAL AND MECHANICAL PROPERTIES

A.1 Abstract

This appendix outlines experimental methods used to determine the mechanical and thermal properties of several common gasket materials. The experimentation enabled the determination of the gasket coefficient of thermal expansion, elastic modulus at temperature and the combined flange/gasket contact and gasket through thickness heat transfer coefficient. The experimental methods used and the resulting thermal properties for the tested gasket types are presented.

A.2 Abbreviations

ASME = American Society of Mechanical Engineers
TTRL = Tightness Testing and Research Laboratory
UGR = Universal Gasket Rig
LVDT = Linear Variable Displacement Transducer
AARH = Arithmetical Average Roughness Height (surface finish)

A.3 Nomenclature

A_c = cross sectional area of the loading cylinder (mm^2)
E_g = gasket modulus of elasticity (MPa)
G_{OD}, G_{ID} = gasket internal diameter, external diameter (mm)
h_c = surface contact heat transfer coefficient ($W/(m^2.°C)$)

h_{cg} = gasket overall heat transfer coefficient (contact and through-thickness)(W/(m².°C))

k_c = loading cylinder material thermal conductivity (W/(m.°C))

L_c = length, between thermocouples, of the loading cylinder (mm)

n_g = number of gaskets being tested

Q = heat flow through gaskets (W)

t_g = gasket thickness in the unloaded state (mm)

t_g' = gasket thickness in the loaded state (mm)

T_{p1}, T_{p2} = Lower, upper platen temperatures (°C)

T_{c1}, T_{c2} = Lower, upper loading cylinder temperatures (°C)

α_g = coefficient of thermal expansion for the gasket (m/m/°C)

α_p = coefficient of thermal expansion for the LVDT pins (m/m/°C)

ΔD_g = Total deflection of all gaskets (mm)

ΔD_{pl} = Total deflection of the platens (mm)

ΔS_g = Change in gasket stress (MPa)

ΔT_g = Change in gasket temperature (°C)

ΔT_{pl} = Change in platen temperature (°C)

A.4 Introduction

In order to analyse the effects of temperature on the integrity of pressure vessel flange joints it is necessary to determine several thermal and mechanical properties of the gasket that is being used. This is not a simple process, however, as gasket materials are generally quite complex in construction, containing several different materials in a variety of configurations. Additionally, the thermal properties of the gasket may change with increasing gasket stress and gasket degradation over a long period of time.

There are three main properties of the gasket that are of interest, as listed below:

1) Gasket elastic modulus at operational temperature (E_g).

2) Gasket coefficient of thermal expansion (α_g).

3) A value for the "overall heat transfer coefficient" of the gasket (h_{cg}). This is a combined value for the contact heat transfer, between the gasket and flange, and also for the heat transfer through the thickness of the gasket. This coefficient is required in order to determine the heat flow between the mating flanges, via the gasket, if the flanges are operating at different temperatures.

The goal of this paper is to determine the above properties of several commonly used gasket types. A description of the methods used for testing the gasket materials is also presented.

A.5 Gasket testing method

Developing an exact testing method for determining the thermal and physical properties of gaskets under stress would be an extremely complex operation. For instance, it is nearly impossible to quantify the actual gasket stress distribution during a compression test. This is due to the difficulty in quantifying the effect of gasket expansion in the radial direction during the test. Similarly with thermal properties, an accurate method of evaluation would determine the properties for the gasket in the deflected state.

However, in order to use these results one would then need to be able to calculate the actual level of deflection expected in the gasket at the point of analysis. The inaccuracies involved in such a calculation (for example establishing the actual bolt load and flange rotation) would negate the advantages obtained in generating the more accurate gasket test data. It was thus deemed sufficient to determine the experimental values for the gasket properties by approximate calculations that use only the initial dimensions (G_{OD}, G_{ID} and t_g) of the gasket.

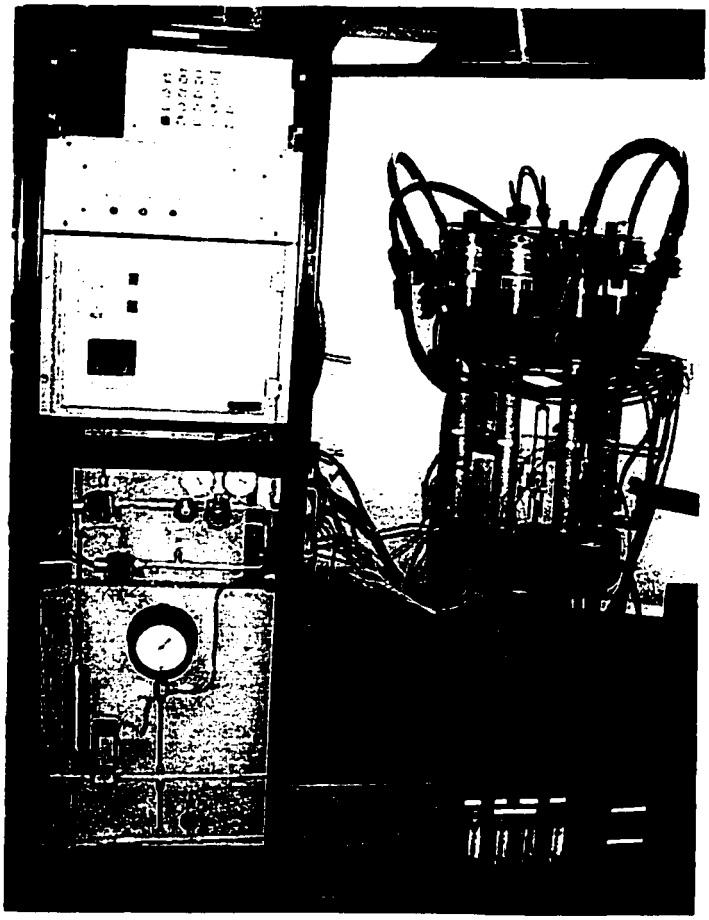

Figure A.1 – TTRL UGR test rig

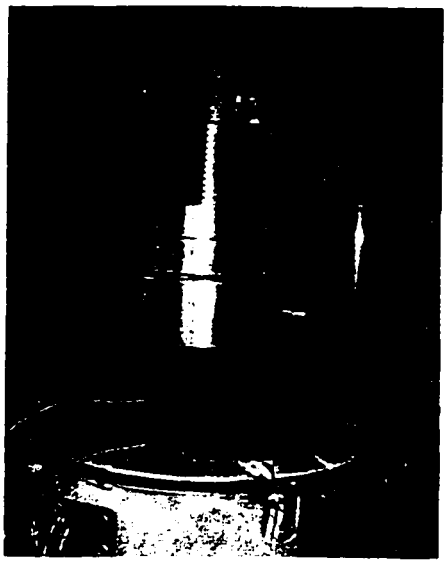

Figure A.2 – UGR loading set-up, insulation removed

The experimental values were generated using the TTRL UGR (Universal Gasket Rig) machine (ref. Figures A.1, A.2). This test rig enables the accurate control of the gasket stress level via hydraulic bolt tensioning, while the gasket deflection is monitored using three LVDT (Linear Voltage Displacement Transducer) set-ups, as shown in Figure A.3. The upper and lower platens are heated electrically and the external surfaces of the platens are insulated to prevent heat loss. Once operational, the gaskets and platens are therefore held at a constant uniform temperature by the UGR heater control system.

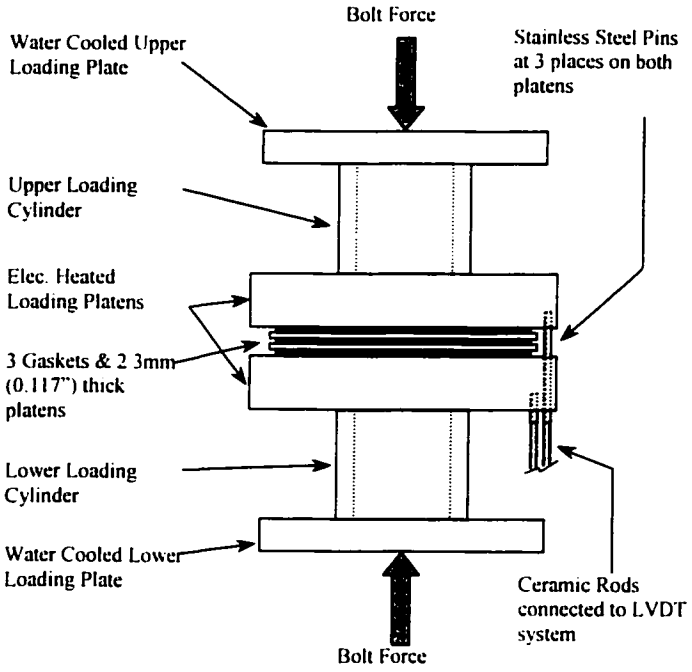

Figure A.3 – UGR platen set-up

In order to increase the sensitivity of the rig, three gaskets of the same specification were tested at the same time (ref. Figure A.3). This also achieved an averaging of the properties over the three specimens. Thin carbon steel platens were inserted between each of the gaskets. These platens and the upper and lower loading platens were machined on all gasket contacting surfaces to a 6.35μm (250μin) AARH surface finish. The UGR machine was initially calibrated (platen deflection vs. temperature) to

determine the level of differential expansion occurring between the platens and the pins and ceramic rods that transfer the upper and lower platen movement to the LVDT's.

In order to establish the thermal expansion coefficient and elastic moduli of the gaskets, the UGR was taken through a set temperature and stress cyclic pattern. This enabled the determination of these properties over a range of gasket stress and temperature values. The overall heat transfer coefficient for the gaskets was somewhat more complex to determine. The heat flux flowing through the gaskets was first established and then, from the platen temperature measurements, the overall gasket heat transfer coefficient was determined.

With the UGR it is possible to turn off the upper platen heating and, since the rig is cooled at both the upper and lower loading sections, a heat flow will be established from the heated lower platen, through the gaskets, to the cooling system on the upper loading plate. The magnitude of the heat flowing through this path may be determined by taking temperature measurements at two points on the upper loading cylinder. Since we know the cylinder material and dimensions, the heat flow resistance between the two points of measurement may be determined. From this, and the temperature measurements, the actual heat flow through that path can be calculated. As the external surfaces of the rig are insulated, the heat flow in other directions should be minimal by comparison to this heat flow path.

The entire test procedure for each gasket type was therefore as follows:

1. Assemble UGR rig with gaskets and platens in position (with insulation = 3 x 3mm thick graphite sheet gasket material inserted into gasket inner diameter, between the upper and lower platens).
2. At ambient temperature, measure deflection vs. load whilst incrementally cycling the gasket load from 0 to 50 MPa.
3. Hold 50MPa load for 1hour to reduce gasket creep rate.
4. Cycle gasket load from 0 to 50 MPa twice.
5. Increase temperature to 100°C.
6. Incrementally load gasket to 50 MPa and hold steady for three hours to reduce the gasket creep rate.
7. Cycle gasket load from 0 to 50 MPa twice.
8. Increase temperature to 200°C (stable) and repeat steps 6 and 7.
9. Increase temperature to 300°C (stable) and repeat steps 6 and 7.
10. Stress gasket to half the maximum cycle stress (25MPa) and hold gasket at temperature and stress for 0.5 hours.
11. Turn off heat and record platen deflection during 8 hour cooling.
12. Repeat steps 2 to 10, with a maximum gasket load of 100MPa.
13. Turn off heat and record platen deflection during 8 hour cooling.
14. Take gasket stress to 25MPa and then heat the lower platen to 100°C and allow the heat flow to stabilise.
15. Take temperature measurements of the lower platen, upper platen and at two positions on the upper loading cylinder portion of the rig, underneath the insulation.
16. Repeat steps 14 and 15 at 200°C and 300°C lower (only) platen temperatures.
17. Heat both platens to 300°C and hold for 2 hours
18. Turn off heat and record platen deflection during 8 hour cooling
19. Disassemble and then repeat test with next gasket type.

The gasket elastic modulus can thus be determined from the measured platen deflection vs. gasket stress taken during steps 2 to 12. The gasket thermal expansion coefficient is determined from the cooling cycles (steps 11, 13 and 18). The overall heat transfer coefficient of the gaskets can be established from the readings taken in steps 15 and 16.

The gaskets tested were as listed in Table A.1:

	Gasket Description	Gasket Dimensions (G_{OD} x G_{ID} x t_g)
Gkt1	Solid Copper Gasket	158 x 132 x 3.05 (6.2" x 5.2" x 0.12")
Gkt2	Double Jacketed Gasket. Soft Iron Outer and Graphite Filler	125.6 x 103 x 3.4 (4.96" x 4.06" x 0.134")
Gkt3	Corrugated Metal Gasket with Graphite Filler	127 x 102 x 1.8 (5.0" x 4.0" x 0.07")
Gkt4	Spiral Wound Gasket with Stainless Steel Windings and Graphite Filler	147 x 127 x 4.57 (5.8" x 5.0" x 0.18")
Gkt5	Compressed Fibre Gasket with Nitrile (NBR) Binder	158 x 114 x 3.12 (6.2" x 4.5" x 0.123")
Gkt6	Compressed Fibre Gasket with Nitrile (NBR) Binder	150 x 125 x 1.6 (5.9" x 4.9" x 0.065")
BLK1	Solid Copper Block (width x length x thickness)	35.6 x 50.8 x 12.5 (1.4" x 2.0" x 0.494")

Table A.1 - Gasket descriptions

A.6 Results

A.6.1 Gasket elastic modulus

The elastic modulus obtained from this experimentation is not comparable with material elastic moduli listed in references. This is due to the fact that it is a compressive modulus obtained by compressing the material between surfaces that have a serrated surface finish. This means that the modulus varies with increasing contact stress due to the embedding of the serrated finish into the softer gasket material. The modulus discussed in this paper is therefore termed an "apparent modulus of elasticity". This modulus relates only to the tested material at the tested thickness in compression between two surfaces with a surface finish similar to the one used during the testing.

The effect of the mating surfaces can be easily highlighted by comparison to the results for the two solid copper items (Gkt1 and BLK1). Item BLK1, a solid copper block, was tested in compression between two flat (no serrated surface finish) steel platens. It can be seen from Figure A.8 that there is still non-linearity in the results, due to the mating

surfaces not being perfectly parallel. While the results are highly repeatable, it can be seen from Figure A.14 that the apparent elastic modulus is still a lot lower than referenced values, at only 2% – 14% of the published Young's modulus of copper (114GPa [16,500 ksi], ASME, 1998a).

When the serrated surface finish is introduced (Gkt1), the effect of the serrations embedding into the gasket material becomes apparent. From the load vs. deflection curve (Figure A.9) it can be seen that the non-linearity of the curve is much higher. Additionally, the deflection is no longer repeatable, rather there is now a degree of permanent set, due to localised yielding of the gasket material at the tip of the serrations. The figure includes the two ambient loading curves only, thus the gap between the two curves is the permanent deformation obtained during the first temperature cycles (steps 5 to 9).

From the stress vs. deflection curve, the apparent elastic modulus of the gasket was calculated between each point of loading. The results of these calculations are graphed in Figure A.15. This graph compares the calculated apparent elastic modulus with the average gasket stress between the two load points from which the modulus was calculated.

The effects of the serrated surface finish are evident in the values obtained for the apparent modulus in the loading direction (marked L1, L3 and L4) and the unloading direction (marked U1-4). The loading moduli are much lower than the unloading moduli. However, there is also a trend that with repetition of the load, the loading modulus increases towards the unloading value, as the serrations imbed in the gasket.

This means that for most mechanical analysis, only the value of the unloading elastic modulus need be used. This is due to the fact that generally, during assembly, the gasket will see sufficient loading cycles to make the unloading and loading moduli comparable. This same effect may be seen for all the gasket types (Figures A.10 to A.13), to varying

degrees. The effect is more pronounced on softer gaskets, such as Gkt4 and Gkt5 (Figures A.18, A.19), than the harder gaskets (Gkt1 and Gkt2, Figures 16, 17). Due to this effect, the apparent modulus always increases with increasing gasket stress. This necessitates using either a non-linear analysis or the use of an approximation that averages the elastic modulus for a specific limited range of gasket stress.

For the majority of the gasket types there was no effect on the apparent elastic modulus due to temperature. There was, however, an increase in the elastic modulus for gasket Gkt2 for the run at 300°C (572°F) and 100 MPa (145 ksi) maximum stress. This may be due to specific changes in material properties of the gasket components at the higher temperature. However, as this result was not apparent in the lower (50 MPa, 72ksi) maximum stress run and there was no gradual increase with temperature, it is equally as likely that these results are due to measurement error.

The one gasket where the effects of temperature on the elastic modulus are apparent is the compressed fibre gasket (Gkt5). The elastic modulus clearly increases with increasing temperature. This is possibly due to two effects; the hardening of the gasket material at higher temperatures, or the fact that at the higher temperatures the gasket flows in the radial direction more. This decreases the thickness of the gasket and, since these calculations are based on initial gasket thickness, would cause an increase in the calculated apparent gasket elastic modulus.

The gasket moduli indicated by this analysis are in the order of 3.5 to 5 times greater than comparable values published by Bazergui (1984b) and Bazergui et. al. (1977) for gasket Gkt4. This is primarily due to two differences in the methods of calculation for the gasket elastic modulus. In the work of Bazergui the modulus is calculated from a straight line drawn between the maximum loading point and some nominal minimum loading point. The analysis method of this paper utilises four points on each unloading cycle. Since the modulus is clearly shown in the results of this paper and also in those of Bazergui (1984b) to vary approximately linearly with stress, it is apparent that the

assumption of a straight line between the upper and lower loading points (constant modulus vs. stress) is inaccurate. It will result in a much lower modulus for the higher stress levels as it has an effect of averaging the modulus over the tested stress range. The results of the calculation using that method also depend heavily on the selection of the value for the nominal lower loading point.

The second difference between the methods is that the Bazergui method (1984b and 1977) utilises the compressed thickness in calculating the gasket elastic modulus, whereas the analysis of this paper uses the initial gasket thickness throughout. This again leads to a higher indicated modulus for the gasket. However, from Figure A.23, which is developed using results from Bazergui (1977), it can be seen that the effect of the difference in procedures results in only a change in the slope of the modulus versus the stress. The method used in this paper eliminates the necessity of publishing the gasket deformation data with the elastic modulus data. It also eliminates the problems associated with establishing the actual zero point, during testing, for gasket deflection vs. load for the calculation of the deformed thickness of the gasket. Additionally, since the values of the modulus calculated for gaskets Gkt2, Gkt3 and Gkt4 from both the 50MPa and 100MPa maximum stress cycles show good agreement, it appears that, for these gasket types, the relationship between the elastic modulus and the stress level is independent from the maximum stress level of the load cycle, within the tested stress range.

If the modulus calculated by the method of Bazergui is used in analysis then it is the deformed thickness of the gasket that must be input as the initial thickness of the gasket. As mentioned previously, this necessitates prior knowledge of the state of deformation or stress at the commencement of the analysis, which is not always possible. However, as long as the analysis in which the modulus is used accounts for the difference in the method of calculation of the modulus, the two methods will actually give the same result. If the modulus for Gkt4 is recalculated, using the deformed thickness, the value of the elastic modulus for the 44MPa gasket stress level is reduced from 8.4GPa to 5.6GPa

(33% reduction). Furthermore if the method of Bazergui is used to calculate the modulus from the unloading curve of Gkt4, the obtained modulus is 2.25GPa, which is in good agreement with the values (2.34GPa and 1.5GPa) for similar gaskets in both Bazergui (1984b) and Bazergui et. al. (1977), respectively.

A.6.2 Gasket coefficient of thermal expansion

The coefficient of thermal expansion for some gaskets has been shown to depend on the initial stress state of the gasket (Bouzid et. al., 2001). This effect is due to the composite nature of the gasket and the existence of microporosity in most gasket filler materials. However, the operational cycle of the gasket needs to be kept in mind when including this effect. A gasket will, in general, be subjected to a high initial stress at assembly. It will then creep and relax with time, so that the actual operational gasket stress will always be lower than the assembly stress. The coefficient of thermal expansion that is required is therefore the coefficient corresponding to a gasket that has been stressed to the assembly stress and then tested at a lower stress. Testing in this way also has the effect of minimising the impact of gasket creep and relaxation on the thermal expansion measurements being taken.

The coefficients of thermal expansion used and calculated during the course of this paper are all assumed to be linear with temperature. It is well known that for most materials the coefficient will vary with increasing temperature (ASME, 1998a). However, due to the limitations of accuracy in the test equipment being used in this testing it was not feasible to establish such trends in the test data. Additionally, due to the limited temperature range this testing was conducted over, this approximation should not greatly affect the end result of any calculation using the determined values.

The initial testing involved testing the platens, without gaskets, to establish the level of differential expansion occurring between the platens and LVDT pins. Several runs were made; the results of which are graphed in Figure A.20, as platen deflection vs. change in

temperature above ambient. The results were approximated by a straight line, which was then subtracted from the subsequent test results to obtain only the differential expansion occurring between the gasket and the LVDT pins.

The next step was to obtain test results on a known material (copper, gasket Gkt1) so that the coefficient of expansion of the pins could be verified. The tests showed repeatable deflection vs. temperature results (Figure A.21). By making the assumption that the copper has a coefficient of expansion of 1.76×10^{-5} m/m/°C (ASME 1998a) in the entire range of testing it can be established that the apparent LVDT pin coefficient of thermal expansion is 1.35×10^{-5} m/m/°C. This is slightly smaller than that expected for 316 Stainless Steel (1.65×10^{-5} m/m/°C, ASME 1998a), however it is still within the limits of what could be expected, due to variations in metal properties which may occur due to the pin fabrication process and subsequent operational thermal cycling of the pin.

The results of the remaining gasket types (ref. Figures A.22 to A.25) were then analysed to establish the coefficient of thermal expansion for those materials. The results of this analysis are tabulated in Table A.2, below:

Gasket	α_g (m/m/°C) x 10^{-6}	α_g' (m/m/°C) x 10^{-6}	t_g' (mm)
Gkt2	9.8	6.8	1.9
Gkt3	8.6	6.8	1.32
Gkt4	11.7	10.3	2.55

Table A.2 - Gasket coefficient of thermal expansion results.

The coefficients of expansion are all within a range that might be expected by examination of the properties of the individual components of the gaskets. Gaskets Gkt2 and Gkt3 are constructed of carbon steel ($\alpha = 11.2 \times 10^{-6}$ m/m/°C, ASME 1998a) and graphite ($\alpha = 2 \times 10^{-6}$ m/m/°C to $\alpha = 4 \times 10^{-6}$ m/m/°C, depending on graphite orientation and type, Touloukian et. al. 1970). One would therefore expect a coefficient of thermal expansion for the gasket between these two values, as was the case. The third gasket,

Gkt4, is constructed of stainless steel (α=16.5x10^{-6} m/m/°C, ASME 1998a) and graphite. Similarly, the result is between these two values and so appears believable.

The second value listed in Table A.2 (α_g') is calculated using the thickness of the gasket in the compressed state. The thickness that was used (t_g') is listed following each value. This value should be used in analysis where the expansion occurring is calculated based on the deformed thickness of the gasket.

The results for gasket Gkt5 (Figure A.25) are not presented, as they were not felt to be conclusive. This gasket exhibited higher relaxation at temperature than other gasket types and was also partially decomposed at the higher temperature. This suggests that the test regime was too severe for this gasket type, and modification to the test procedure would be required to obtain more accurate results.

In all cases there appeared to be runs where the coefficient of expansion of the gasket was higher than that of the pins (noted by a positive platen deflection with increasing temperature). This effect did not appear to be related to the initial gasket stress level or the number of testing cycles conducted. They are perhaps real results, however, it is equally as likely that they are due to errors in the deflection measurement (such as sticking deflection pins). Ideally this effect should have been examined further, perhaps using ceramic pins, which would have given a higher differential expansion measurement, and therefore increased the measurement accuracy.

However, as mechanical calculations using a higher gasket coefficient of thermal expansion will always result in a higher gasket stress, by considering only the negative platen deflection results the mechanical calculations will always be conservative. The positive results were therefore disregarded, although they should be kept in mind when developing further thermal expansion tests.

As mentioned earlier, it is important to eliminate such factors as creep and relaxation from influencing the test results. In examining Figure A.26, an example of the platen deflection and temperature with respect to time, it is clear that the obtained results should not be influenced by such factors as relaxation, as the gasket deformation is steady (at constant stress and temperature) for an hour beforehand. There appears to be a dynamic effect, possibly due to differential cooling between the platens and LVDT pins when the heating is initially turned off. However, this should not affect the validity of the results, as this section is excluded from the results. Additionally, it can be seen from this figure that the platen deflection follows the temperature curve very closely, a good sign that the results are accurate.

A.6.3 Gasket overall heat transfer coefficient

The determination of the gasket overall heat transfer coefficient for the gaskets was quite successful and it was possible to determine the coefficient in a repeatable fashion (Table A.3.). Initial tests were done on the platens, without any gaskets, and also using the solid copper gaskets (Gkt1). These tests were compared to generic results for contact heat flow from Ozisik (1985).

The values in Table A.4, for platens alone and also for the copper gasket (Gkt1), were adjusted to remove the through platen (and through gasket) thickness resistance. The remainder is therefore due only to the surface contact resistance. The values for the thermal conductance of copper (16.8×10^{-6} W/(m.°C)) and carbon steel (43×10^{-6} W/(m.°C)) were obtained from ASME (1998a). From Ozisik (1985) surface contact between stainless steel, in air, of surface roughness 2.54μm, results in a heat transfer coefficient of around 3,000 W/(m².°C) to 4,000 W/(m².°C). Additionally the value increases with increasing temperature and decreasing surface roughness.

Gasket	h_{cg} at 100°C (212°F) W/(m².°C) (Btu/h/ft²/°F)	h_{cg} at 200°C (392°F) W/(m².°C) (Btu/h/ft²/°F)	h_{cg} at 300°C (572°F) W/(m².°C) (Btu/h/ft²/°F)
Platens	740 (130)	958 (169)	1048 (185)
Gkt1	1756 (309)	1959 (345)	2114 (372)
Gkt2	1369 (241)	1569 (276)	1769 (312)
Gkt3	1310 (231)	1535 (270)	1723 (303)
Gkt4	2865 (505)	3037 (535)	3276 (577)
Gkt5	368 (65)	458 (81)	469 (83)
Gkt6	194 (34)	321 (57)	-

Table A.3 - Overall heat transfer coefficient results

Gasket	h_c at 100°C (212°F) W/(m².°C)	h_c at 200°C (392°F) W/(m².°C)	h_c at 300°C (572°F) W/(m².°C)
Platens	1575	2050	2250
Gkt1	5875	7075	8225

Table A.4 - Surface contact heat transfer coefficient results

The obtained surface contact heat transfer coefficients for the platens therefore appear to give good agreement with these values. The trends of increasing resistance with increasing surface roughness and decreasing resistance with increasing temperature were maintained by the test results. The results presented for copper (in a vacuum) in Ozisik (1985), indicate that the contact coefficient of heat transfer for copper should be in the order of 1.3 to 21 times that obtained for a stainless steel interface. Once again this trend is confirmed by the obtained test results, with the value for copper being around 3.5 times higher than that of the platen contact.

For all gasket types there appears to be only a small variation in the value of the coefficient for gaskets of similar construction (gaskets Gkt2 and Gkt3). However, as would be expected, the gaskets with a more direct channel of heat flow (Gkt4) have a

higher coefficient and those constructed of a lower conductivity material (Gkt5 and Gkt6) have a much lower coefficient.

During all calculations the heat transfer occurring between the exposed surface areas of the platens on either side of the gasket was ignored, on the basis that it would be of at least a magnitude smaller than the heat transfer through the gasket. The validity of this assumption was confirmed by comparison of the results of the Gkt5 and Gkt6 gasket tests. In the first test the platen surface area was, essentially, fully covered by the gasket. Whereas, in test Gkt6 the exposed platen surface area was greater than the gasket area. It can be seen that for Gkt6, the gasket overall coefficient of heat transfer is actually lower than that of Gkt5, but of the same order. This confirms the validity of the assumption, as the heat transfer between the exposed platen surfaces in test Gkt6 is obviously not contributing greatly to the overall heat transfer level.

The higher resistance of Gkt6 is probably due to the fact that it was not subjected to the same rigorous level of testing as Gkt5 and therefore the thickness was greater (the final compressed thicknesses of Gkt5 and Gkt6 were 1.02mm and 1.5mm respectively). As stated previously, the test appeared too rigorous for the Gkt5 gasket material and so caution should be used when applying the Gkt5 results. In the case of the overall heat transfer coefficient, the test result will indicate a higher transfer of heat than is perhaps the case in reality, unless operational conditions are similar to the test procedure.

A.7 Equations

Calculation of the modulus of elasticity:

$$E_g = \frac{\Delta S_g}{\Delta D_g} t_g \qquad (A.1)$$

Calculation of the coefficient of expansion (for constant gasket stress):

$$\alpha_g = \alpha_p + \frac{1}{n_g t_g}\left(\frac{\Delta D_g}{\Delta T_g} - \frac{\Delta D_{pl}}{\Delta T_{pl}}\right) \qquad (A.2)$$

Calculation of the overall coefficient of heat transfer:

$$Q = (T_{c1} - T_{c2}) \cdot A_c k_c / L_c \tag{A.3}$$

$$h_{cg} = (T_{p1} - T_{p2}) / Q \tag{A.4}$$

A.8 Conclusions

The gasket properties determined during the course of this testing appear to be of sufficient accuracy that they may be confidently used in mechanical analysis. However, the results require further confirmation with other gasket types, other gasket manufacturers and perhaps even other testing methods in order to determine the overall variability of the properties.

In particular, it is thought that further testing to examine the value of the coefficient of thermal expansion for gaskets needs to be conducted, perhaps using ceramic LVDT pins to improve the accuracy of the test method. It appears from this initial test program that, for certain gasket types of similar construction, it may be possible to standardize the thermal property values.

It is also important that further research into the gasket apparent elastic modulus be conducted. Specific attention should be paid to the variability of the modulus with respect to gasket stress, ensuring that several points on the unloading curve are used in the calculation. Great care must also be taken when using the calculated values in any subsequent analysis that the modulus is correctly applied. As demonstrated, if an unloading modulus base on two points and the loaded thickness is used in an finite element analysis without suitable precaution it may in fact be in the order of five times smaller than reality.

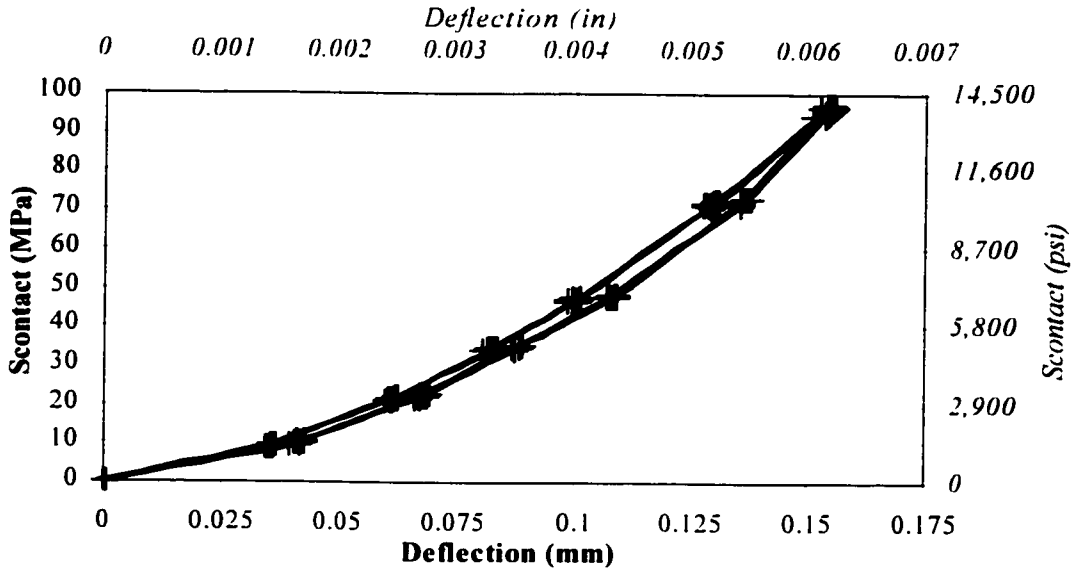

Figure A.4 – Stress vs. deflection for sample BLK1

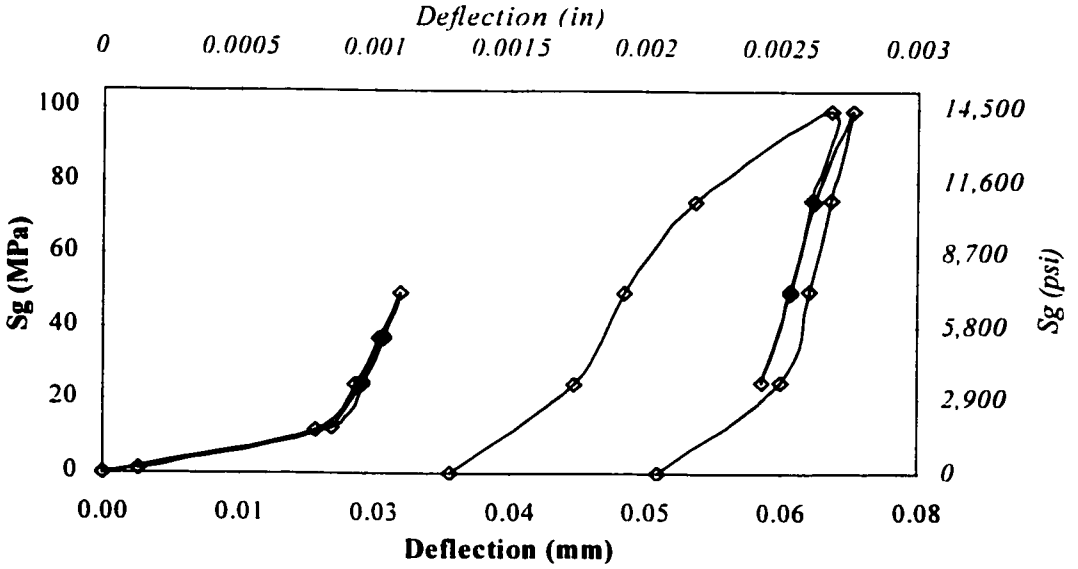

Figure A.5 – Stress vs. deflection for Gkt1 (steps 3-6, 11)

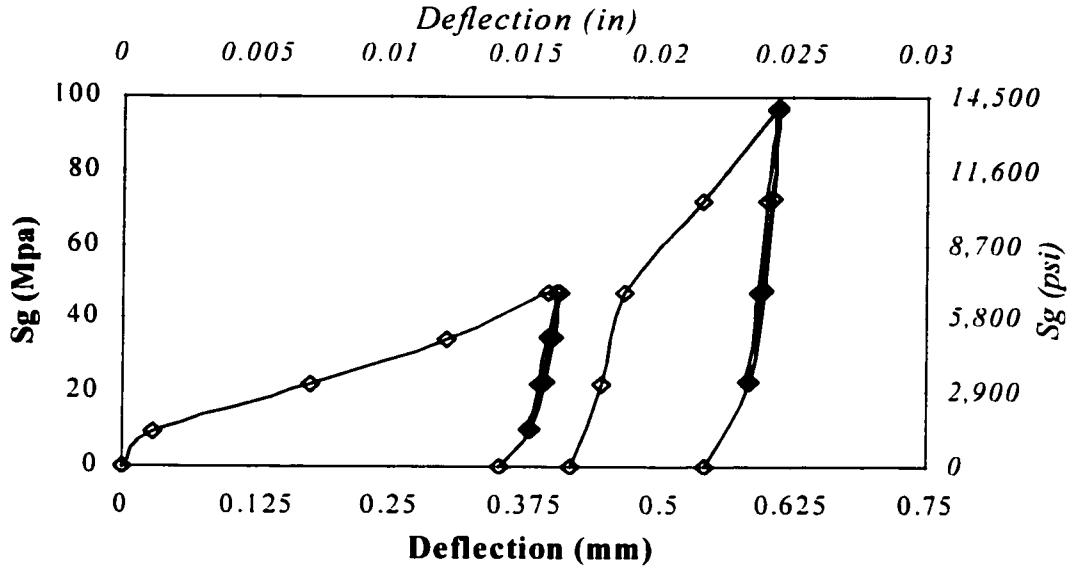

Figure A.6 – Stress vs. deflection for Gkt2 (steps 3-6, 11)

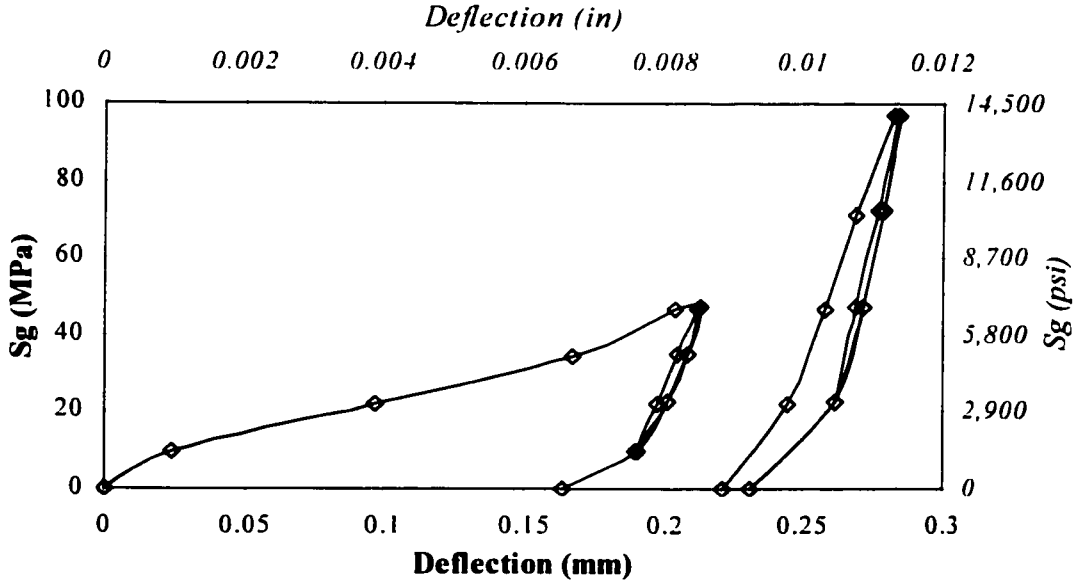

Figure A.7 – Stress vs. deflection for Gkt3 (steps 3-6,11)

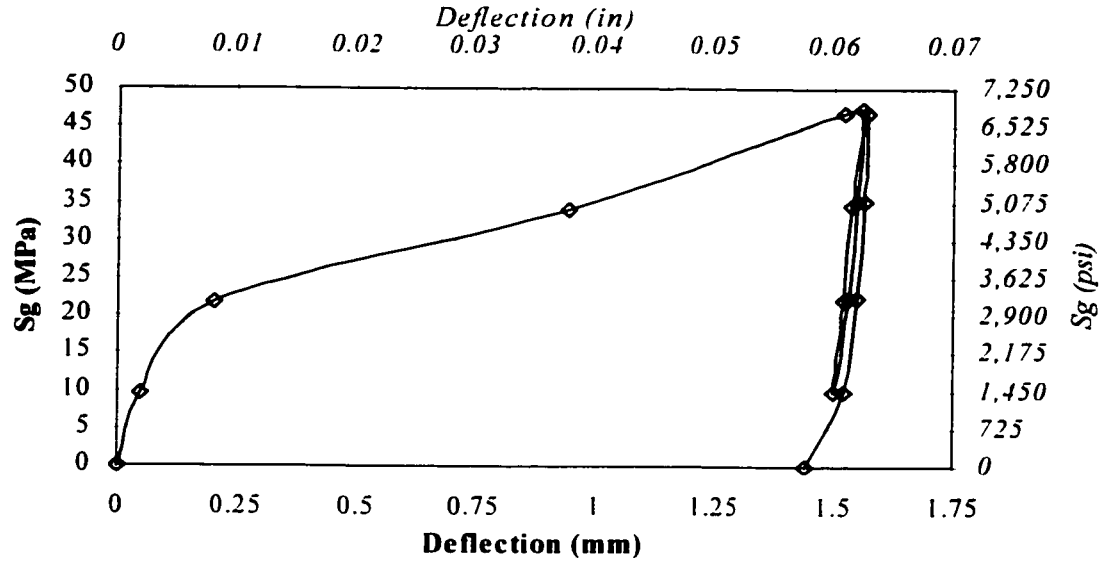

Figure A.8 – Stress vs. deflection for sample Gkt4 (steps 3-6)

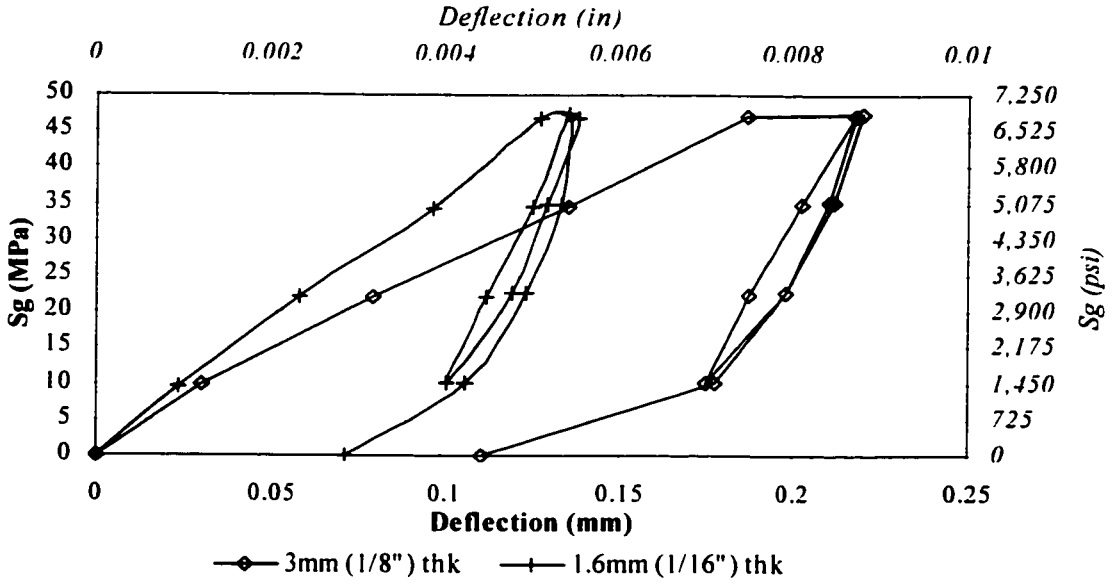

Figure A.9 – Stress vs. deflection for Gkt5 & 6 (steps 3-6)

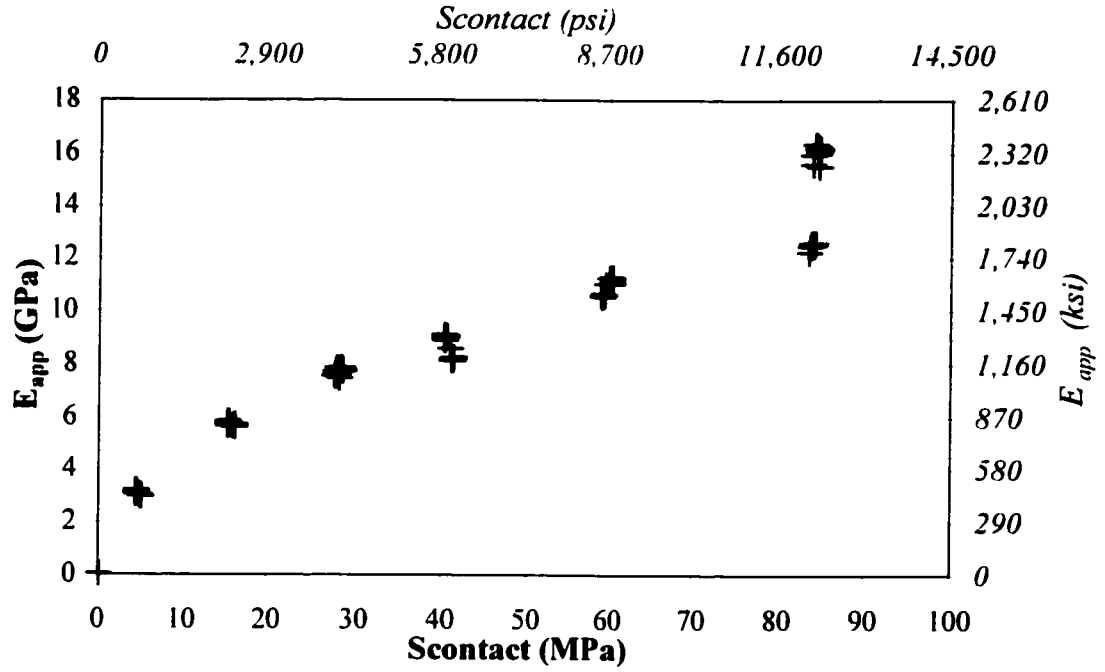

Figure A.10 – Stress vs. apparent elasticity, sample BLK1

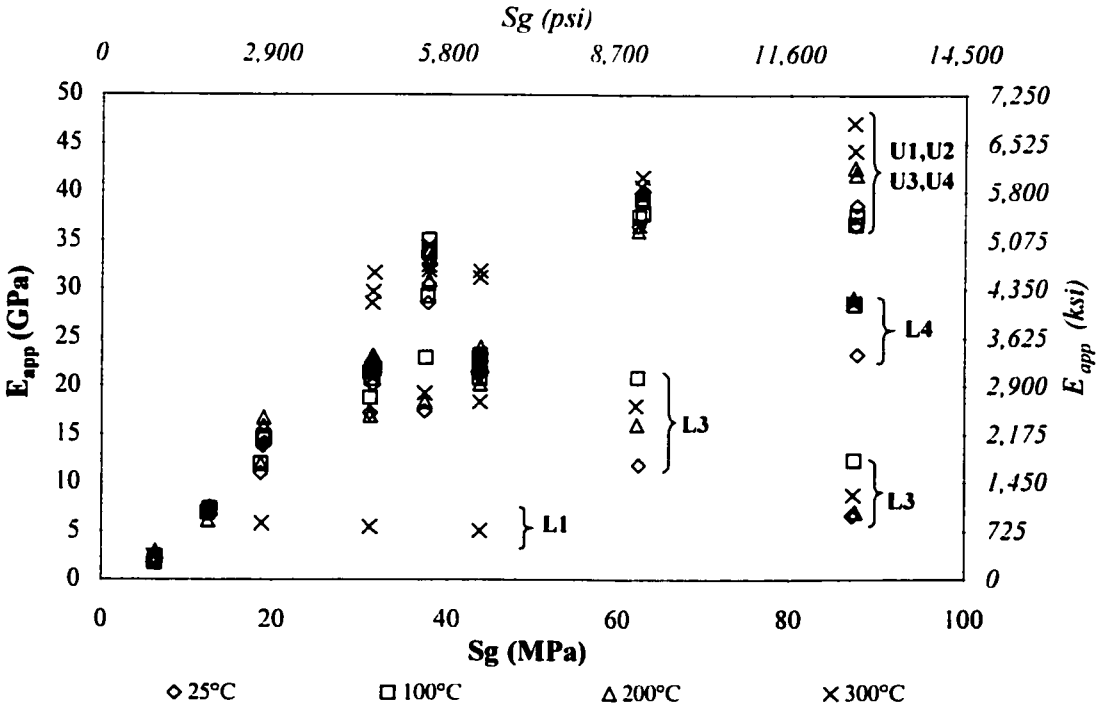

Figure A.11 – Stress vs. apparent elasticity, Gkt1 (steps 3-11)

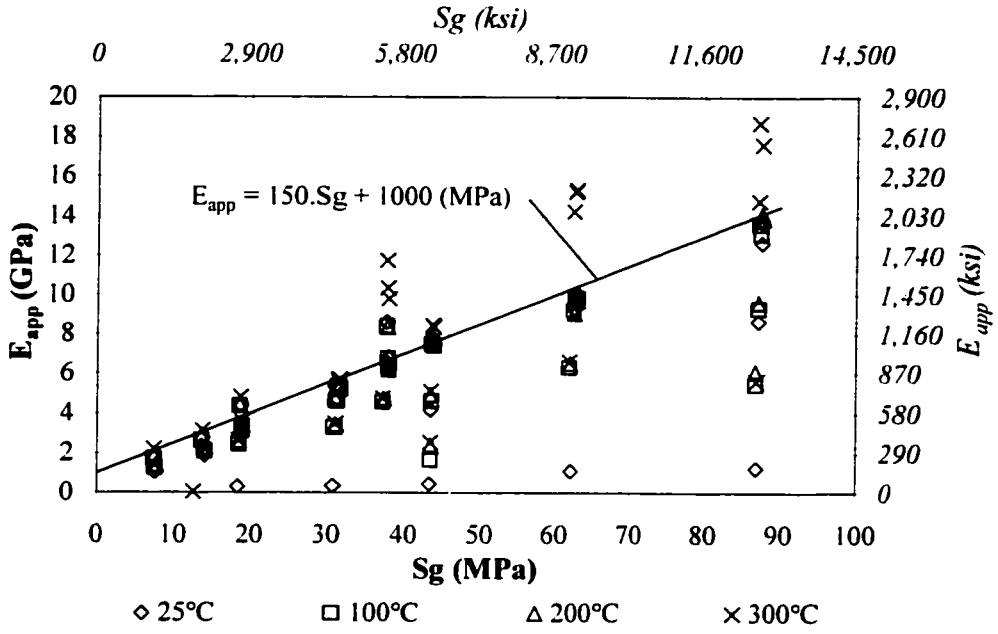

Figure A.12 – Stress vs. apparent elasticity, Gkt2 (steps 3-11)

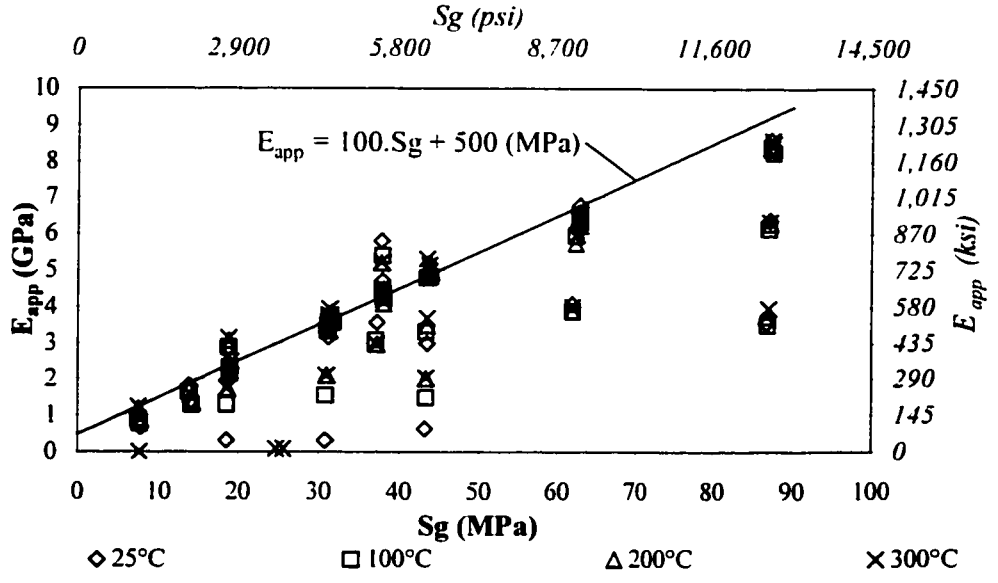

Figure A.13 – Stress vs. apparent elasticity, Gkt3 (steps 3-11)

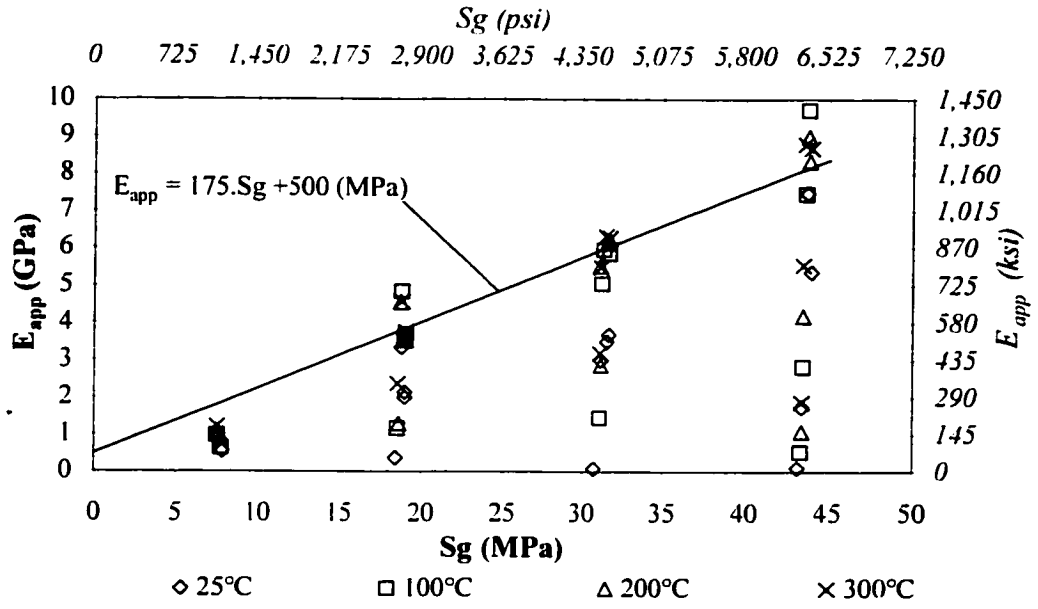

Figure A.14 – Stress vs. apparent elasticity, Gkt4 (steps 3-11)

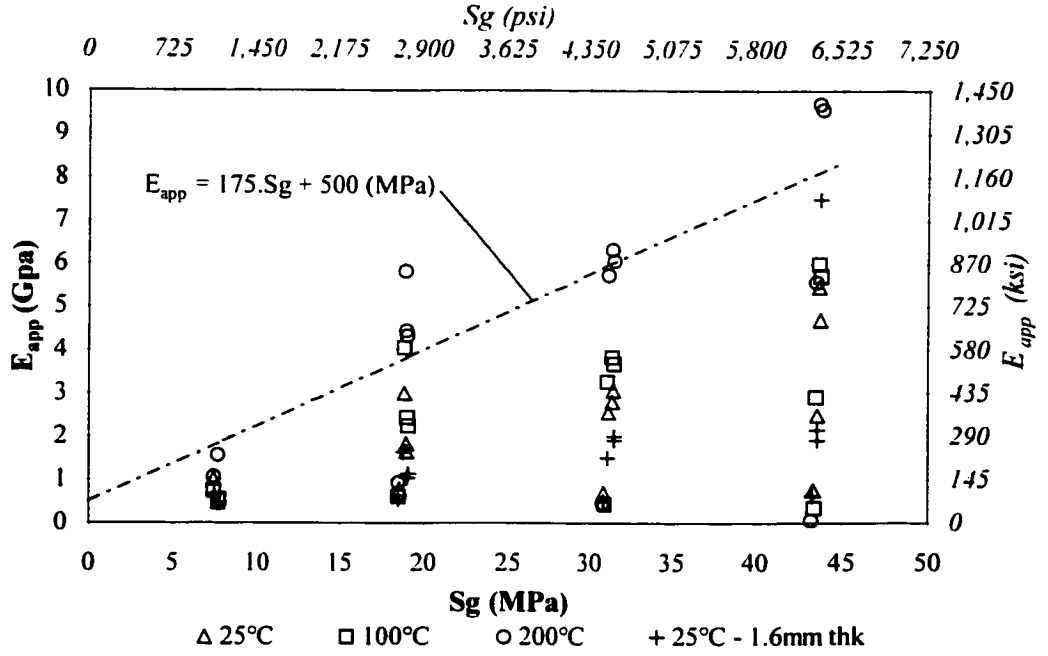

Figure A.15 – Stress vs. apparent elasticity, Gkt5 & 6 (3-11)

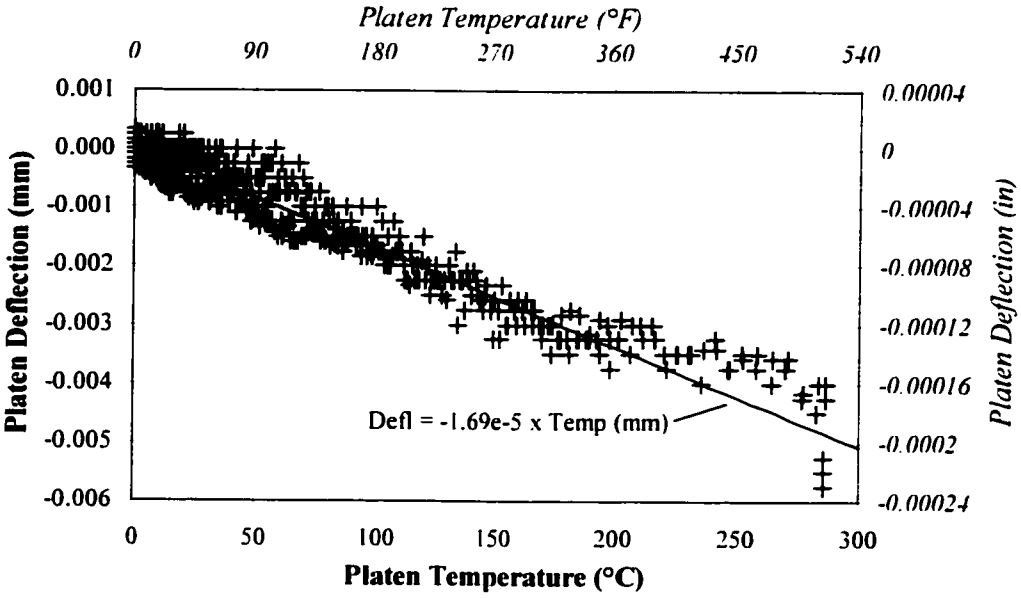

Figure A.16 – Deflection vs. temperature, platens only

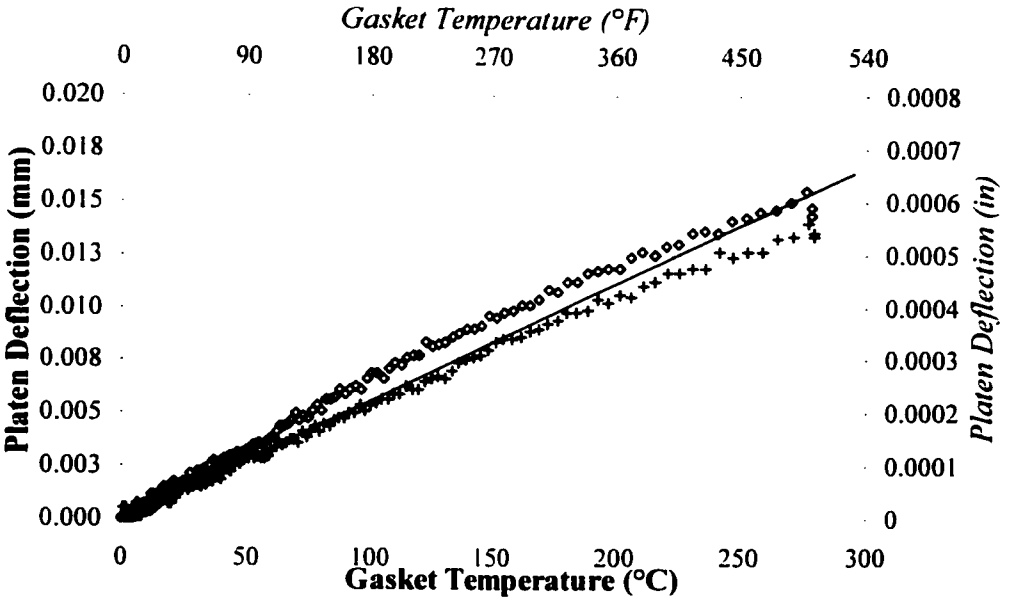

Figure A.17 – Deflection vs. temperature, sample Gkt1

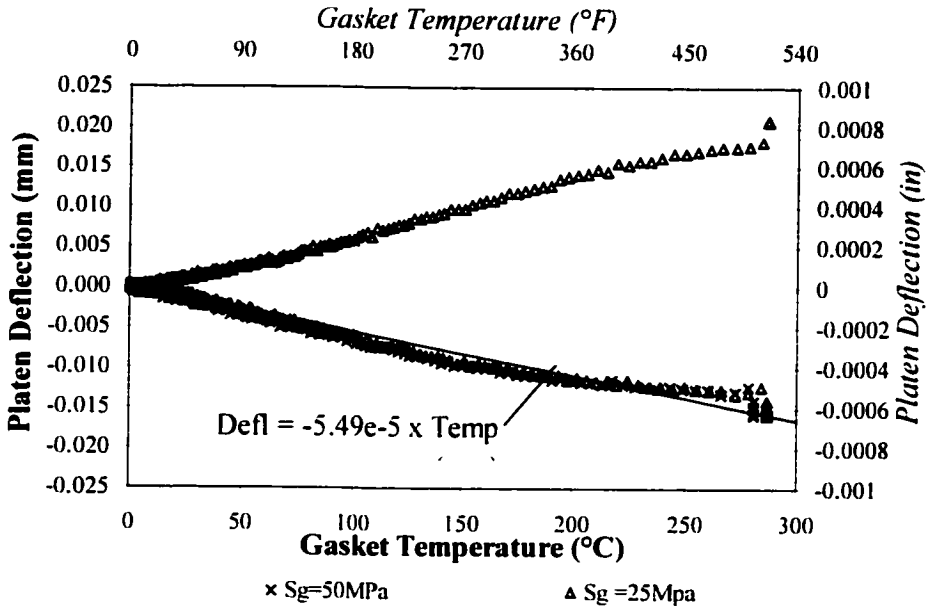

Figure A.18 – Deflection vs. temperature, sample Gkt2

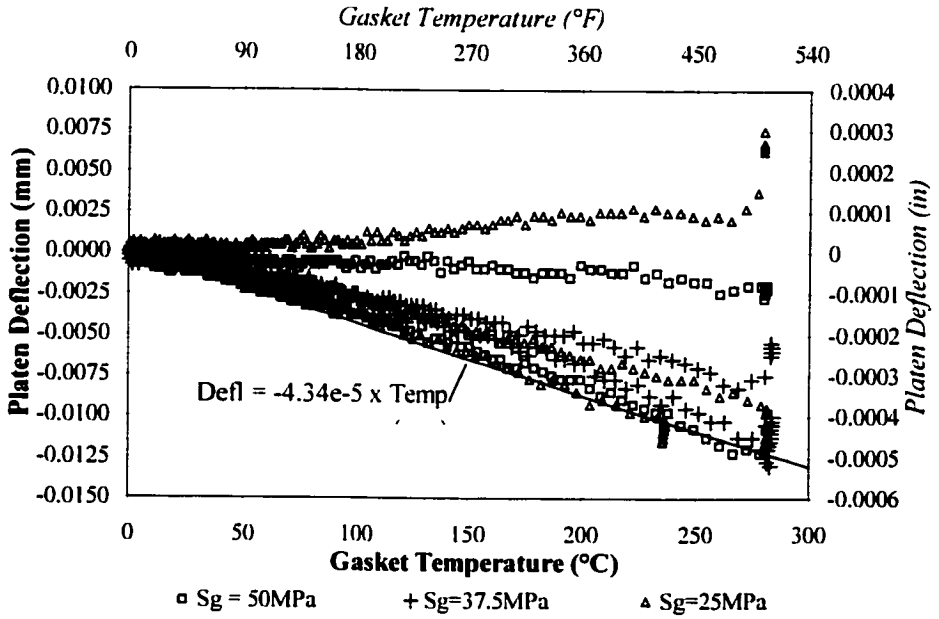

Figure A.19 – Deflection vs. temperature, sample Gkt3

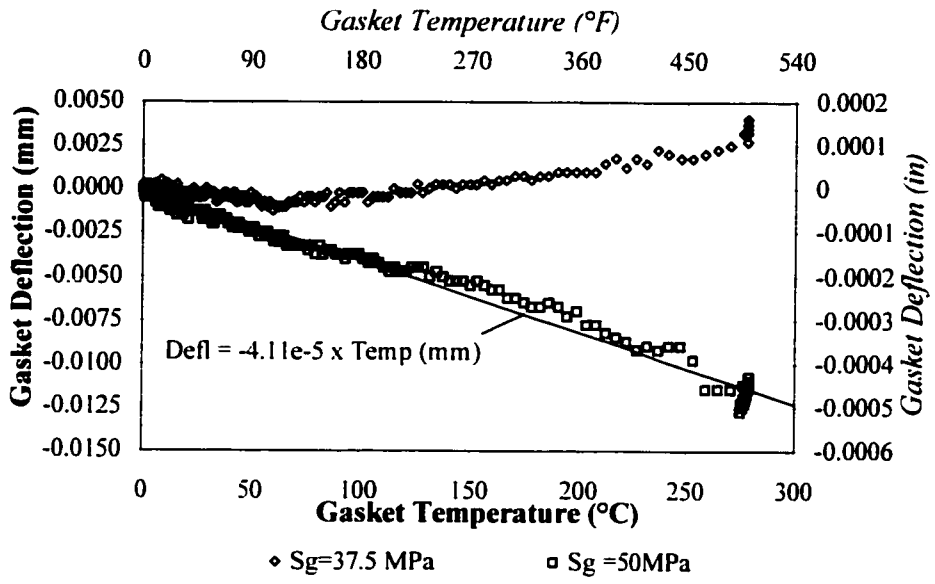

Figure A.20 – Deflection vs. temperature, sample Gkt4

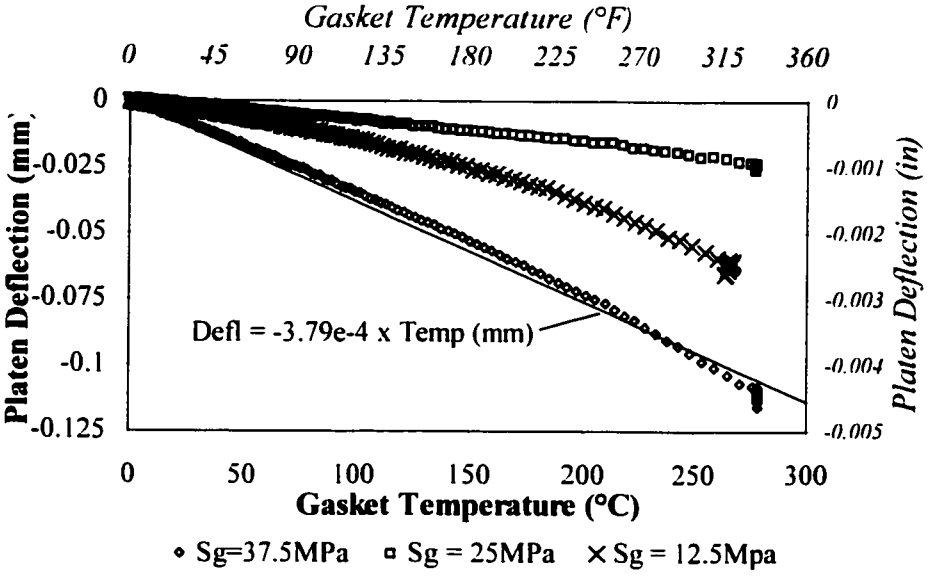

Figure A.21 – Deflection vs. temperature, sample Gkt5

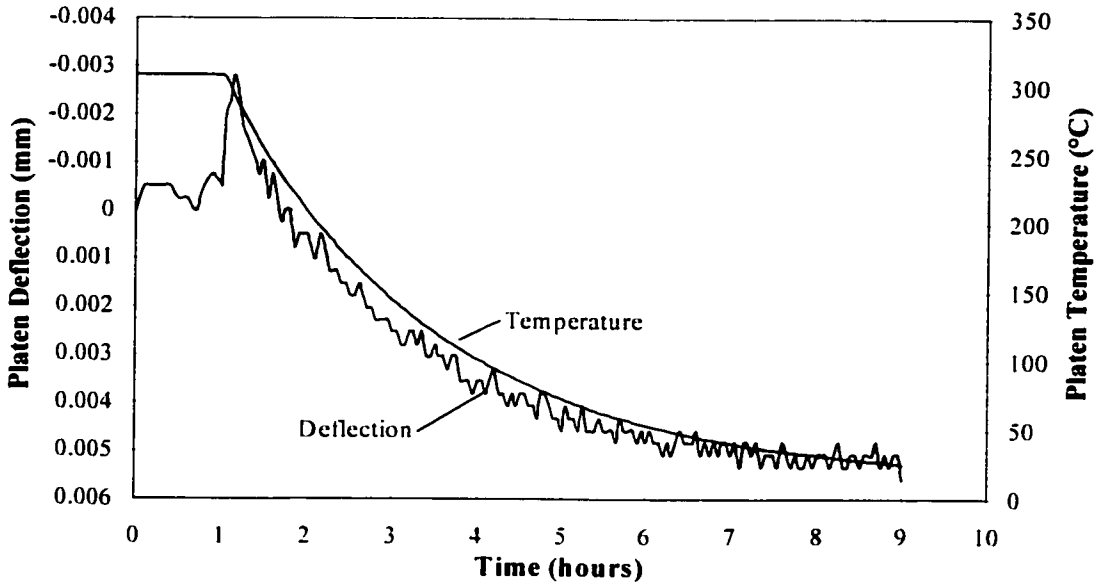

Figure A.22 – Deflection & temperature vs. time, Gkt3

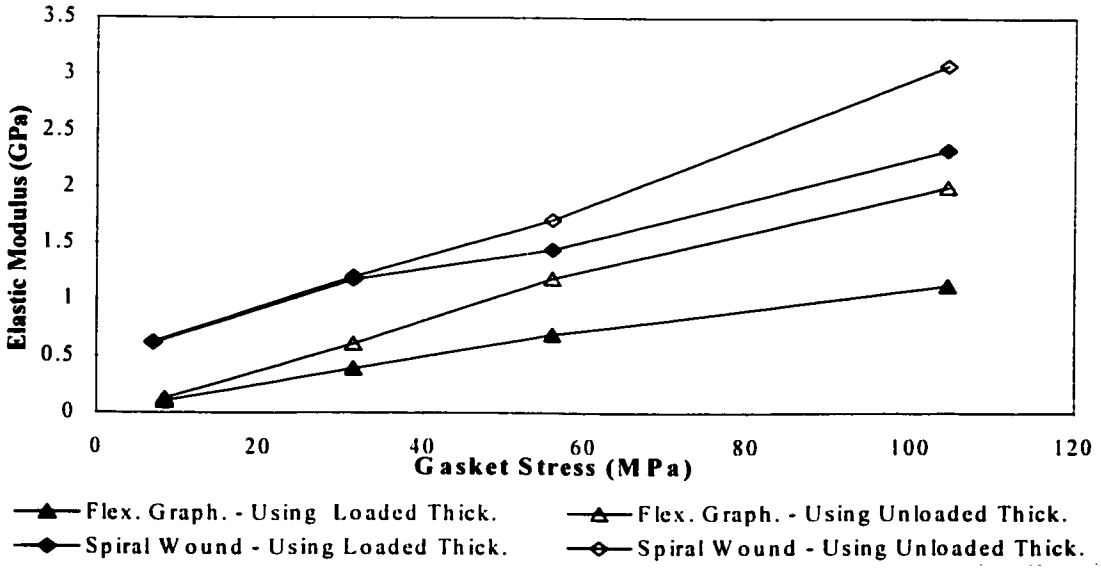

Figure A.23– Calculation comparison (data from Bazergui,1984b)

APPENDIX B

FINITE DIFFERENCE HEAT TRANSFER EQUATIONS

B.1 Description of method

The following equations were developed to analyse the variation of both finite length and infinite length hollow cylinders, when subjected to an instantaneous increase in internal fluid temperature. The governing equation, assuming infinitesimally small element volume, for heat flow through an axisymmetric cylinder (Equation B.1) is obtained from Carslaw et. al.(1959).

$$\frac{\partial T}{\partial t} = \alpha\left(\frac{\partial^2 T}{\partial r^2} + \frac{1}{r}\frac{\partial T}{\partial r} + \frac{\partial^2 T}{\partial z^2}\right) \qquad \text{B.1}$$

Where

$$\alpha = \left(\frac{k_f}{\rho c}\right) \qquad \text{B.2}$$

The boundary conditions are assumed to follow Newton's law of cooling, and may therefore be expressed as following:

At the cylinder internal diameter:

$$q = -k_f \frac{\partial T}{\partial r} = h_i(T_i - T) \qquad \text{B.3}$$

At the cylinder external diameter:

$$q = -k_f \frac{\partial T}{\partial r} = h_e(T - T_e) \qquad \text{B.4}$$

At the finite length cylinder upper and lower surfaces:

$$q = -k_f \frac{\partial T}{\partial z} = h_e(T - T_e) \qquad \text{B.5}$$

In order to simplify the equations, the external temperature (T_e) is assumed to be zero. The calculations are further simplified by non-dimensionalisation of the equations as following:

Non-dimensional temperature:

$$\theta = \frac{T}{T_i} \qquad \text{B.6}$$

Non-dimensional time:

$$\tau = \frac{\alpha t}{r_i^2} \qquad \text{B.7}$$

Non-dimensional radius:

$$R = \frac{r}{r_i} \qquad \text{B.8}$$

Non-dimensional axial distance:

$$Z = \frac{z}{r_i} \qquad \text{B.9}$$

Non-dimensional Heat Transfer Coefficients (Biot No. – radius based):

$$H_i = \frac{h_i r_i}{k} \qquad \text{B.10}$$

$$H_e = \frac{h_e r_i}{k} \qquad \text{B.11}$$

The non-dimensional governing equations and boundary conditions therefore become:

$$\frac{\partial \theta}{\partial \tau} = \alpha\left(\frac{\partial^2 \theta}{\partial R^2} + \frac{1}{R}\frac{\partial \theta}{\partial R} + \frac{\partial^2 \theta}{\partial Z^2}\right) \qquad \text{B.12}$$

$$-\left.\frac{\partial \theta}{\partial R}\right|_{R=1} = H_i(\theta_i - \theta) \qquad \text{B.13}$$

$$-\left.\frac{\partial \theta}{\partial R}\right|_{R=\frac{r_e}{r_i}} = H_e \theta \qquad \text{B.14}$$

$$-\left.\frac{\partial\theta}{\partial Z}\right|_{Z=0,\frac{t}{r_i}} = H_c\theta$$

B.15

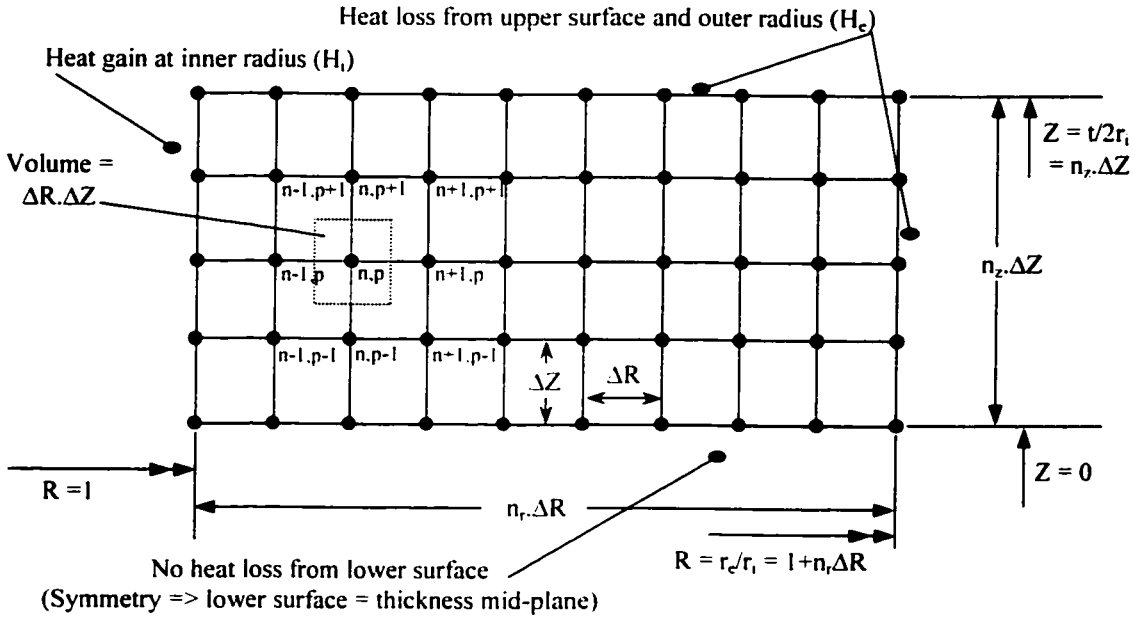

Figure B1 – Finite difference model diagram

The finite difference model is therefore defined as in Figure B1. From energy balance equations on the finite volume, the finite difference equations may be developed as following.

For an internal node:

$$\theta_{m+1,n,p} = \frac{\Delta\tau}{\Delta R^2}\left(\theta_{m,n+1,p} + \theta_{m+1,n-1,p}\right) + \left(1 - \frac{2\Delta\tau}{\Delta R^2} - \frac{2\Delta\tau}{\Delta Z^2}\right)\theta_{m,n,p} + \frac{\Delta\tau}{2\Delta R\left(1+n\Delta R\right)}\left(\theta_{m,n+1,p} - \theta_{m,n-1,p}\right) + \frac{\Delta\tau}{\Delta Z^2}\left(\theta_{m,n,p+1} + \theta_{m,n,p-1}\right)$$

B.16

Where m is the time co-ordinate, n is the radius co-ordinate and p is the thickness co-ordinate.

For inner radius nodes:

$$\theta_{m+1,0,p} = \frac{\Delta\tau}{\Delta R^2}\left(\theta_{m,1,p}\right) + \left(1 - \frac{H_i\Delta\tau}{\Delta R} - \frac{\Delta\tau}{\Delta R^2} - \frac{2\Delta\tau}{\Delta Z^2}\right)\theta_{m,0,p} + \frac{H_i\Delta\tau}{\Delta R} + \frac{\Delta\tau}{\Delta Z^2}\left(\theta_{m,0,p+1} + \theta_{m,0,p-1}\right)$$

B.17

For outer radius nodes:

$$\theta_{m+1,n_r,p} = \frac{\Delta\tau}{\Delta R^2}\left(\theta_{m,n_r-1,p}\right) + \left(1 - \frac{H_e\Delta\tau}{\Delta R} - \frac{\Delta\tau}{\Delta R^2} - \frac{2\Delta\tau}{\Delta Z^2}\right)\theta_{m,n_r,p} + \frac{\Delta\tau}{\Delta Z^2}\left(\theta_{m,n_r,p+1} + \theta_{m,n_r,p-1}\right)$$

B.18

For lower surface nodes:

$$\theta_{m+1,n,0} = \frac{\Delta\tau}{\Delta R^2}\left(\theta_{m,n+1,0} + \theta_{m,n-1,0}\right) + \left(1 - \frac{2\Delta\tau}{\Delta R^2} - \frac{\Delta\tau}{\Delta Z^2}\right)\theta_{m,n,0} + \frac{\Delta\tau}{2\Delta R\left(1 + n\Delta R\right)}\left(\theta_{m,n+1,0} - \theta_{m,n-1,0}\right) + \frac{\Delta\tau}{\Delta Z^2}\left(\theta_{m,n,1}\right)$$

B.19

For upper surface nodes:

$$\theta_{m+1,n,n_z} = \frac{\Delta\tau}{\Delta R^2}\left(\theta_{m,n+1,n_z} + \theta_{m,n-1,n_z}\right) + \left(1 - \frac{H_e\Delta\tau}{\Delta Z} - \frac{2\Delta\tau}{\Delta R^2} - \frac{\Delta\tau}{\Delta Z^2}\right)\theta_{m,n,n_z} + \frac{\Delta\tau}{2\Delta R\left(1 + n\Delta R\right)}\left(\theta_{m,n+1,n_z} - \theta_{m,n-1,n_z}\right) + \frac{\Delta\tau}{\Delta Z^2}\left(\theta_{m,n,n_z-1}\right)$$

B.20

Equations B.16 to B.18 are further simplified for infinite length cylinders by deleting the ΔZ, $\theta_{(\,,\,,p-1)}$ and $\theta_{(\,,\,,p+1)}$ terms.

These equations may then be solved using explicit methods, with the time increment $\Delta\tau$ limited by the relationship defined in Equations B.21 and B.22. These equations are based on the analysis stability criterion outlined in Ozisik (1985), modified for non-dimensional cylindrical analysis.

For an infinite cylinder, $\Delta\tau$ was taken as:

$$\Delta\tau \leq \frac{\Delta R^2}{2(1 + H_i \Delta R)} \qquad \text{B.21}$$

For a finite length cylinder, $d\tau$ was taken as equal to, or less than the smaller of:

$$\left.\begin{aligned} \Delta\tau &\leq \frac{\Delta R^2}{2(2 + H_i \Delta R)} \\ \Delta\tau &\leq \frac{\Delta Z^2}{2(2 + H_i \Delta Z)} \\ \Delta\tau &\leq \frac{\Delta R^2}{4(1 + H_e \Delta R)} \\ \Delta\tau &\leq \frac{\Delta Z^2}{4(1 + H_e \Delta Z)} \end{aligned}\right\} \qquad \text{B.22}$$

B.2 Convergence of results

The above finite difference equations were developed into a computer program, written in C++. This program was run for the cases listed previously in Section 4.1. In order to determine the optimal number of nodes for each type of analysis (infinite and finite length cylinders), selected cases were run with increasing numbers of nodes, such that the convergence of the results could be examined.

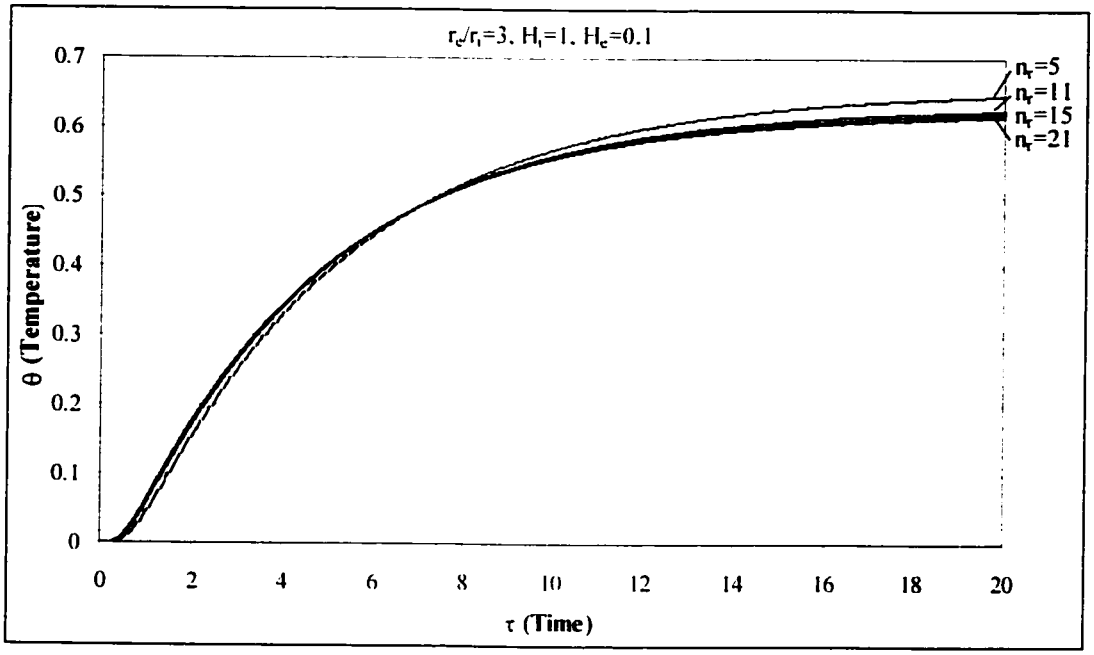

Figure B.2 – Convergence results, outer radius temperature, infinite cylinder

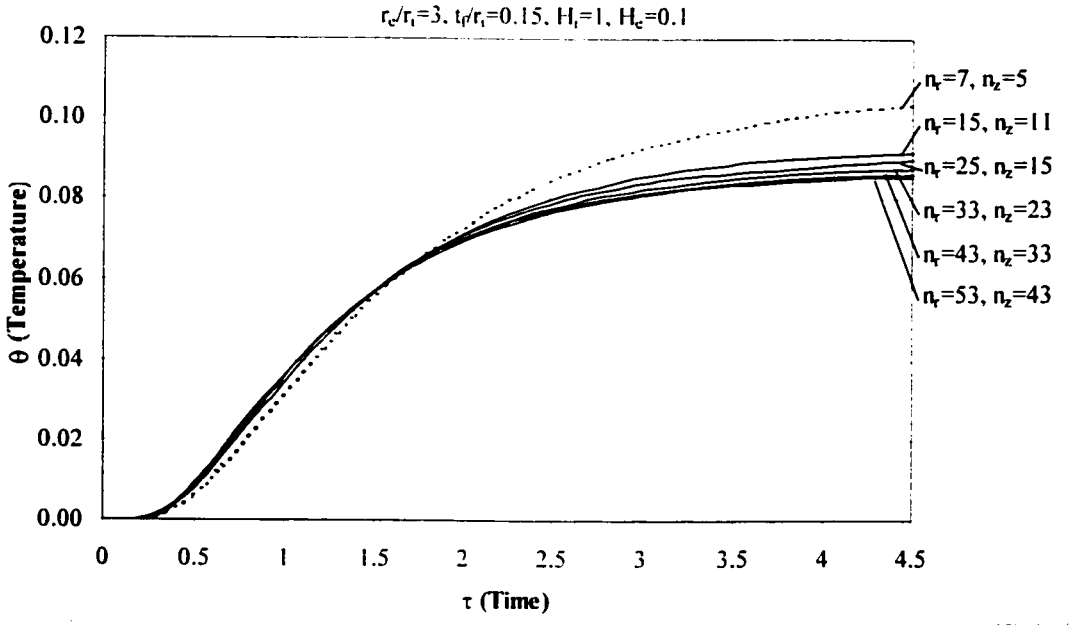

Figure B.3 – Convergence results, outer radius temperature, finite cylinder

For the infinite length case, the results appear below in Figure B.2. It is apparent that convergence of the results is obtained very quickly and that the use of more than 21 radial nodes results in very little difference in the results. All subsequent analysis was therefore performed using at least 21 nodes in the radial direction.

The finite length case was similarly analysed. With reference to Fig B.3, it is apparent that the results converge with greater than 43 and 33 nodes in the r and z directions, respectively. However, the solution is quite slow when using this number of nodes. Additionally, the solution using 33 and 23 nodes was not much more inaccurate, whilst being more than twice as quick to run. All subsequent analyses were therefore run using at least 33 and 23 nodes in the radial and axial directions respectively.

B.3 Development of a graphical solution

Historically, the effects of thermal transients on cylinders have commonly been examined using an analogy to the flow of heat through a thick slab with an insulated external surface (McNeill, et.al, 1971). This approach allows the solution to be developed analytically. However, it neglects the effects of the increasing cylinder radius and also the effects of an external surface that is not insulated. These effects diminish for thin walled cylinders and very small ratios of external/internal heat transfer coefficients. However, this approach would result in excessive error if applied to the analysis of the flange ring in a joint.

By using the finite difference solution previously outlined, a similar graphical analysis can be developed which eliminates the inaccuracies involved in treating the cylinder as a thick slab. To facilitate later simplifications involving the use of the temperature results in stress analysis, the graphical approach will be based on the graphing of the 0.05 and 0.95 values of the non-dimensional temperature (θ).

The graphs were constructed by running the finite difference analysis over the full range of analysis variables, varying each of these slightly from one run to another. In this way the change in the temperature versus time profile with each variable could be determined. It was found that the use of a thickness based Biot number, rather than the radius based Biot number used in the analysis, allowed the simplest graphical representation of the variation of the time taken to reach 0.05 and 0.95 of the steady state temperature. For each radial position it was therefore possible to construct a graph which showed the variation of these times with respect to not only the Biot number (H_i), but also with respect to the ratios of internal to external heat transfer coefficient (H_e/H_i) and external radius to internal radius (r_e/r_i) (ref. Figures 4.3a to 4.4c). These graphs can also be used to gain an understanding of the error that would be associated with using the analysis of McNeill, et.al (1971), which does not account for the effects of the variation in the heat transfer coefficient ratio or external radius ratio. The results of the analysis of McNeill, et.al (1971) always correspond to the smallest ratio of both the heat transfer coefficient ratio and the external radius ratio.

The final graph (Figure 4.5) was constructed by comparing the finite difference results for each case with a series of standard curves. These curves graphed the variation of temperature in the cylinder, versus the ratio of the time between the 0.05 time and the present time over the time between the 0.05 and 0.95 time values. Since the geometry of the infinite length hollow cylinder is very simple, there is not a lot of variation in the shape of the temperature transient. It was therefore possible to use only eight standard curves, with user performing a linear interpolation between values as necessary. In this way, even with poor interpolation, it is evident that the error involved will be less than 10% of the value at any given time. For the required analysis purposes this is not considered a very large error.

APPENDIX C

SAMPLE TRANSIENT MECHANICAL EFFECTS CALCULATION

Input Values

	14" cl. 150	16" cl. 600	24" H. Ex.	37" H. Ex.	Source
h_i =	400	400	400	400	
H_i =	1.77	2.01	3.11	4.95	
h_e/h_i =	0.0575	0.0575	0.0575	0.0575	
r_i =	0.1683	0.1905	0.2953	0.4699	
r_f =	0.2666		0.3747	0.5446	
t_s =	0.00953	0.0127	0.00953	0.0127	
t_f =	0.0334	0.0762	0.0476	0.0841	
L_h =	0.07	0.156	0.12	0.235	
t_{ts} =	-	-	-	0.0632	
α =	0.0000103	0.0000103	0.0000103	0.0000103	
ρ =	7850	7850	7850	7850	
c =	470	470	470	470	
k =	38	38	38	38	

Calculated Steady State Values

$\Delta\sigma_{bSS\ 1}$ =	15.2	14.6	3.88	6.3	
$\Delta\sigma_{bSS\ 1ts}$ =	-	-	-	21	
$\Delta\sigma_{bSS\ 2}$ =	-4.8	-2.9	-2.23	-0.8	
$\Delta\sigma_{bSS\ 3}$ =	-36.8	-27.7	-14	-9.3	
T^{s}_{SS} =	281.9	281.5	281.3	282	
T^{fi}_{SS} =	260.9	250.7	267.2	271.3	
T^{fin}_{SS} =	230.7	204.6	249.5	256.5	
T^{fo}_{SS} =	221.7	190.9	244.5	244.7	
T^{h}_{SS} =	225.2	195.9	239.3	235.4	
T^{ts}_{SS} =	-	-	-	282.9	

Calculated Values

$(H_e/H_i)^{new}$ =	0.173	0.206	0.211	0.137	Eqn. 4.1
$(t^{sm}_{0.95})$ =	255.7	328.8	255.7	328.8	Fig. 4.4b
$(t^{fi}_{0.05})$ =	3.0	6.3	3.1	3.3	Fig. 4.3a
$(t^{fi}_{0.95})$ =	3001.3	6694.3	2139.6	2167.8	Fig. 4.4a
$(t^{fin}_{0.05})$ =	89.1	264.2	64.2	58.0	Fig. 4.3b

Calculated Values (Continued)

	14" cl. 150	16" cl. 600	24" H. Ex.	37" H. Ex.	Source
$(t^{fm}_{0.95})$ =	3470.2	7399.0	2475.8	2276.2	Fig. 4.4b
$(t^{fo}_{0.05})$ =	178.2	493.3	125.3	113.8	Fig. 4.3c
$(t^{fo}_{0.95})$ =	3564.0	7399.0	2506.3	2384.6	Fig. 4.4c
$\theta_b(t^{sm}_{0.95})$ =	0.88	0.43	0.52	0.22	Eqn. 4.3
$\theta_b(t^{fo}_{0.95})$ =	1.00	1.00	1.00	0.83	Eqn. 4.3
$\theta_b(t^{ts}_{0.95})$ =	-	-	-	0.48	Eqn. 4.3
$(t^{ts}_{0.95})$ =	-	-	-	873.2	Eqn. 6.1
$dT^{fi}(t^{sm}_{0.95})$=	0.46	0.49	0.47	0.48	Figs. 4.3a, 4.4a & 4.5
$dT^{fm}(t^{sm}_{0.95})$=	0.18	0.14	0.25	0.32	Figs. 4.3b, 4.4b & 4.5
$dT^{fo}(t^{sm}_{0.95})$=	0.1	0.05	0.18	0.28	Figs. 4.3c, 4.4c & 4.5
$dT^{fi}(t^{ts}_{0.95})$=	-	-	-	0.66	Figs. 4.3a, 4.4a & 4.5
$dT^{fm}(t^{ts}_{0.95})$=	-	-	-	0.51	Figs. 4.3b, 4.4b & 4.5
$dT^{fo}(t^{ts}_{0.95})$=	-	-	-	0.49	Figs. 4.3c, 4.4c & 4.5
T^{s}_{1}=	268	267	267	268	$0.95T^{s}_{ss}$
T^{fi}_{1}=	120	123	126	130	
T^{fm}_{1}=	42	29	62	82	
T^{fo}_{1}=	22	10	44	69	
T^{b}_{1}=	20	4	22	14	
T^{s}_{2}=	-	-	-	282	
T^{fi}_{2}=	-	-	-	179	
T^{fm}_{2}=	-	-	-	131	
T^{fo}_{2}=	-	-	-	120	
T^{b}_{2}=	-	-	-	55	
T^{ts}_{2}=	-	-	-	269	$0.95T^{ts}_{ss}$
Minima					
$\Delta\sigma_{b1\,1}$=	59.8	41.1	15.2	20.2	Eqn. 5.2a
$\Delta\sigma_{b1\,2}$=	-33.8	-13.6	-22.4	-10.3	Eqn. 5.2b
$\Delta\sigma_{b1\,3}$=	-137.8	-75.0	-75.8	-54.0	Eqn. 5.2c
$\Delta\sigma_{b1}$=	-112	-48	-83	-44	Eqn. 5.2d
Maxima					
$\Delta\sigma_{b2\,1}$=	15.2	14.6	3.9	22.6	Eqn. 5.3a or 5.4a
$\Delta\sigma_{b2\,2}$=	-4.8	-2.9	-2.2	-7.7	Eqn. 5.3b or 5.4b
$\Delta\sigma_{b2\,3}$=	-36.8	-27.7	-14.0	-46.0	Eqn. 5.3c or 5.4c
$\Delta\sigma_{b2\,1ts}$=	-	-	-	94.4	Eqn. 5.4c
$\Delta\sigma_{b2}$=	-26	-16	-12	63	Eqn. 5.3d or 5.4d

APPENDIX D

CALIBRATION OF THE BOLT GAUGE SYSTEM

D.1 Calibration requirements

The bolt gauges are designed to measure the bolt load during initial bolt-up and also during subsequent thermal cycling. The gauges must therefore be calibrated not only with respect to bolt load, but also with respect to the zero offset and calibration factor effects of elevated temperature operation. The calibration included voltage output versus applied load, change in voltage output versus temperature and also the effect of temperature on the change in voltage output versus load.

D.2 Bolt gauge specifications

The strain gauged beams used to measure the bolt central rod deflection were Omega LCL-113G full bridge thin beam load cells. These beams are constructed from Berrylium-Copper and have four 1200ohm resistance strain gauges etched onto the upper surface. The beams are supplied with special mounting blocks at either end, which are require to ensure that the optimum deflected shape is obtained with deflection of the beam free end. The excitation voltage used was a 10Vdc regulated power source. The gauges are configured in a full Wheatstone bridge configuration. They have a rated output of 2mV/V and a listed combined error of 0.25% of the full scale reading. However, in the configuration used for this project the error is increased, due to the inaccuracies introduced by mounting the bolt gauge on the bolt and therefore introducing two sets of contacting surfaces.

D.3 Calibration procedure

The bolt gauge calibration was conducted in two phases, load calibration and transient temperature calibration. The first phase was to calibrate the gauges at ambient, 100°C and 200°C steady state temperatures in a calibrated Amsler tensile test machine. The second phase was to examine the transient temperature effects on the output signal of the unloaded bolts. This was performed in the actual test rig, by running several thermal cycles prior to applying load on the bolts.

D.3.1 Load calibration

The bolt gauges were calibrated by applying a known load to them using a calibrated Amsler test machine (ref. Figure D.1) and measuring the output voltage. The gauge excitation voltage and data acquisition system were the same as those used during the principal testing. The bolt stress was initially cycled three times from 0MPa to 360 MPa bolt stress (calculated on the remaining bolt stress area of 250mm^2) at ambient temperature. It was then cycled two more times, over the same stress range, except that this time the load was applied incrementally. The bolt and gauge were then heated, by an externally fitted electric band heater (ref. Figure D.2), to give a bolt temperature of 100°C. Two more incremental full range stress cycles were then applied. The bolt temperature was then raised to 200°C and two further incremental full range stress cycles applied. For every second bolt, the system was left loaded to 300MPa and at 200°C for 8 hours. The load was then released and another full range incremental stress cycle applied (this examined temperature driven or load driven signal drift with time).

In addition to testing each bolt as above, two bolts were tested at varying grip lengths, to confirm that the variation in the bolt calibration figure varied linearly with varying grip length, as would be expected. Most of the bolt gauges were kept mounted on the same bolt, at the same location, throughout both the calibration and subsequent testing.

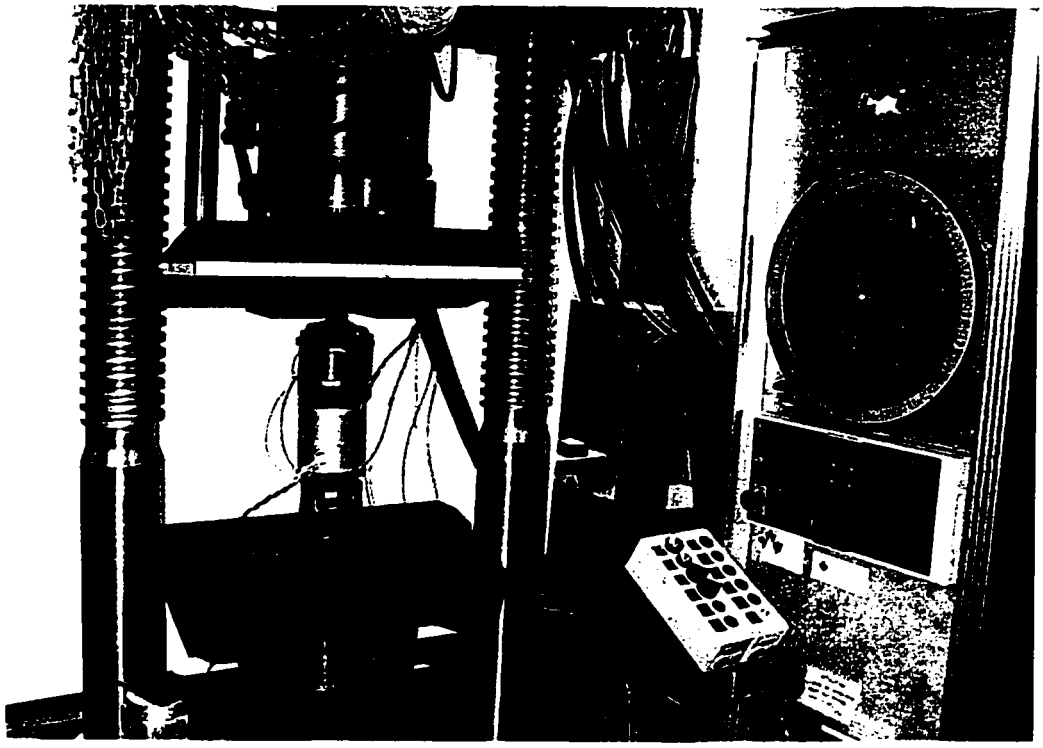

Figure D.1 – Amsler bolt gauge calibration set-up

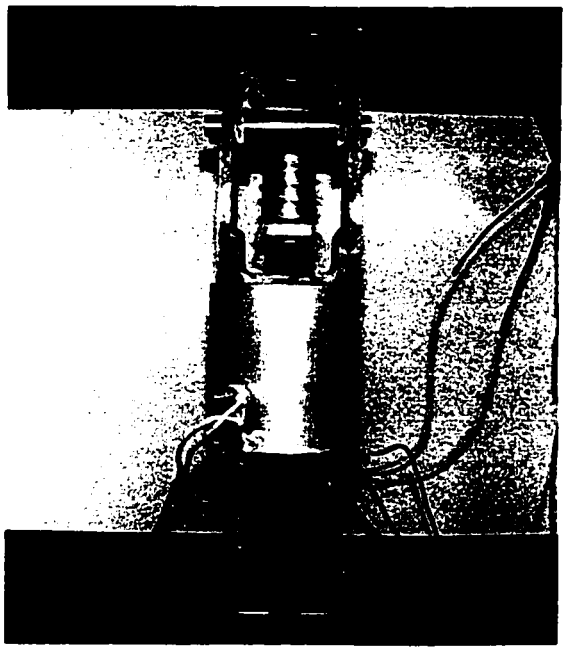

Figure D.2 – View of mounted bolt gauge

However, to examine the effects of re-mounting the bolts and also the bolt gauge, several bolt gauges were removed from the Amsler after testing and then replaced and retested. Additionally three bolt gauges were completely removed from their bolts and then remounted and retested.

D.3.2 Transient temperature calibration

To examine the effects of the gauge zero offset due to differential expansion of both the bolt and central rod and the gauge components during the temperature transients, the bolts were mounted on the test rig and the output signals were zeroed. The rig was assembled, complete with gasket, but the bolts were not tightened. The test rig was then heated, at both the 48°C/min transient and also the 16°C/min transient rates. The output signal variations for all bolts and the temperature of three bolts were recorded during the test rig heating cycle and also the cooling cycle. This enabled a standard signal offset for each bolt to be established for both the heating and cooling cycles, versus the average bolt temperature for the three bolts with thermocouples.

D.4 Calibration results

D.4.1 Load calibration

The results of the load calibration tests are detailed in the test datasheets following. The effect of bolt grip length on the signal, and the confirmation that this effect is linear as expected is detailed in tests on Bolts #1 and #10 in Figures D.3 and D.4. The calculations at the bottom of each datasheet, the calibration constant divided by the grip length, confirm that the effect is linear. Therefore the calibration constant input into the data acquisition system may be easily adjusted for the effect of different grip lengths.

The remaining bolt load calibration datasheets (Figures D.5a to D.28) outline the results of the bolt load calibration on all of the bolt gauges. There are four bolts that have two

datasheets (Bolts #1, #7, #13 and #19), in these cases the bolt gauge was removed from the bolt, remounted and then the gauge was retested. In addition, for two of the bolts (Bolts #7 and #19) the actual strain gauged load beam was remounted prior to retesting. It is evident from these retests that the bolt gauge calibration factor is not greatly affected by movement of the bolt gauge on the bolts. One can therefore be confident that the bolt gauge calibration factors will apply even if the bolt gauge is knocked or the bolt must be removed between tests.

D.4.2 Temperature transient calibration

The results for the bolt gauge zero offset during the thermal transients for three sample bolts are outlined in Figures D.29a to D.31b. These results were analysed for each bolt gauge and an average value for the change in gauge zero offset during bolt the heating and cooling transients, both with and without the tubesheet fitted, were established (ref. Figures D.32a to D.33a). These curves were then, using an excel macro, used to adjust the acquired test data during the temperature transient by subtracting the zero offset from the bolt gauge reading relative to the average bolt temperature during the transient. In this way the effects of the changes in temperature driven zero offset for each bolt are accounted for.

It can be seen from the individual bolt gauge curves (Figures D.29a to D.33b) that the variation in zero offset is not uniform for each gauge, however it is repeatable for each gauge. The average value for twice the standard deviation (95% confidence interval) is 2.27MPa without the tubesheet and 1.85 with the tubesheet. This means that with the adjustment made, we can be 95% confident that the zero offset error in average bolt stress during the transient should be less than ±2.3MPa and ±1.9MPa respectively. The maximum twice standard deviation values are 5.96 and 11.46 respectively. If the results for all gauges during heating and cooling (ref. Figures D.34 to D.37) are examined, it may be seen that most bolt loads change less than 10MPa, during the heating transient.

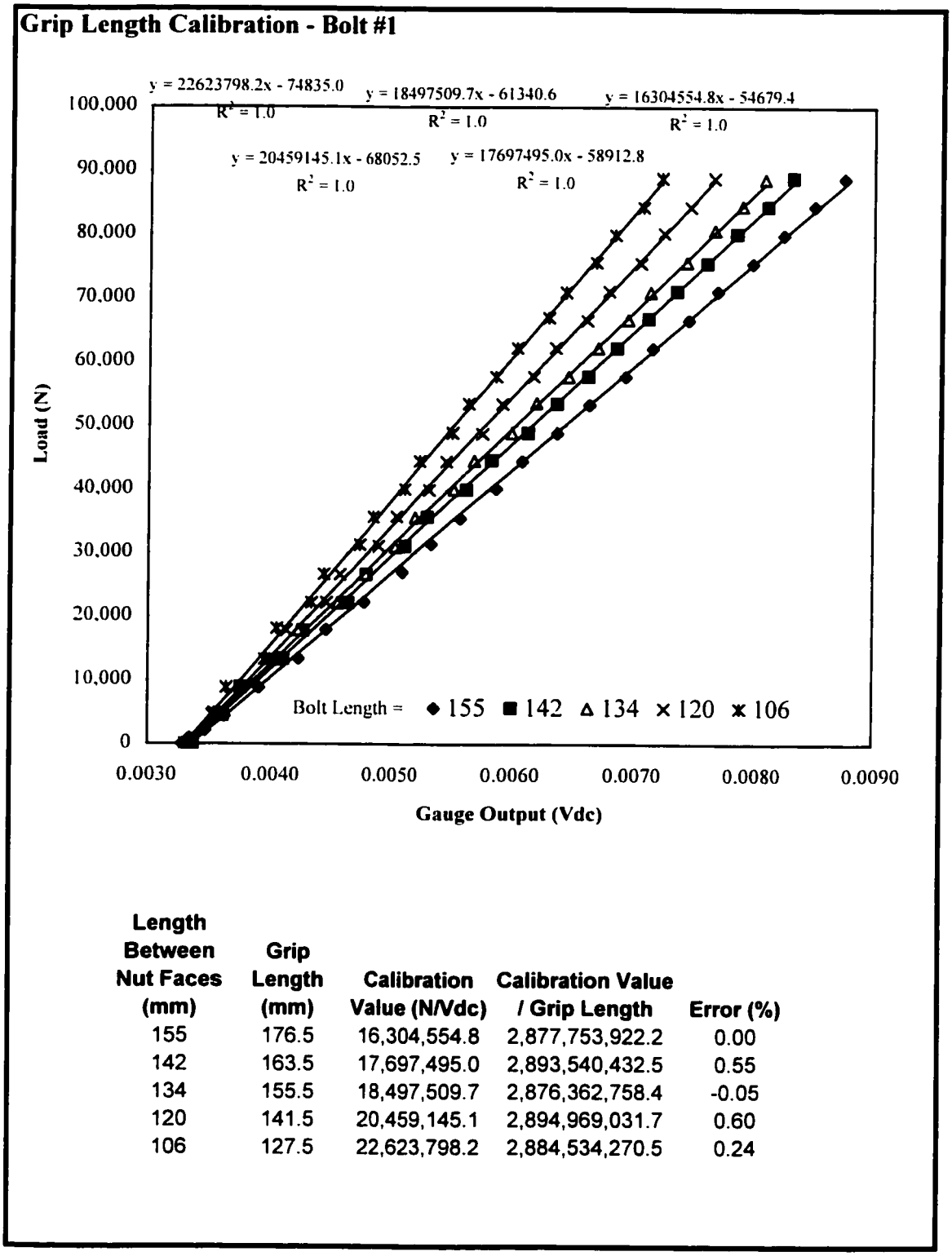

Length Between Nut Faces (mm)	Grip Length (mm)	Calibration Value (N/Vdc)	Calibration Value / Grip Length	Error (%)
155	176.5	16,304,554.8	2,877,753,922.2	0.00
142	163.5	17,697,495.0	2,893,540,432.5	0.55
134	155.5	18,497,509.7	2,876,362,758.4	-0.05
120	141.5	20,459,145.1	2,894,969,031.7	0.60
106	127.5	22,623,798.2	2,884,534,270.5	0.24

Figure D.3 - The effect of bolt length on the calibration signal - Bolt #1

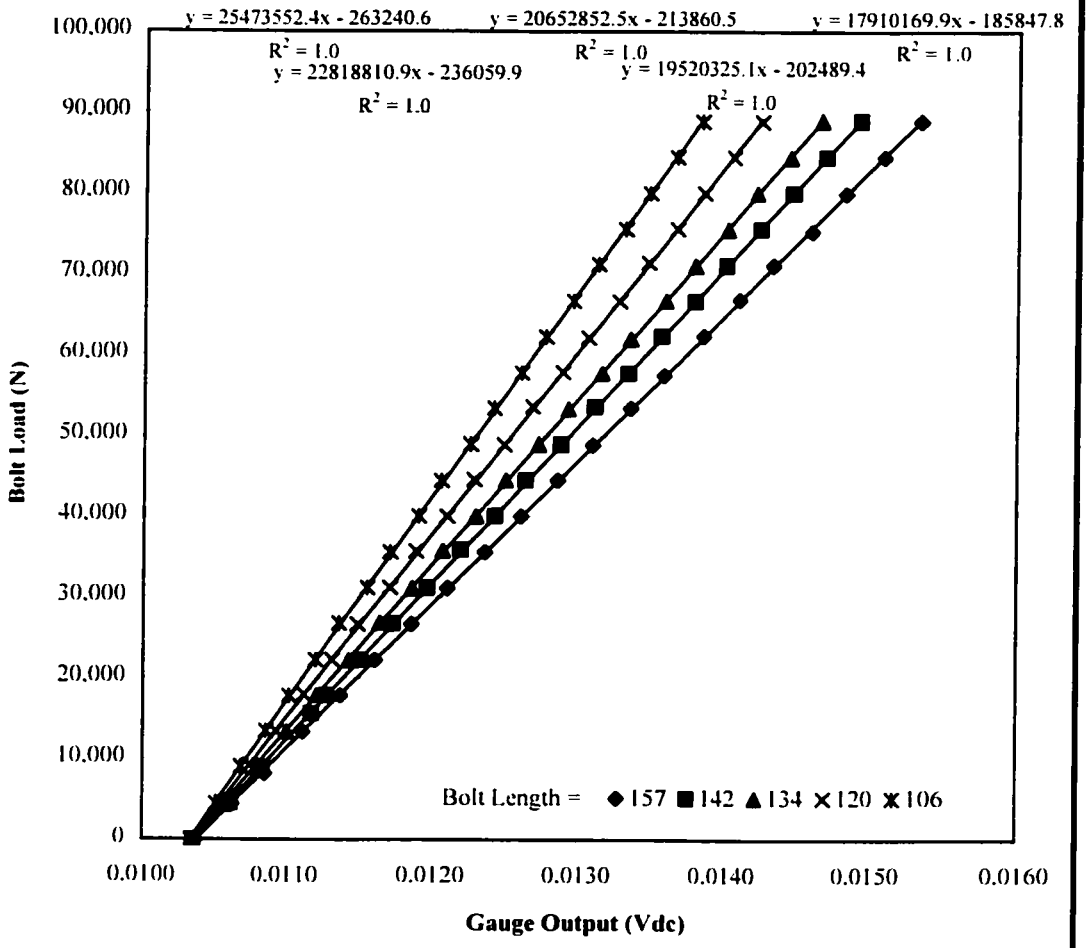

Length Between Nut Faces (mm)	Grip Length (mm)	Calibration Value (N/Vdc)	Calibration Value / Grip Length	Error (%)
157	178.5	17,910,169.9	3,196,965,327.2	0.00
142	163.5	19,520,325.1	3,191,573,153.9	-0.17
134	155.5	20,652,852.5	3,211,518,563.8	0.46
120	141.5	22,818,810.9	3,228,861,742.4	1.00
106	127.5	25,473,552.4	3,247,877,931.0	1.59

Figure D.4 - The effect of bolt length on the calibration signal - Bolt #10

BOLT GAUGE CALIBRATION DATASHEET

BOLT GAUGE NUMBER: 1 - Test II (Gauge re-mounted on bolt)

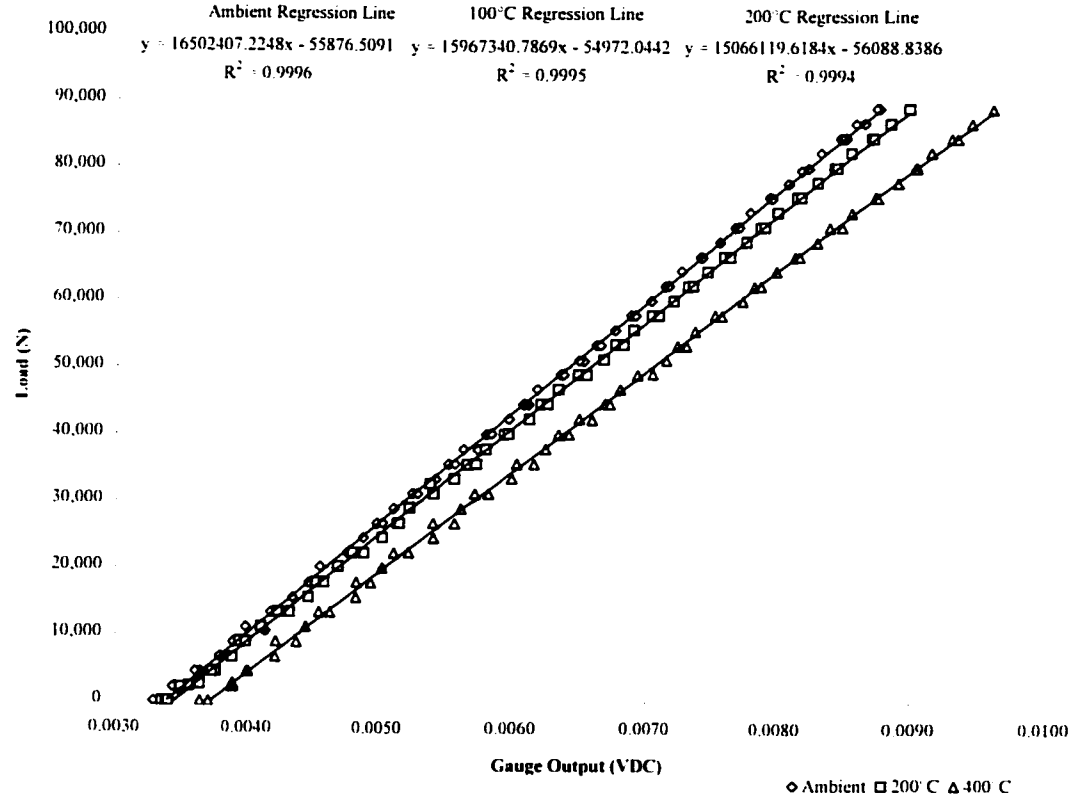

Calibration constant vs. temperature

		Signal Ratio
Ambient :	16502407.22	1
100°C :	15967340.79	1.033510053
200°C :	15066119.62	1.095332285

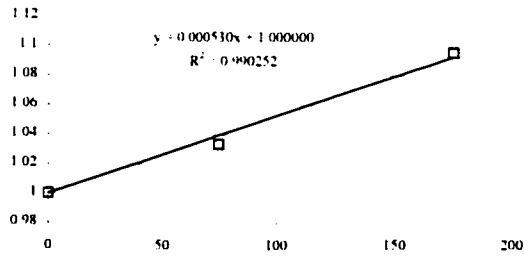

Calibration Equation: (T_b absolute)

$$\sigma_b = 16502407.(1 - 0.00053.T_b).Signal(VDC)/250$$

Overall Error:

	Max. Offset (Abs)	% of Full Scale	99.5% Error Range (MPa)	
Ambient :	13.8 MPa	4.0 %	7.26 5.73	Listed 99.5% Error
100°C :	9.6 MPa	2.8 %	6.48 4.89	± 7.26 MPa
200°C :	10.1 MPa	2.9 %	6.04 4.12	

Point to Point Error:

	Max. Offset (Abs)	% of Full Scale	99.5% Error Range (MPa)	
Ambient :	9.4 MPa	2.7 %	0.81 -0.74	Listed 99.5% Error
100°C :	8.1 MPa	2.3 %	0.65 -0.89	± 0.89 MPa
200°C :	4.7 MPa	1.3 %	0.65 -0.64	

Figure D.5a - Bolt gauge calibration datasheet - Bolt #1 (Test II)

BOLT GAUGE CALIBRATION DATASHEET

BOLT GAUGE NUMBER: 1

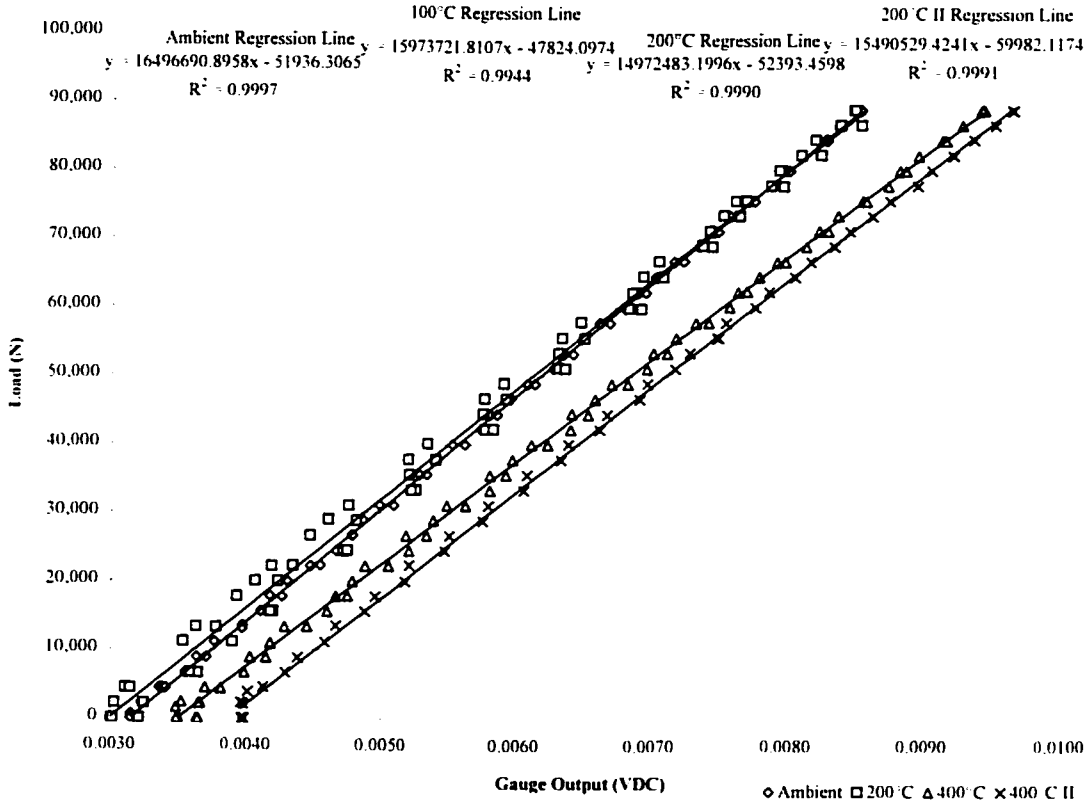

Calibration constant vs. temperature

		Signal Ratio
Ambient :	16623951.25	1
100°C :	16342950.83	1.017193983
200°C :	15231506.31	1.091418729

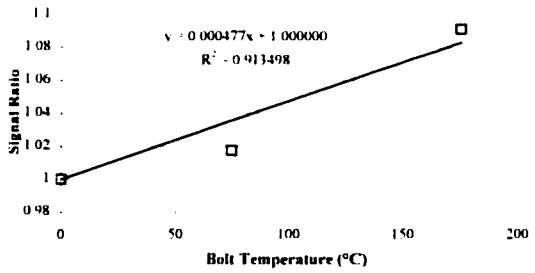

Calibration Equation: (T_b absolute)

$$\sigma_b = 16623951.(1 - 0.000477.T_b).Signal(VDC)/250$$

Overall Error:

	Max. Offset (Abs)	% of Full Scale	99.5% Error Range (MPa)	
Ambient :	7.0 MPa	2.0 %	-1.44 -3.12	Listed 99.5% Error
100°C :	16.1 MPa	4.6 %	5.63 -0.66	± 5.63 MPa
200°C :	9.0 MPa	2.6 %	4.94 1.86	

Point to Point Error:

	Max. Offset (Abs)	% of Full Scale	99.5% Error Range (MPa)	
Ambient :	7.0 MPa	2.0 %	0.51 -0.69	Listed 99.5% Error
100°C :	13.7 MPa	3.9 %	1.17 -0.84	± 1.17 MPa
200°C :	6.4 MPa	1.8 %	0.70 -0.48	

Figure D.5b - Bolt gauge calibration datasheet - Bolt #1 (Test I)

BOLT GAUGE CALIBRATION DATASHEET

BOLT GAUGE NUMBER: 2

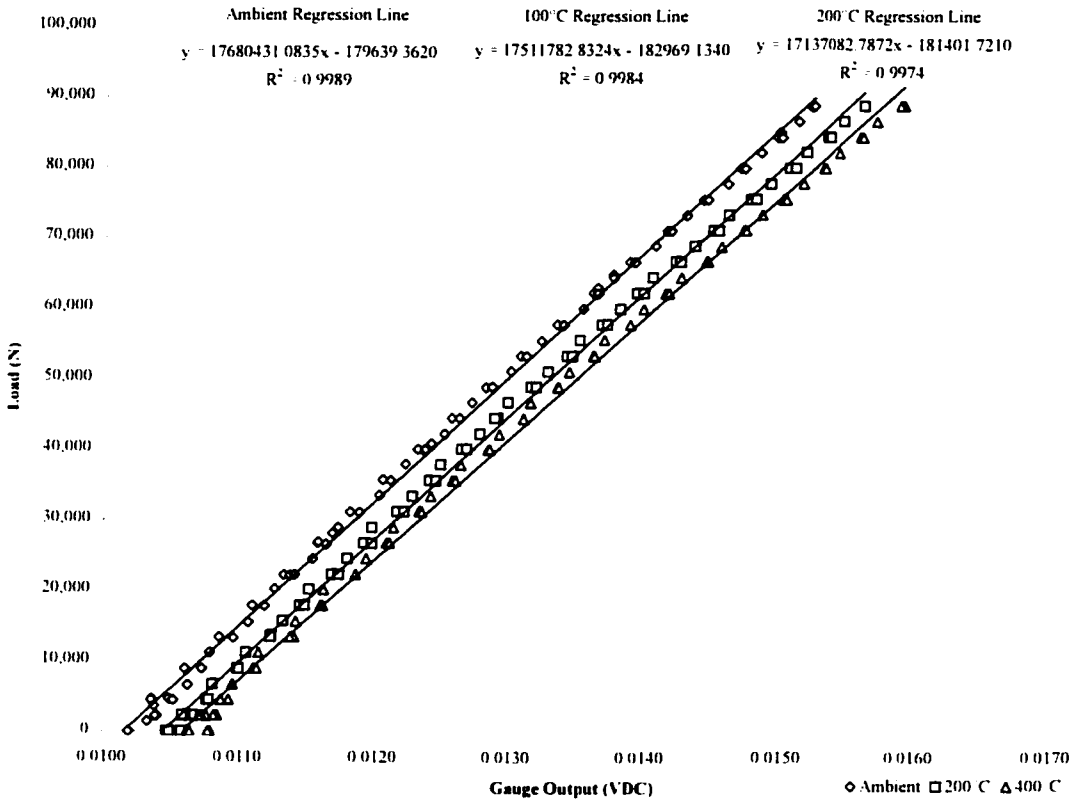

Calibration constant vs. temperature

		Signal Ratio
Ambient :	17680431.08	1
100°C :	17511782.83	1.009630559
200°C :	17137082.79	1.031705997

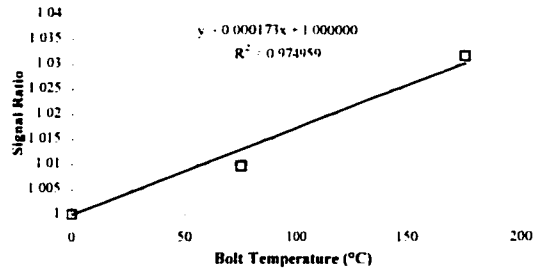

Calibration Equation: (T_b absolute)

$$\sigma_b = 17680431.(1 - 0.000173.T_b).Signal(VDC)/250$$

Overall Error:

	Max. Offset (Abs)	% of Full Scale	99.5% Error Range (MPa)	
Ambient :	10.5 MPa	3.0 %	-1.41 -4.11	Listed 99.5% Error
100°C :	17.6 MPa	5.0 %	-8.37 -11.34	± 15.90 MPa
200°C :	23.1 MPa	6.6 %	-12.30 -15.90	

Point to Point Error:

	Max. Offset (Abs)	% of Full Scale	99.5% Error Range (MPa)	
Ambient :	8.7 MPa	2.5 %	1.06 -0.96	Listed 99.5% Error
100°C :	7.8 MPa	2.2 %	0.64 -0.92	± 1.06 MPa
200°C :	8.8 MPa	2.5 %	0.65 -1.06	

Figure D.6 - Bolt gauge calibration datasheet - Bolt #2

BOLT GAUGE CALIBRATION DATASHEET

BOLT GAUGE NUMBER: 3

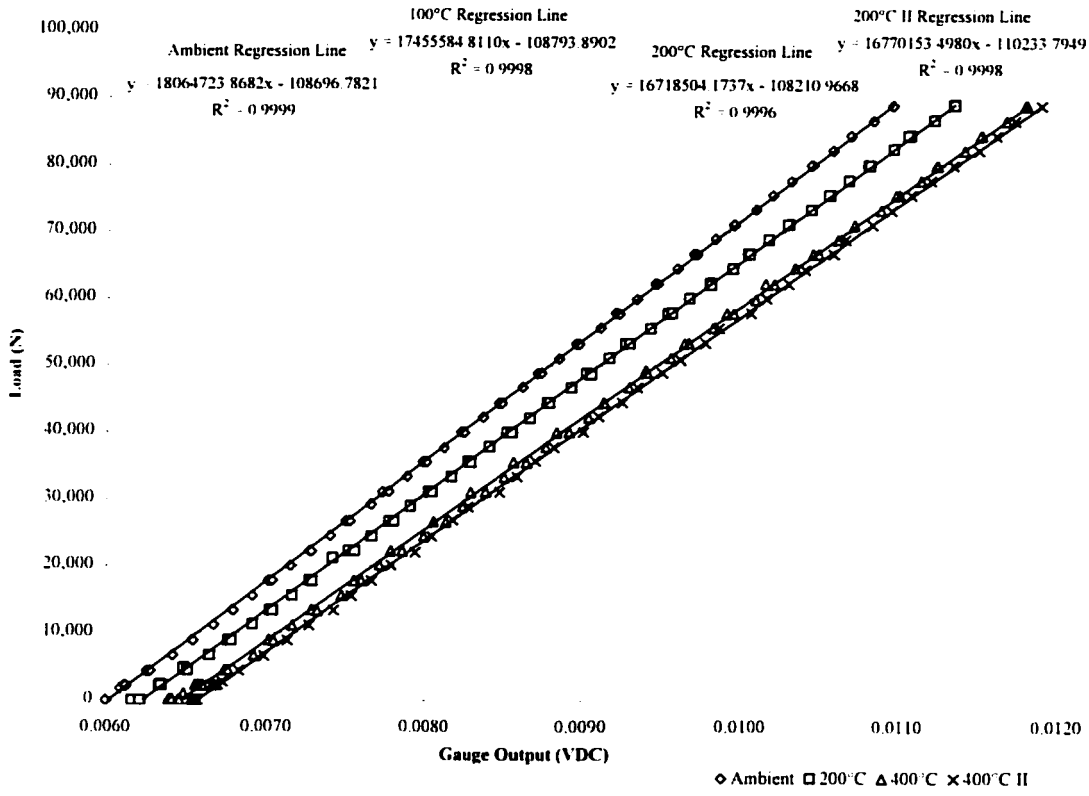

Calibration constant vs. temperature

		Signal Ratio
Ambient :	18064723.9	1
100°C :	17455584.8	1.03489651
200°C :	16718504.2	1.08052274

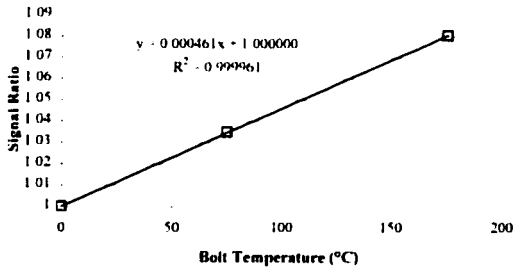

Calibration Equation: (T_b absolute)

$$\sigma_b = 18064723.(1 - 0.000461.T_b).Signal(VDC)/250$$

Overall Error:

	Max. Offset (Abs)	% of Full Scale	99.5% Error Range (MPa)	
Ambient :	6.8 MPa	2.0 %	2.09 1.23	Listed 99.5% Error
100°C :	6.8 MPa	2.0 %	4.62 3.64	± 5.08 MPa
200°C :	8.7 MPa	2.5 %	5.08 3.51	

Point to Point Error:

	Max. Offset (Abs)	% of Full Scale	99.5% Error Range (MPa)	
Ambient :	3.0 MPa	0.9 %	0.30 -0.29	Listed 99.5% Error
100°C :	3.0 MPa	0.9 %	0.49 -0.40	± 0.49 MPa
200°C :	4.5 MPa	1.3 %	0.48 -0.37	

Figure D.7 - Bolt gauge calibration datasheet - Bolt #3

BOLT GAUGE CALIBRATION DATASHEET

BOLT GAUGE NUMBER: 4

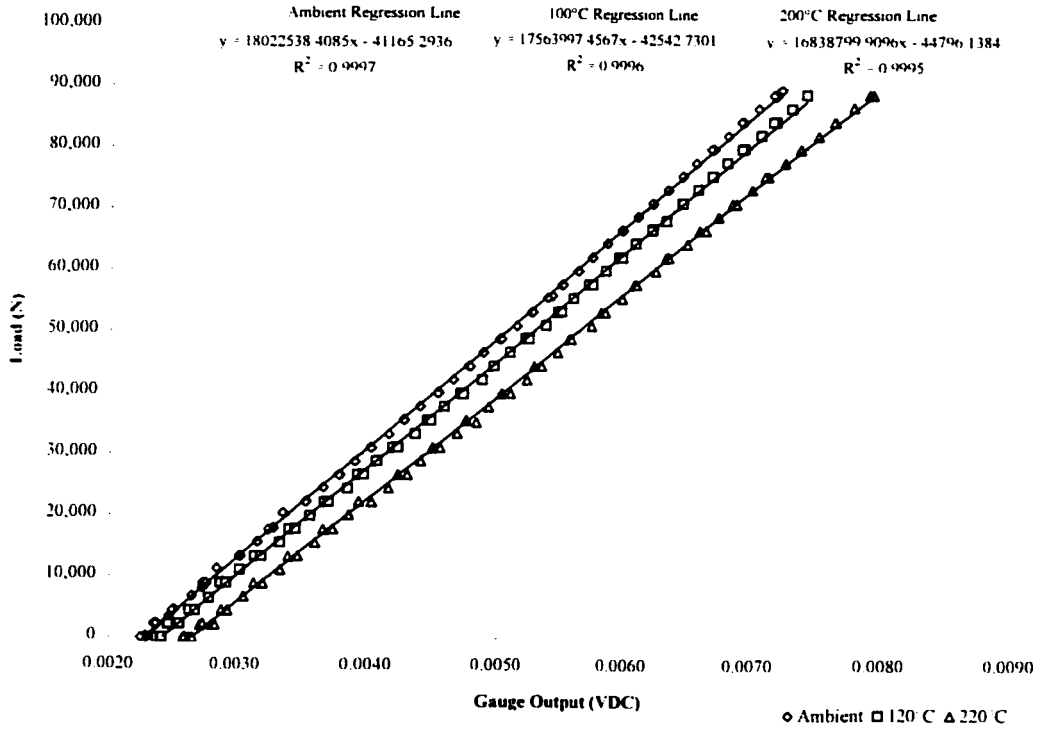

Calibration constant vs. temperature

		Signal Ratio
Ambient :	18022538.4	1
100°C :	17563997.5	1.02610687
200°C :	16838799.9	1.07029827

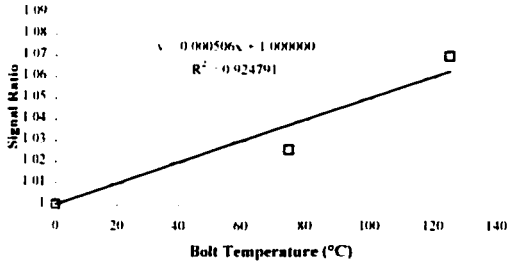

Calibration Equation: (T_b absolute)

$$\sigma_b = 18069514.(1 - 0.000506.T_b).Signal(VDC)/250$$

Overall Error:

	Max. Offset (Abs)	% of Full Scale	99.5% Error Range (MPa)	
Ambient :	5.2 MPa	1.5 %	-0.21 -1.50	Listed 99.5% Error
100°C :	6.8 MPa	1.9 %	4.01 2.42	± 5.31 MPa
200°C :	9.5 MPa	2.7 %	5.31 3.63	

Point to Point Error:

	Max. Offset (Abs)	% of Full Scale	99.5% Error Range (MPa)	
Ambient :	6.1 MPa	1.7 %	0.45 -0.56	Listed 99.5% Error
100°C :	4.8 MPa	1.4 %	0.47 -0.36	± 0.56 MPa
200°C :	3.1 MPa	0.9 %	0.55 -0.31	

Figure D.8 - Bolt gauge calibration datasheet - Bolt #4

BOLT GAUGE CALIBRATION DATASHEET

BOLT GAUGE NUMBER: 5

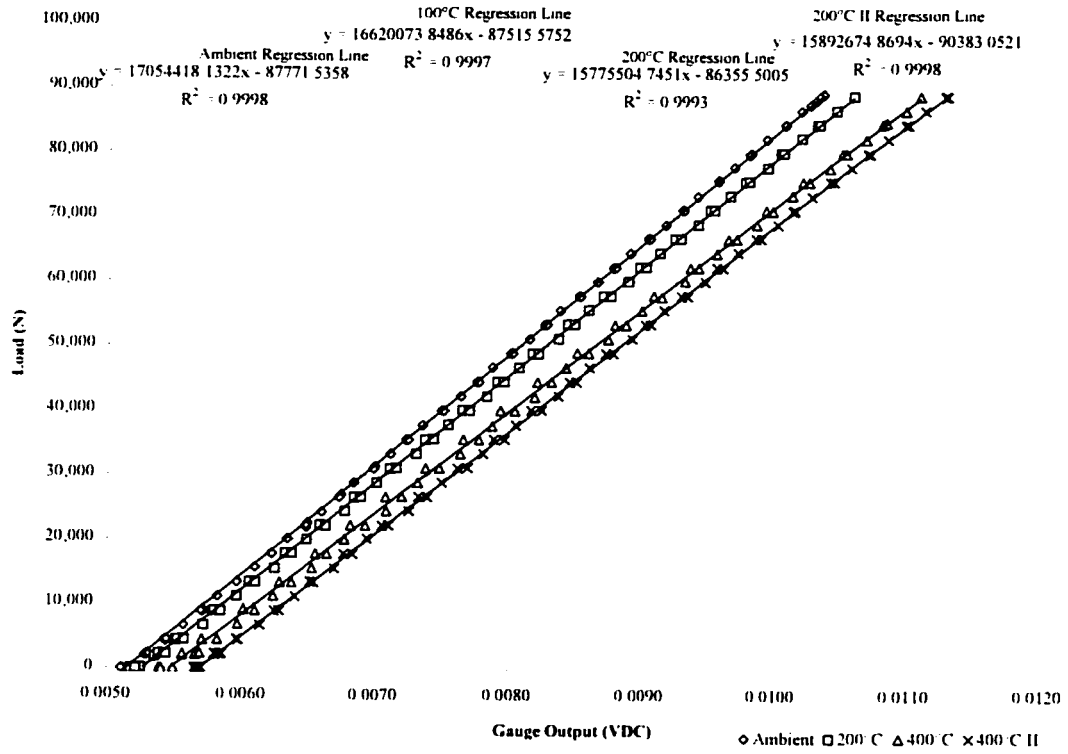

Calibration constant vs. temperature

		Signal Ratio
Ambient :	17054418.1	1
100°C :	16620073.8	1.02394821
200°C :	15775504.7	1.05181986

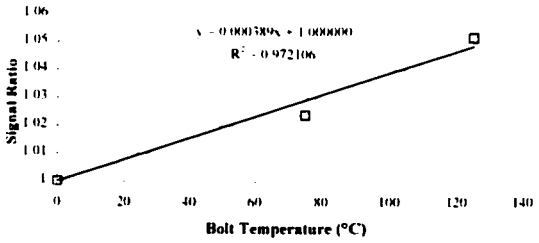

Calibration Equation: (T_b absolute)

$$\sigma_b = 17054418.(1 - 0.000389.T_b).Signal(VDC)/250$$

Overall Error:

	Max. Offset (Abs)	% of Full Scale	99.5% Error Range (MPa)	
Ambient :	5.6 MPa	1.6 %	3.10 2.21	Listed 99.5% Error
100°C :	9.0 MPa	2.6 %	6.51 5.38	± 6.51 MPa
200°C :	9.6 MPa	2.7 %	6.25 4.28	

Point to Point Error:

	Max. Offset (Abs)	% of Full Scale	99.5% Error Range (MPa)	
Ambient :	3.8 MPa	1.1 %	0.34 -0.28	Listed 99.5% Error
100°C :	4.1 MPa	1.2 %	0.34 -0.09	± 0.35 MPa
200°C :	3.2 MPa	0.9 %	0.35 -0.15	

Figure D.9 - Bolt gauge calibration datasheet - Bolt #5

BOLT GAUGE CALIBRATION DATASHEET

BOLT GAUGE NUMBER: 6

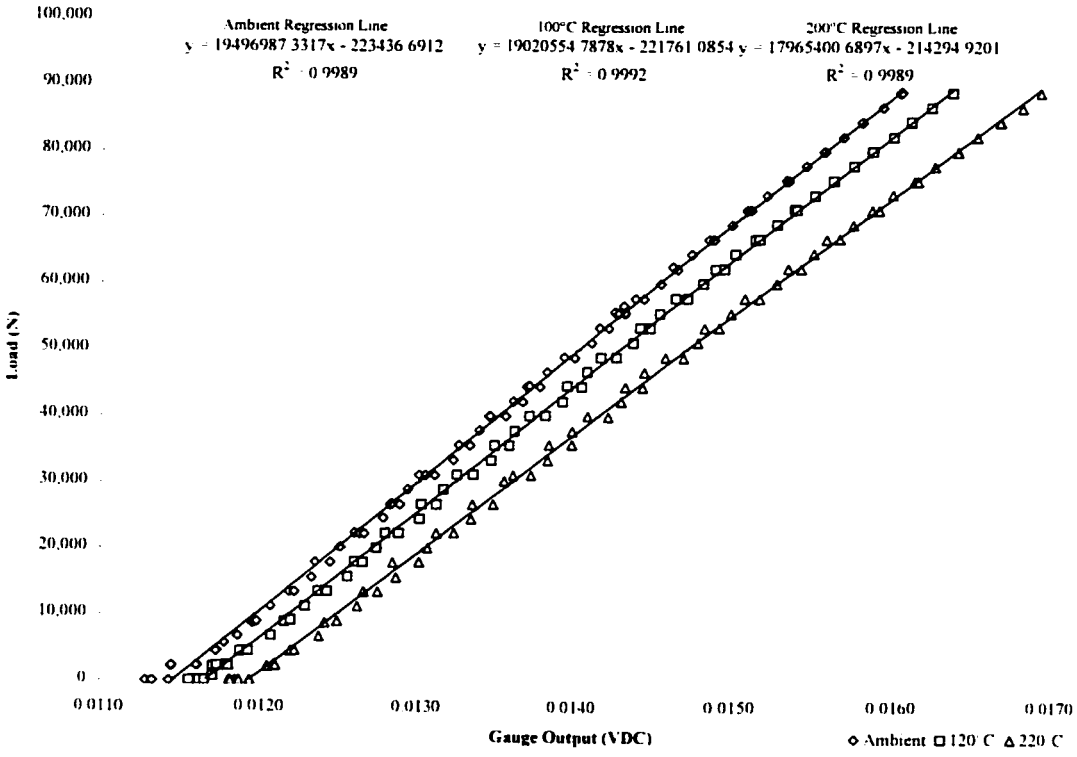

Calibration constant vs. temperature

		Signal Ratio
Ambient :	19496987.3	1
100°C :	19020554.8	1.0250483
200°C :	17965400.7	1.08525202

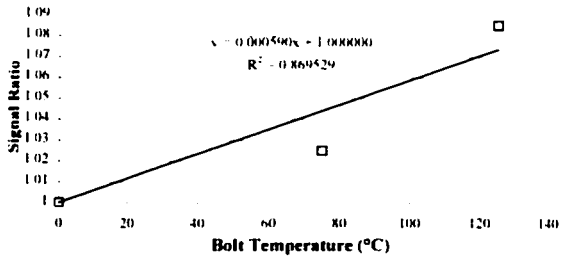

Calibration Equation: (T_b absolute)

$$\sigma_b = 19496987.(1 - 0.000590.T_b).Signal(VDC)/250$$

Overall Error:

	Max. Offset (Abs)	% of Full Scale	99.5% Error Range (MPa)	
Ambient :	9.0 MPa	2.6 %	2.00 0.09	Listed 99.5% Error
100°C :	12.1 MPa	3.5 %	7.91 5.90	± 7.91 MPa
200°C :	10.3 MPa	2.9 %	5.87 3.40	

Point to Point Error:

	Max. Offset (Abs)	% of Full Scale	99.5% Error Range (MPa)	
Ambient :	8.2 MPa	2.3 %	0.78 -0.49	Listed 99.5% Error
100°C :	3.2 MPa	0.9 %	0.58 -0.30	± 0.78 MPa
200°C :	5.5 MPa	1.6 %	0.77 -0.54	

Figure D.10 - Bolt gauge calibration datasheet - Bolt #6

BOLT GAUGE CALIBRATION DATASHEET

BOLT GAUGE NUMBER: 7 - Test II

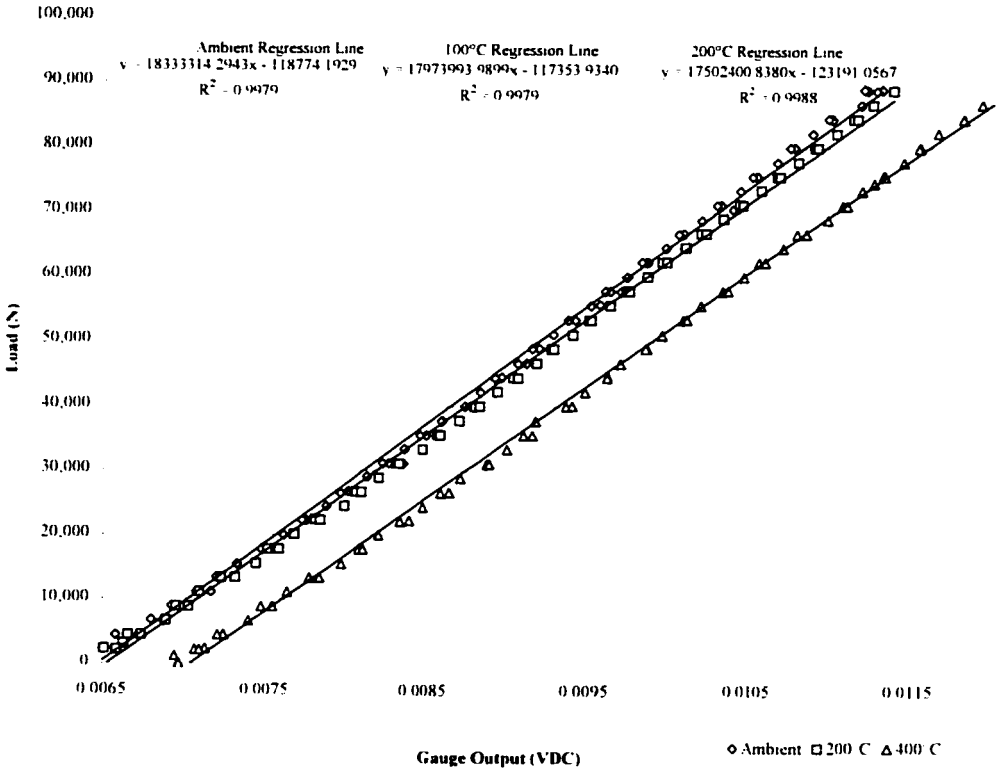

Calibration constant vs. temperature

		Signal Ratio
Ambient :	18333314.29	1
100°C :	17973993.99	1.023948208
200°C :	17502400.84	1.051819859

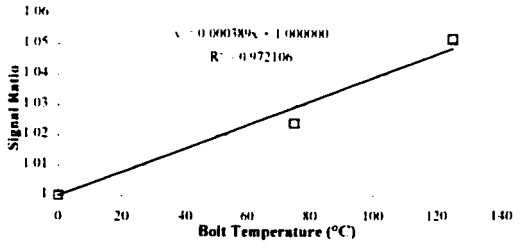

Calibration Equation: (T_b absolute)

$$\sigma_b = 18333314.(1 - 0.000389.T_b).Signal(VDC)/250$$

Overall Error:

	Max. Offset (Abs)	% of Full Scale	99.5% Error Range (MPa)	
Ambient :	13.1 MPa	3.7 %	4.12 0.75	Listed 99.5% Error
100°C :	24.3 MPa	6.9 %	18.58 16.50	± 18.58 MPa
200°C :	13.3 MPa	3.8 %	-4.81 1.25	

Point to Point Error:

	Max. Offset (Abs)	% of Full Scale	99.5% Error Range (MPa)	
Ambient :	3.7 MPa	1.0 %	0.50 -0.52	Listed 99.5% Error
100°C :	9.2 MPa	2.6 %	0.77 -0.94	± 0.94 MPa
200°C :	6.0 MPa	1.7 %	0.73 -0.78	

Figure D.11a - Bolt gauge calibration datasheet - Bolt #7 (Test II)

BOLT GAUGE CALIBRATION DATASHEET

BOLT GAUGE NUMBER: 7

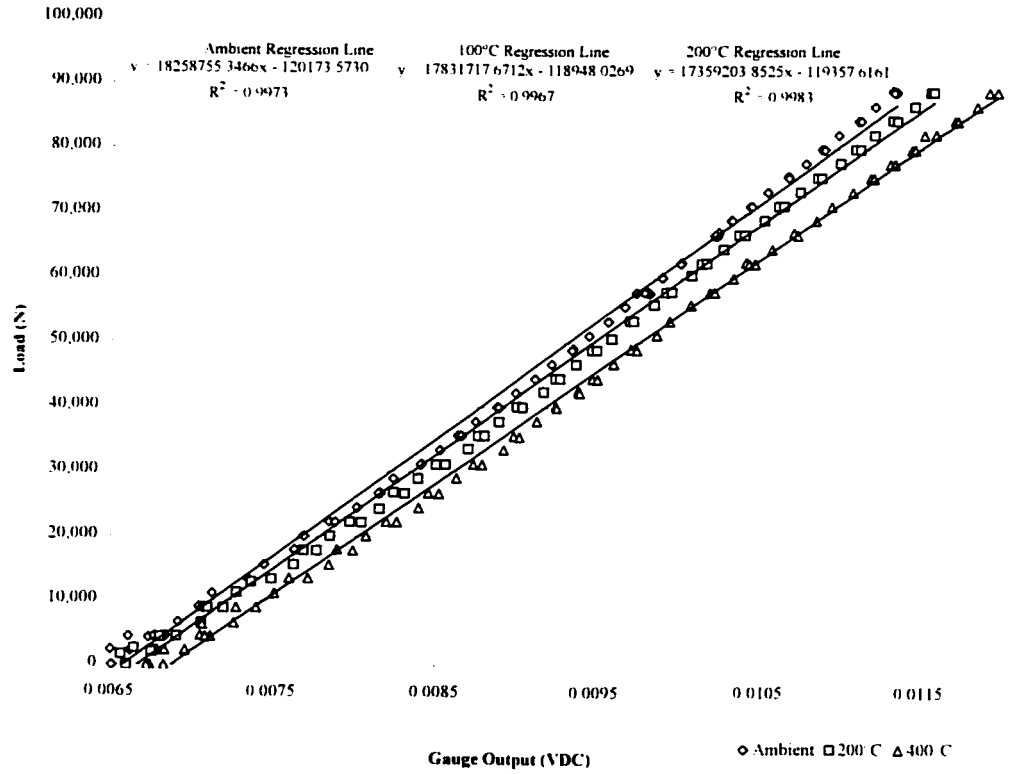

Calibration constant vs. temperature

		Signal Ratio
Ambient :	18258755.35	1
100°C :	17831717.67	1.023948208
200°C :	17359203.85	1.051819859

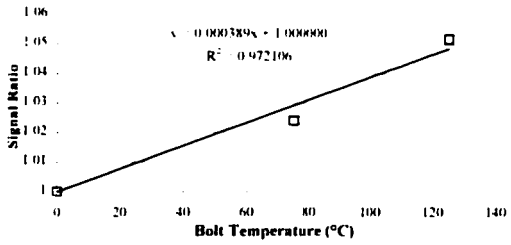

Calibration Equation: (T_b absolute)

$$\sigma_b = 18258755.(1 - 0.000389.T_b).Signal(VDC)/250$$

Overall Error:

	Max. Offset (Abs)	% of Full Scale	99.5% Error Range (MPa)	
Ambient :	14.0 MPa	4.0 %	8.19 4.38	Listed 99.5% Error
100°C :	25.6 MPa	7.3 %	17.89 13.40	± 17.89 MPa
200°C :	11.0 MPa	3.1 %	4.58 1.45	

Point to Point Error:

	Max. Offset (Abs)	% of Full Scale	99.5% Error Range (MPa)	
Ambient :	8.6 MPa	2.5 %	0.89 -1.23	Listed 99.5% Error
100°C :	5.5 MPa	1.6 %	0.88 -0.56	± 1.23 MPa
200°C :	4.3 MPa	1.2 %	0.92 -0.64	

Figure D.11b - Bolt gauge calibration datasheet - Bolt #7 (Test I)

BOLT GAUGE CALIBRATION DATASHEET

BOLT GAUGE NUMBER: 8

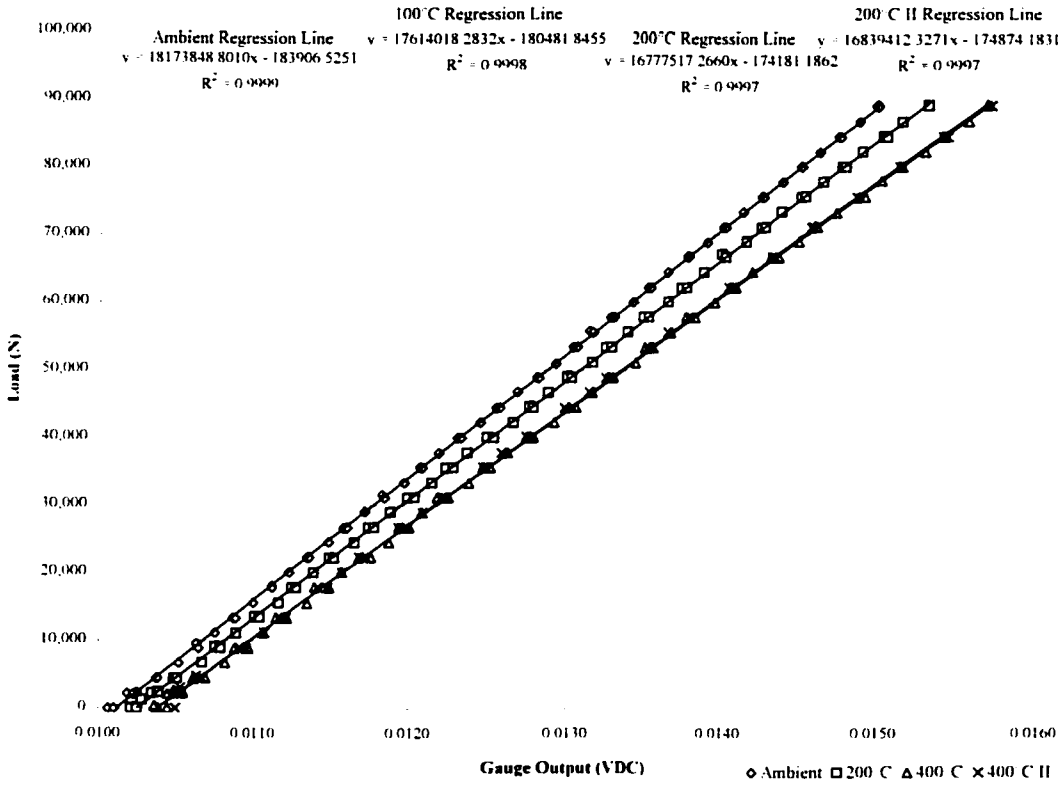

Calibration constant vs. temperature

		Signal Ratio
Ambient :	18173848.8	1
100°C :	17614018.3	1.03178324
200°C :	16777517.3	1.08322635

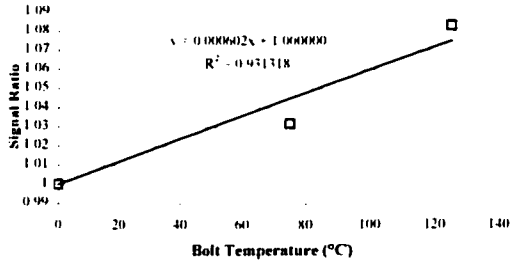

Calibration Equation: (T_b absolute)

$$\sigma_b = 18173848.(1 - 0.000602.T_b).Signal(VDC)/250$$

Overall Error:

	Max. Offset (Abs)	% of Full Scale	99.5% Error Range (MPa)	
Ambient :	6.6 MPa	1.9 %	4.59 3.82	Listed 99.5% Error
100°C :	5.0 MPa	1.4 %	2.85 1.91	± 4.90 MPa
200°C :	7.9 MPa	2.3 %	-3.49 -4.90	

Point to Point Error:

	Max. Offset (Abs)	% of Full Scale	99.5% Error Range (MPa)	
Ambient :	2.0 MPa	0.6 %	0.35 -0.18	Listed 99.5% Error
100°C :	2.2 MPa	0.6 %	0.29 -0.20	± 0.52 MPa
200°C :	2.8 MPa	0.8 %	0.52 -0.25	

Figure D.12 - Bolt gauge calibration datasheet - Bolt #8

BOLT GAUGE CALIBRATION DATASHEET

BOLT GAUGE NUMBER: 9

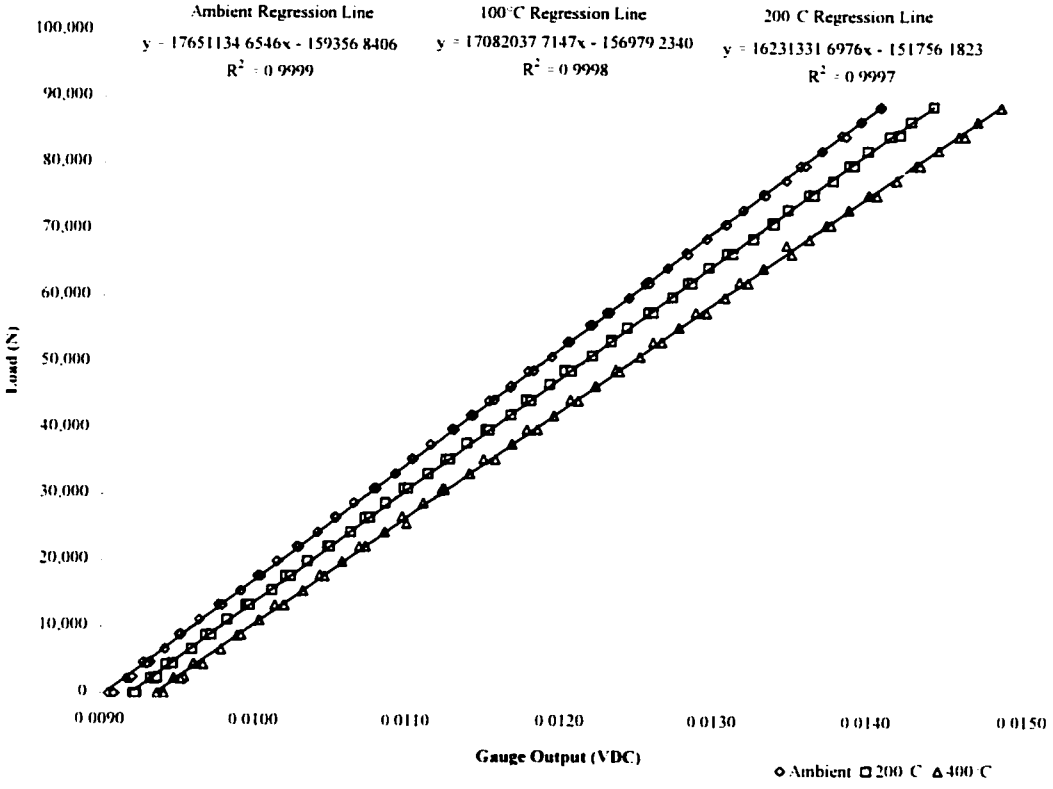

Calibration constant vs. temperature

		Signal Ratio
Ambient :	17651134.7	1
120°C :	17082037.7	1.03331552
220°C :	16231331.7	1.08747298

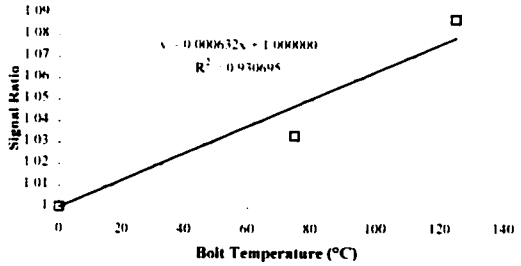

Calibration Equation: (T_b absolute)

$$\sigma_b = 17651134.(1 - 0.000632.T_b).Signal(VDC)/250$$

Overall Error:

	Max. Offset (Abs)	% of Full Scale	99.5% Error Range (MPa)	
Ambient :	3.6 MPa	1.0 %	-1.68 -2.39	Listed 99.5% Error
120°C :	4.3 MPa	1.2 %	-1.37 -2.33	± 2.39 MPa
220°C :	6.2 MPa	1.8 %	-0.29 -1.66	

Point to Point Error:

	Max. Offset (Abs)	% of Full Scale	99.5% Error Range (MPa)	
Ambient :	3.9 MPa	1.1 %	0.31 -0.38	Listed 99.5% Error
120°C :	3.1 MPa	0.9 %	0.33 -0.31	± 0.61 MPa
220°C :	4.7 MPa	1.4 %	0.61 -0.44	

Figure D.13 - Bolt gauge calibration datasheet - Bolt #9

BOLT GAUGE CALIBRATION DATASHEET

BOLT GAUGE NUMBER: 10

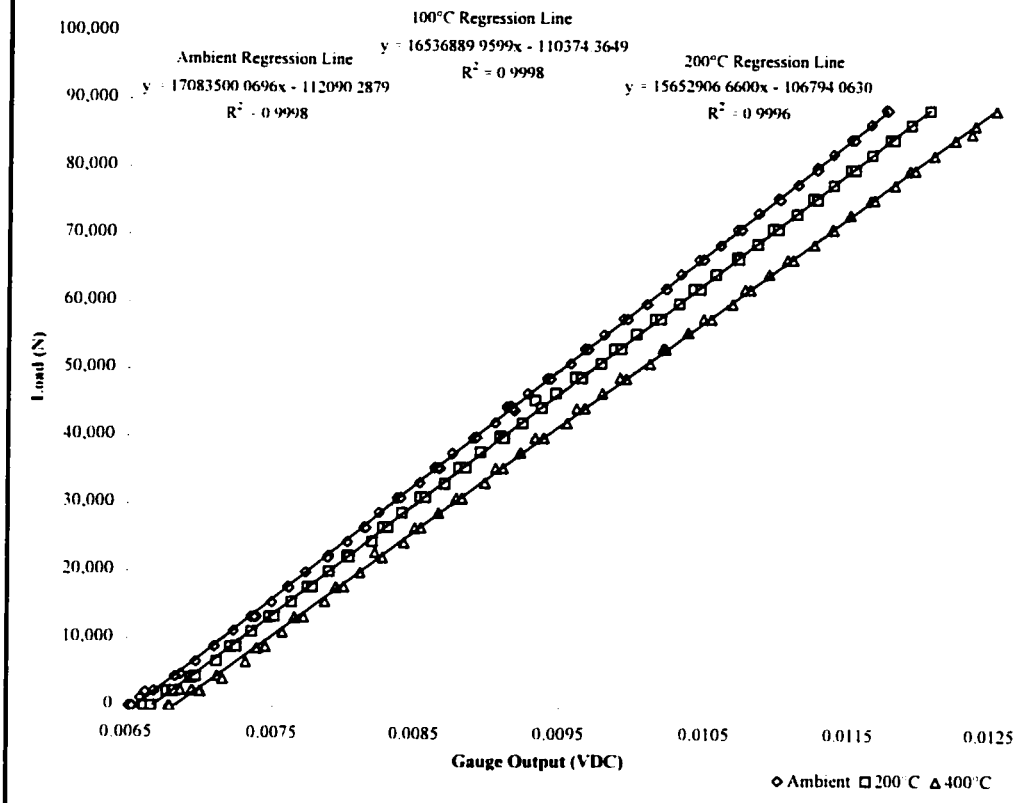

Calibration constant vs. temperature

		Signal Ratio
Ambient :	17083500.1	1
100°C :	16536890	1.03305399
200°C :	15652906.7	1.09139474

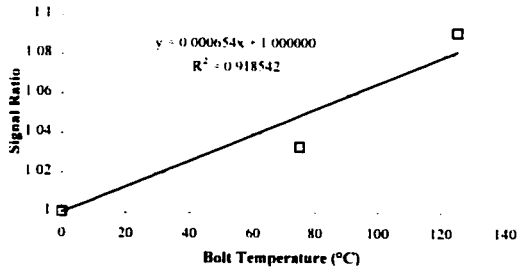

Calibration Equation: (T_b absolute)

$$\sigma_b = 17083500.(1 - 0.000654.T_b).Signal(VDC)/250$$

Overall Error:

	Max. Offset (Abs)	% of Full Scale	99.5% Error Range (MPa)	
Ambient :	6.1 MPa	1.7 %	3.56 2.70	Listed 99.5% Error
100°C :	6.1 MPa	1.7 %	4.26 3.15	± 4.26 MPa
200°C :	6.8 MPa	2.0 %	3.20 1.69	

Point to Point Error:

	Max. Offset (Abs)	% of Full Scale	99.5% Error Range (MPa)	
Ambient :	4.4 MPa	1.3 %	0.37 -0.30	Listed 99.5% Error
100°C :	4.4 MPa	1.3 %	0.49 -0.34	± 0.78 MPa
200°C :	5.6 MPa	1.6 %	0.78 -0.62	

Figure D.14 - Bolt gauge calibration datasheet - Bolt #10

BOLT GAUGE CALIBRATION DATASHEET

BOLT GAUGE NUMBER: 11

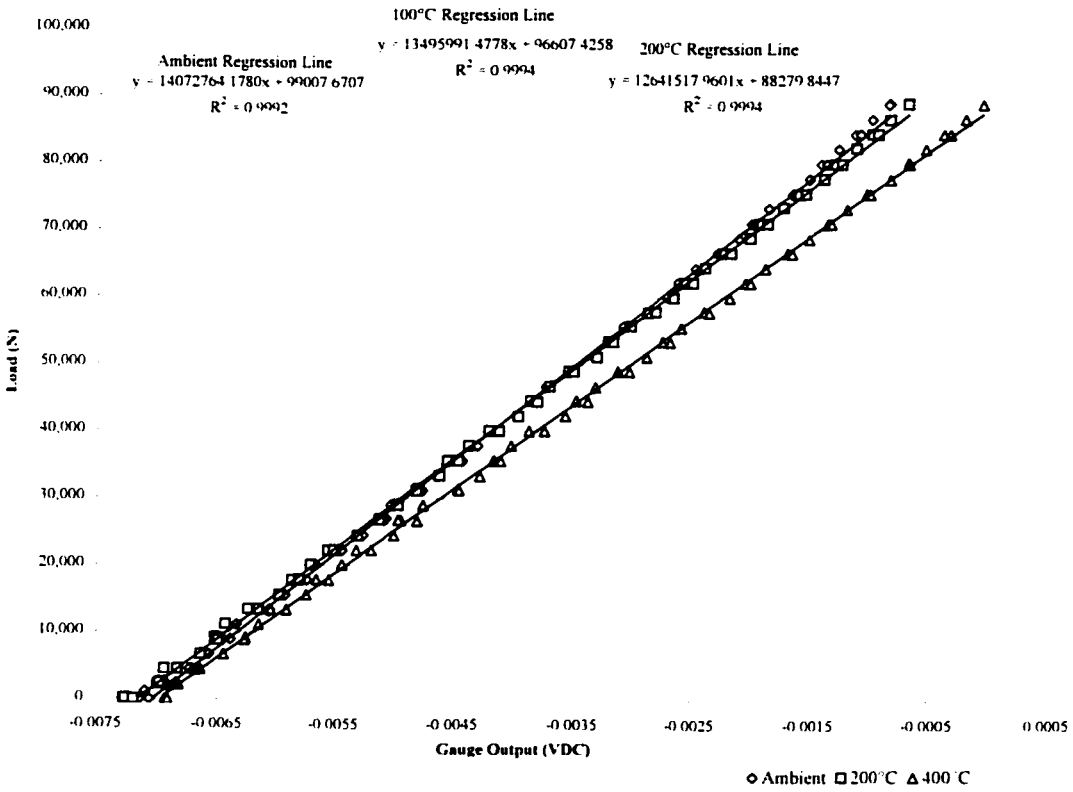

Calibration constant vs. temperature

		Signal Ratio
Ambient :	14072764.2	1
100°C :	13495991.5	1.04273659
200°C :	12641518	1.11321791

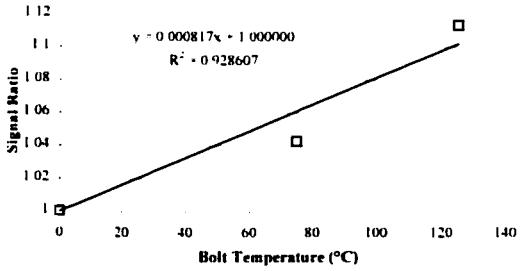

Calibration Equation: (T_b absolute)

$$\sigma_b = 14072764.(1 - 0.000817.T_b).Signal(VDC)/250$$

Overall Error:

	Max. Offset (Abs)	% of Full Scale	99.5% Error Range (MPa)	
Ambient :	10.0 MPa	2.8 %	2.76 0.65	Listed 99.5% Error
100°C :	10.0 MPa	2.8 %	7.12 5.20	± 7.12 MPa
200°C :	8.5 MPa	2.4 %	-1.61 -3.46	

Point to Point Error:

	Max. Offset (Abs)	% of Full Scale	99.5% Error Range (MPa)	
Ambient :	11.3 MPa	3.2 %	1.05 -1.10	Listed 99.5% Error
100°C :	11.3 MPa	3.2 %	0.95 -0.74	± 1.10 MPa
200°C :	6.7 MPa	1.9 %	0.83 -0.91	

Figure D.15 - Bolt gauge calibration datasheet - Bolt #11

BOLT GAUGE CALIBRATION DATASHEET

BOLT GAUGE NUMBER: 12

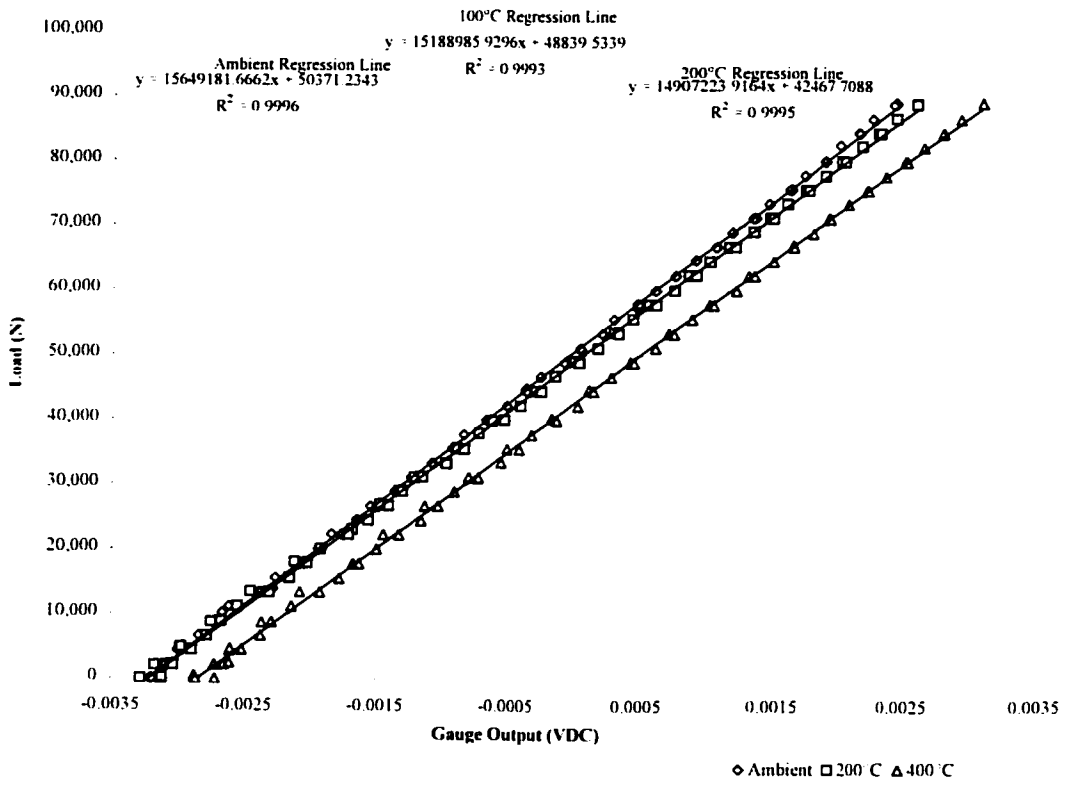

Calibration constant vs. temperature

		Signal Ratio
Ambient :	15649181.7	1
100°C :	15188985.9	1.03029799
200°C :	14907223.9	1.04977169

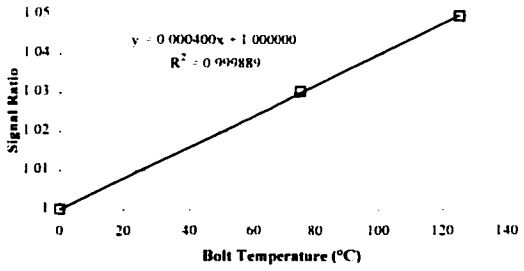

Calibration Equation: (T_b absolute)

$$\sigma_b = 15649181.(1 - 0.0004.T_b).Signal(VDC)/250$$

Overall Error:

	Max. Offset (Abs)	% of Full Scale	99.5% Error Range (MPa)	
Ambient :	7.3 MPa	2.1 %	-0.22 -1.71	Listed 99.5% Error
100°C :	7.3 MPa	2.1 %	4.71 2.82	± 4.71 MPa
200°C :	6.3 MPa	1.8 %	2.07 0.37	

Point to Point Error:

	Max. Offset (Abs)	% of Full Scale	99.5% Error Range (MPa)	
Ambient :	8.2 MPa	2.3 %	0.89 -0.92	Listed 99.5% Error
100°C :	8.2 MPa	2.3 %	0.73 -0.53	± 0.92 MPa
200°C :	6.4 MPa	1.8 %	0.71 -0.52	

Figure D.16 - Bolt gauge calibration datasheet - Bolt #12

BOLT GAUGE CALIBRATION DATASHEET

BOLT GAUGE NUMBER: 13 - Test II (Gauge Re-mounted)

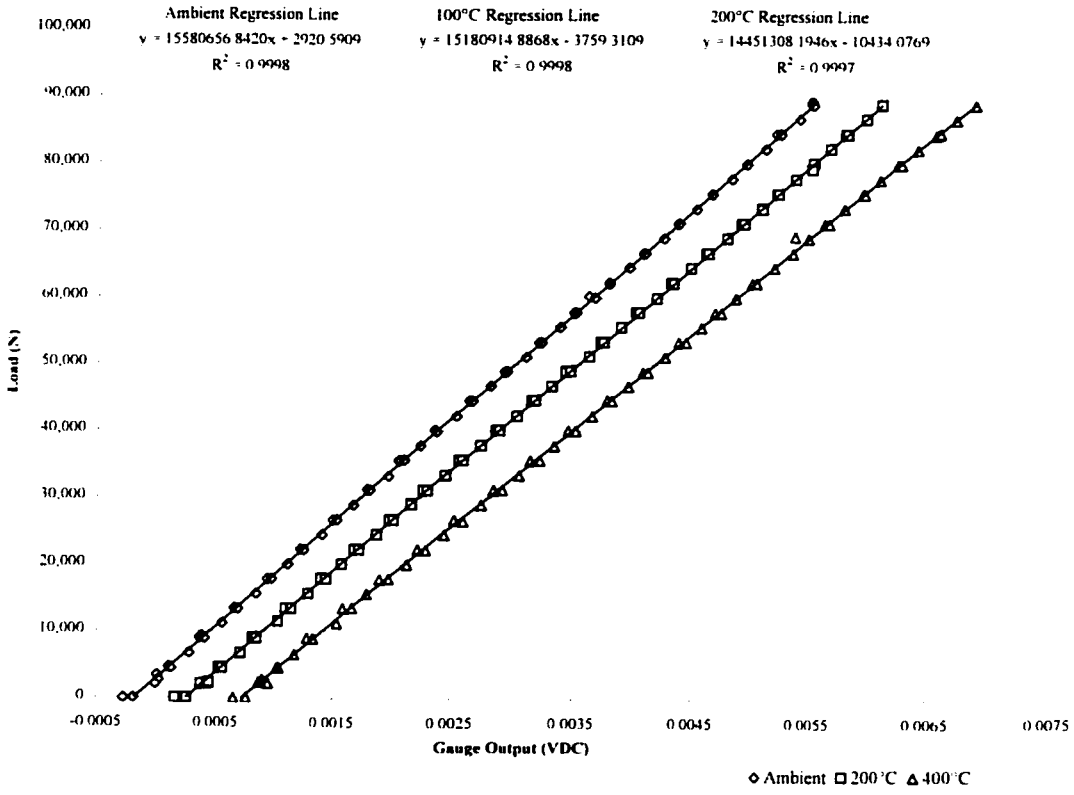

Calibration constant vs. temperature

		Signal Ratio
Ambient :	15580656.8	1
100°C :	15180914.9	1.02633188
200°C :	14451308.2	1.07814854

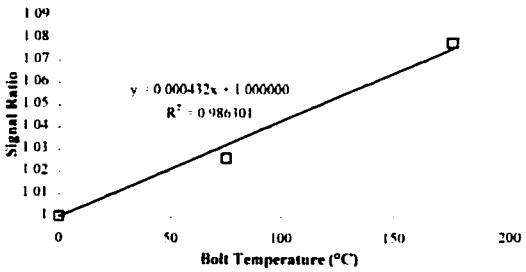

Calibration Equation: (T_b absolute)

$$\sigma_b = 15580656.(1 - 0.000432.T_b).Signal(VDC)/250$$

Overall Error:

	Max. Offset (Abs)	% of Full Scale	99.5% Error Range (MPa)	
Ambient :	8.5 MPa	2.4 %	5.94 5.07	Listed 99.5% Error
100°C :	8.5 MPa	2.4 %	5.93 5.10	± 5.94 MPa
200°C :	8.3 MPa	2.4 %	4.79 3.45	

Point to Point Error:

	Max. Offset (Abs)	% of Full Scale	99.5% Error Range (MPa)	
Ambient :	3.5 MPa	1.0 %	0.32 -0.08	Listed 99.5% Error
100°C :	3.5 MPa	1.0 %	0.46 -0.20	± 0.73 MPa
200°C :	4.7 MPa	1.4 %	0.73 -0.46	

Figure D.17a - Bolt gauge calibration datasheet - Bolt #13a (Test II)

BOLT GAUGE CALIBRATION DATASHEET

BOLT GAUGE NUMBER: 13

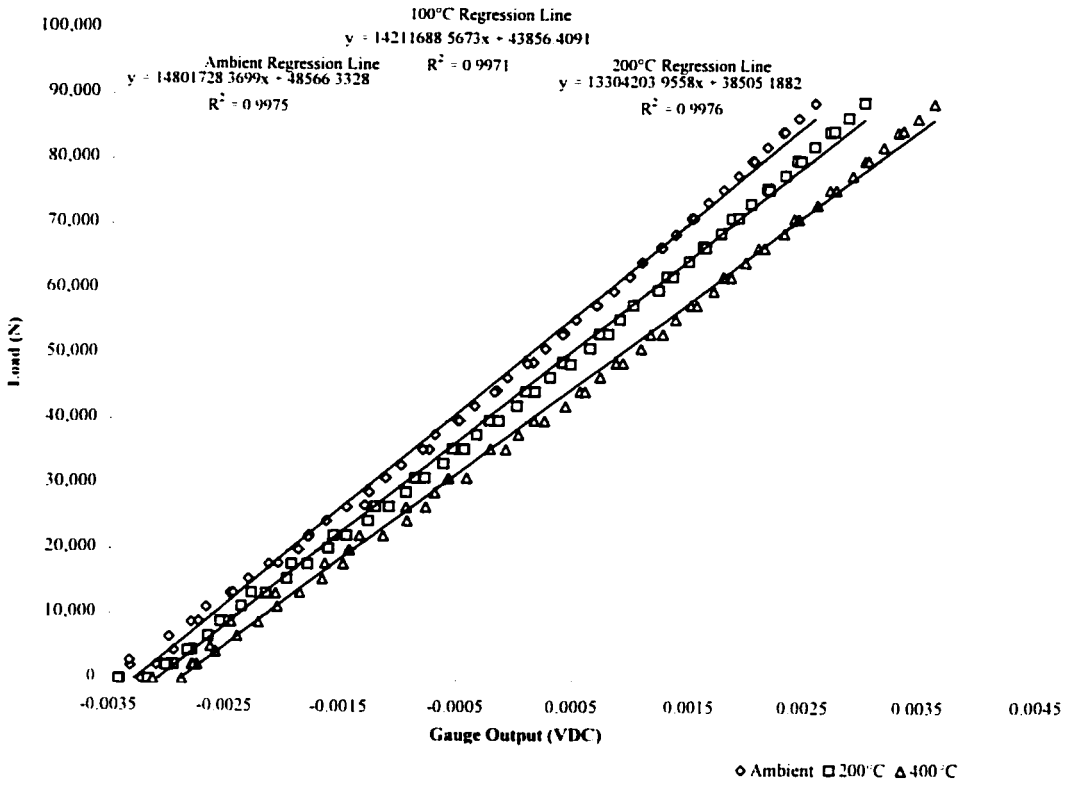

Calibration constant vs. temperature

		Signal Ratio
Ambient :	14801728.4	1
100°C :	14211688.6	1.04151792
200°C :	13304204	1.11256024

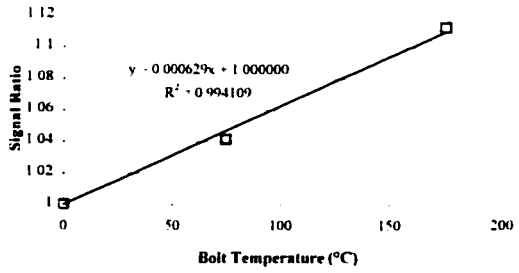

Calibration Equation: (T_b absolute)

$$\sigma_b = 14801728.(1 - 0.000629.T_b).Signal(VDC)/250$$

Overall Error:

	Max. Offset (Abs)	% of Full Scale	99.5% Error Range (MPa)	
Ambient :	26.7 MPa	7.6 %	-1.75 -5.52	Listed 99.5% Error
100°C :	26.7 MPa	7.6 %	21.08 17.54	± 21.08 MPa
200°C :	20.1 MPa	5.7 %	14.38 10.62	

Point to Point Error:

	Max. Offset (Abs)	% of Full Scale	99.5% Error Range (MPa)	
Ambient :	12.7 MPa	3.6 %	0.94 -1.52	Listed 99.5% Error
100°C :	12.7 MPa	3.6 %	1.42 -0.94	± 1.52 MPa
200°C :	17.6 MPa	5.0 %	1.20 -0.89	

Figure D.17b - Bolt gauge calibration datasheet - Bolt #13 (Test I)

BOLT GAUGE CALIBRATION DATASHEET

BOLT GAUGE NUMBER: 14

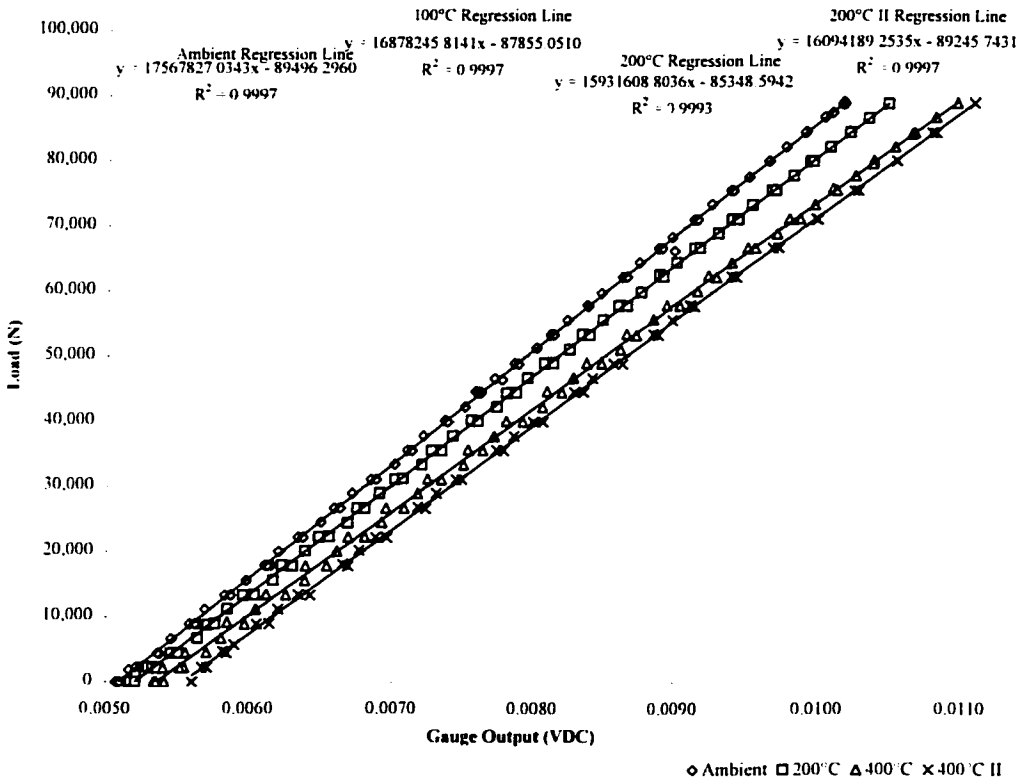

Calibration constant vs. temperature

		Signal Ratio
Ambient :	17567827	1
100°C :	16878245.8	1.04085621
200°C :	15934064.8	1.10253267

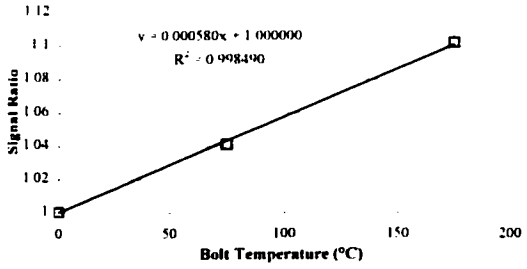

Calibration Equation: (T_b absolute)

$$\sigma_b = 17567827.(1 - 0.000580.T_b).Signal(VDC)/250$$

Overall Error:

	Max. Offset (Abs)	% of Full Scale	99.5% Error Range (MPa)	
Ambient :	5.7 MPa	1.6 %	2.01 0.81	Listed 99.5% Error
100°C :	5.7 MPa	1.6 %	3.23 1.95	± 3.23 MPa
200°C :	5.4 MPa	1.6 %	2.14 0.03	

Point to Point Error:

	Max. Offset (Abs)	% of Full Scale	99.5% Error Range (MPa)	
Ambient :	9.8 MPa	2.8 %	0.61 -0.58	Listed 99.5% Error
100°C :	9.8 MPa	2.8 %	0.32 -0.17	± 0.61 MPa
200°C :	3.1 MPa	0.9 %	0.45 -0.36	

Figure D.18 - Bolt gauge calibration datasheet - Bolt #14

BOLT GAUGE CALIBRATION DATASHEET

BOLT GAUGE NUMBER: 15

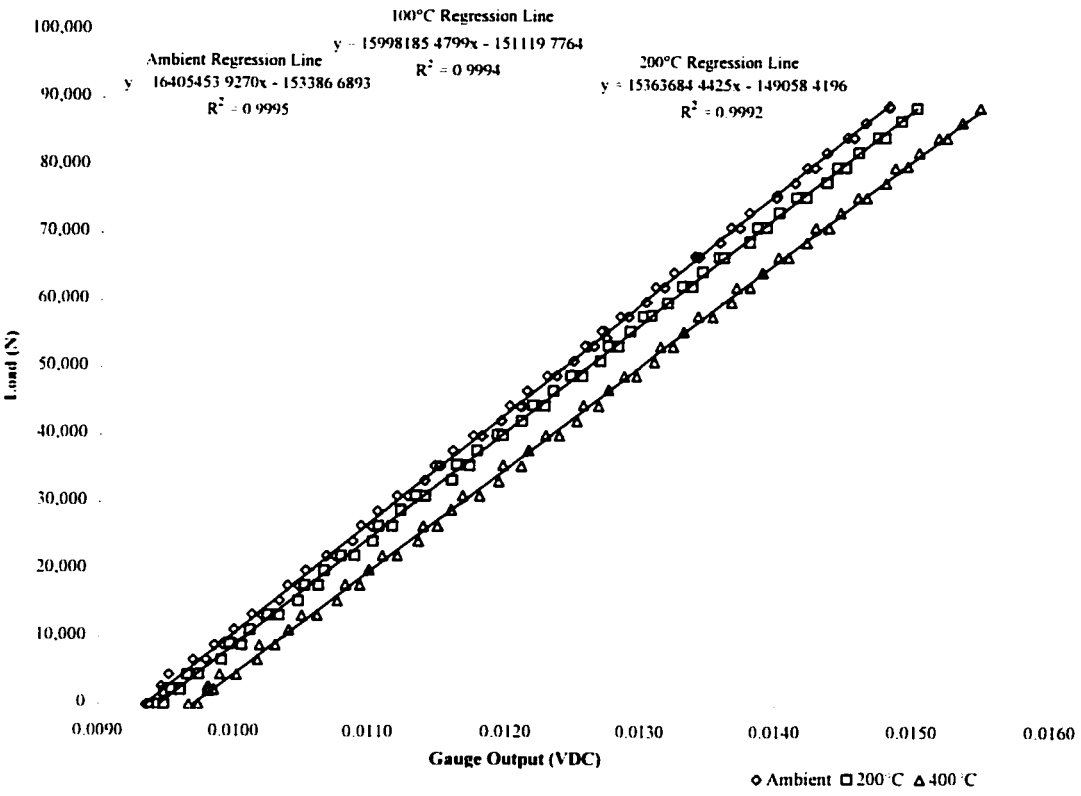

Calibration constant vs. temperature

		Signal Ratio
Ambient :	16405453.9	1
100°C :	15998185.5	1.02545716
200°C :	15363684.4	1.06780727

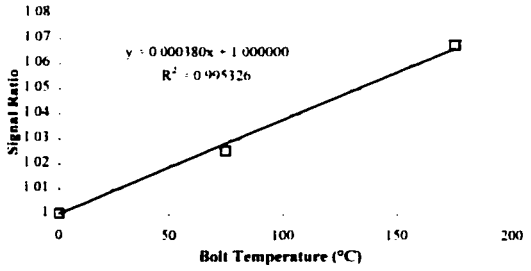

Calibration Equation: (T_b absolute)

$$\sigma_b = 16405453.(1 - 0.000380.T_b).Signal(VDC)/250$$

Overall Error:

	Max. Offset (Abs)	% of Full Scale	99.5% Error Range (MPa)	
Ambient :	4.4 MPa	1.3 %	0.07 -1.64	Listed 99.5% Error
100°C :	4.4 MPa	1.3 %	0.96 -0.89	± 3.30 MPa
200°C :	7.4 MPa	2.1 %	3.30 1.12	

Point to Point Error:

	Max. Offset (Abs)	% of Full Scale	99.5% Error Range (MPa)	
Ambient :	6.0 MPa	1.7 %	0.59 -0.60	Listed 99.5% Error
100°C :	6.0 MPa	1.7 %	0.54 -0.49	± 0.60 MPa
200°C :	4.2 MPa	1.2 %	0.44 -0.42	

Figure D.19 - Bolt gauge calibration datasheet - Bolt #15

BOLT GAUGE CALIBRATION DATASHEET

BOLT GAUGE NUMBER: 16

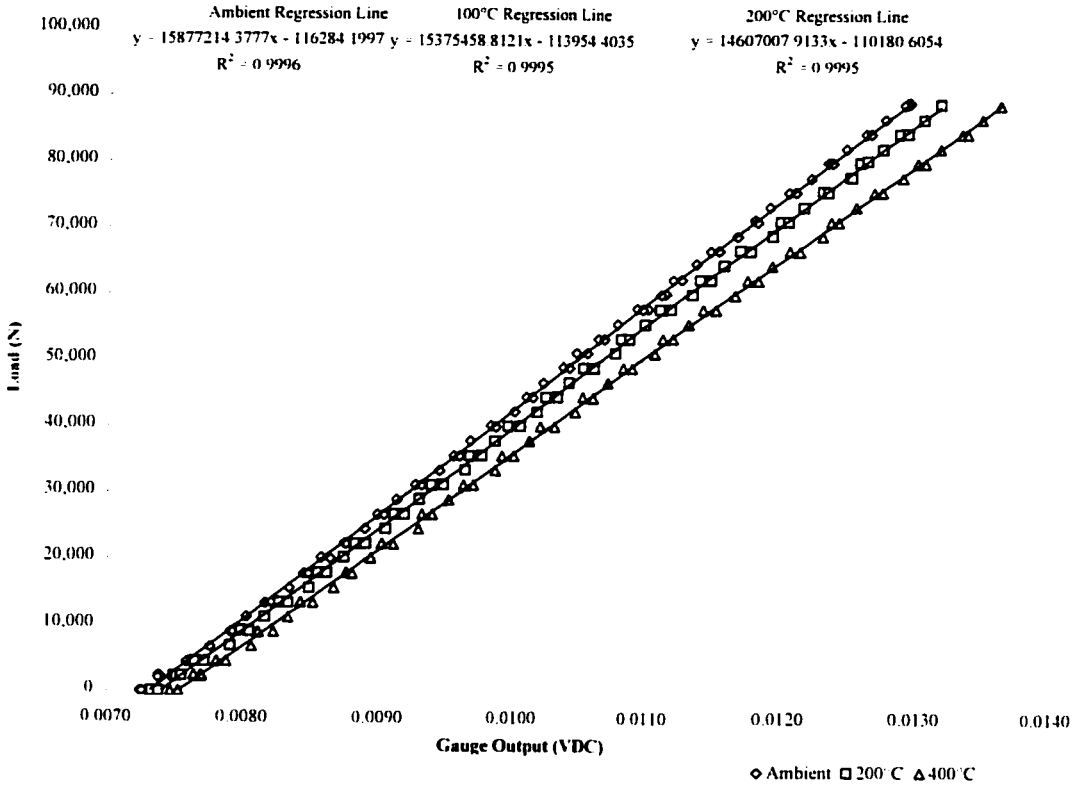

Calibration constant vs. temperature

		Signal Ratio
Ambient :	15877214.4	1
100°C :	15375458.8	1.03263353
200°C :	14607007.9	1.0869587

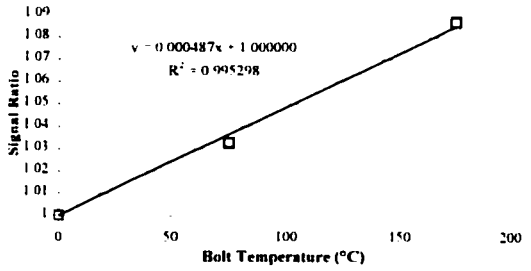

Calibration Equation: (T_b absolute)

$$\sigma_b = 15877214.(1 - 0.000487.T_b).Signal(VDC)/250$$

Overall Error:

	Max. Offset (Abs)	% of Full Scale	99.5% Error Range (MPa)	
Ambient :	8.8 MPa	2.5 %	5.38 3.95	Listed 99.5% Error
100°C :	8.8 MPa	2.5 %	5.73 4.10	± 5.73 MPa
200°C :	8.0 MPa	2.3 %	4.55 2.88	

Point to Point Error:

	Max. Offset (Abs)	% of Full Scale	99.5% Error Range (MPa)	
Ambient :	5.9 MPa	1.7 %	0.57 -0.55	Listed 99.5% Error
100°C :	5.9 MPa	1.7 %	0.49 -0.32	± 0.57 MPa
200°C :	3.7 MPa	1.1 %	0.44 -0.33	

Figure D.20 - Bolt gauge calibration datasheet - Bolt #16

BOLT GAUGE CALIBRATION DATASHEET

BOLT GAUGE NUMBER: 17

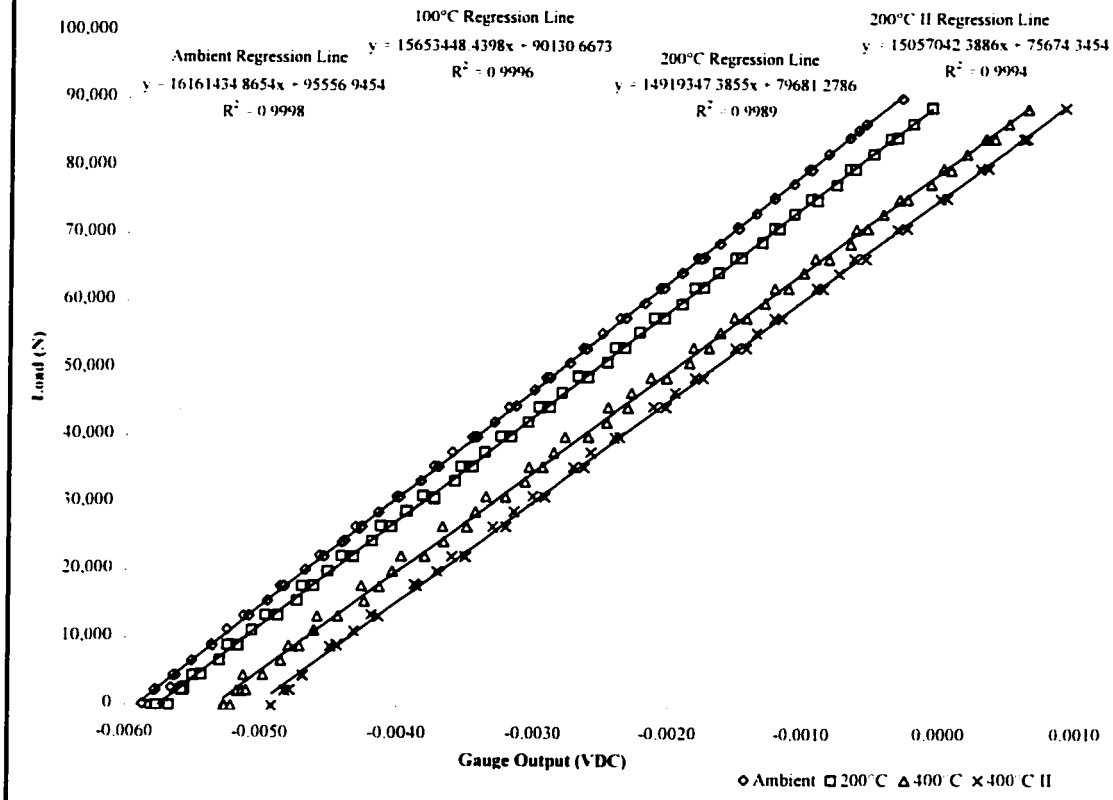

Calibration constant vs. temperature

		Signal Ratio
Ambient :	16161434.9	1
100°C :	15653448.4	1.03245205
200°C :	14919347.4	1.08325347

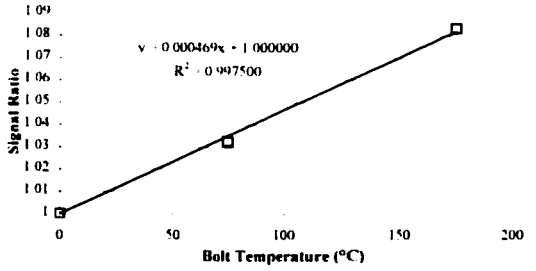

Calibration Equation: (T_b absolute)

$$\sigma_b = 16161434.(1 - 0.000469.T_b).Signal(VDC)/250$$

Overall Error:

	Max. Offset (Abs)	% of Full Scale	99.5% Error Range (MPa)	
Ambient :	3.7 MPa	1.1 %	-5.17 -6.11	Listed 99.5% Error
100°C :	3.7 MPa	1.1 %	1.23 -0.37	± 6.11 MPa
200°C :	11.7 MPa	3.4 %	-3.01 -5.56	

Point to Point Error:

	Max. Offset (Abs)	% of Full Scale	99.5% Error Range (MPa)	
Ambient :	5.8 MPa	1.6 %	0.29 -0.47	Listed 99.5% Error
100°C :	5.8 MPa	1.6 %	0.41 -0.33	± 0.64 MPa
200°C :	3.8 MPa	1.1 %	0.64 -0.60	

Figure D.21 - Bolt gauge calibration datasheet - Bolt #17

BOLT GAUGE CALIBRATION DATASHEET

BOLT GAUGE NUMBER: 18

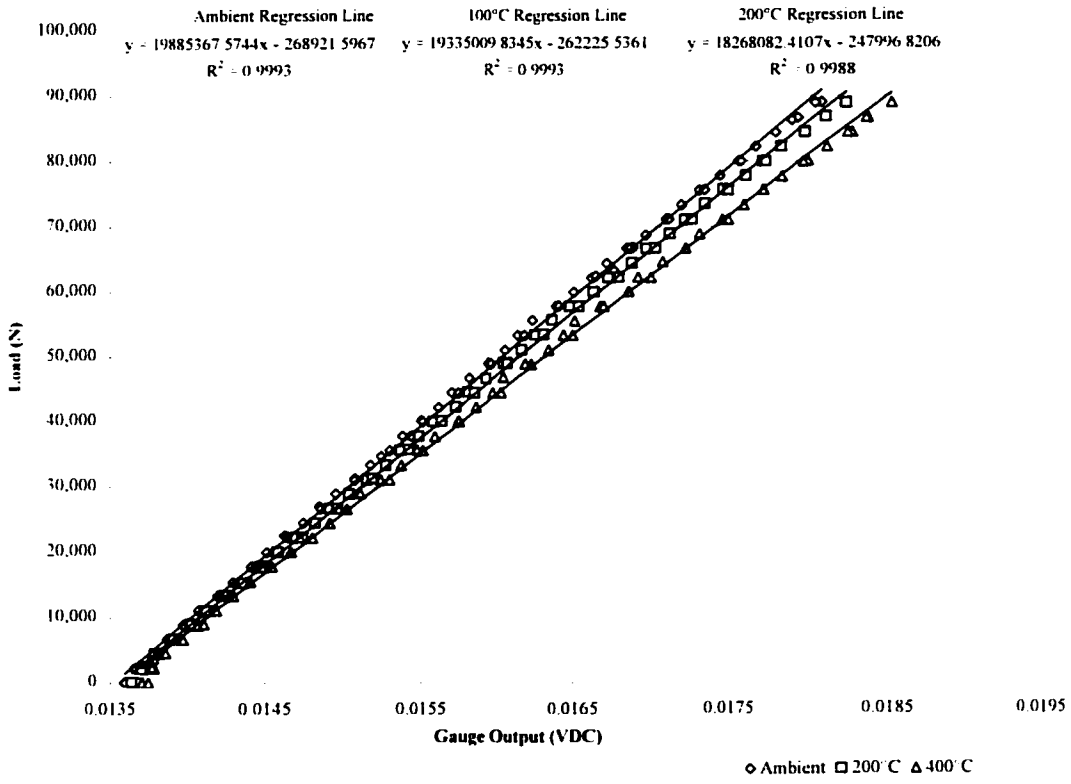

Calibration constant vs. temperature

		Signal Ratio
Ambient :	19885367.6	1
100°C :	19335009.8	1.02846431
200°C :	18268082.4	1.08853065

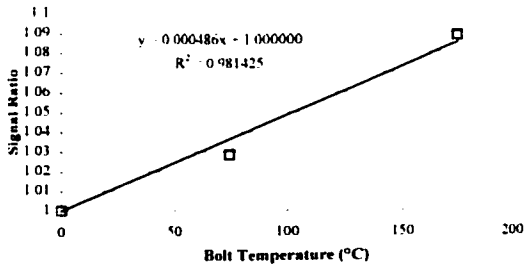

Calibration Equation: (T_b absolute)

$$\sigma_b = 19885367.(1 - 0.000486.T_b).Signal(VDC)/250$$

Overall Error:

	Max. Offset (Abs)	% of Full Scale	99.5% Error Range (MPa)	
Ambient :	14.7 MPa	4.2 %	-4.92 -6.77	Listed 99.5% Error
100°C :	14.7 MPa	4.2 %	-8.46 -10.35	± 11.01 MPa
200°C :	16.9 MPa	4.8 %	-8.72 -11.01	

Point to Point Error:

	Max. Offset (Abs)	% of Full Scale	99.5% Error Range (MPa)	
Ambient :	5.5 MPa	1.6 %	0.58 -0.70	Listed 99.5% Error
100°C :	5.5 MPa	1.6 %	0.58 -0.79	± 1.02 MPa
200°C :	7.1 MPa	2.0 %	0.87 -1.02	

Figure D.22 - Bolt gauge calibration datasheet - Bolt #18

BOLT GAUGE CALIBRATION DATASHEET

BOLT GAUGE NUMBER: 19 - Test II (Gauge Re-mounted)

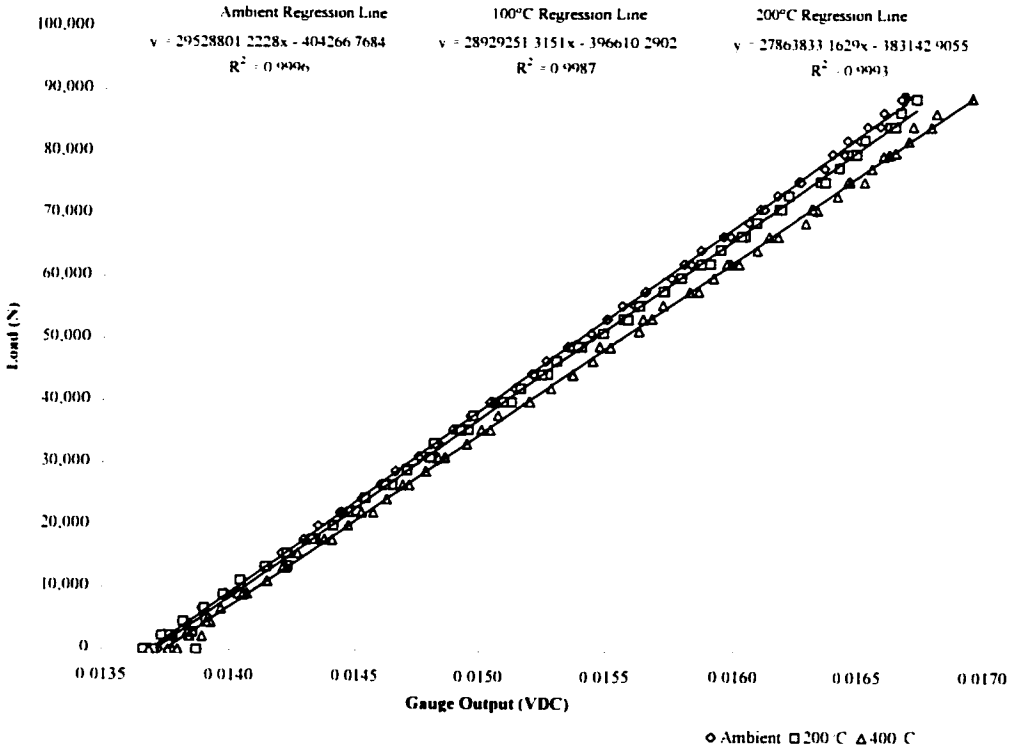

Calibration constant vs. temperature

		Signal Ratio
Ambient :	29528801.2	1
100°C :	28929251.3	1.02072469
200°C :	27863833.2	1.05975373

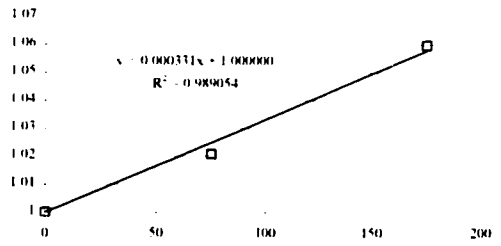

Calibration Equation: (T_b absolute)

$$\sigma_b = 29528801.(1 - 0.000331.T_b).Signal(VDC)/250$$

Overall Error:

	Max. Offset (Abs)	% of Full Scale	99.5% Error Range (MPa)	
Ambient :	25.6 MPa	7.3 %	-2.55 -4.09	Listed 99.5% Error
100°C :	25.6 MPa	7.3 %	-17.71 -19.90	± 19.90 MPa
200°C :	11.1 MPa	3.2 %	-1.90 -3.83	

Point to Point Error:

	Max. Offset (Abs)	% of Full Scale	99.5% Error Range (MPa)	
Ambient :	8.2 MPa	2.4 %	0.76 -0.93	Listed 99.5% Error
100°C :	8.2 MPa	2.4 %	0.80 -1.61	± 1.61 MPa
200°C :	13.0 MPa	3.7 %	1.12 -1.25	

Figure D.23a - Bolt gauge calibration datasheet - Bolt #19 (Test II)

BOLT GAUGE CALIBRATION DATASHEET

BOLT GAUGE NUMBER: 19

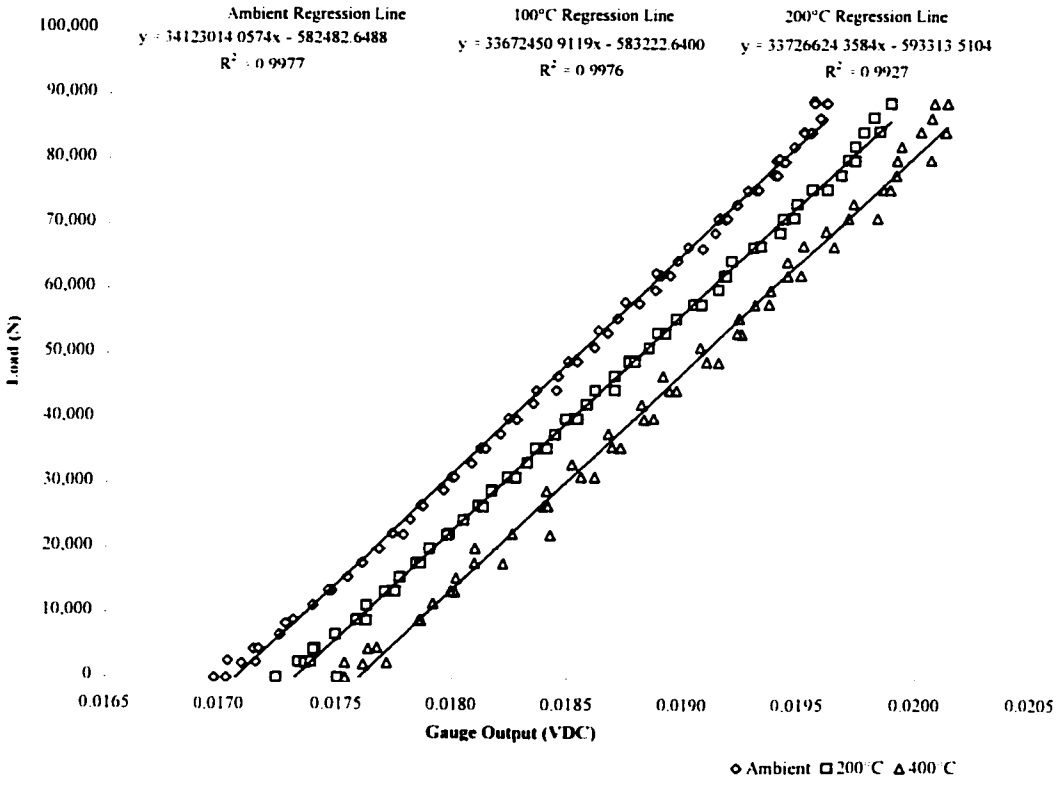

Calibration constant vs. temperature

		Signal Ratio
Ambient :	34123014.1	1
100°C :	33672450.9	1.01338076
200°C :	33726624.4	1.01175302

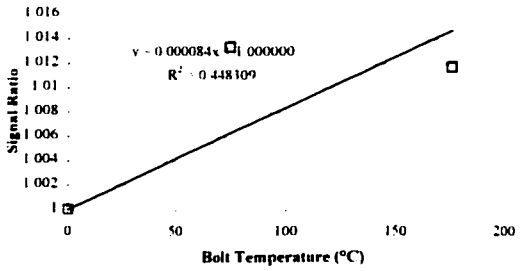

Calibration Equation: (T_b absolute)

$$\sigma_b = 34123014.(1 - 0.000084.T_b).Signal(VDC)/250$$

Overall Error:

	Max. Offset (Abs)	% of Full Scale	99.5% Error Range (MPa)	
Ambient :	36.3 MPa	10.4 %	14.38 10.98	Listed 99.5% Error
100°C :	36.3 MPa	10.4 %	-23.20 -26.17	± 26.17 MPa
200°C :	31.5 MPa	9.0 %	11.21 4.53	

Point to Point Error:

	Max. Offset (Abs)	% of Full Scale	99.5% Error Range (MPa)	
Ambient :	16.7 MPa	4.8 %	1.55 -1.15	Listed 99.5% Error
100°C :	16.7 MPa	4.8 %	1.70 -2.51	± 2.97 MPa
200°C :	31.5 MPa	9.0 %	2.97 -2.90	

Figure D.23b - Bolt gauge calibration datasheet - Bolt #19 (Test I)

BOLT GAUGE CALIBRATION DATASHEET

BOLT GAUGE NUMBER: 20

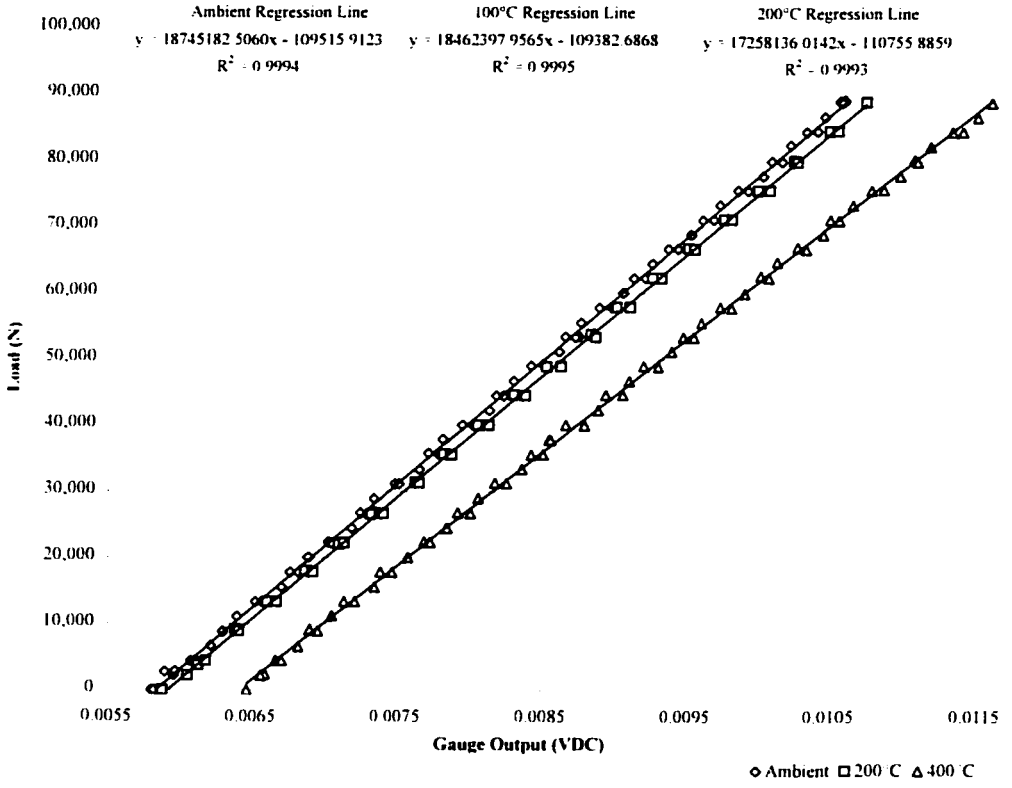

Calibration constant vs. temperature

		Signal Ratio
Ambient :	18745182.5	1
100°C :	18462398	1.01531678
200°C :	17258136	1.08616495

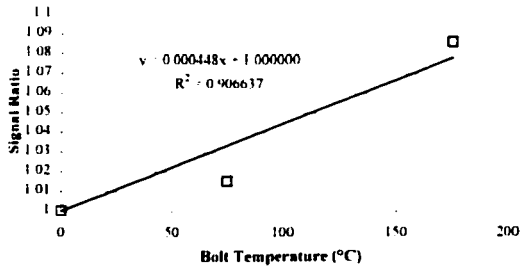

Calibration Equation: (T_b absolute)

$$\sigma_b = 18745182.(1 - 0.000448.T_b).Signal(VDC)/250$$

Overall Error:

	Max. Offset (Abs)	% of Full Scale	99.5% Error Range (MPa)	
Ambient :	6.8 MPa	1.9 %	3.26 1.39	Listed 99.5% Error
100°C :	6.8 MPa	1.9 %	4.03 1.87	± 4.89 MPa
200°C :	9.1 MPa	2.6 %	-2.96 -4.89	

Point to Point Error:

	Max. Offset (Abs)	% of Full Scale	99.5% Error Range (MPa)	
Ambient :	7.0 MPa	2.0 %	0.74 -0.72	Listed 99.5% Error
100°C :	7.0 MPa	2.0 %	0.85 -0.64	± 0.85 MPa
200°C :	3.6 MPa	1.0 %	0.50 -0.56	

Figure D.24 - Bolt gauge calibration datasheet - Bolt #20

BOLT GAUGE CALIBRATION DATASHEET

BOLT GAUGE NUMBER: 21

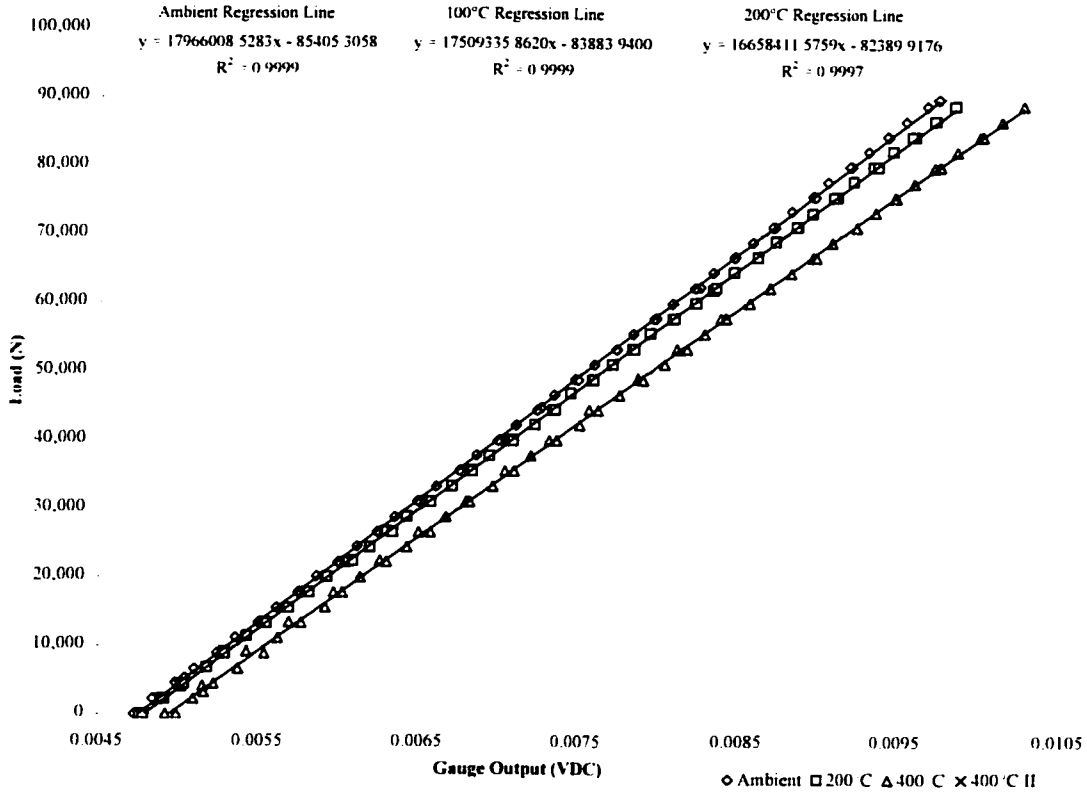

Calibration constant vs. temperature

		Signal Ratio
Ambient :	17966008.5	1
100°C :	17509335.9	1.02608167
200°C :	16658411.6	1.0784947

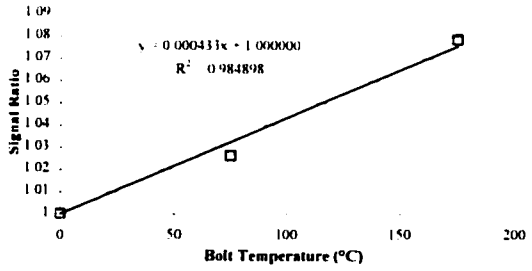

Calibration Equation: (T_b absolute)

$$\sigma_b = 17966008.(1 - 0.000433.T_b).Signal(VDC)/250$$

Overall Error:

	Max. Offset (Abs)	% of Full Scale	99.5% Error Range (MPa)	
Ambient :	3.9 MPa	1.1 %	1.57 0.69	Listed 99.5% Error
100°C :	3.9 MPa	1.1 %	2.42 1.73	± 2.52 MPa
200°C :	6.0 MPa	1.7 %	2.52 1.27	

Point to Point Error:

	Max. Offset (Abs)	% of Full Scale	99.5% Error Range (MPa)	
Ambient :	3.2 MPa	0.9 %	0.29 -0.34	Listed 99.5% Error
100°C :	3.2 MPa	0.9 %	0.29 -0.26	± 0.48 MPa
200°C :	2.7 MPa	0.8 %	0.48 -0.36	

Figure D.25 - Bolt gauge calibration datasheet - Bolt #21

BOLT GAUGE CALIBRATION DATASHEET

BOLT GAUGE NUMBER: 22

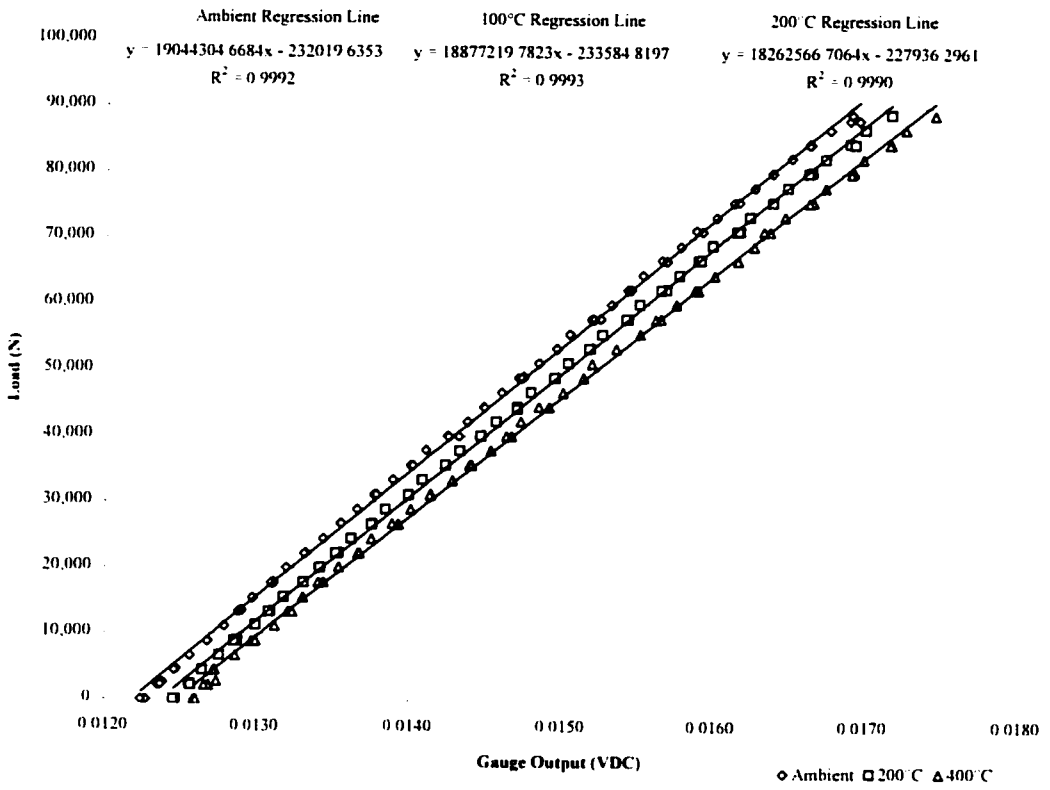

Calibration constant vs. temperature

		Signal Ratio
Ambient :	19044304.7	1
100°C :	18877219.8	1.00885114
200°C :	18262566.7	1.04280548

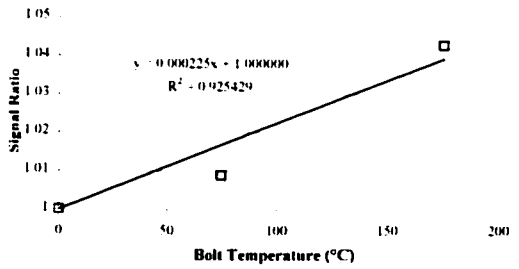

Calibration Equation: (T_b absolute)

$$\sigma_b = 19044304.(1 - 0.000225.T_b).Signal(VDC)/250$$

Overall Error:

	Max. Offset (Abs)	% of Full Scale	99.5% Error Range (MPa)	
Ambient :	11.7 MPa	3.3 %	-6.28 -8.14	Listed 99.5% Error
100°C :	11.3 MPa	3.2 %	-6.61 -8.38	± 9.40 MPa
200°C :	14.3 MPa	4.1 %	-7.12 -9.40	

Point to Point Error:

	Max. Offset (Abs)	% of Full Scale	99.5% Error Range (MPa)	
Ambient :	9.3 MPa	2.6 %	0.57 -0.81	Listed 99.5% Error
100°C :	4.8 MPa	1.4 %	0.56 -0.57	± 1.12 MPa
200°C :	6.4 MPa	1.8 %	1.12 -0.82	

Figure D.26 - Bolt gauge calibration datasheet - Bolt #22

BOLT GAUGE CALIBRATION DATASHEET

BOLT GAUGE NUMBER: 23

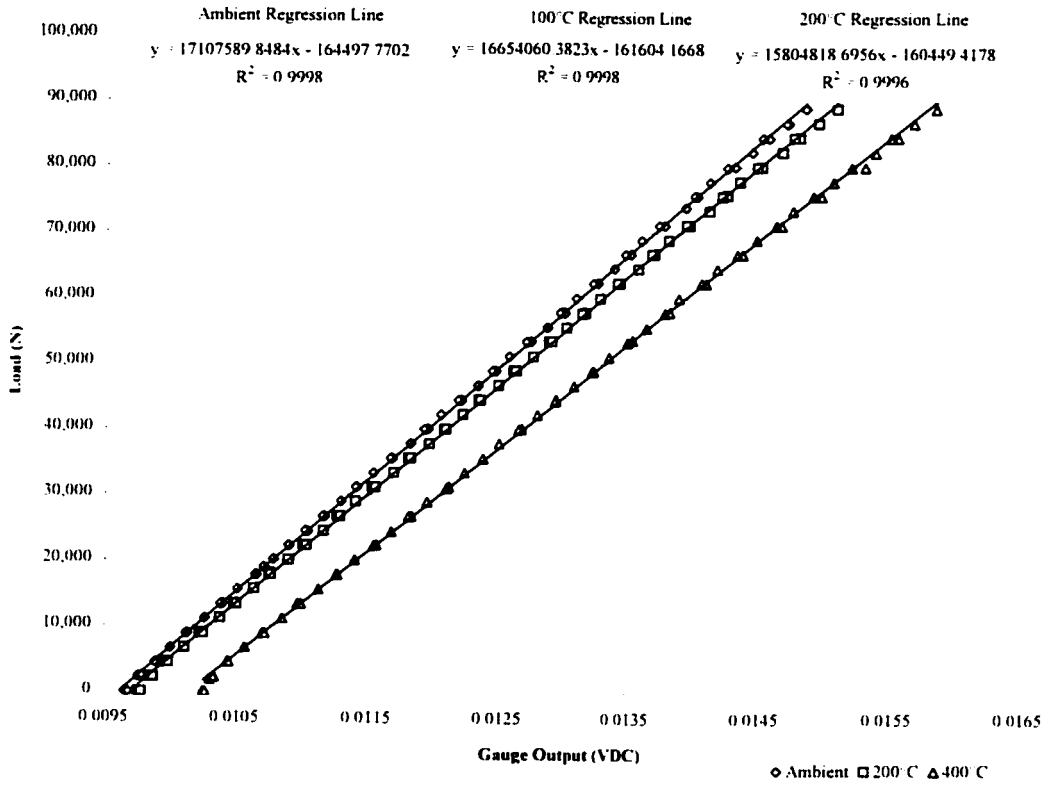

Calibration constant vs. temperature

		Signal Ratio
Ambient :	17107589.8	1
100°C :	16654060.4	1.02723237
200°C :	15804818.7	1.08242873

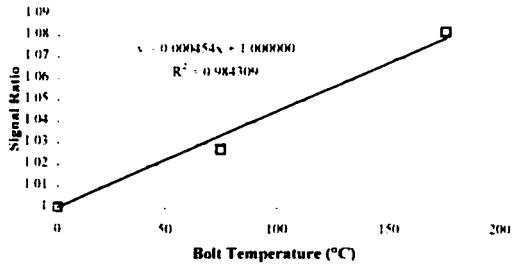

Calibration Equation: (T_b absolute)

$$\sigma_b = 17107589.(1 - 0.000454.T_b).Signal(VDC)/250$$

Overall Error:

	Max. Offset (Abs)	% of Full Scale	99.5% Error Range (MPa)	
Ambient :	4.8 MPa	1.4 %	-2.43 -3.42	Listed 99.5% Error
100°C :	6.3 MPa	1.8 %	-3.45 -4.51	± 7.46 MPa
200°C :	9.6 MPa	2.7 %	-5.98 -7.46	

Point to Point Error:

	Max. Offset (Abs)	% of Full Scale	99.5% Error Range (MPa)	
Ambient :	4.4 MPa	1.2 %	0.49 -0.52	Listed 99.5% Error
100°C :	3.9 MPa	1.1 %	0.43 -0.35	± 0.65 MPa
200°C :	4.7 MPa	1.3 %	0.65 -0.41	

Figure D.27 - Bolt gauge calibration datasheet - Bolt #23

BOLT GAUGE CALIBRATION DATASHEET

BOLT GAUGE NUMBER: 24

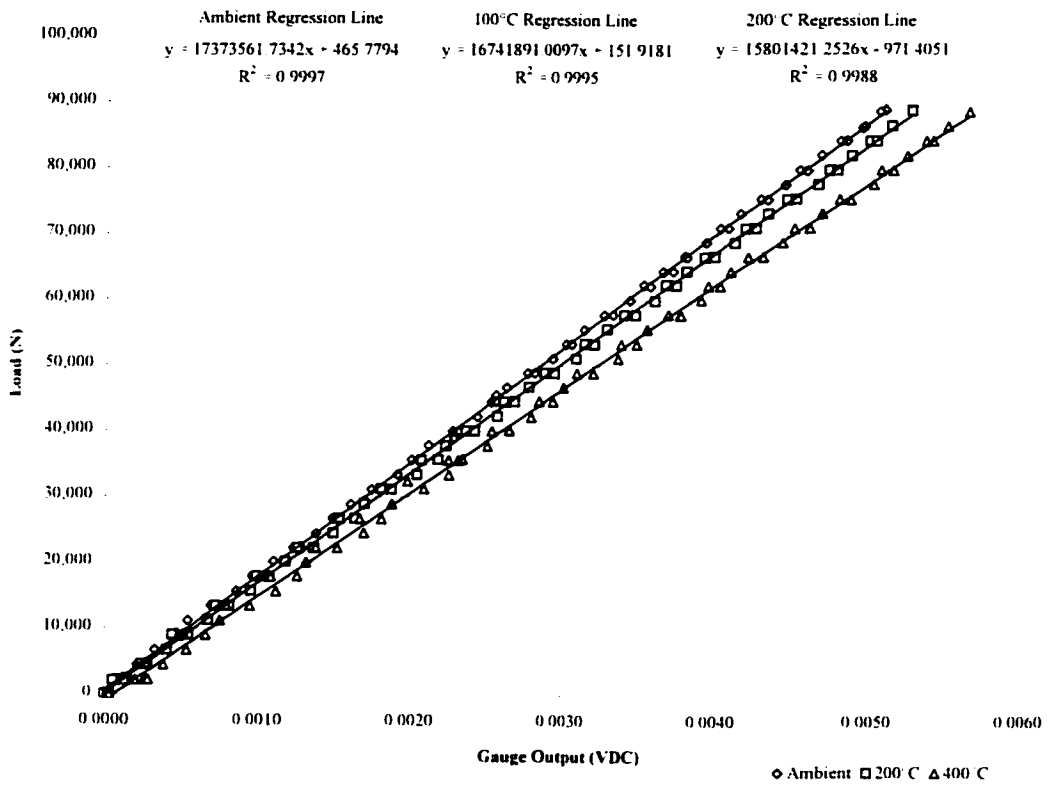

Calibration constant vs. temperature

		Signal Ratio
Ambient :	17373561.7	1
100°C :	16741891	1.03772995
200°C :	15801421.3	1.09949361

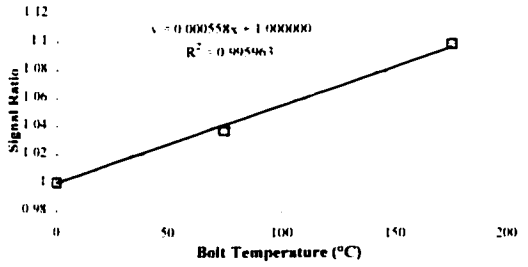

Calibration Equation: (T_b absolute)

$$\sigma_b = 17373561.(1 - 0.000558.T_b).Signal(VDC)/250$$

Overall Error:

	Max. Offset (Abs)	% of Full Scale	99.5% Error Range (MPa)	
Ambient :	8.9 MPa	2.5 %	-3.46 -4.78	Listed 99.5% Error
100°C :	6.2 MPa	1.8 %	3.27 1.44	± 4.78 MPa
200°C :	7.0 MPa	2.0 %	3.26 0.65	

Point to Point Error:

	Max. Offset (Abs)	% of Full Scale	99.5% Error Range (MPa)	
Ambient :	6.3 MPa	1.8 %	0.53 -0.66	Listed 99.5% Error
100°C :	4.6 MPa	1.3 %	0.45 -0.39	± 0.71 MPa
200°C :	4.5 MPa	1.3 %	0.71 -0.37	

Figure D.28 - Bolt gauge calibration datasheet - Bolt #24

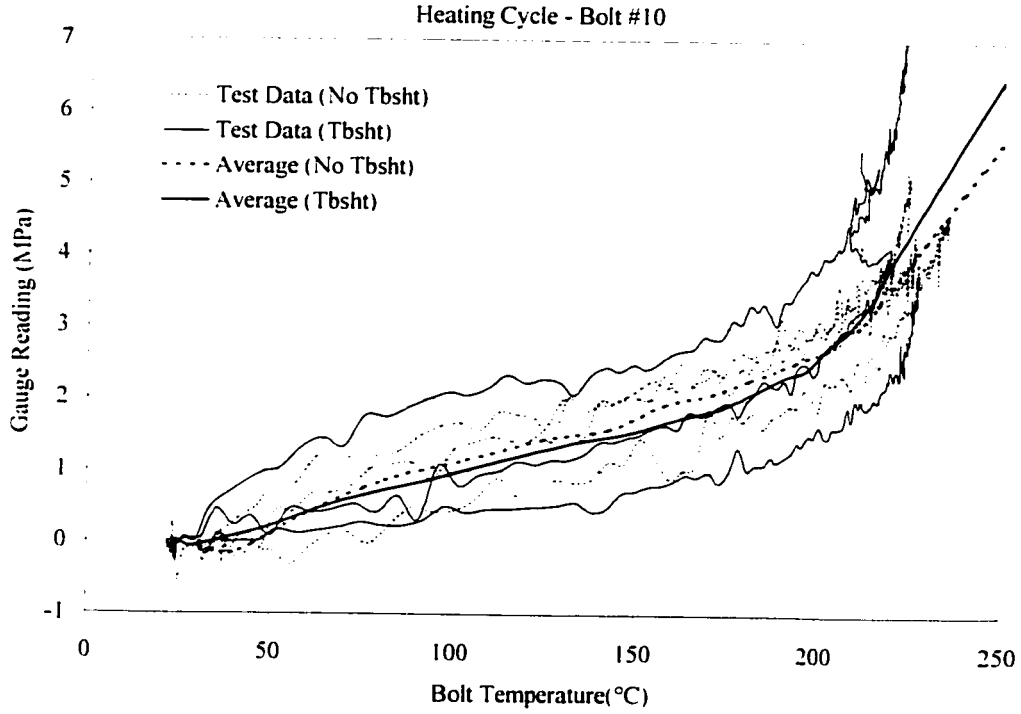

Figure D.29a – Heating cycle zero offset – Bolt #10

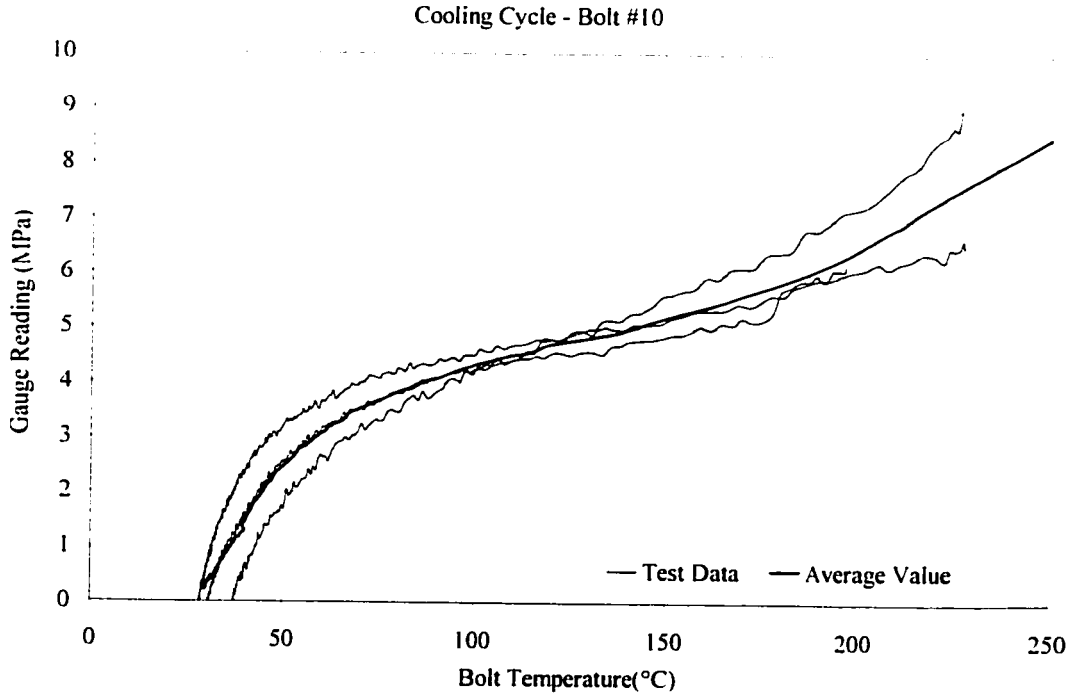

Figure D.29b – Cooling cycle zero offset – Bolt #10

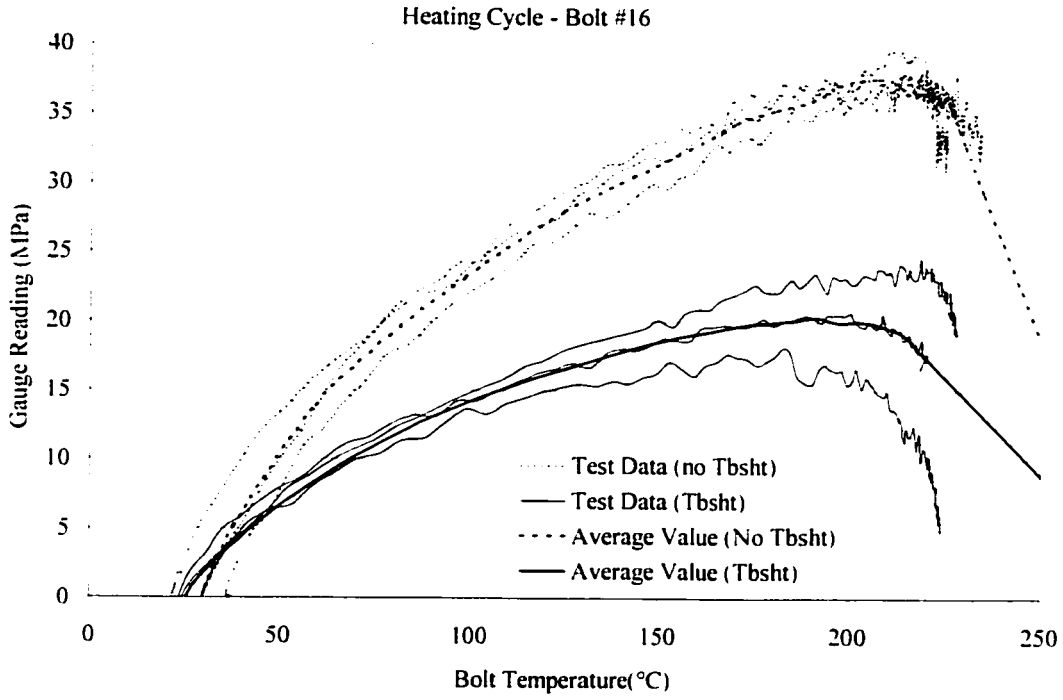

Figure D.30a – Heating cycle zero offset – Bolt #16

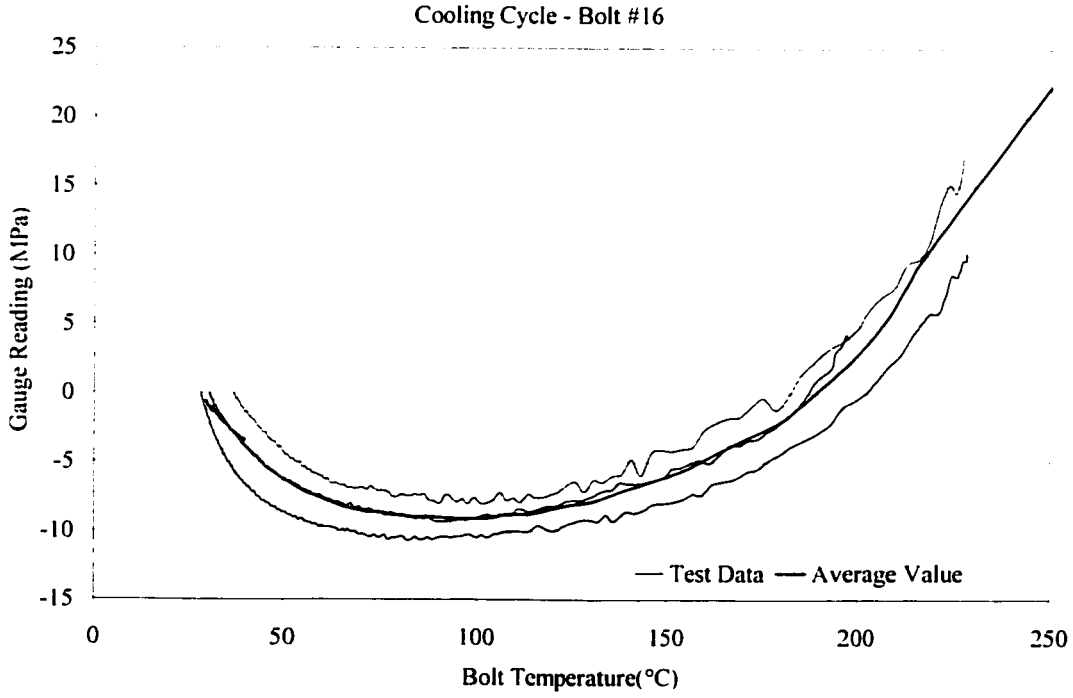

Figure D.30b – Cooling cycle zero offset – Bolt #16

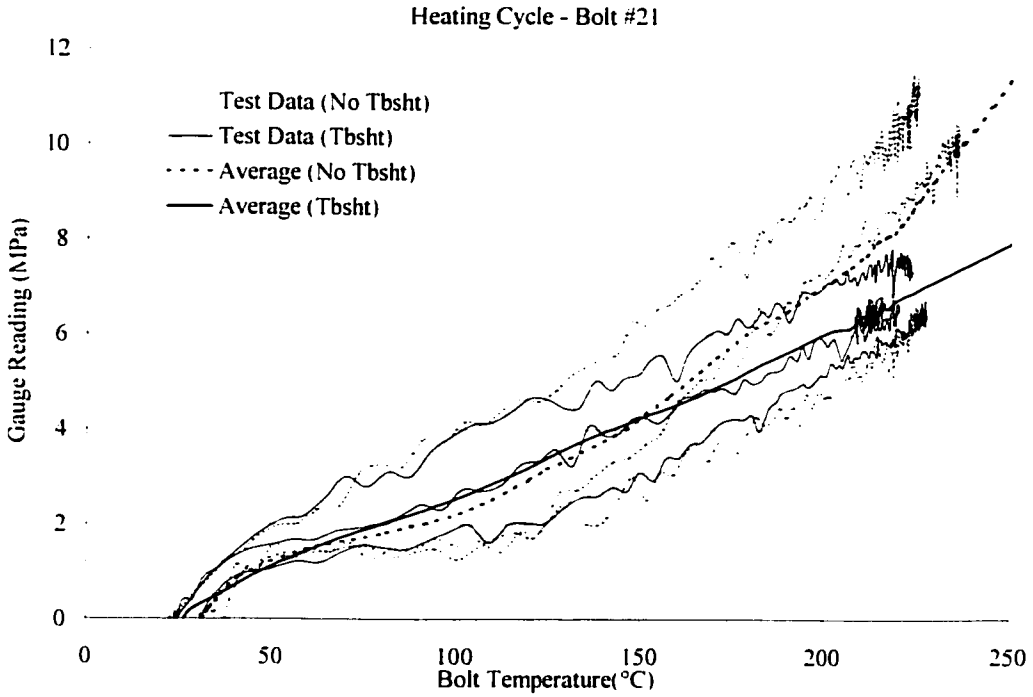

Figure D.31a – Heating cycle zero offset – Bolt #21

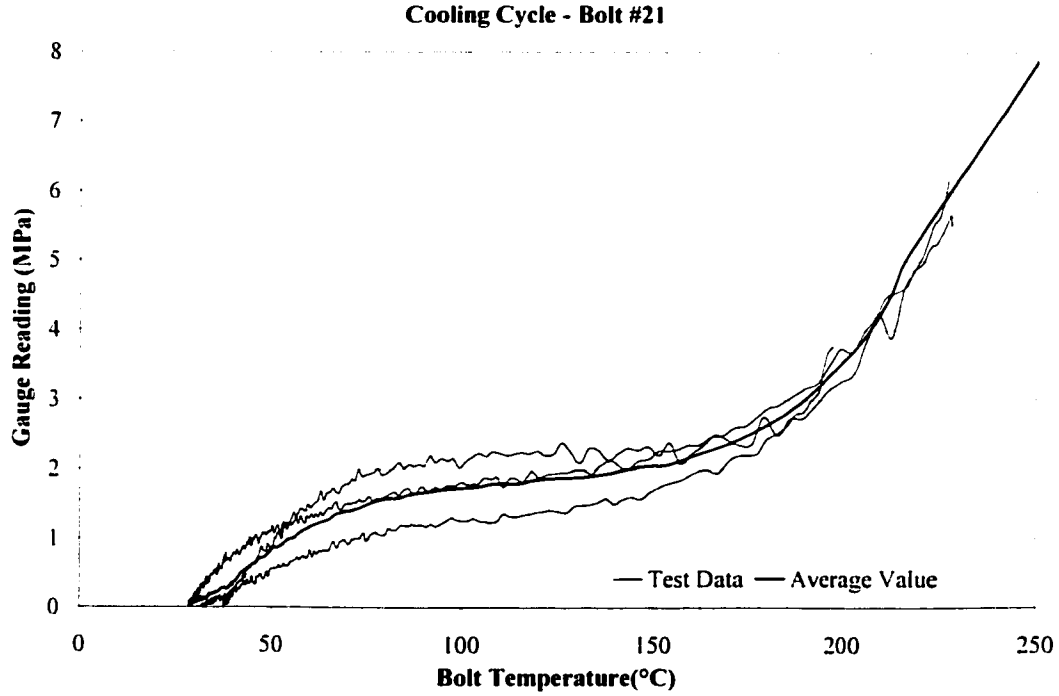

Figure D.31b – Cooling cycle zero offset – Bolt #21

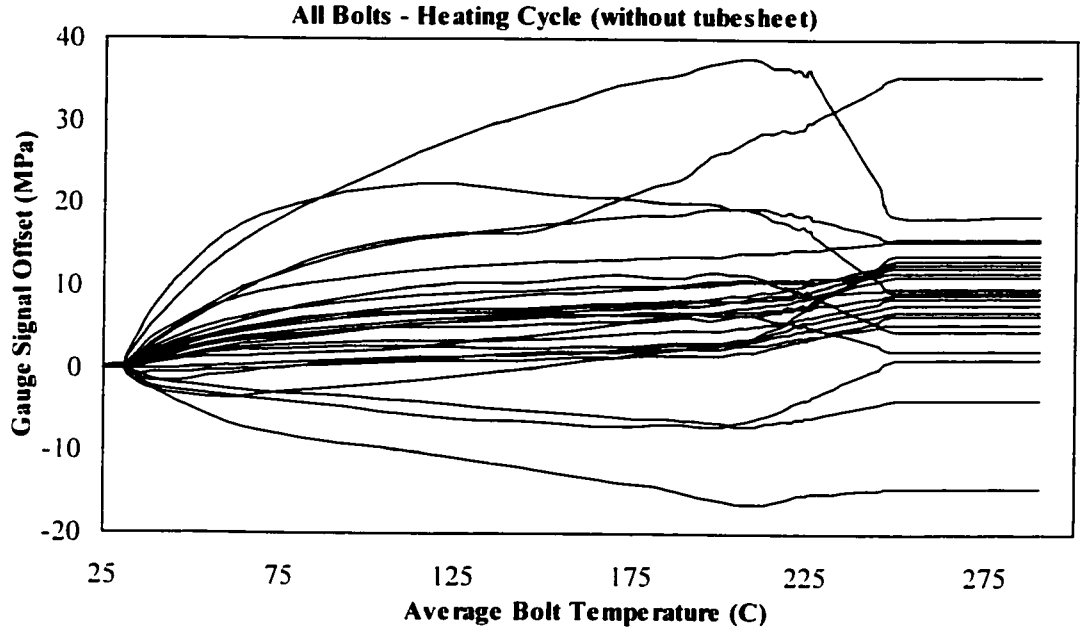

Figure D.32a – Average heating cycle zero offset – all bolts, no tubesheet

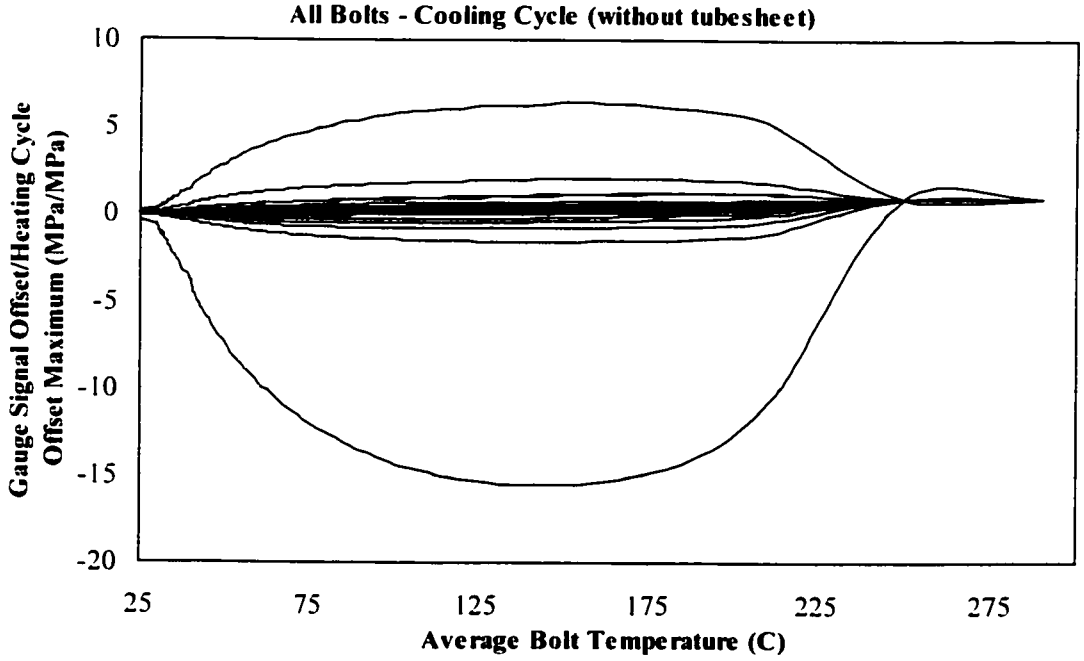

Figure D.32b – Average cooling cycle zero offset – all bolts, no tubesheet

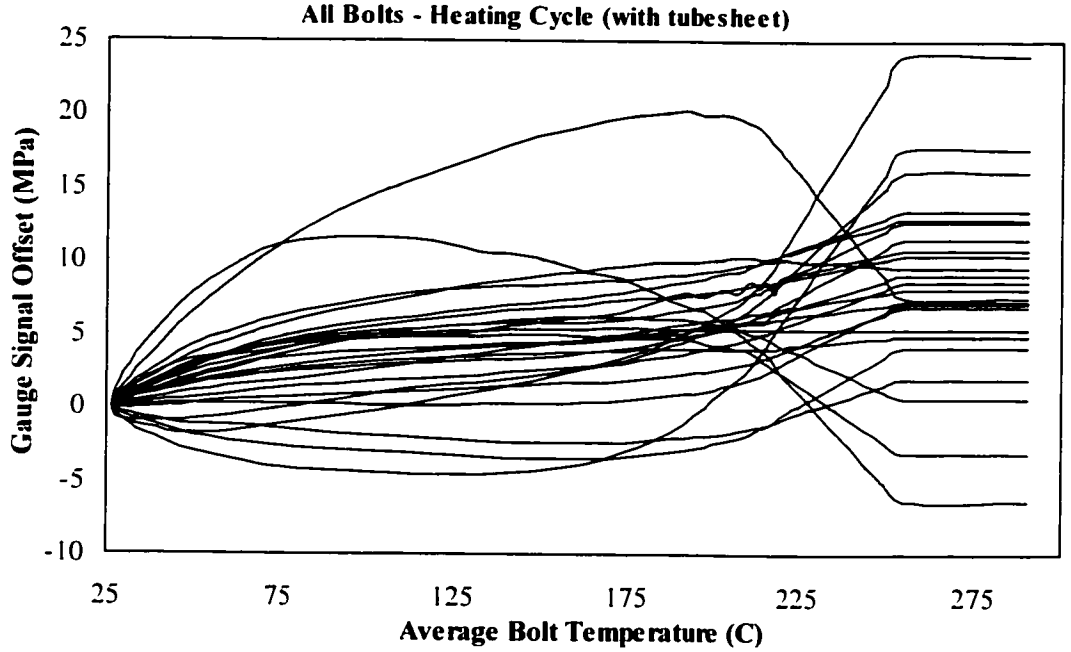

Figure D.33a – Average heating cycle zero offset – all bolts, with tubesheet

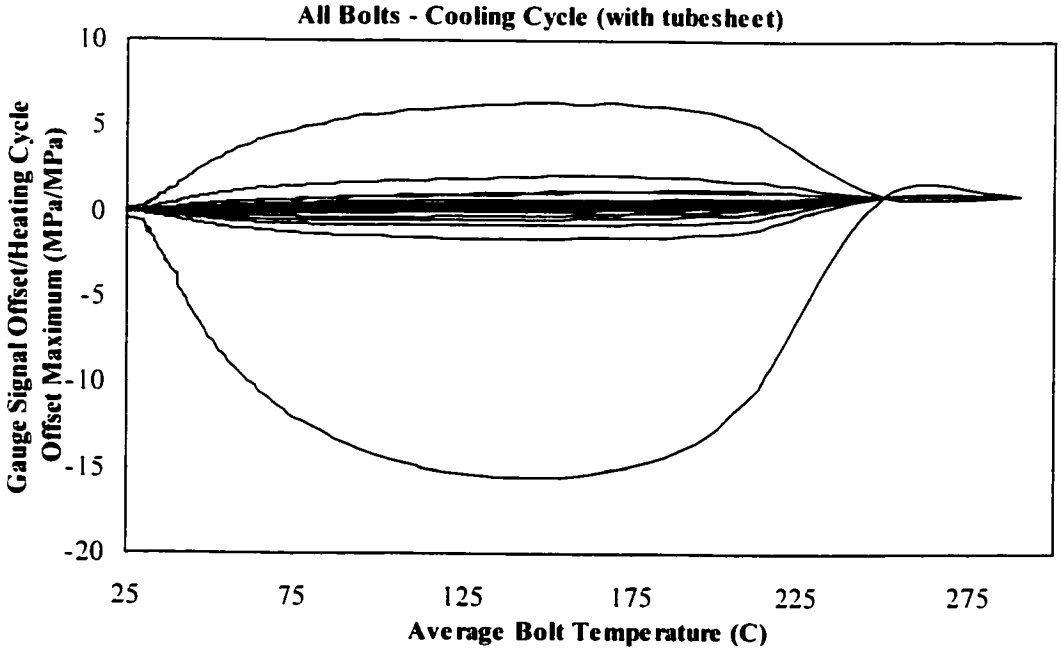

Figure D.33b – Average cooling cycle zero offset – all bolts, with tubesheet

APPENDIX E

CALIBRATION OF THE LVDT SYSTEM

E.1 Calibration requirements

The LVDT system measures the flange deflections during initial assembly and subsequent thermal cycling. The LVDTs were therefore calibrated for plunger movement versus the output signal, at the supply voltage used during testing. Due to the fact that there is flange movement during any thermal cycling, even if the flange is unloaded, it was not feasible to calibrate the LVDTs with temperature.

E.2 LVDT specifications

The LVDTs used to measure the flange rotation were Omega LD400-5mm stroke Linear Variable Displacement Transducers (LVDTs). These transducers have a displacement measurement capability of 10mm ($\pm$5mm) and are listed as linear to within 0.30% across the full stroke. The plunger is guided by Delrin bearings at either end, to ensure it is held central within the LVDT body. The excitation voltage used during testing was a 10VDC regulated power supply.

E.3 Calibration procedure

The LVDTs were mounted in a specially constructed calibration stand (ref. Figure E.1), which allowed the LVDT body to be clamped in place, perpendicular to the plunger of a micrometer. The LVDT plunger was held against the micrometer with a spring (ref. Figure E.2) and the LVDT output could then be compared to the micrometer movement to obtain the calibration value for displacement versus voltage output for each LVDT used. The test consisted of commencing with the plunger fully inserted into the LVDT

and then retracting the LVDT plunger by moving the micrometer in 0.635mm increments, until the plunger was fully retracted. The micrometer was then advanced inward by 0.3675mm and then fully inserted back into the LVDT in 0.635mm increments. The output voltage for each increment was collected using the Agilent data acquisition system, the 10VDC power supply and the same wiring used during the main testing. This eliminated these variables from the calibration process.

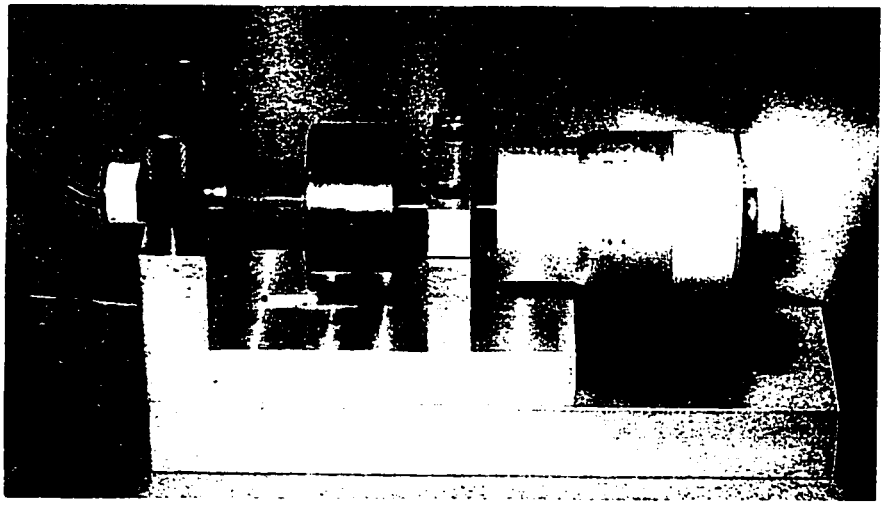

Figure E.1 – LVDT calibration set-up

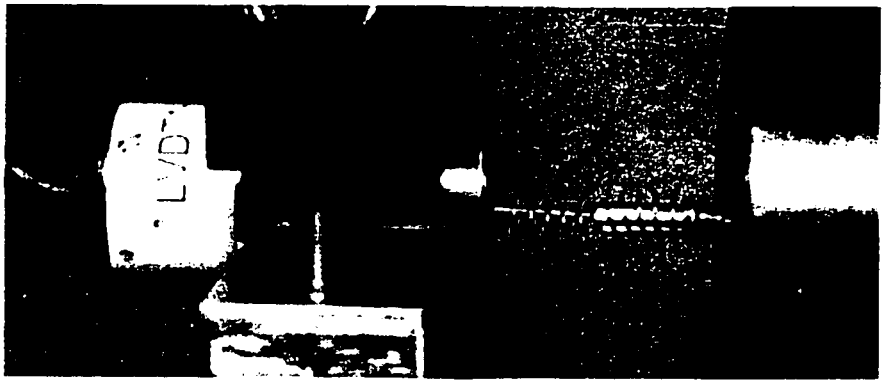

Figure E.2 – View of mounted LVDT

E.4 Calibration results

The results, for voltage output versus displacement and also the calibration constant, for each LVDT used are presented following in Figures E.3 to E.10.

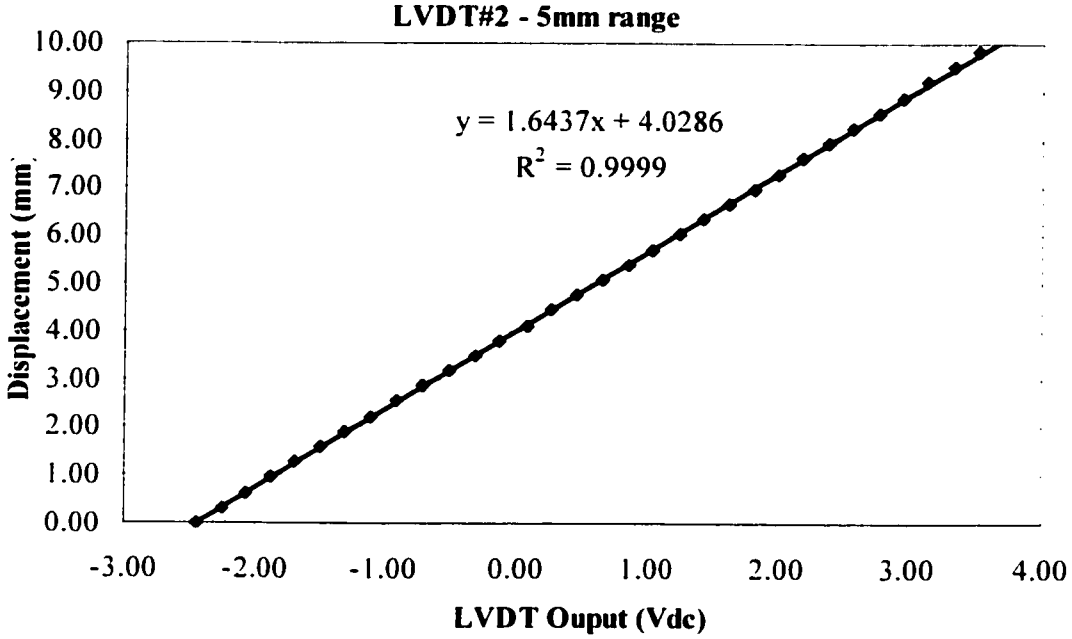

Calibration Constant = 1.6437 mm/V

Figure E.3 – Calibration results – LVDT#2

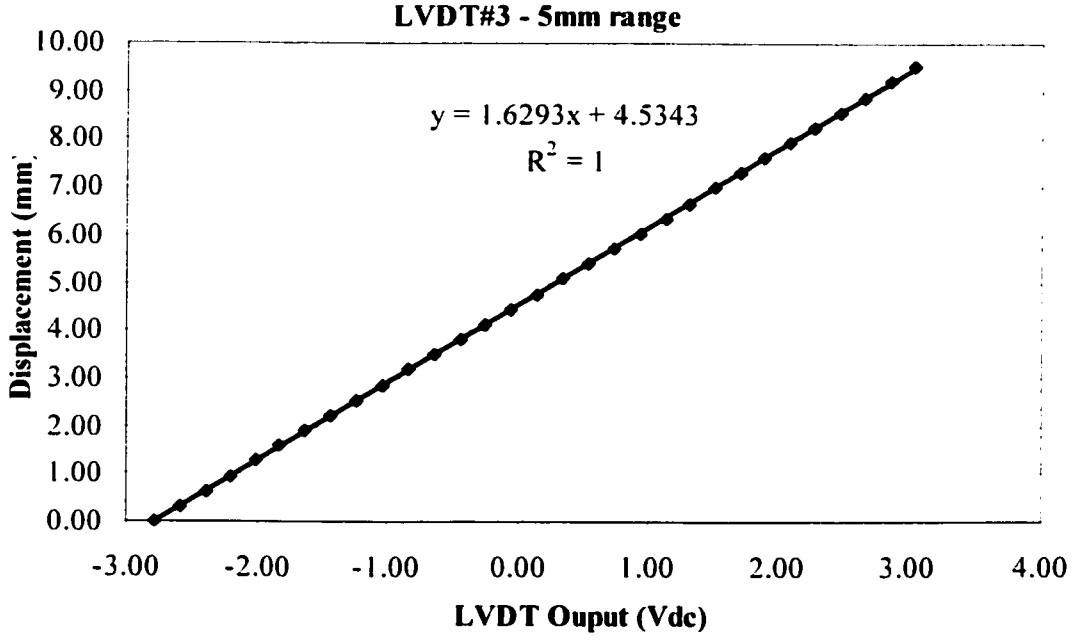

Calibration Constant = 1.6293 mm/V

Figure E.4 – Calibration results – LVDT#3

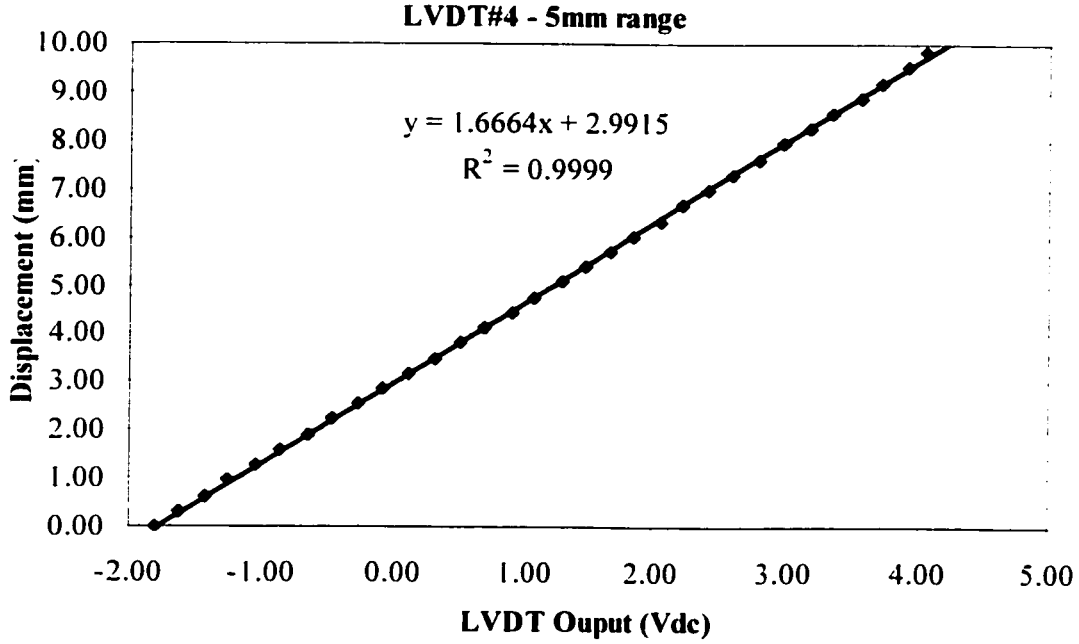

Calibration Constant = 1.6664 mm/V

Figure E.5 – Calibration results – LVDT#4

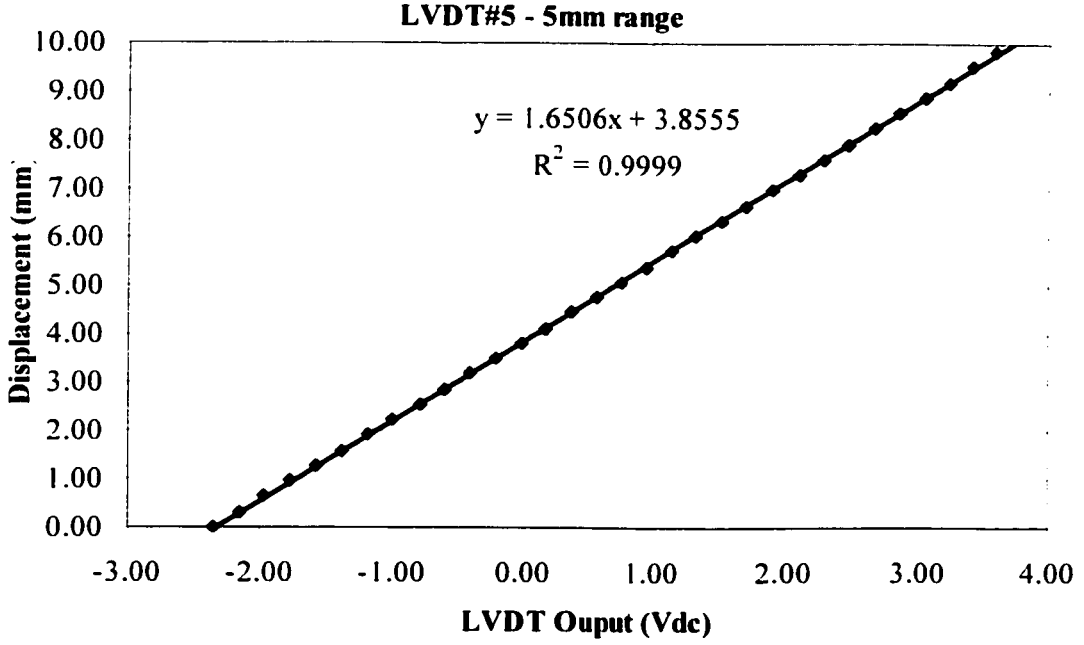

Calibration Constant = 1.6506 mm/V

Figure E.6 – Calibration results – LVDT#5

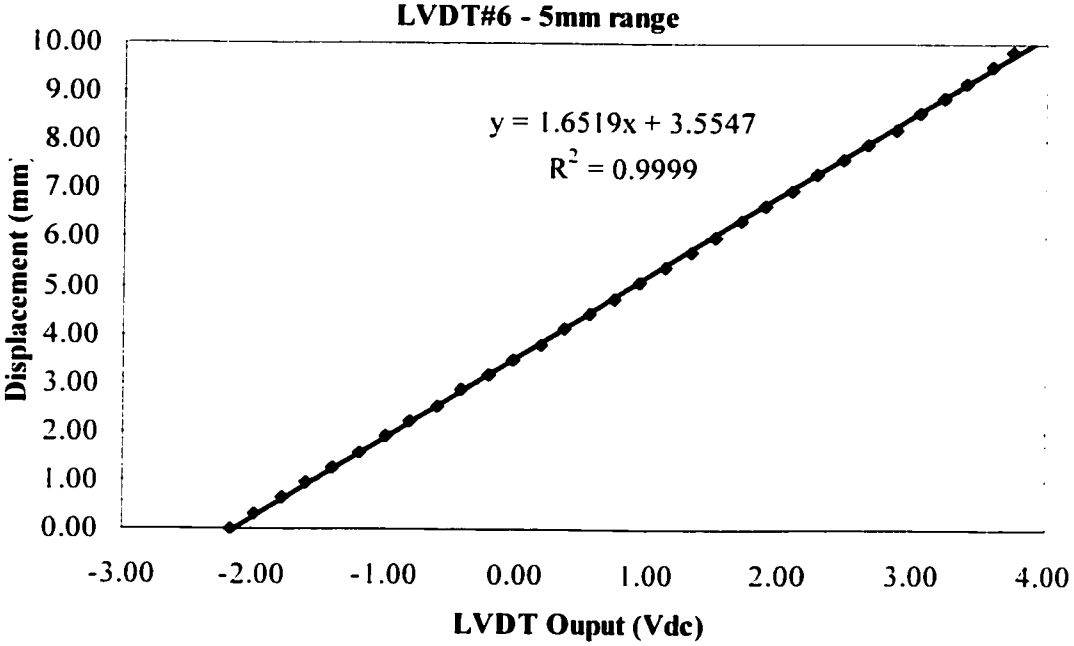

Calibration Constant = 1.6519 mm/V

Figure E.7 – Calibration results – LVDT#6

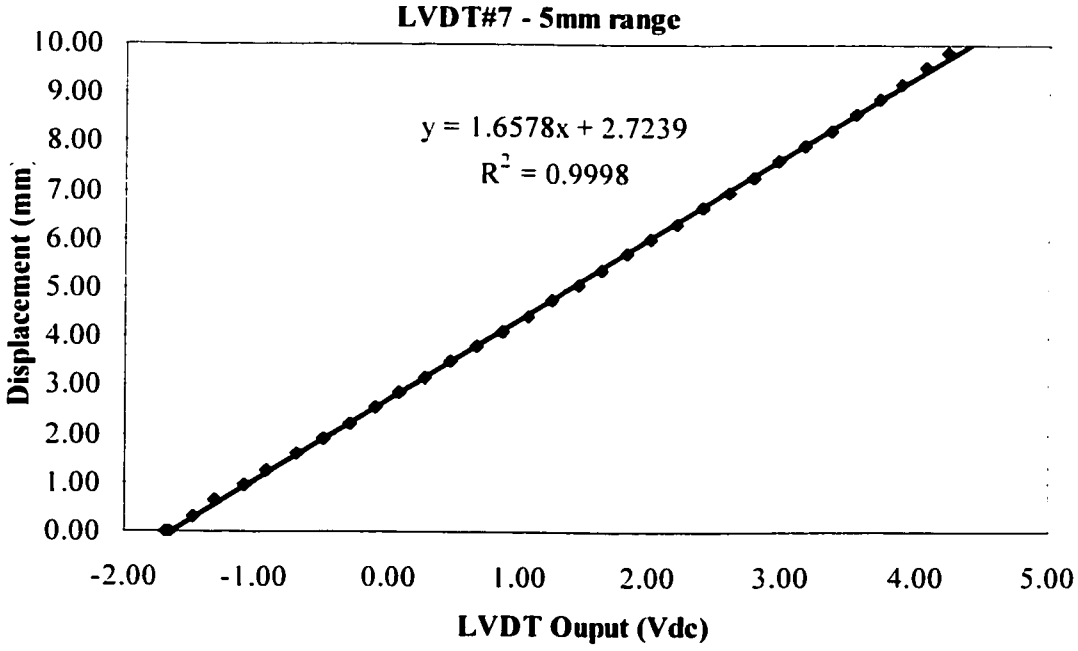

Calibration Constant = 1.6578 mm/V

Figure E.8 – Calibration results – LVDT#7

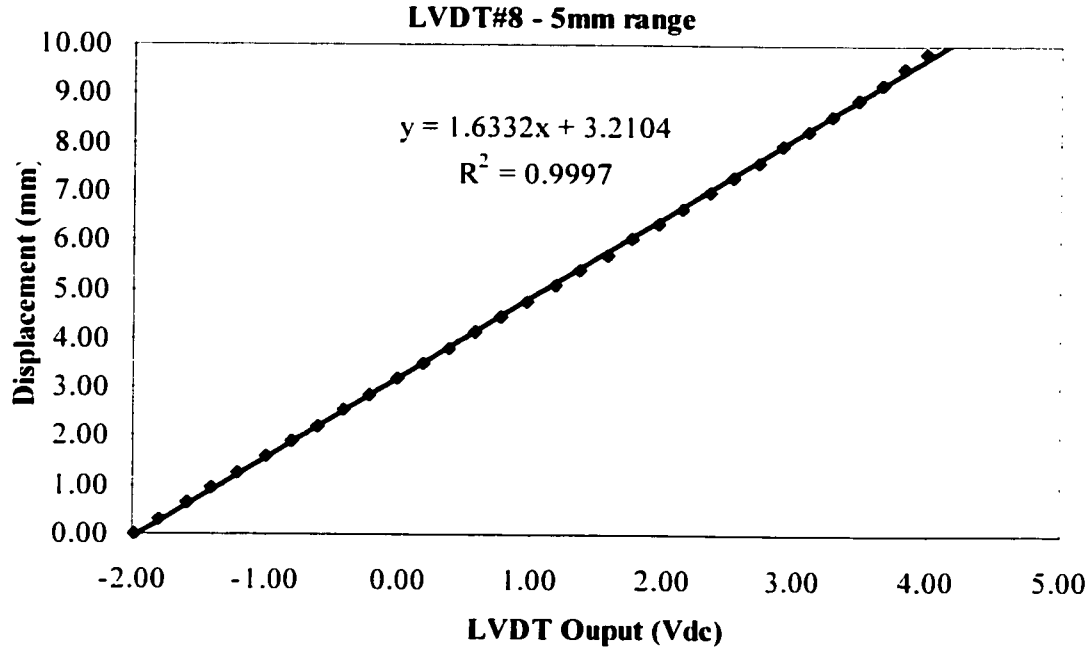

Calibration Constant = 1.6332 mm/V

Figure E.9 – Calibration results – LVDT#8

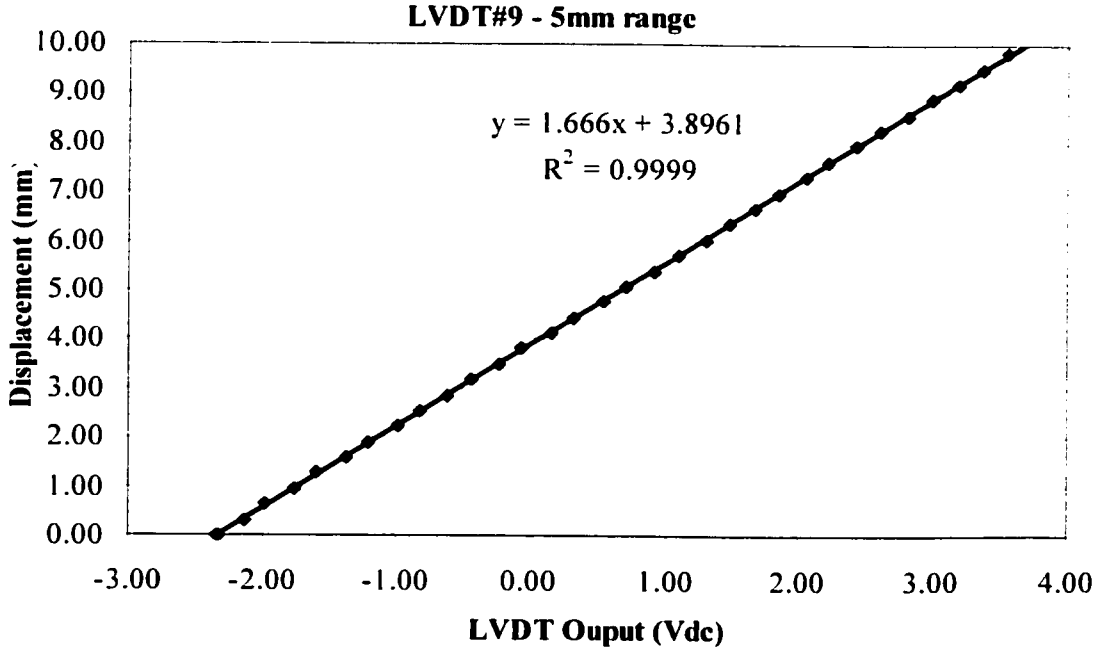

Calibration Constant = 1.666 mm/V

Figure E.10 – Calibration results – LVDT#9